The University Of Sheffield.

Department
Of
Mechanical
Engineering

Thesis

Non-destructive Evaluation and Condition Monitoring of Tool Wear

Author: Nopparat Seemuang

Supervisors: Dr. Tom Slatter

Dr. Matt Marshall

Date: April 2016

Thesis submitted to the University of Sheffield in partial fulfilment of the requirements for the degree of Doctor of Philosophy

Abstract

Non-destructive Evaluation and Condition Monitoring of Tool Wear

Author: Nopparat Seemuang

As tool wear is unavoidable, a tool condition monitoring system is an essential system to prevent machine tool downtime due to unnecessary tool replacement, tool breakage caused by using worn tools, and to reduce part rejections. Currently, multiple indirect sensing signals are commonly fused and used to detect tool wear to enhance the system reliability and generalisation. Many of the recently developed systems uses expensive sensing methods which are seemingly not suitable for real machining. Almost all of these monitoring systems were also developed in a laboratory control environment, resulting in lower performance if they are utilised in real machining operations.

This thesis takes these discrepancies as motivation to investigate and develop low-cost based tool condition monitoring systems. The cost effective tool monitoring systems were developed from a non-destructive evaluation (NDE) method and a multiple sensor fusion approach in order to monitor tool wear of common machining processes (turning, drilling, and gear hobbing). First, Barkhausen noise technique, an off-line NDT method commonly used in the hardened case-depth evaluation, was used to evaluate the coating thickness of TiN and CrN layers on HSS cutting tools. The results confirm that this proposed measurement system can be successfully used to indicate between different coating thicknesses.

Secondly, an on-line tool condition monitoring system based on multiple sensor fusion using a combination of inexpensive sensors (AE, microphone, and power monitoring system) was developed. Sensory features extracted from those sensors were trained by neural networks to obtain the tool wear prediction and tool wear state classification models. The system was successfully used to predict flank wear width and classify the tool wear states during a turning operation.

Furthermore, a novel sensing feature extracted from cutting sound, named '*spindle noise*', was first introduced in this study as this feature can successfully detect the excessive tool wear in turning and drilling or any other machining process which has a rotary spindle.

The cost-effective systems proposed in this study can be utilised in small and medium sized manufacturing companies and will improve productivity and add more value to the manufacturing processes.

Acknowlegements

Throughout this research I have called upon the assistance of a large number of people both within and outside the University. First and foremost, I would like to express my gratitude for the guidance and encouragement offered by my Director of Studies, Dr.Tom Slatter, who has excelled as a supervisor, both as a constant source of advice, support and encouragement throughout the project, and more specifically in the reading of countless draft chapters which has helped enormously in the preparation of this thesis.

Also, I would like to express my gratitude to Professor Rob Dwyer Joyce, Dr. Matt Marshall, for their comments and valuable ideas which helped in the development of the thesis. The author has a deep gratitude towards AMRC / NARMC and the staff, especially Tom McLeay, Jay Shaw, Kathryn Jackson, Ross Barrable, who are mentors and facilitators throughout the machining experiment.

The help and support of colleagues and members of staff at the University of Sheffield are also gratefully acknowledged. On this front thanks must also go to John Wilkinson, who made a U-core for Barkhasen noise study, John Bradley, who made various mechanical elements for the experiment, Ben Kitchener who is a departmental electronic supervisor, and Carl Wilson who pays his time to operate a CNC machine during long-period data collection.

During my time as a PhD student, the enthusiastic supports of Tribology group's members, Rob Thornton, Adli Bahari, Liam Chisman, Niki Hilton, Thomas Howard, were vital towards the completion of the experimental set-up and conduction.

I would like to acknowledge the financial support through years of study provided by the Royal Thai Government. Other thanks must also go to the Advanced Manufacturing Research Centre (AMRC) and Nuclear AMRC, who are responsible for the experimental studies in this thesis.

Most importantly, the author wishes to express special thanks to Dad, Mom, sister, lovely friends, departmental colleagues at the department of production engineering (KMUTNB), and people at the Office of Education Affairs (OEA-UK) for all kind support during this hard time. I would not have made it this far without you.

Abbreviations

2D, 3D	Two/Three Dimension
AC	Alternating Current
ACC	Average Classification Accuracy
AE	Acoustic Emission
AF	Activation Function (transfer function)
AI	Artificial Intelligence
AISI	American Iron and Steel Institute
AMRC	Advanced Manufacturing Research Centre
ANFIS	Adaptive Neuro-Fuzzy Inference System
ANN	Artificial Neural Network
AWG	American Wire Gauge
BHN	Barkhausen Noise
BP	Back-Propagation
BUE	Build Up Edge
CCD	Charge Coupled Device
CFS	Correlation Based Feature Selection
CNC	Computer Numerical Control
DAQ	Data Acquisition
DHL	Double Hidden Layer
DIP	Digital Image Processing
DOC/DoC	Depth of Cut
DOE	Design of Experiment
DWT	Discrete Wavelet Transform
EBPAPVD	Electron Beam Plasma Assisted Physical Vapour Deposition
EDM	Electrode Discharge Machine
ESD	Energy Spectral Density
F	Feed
FFT	Fast Fourier Transform
FS	Feature Set
FWWL	Flank Wear Width at Left Side (flank face)

Abbreviations

FWWN	Flank Wear Width at Nose Radius (Nose Wear)
FWWR	Flank Wear Width at Right Side (flank face)
GA	Genetic Algorithm
GDP	Gross Domestic Product
HHT	Hilbert-Huang Transform
HSS	High Speed Steel
HVM	High Value Manufacturing
IACS	International Annealed Copper Standard
LED	Light Emitting Diode
MAE	Magnetoacoustic Emission
MAE	Mean Absolute Error
MBE	Magnetic Barkhausen Emission
MBN	Magnetic Barkhausen Noise
MFS	Magnetising Frequency Sweep
MLP	Multilayer Perceptron
MMR	Metal Removal Rate
MP	Magnetoelastic Parameter
MVS	Magenetising Voltage Sweep
NAMRC	Nuclear Advanced Manufacturing Research Centre
NaN	Not a Number
NDT	Non-Destructive Testing
NHL	Nodes in Hidden Layer
NN	Neural Network
NNHL	Number of Nodes in Hidden Layer
PCA	Principal Component Analysis
PSD	Power Spectral Density
PVD	Physical Vapour Deposition
RMS	Root Mean Sqaured
RMSE	Root Mean Squared Error
RPM	Revolution per Minute

Abbreviations

RUL	Remaining Useful Life
SAE	Society of Automotive Engineers
SHL	Single Hidden Layer
SLD	Stability Lobe Diagram
SSA	Singular Spectrum Analysis
SSE	Sum of Squared Error
STFT	Short-Time Fourier Transform
SVM	Support Vector Machine
TA	Training Algorithms
TCM	Tool Condition Monitoring
TCMS	Tool Condition Monitoring System
TDMS	Technical Data Management Streaming
USB	Universal Serial Bus
Vc	Cutting Speed
VTL	Vertical Turning/Milling Lathe
WEKA	Waikato Environment for Knowledge Analysis
WT	Wavelet Transform

Table of Contents

Table of Contents

Table of Contents

Table of Contents

Table of Contents

Chapter 1

Introduction

1.1 Motivation for the Development of Tool Condition Monitoring

The machining process is one of the important manufacturing processes that are normally used to produce semi-finished and final products by changing the geometry of bulk materials. Cutting tools are normally used to remove material in the form of chips. Although recent developments in cutting tool materials and control technology of machine tools have allowed longer tool life, the tools still wear out when used over periods of time.

Inevitably, tool wear has a direct influence on surface finish and part accuracy of finished workpiece leading to rejections. Also, tool replacement and unplanned stoppages due to using worn tools can cause machine downtime and part non-conformance leading to economic loss. Therefore, it is essential to prevent downtime during production from unplanned incidents which have a direct impact on productivity. To avoid this, tool condition monitoring systems have been developed for almost two decades and this monitoring system is included as a basic necessity of recent machine tools.

As mass production has been recently established in developing countries, developed economies such as USA and UK have to maintain the manufacturing contribution to their GDP by adding value to manufactured goods in terms of manufacturing technology improvement. As a major part of production, the value of machining processes is increased by, for example, optimum tool preparation, shorter machining time, micro/nano machining, extended tool life and reduction of tool change time. In terms of tool wear, not only can such a tool failure be avoided by tool condition monitoring system but also maximum use should be obtained from the tools.

Tool condition monitoring (tool wear monitoring) can be achieved by direct and indirect methods. As for direct methods, the actual tool wear in terms of material loss is directly measured and observed by using optical sensor, radioactivity and lasers which are considered as a high accuracy and reliability method. However, these methods are still very expensive, impractical to apply in the shop-floor, and they can only be used for off-line or in-cycle measurement, leading to machine downtime. In contrast, indirect methods based on inferring condition from the outputs of indirect sensors are more favourable to use as they are more cost effective, robust, easy to use, and can still be used for on-line monitoring although they provide less accuracy.

Coated tools are commonly used in machining processes (e.g. TiN coated HSS for gear hob cutters) as they offer longer tool life and good machinability compared with uncoated tools. During production operations assessment of the remaining coating depth of coated tools could be helpful information for the machine operator to avoid using the worn tool. Destructive methods such as micro-hardness profiling and metallography are used to evaluate the thickness of coating layer; however, they are also expensive, time-consuming, and inconvenient use.

Thus, non-destructive methods, evaluating the properties of materials, parts, products without causing any damage, are more often used as they are very fast in evaluation. The most frequently used to evaluate tool wear are visual testing, acoustic emission testing, ultrasonic testing, thermal/infrared testing, magnetic/electromagnetic techniques, and radioactivity. Also, the cost and characteristics of each technique should be considered in order to ensure the best fit for a given monitoring purpose and application.

Many magnetic methods have been attempted to evaluate hardness and case depth such as Barkhausen effect, magnetic hysteresis properties, and magneto-acoustic emission. The "Barkhausen noise (BHN)" can be used successfully in several applications such as hardening depth evaluation, residual stresses and fatigue monitoring, and surface integrity evaluation. However, this technique has not been well studied for monitoring coated layer in coated high speed cutting tool. It would be worth to apply this non-destructive technique as in a similar fashion to the use of magnetic methods to measure case hardening.

Automated machining processes are increasingly used in manufacturing systems which consequently need the development of more reliable and robust monitoring systems. Accordingly, the demand of tool condition monitoring systems has been increased as companies have attempted to minimise the consequence of failures, to increase product quality, safety and reliability. To achieve robust prediction and evaluation of tool wear in machining processes, the use of more than one sensing technique to monitor the tool wear has been developed, known as multiple "sensor fusion". Due to varying machining conditions, it is more useful to use several sensor signals instead of only single sensor signal in order to increase the reliability of the sensor and monitoring system. Consequently, the data acquisition systems consisting of multiple sensors are required to acquire sensor signals from machining processes, and this needs high performance computers to interface these sensors, data collection, perform data processing, and machine control. This can be achieved as the computer system and software have also been developed to meet the requirements of large data storage, faster, more effective data analysis.

Nevertheless, the majority of tool condition monitoring system found in currently-published research has used expensive sensing systems not suitable for production, such as force dynamometers. Even with expensive data acquisition hardware, obtaining high quality data to train the system is difficult and time-consuming because of the complexity of the signals that can be recorded from an operating machine.

With this in mind, it is clear that there is a research opportunity to investigate, and develop, low-cost based tool condition monitoring system that take advantage of these recent developments.

1.2 Statement of Purpose and Scope of Thesis

The development of cost effective tool monitoring systems is defined as the core purpose of this study. The wear on cutting tools was variously monitored by non-destructive evaluation techniques and a multiple sensor fusion approach in order to help prevent unnecessary tool replacement, tool breakages, and part rejections caused by using worn tools. Both off-line and on-line measurement approaches were developed in order to monitor tool wear of common machining processes such as turning, drilling and hobbing.

At its core, this thesis consists of two main studies:

Coating-depth evaluation using the Barkhausen noise (BHN) technique: this off-line measurement technique was studied for evaluating the thickness of the coating layer in coated HSS, which is the cutting tool normally used in the gear manufacturing process. A cost effective BHN system has been developed and the effective working setup of the system was identified that can distinguish between different coating thicknesses.

and;

Tool condition monitoring based on sensor fusion: this on-line monitoring method, based on sensor fusion, has been developed by using multiple sensors (AE sensor, microphone, power consumption of spindle motor) and an artificial neural network. This system was first used to monitor the tool wear and the tool condition in turning process and includes an image processing technique used to monitor the wear.

1.3 Formal Statement of Aim and Practical Objectives

1.3.1 Aim

The aim of this work was to design, test and evaluate the off-line and on-line measurement methods in order to have a potential of the tool condition monitoring system in common machining processes.

1.3.2 Objectives

To achieve the aim, the following objectives are defined:

1. To review past work and the current state of the art in tool condition monitoring, in particular, sensor fusion for tool condition monitoring and magnetic Barkhausen noise technique.

2. To establish the measurement requirements of the chosen processes for use in sensing, pre-processing and analysing signals generated from the machining process.

3. To propose a cost-effective off-line measuring the coating thickness of CrN/TiN coated HSS tools.

4. To propose a systematic approach to design a multi-sensor monitoring system based on the concept of data fusion.

5. To implement suitable data processing technique (Neural network) on multi-sensory signals obtained from cutting processes and to validate the performance effectiveness of the monitoring system.

The aim and objectives of this thesis can be illustrated in the block diagram shown in Figure 1.1.

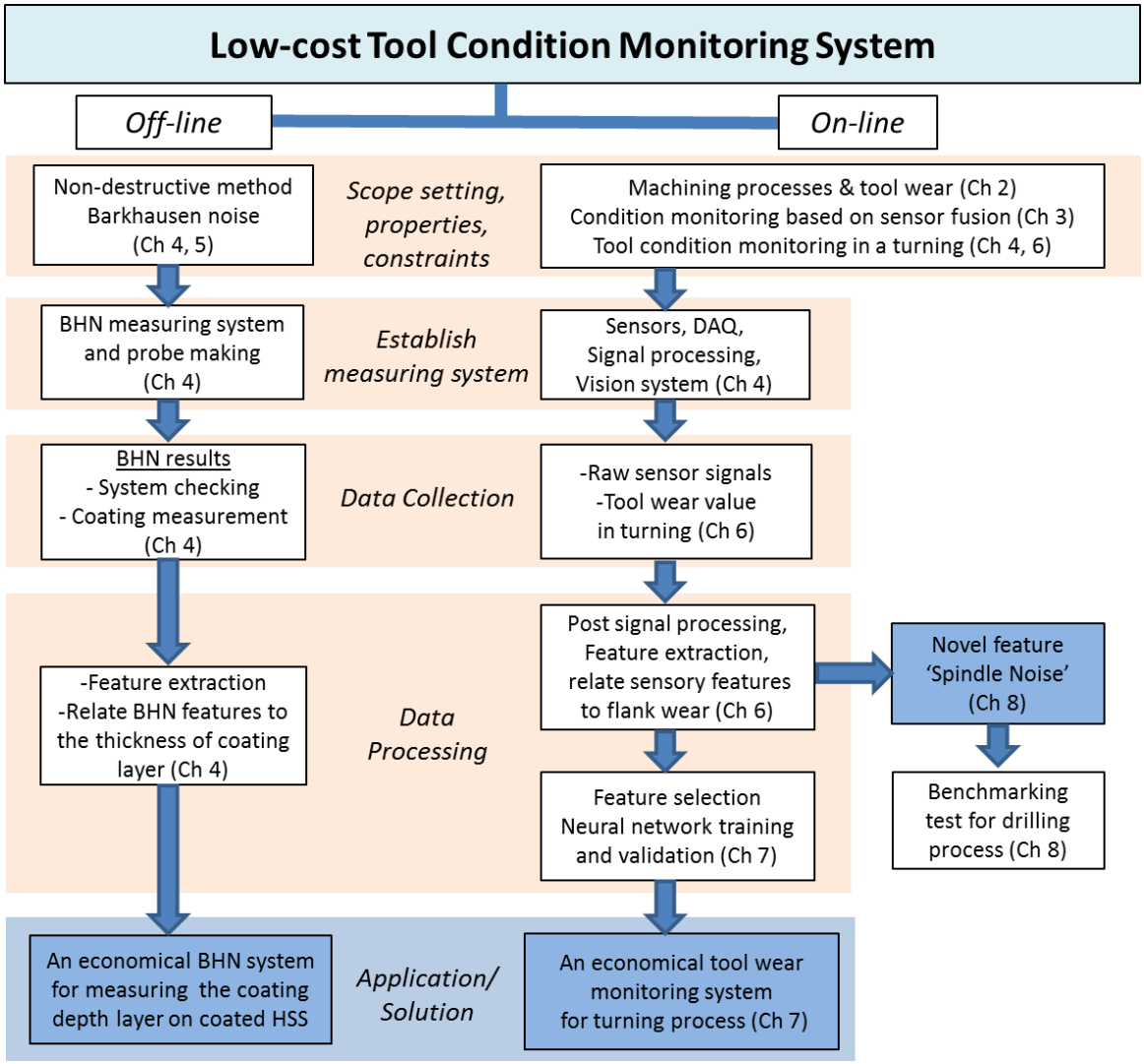

Figure 1.1 Diagram showing the main tasks of the research programme

1.4 Thesis Structure

This thesis is organised as follows.

Chapter 1 introduces the motivation for the development of tool condition monitoring system. General purposes, scope of study, aim and practical objectives, have been stated.

Chapter 2 details general manufacturing processes, focusing on machining processes. The fundamental knowledge in machining science is introduced, such as cutting tool geometry, chip formation, and process parameters. Tool wear and wear determination in the machining process are also described.

Chapter 3 describes condition monitoring, especially of a machining process. The sensor fusion approach, including sensors, signal processing, artificial intelligences normally used in tool condition monitoring is also discussed.

The general methodology presented in Chapter 4, consists of general background and development of the both the off-line and on-line monitoring systems in this thesis. Firstly, the characteristics and principles of BHN are introduced and the development of the BHN-based measuring off-line system is then described. Secondly, the development of the on-line tool condition monitoring system is explained including the machining experimental setups and the feature extraction and selection methods. Finally, the artificial neural networks for tool condition monitoring and validation method used in this study are introduced.

Chapter 5 begins with a short review of previous attempts to use the BHN technique in condition monitoring. The bulk of this chapter gives details of the experimental setup and presents the results. A procedure for the use of the BHN system for tool condition monitoring is proposed and its success discussed.

Similarly, Chapter 6 begins with a short review of on-line tool condition monitoring and then the specific experimental setup, materials and methods are described. The results, particularly of the sensing of tool wear, are presented and the effect of cutting parameters on the sensing signals is discussed in this chapter. These are combined in order to compare the sensing features with flank wear progression.

Chapter 7 builds on the results of Chapter 6, by beginning with feature extraction and selection of the sensing signals. Feature selection based on correlation coefficient and correlation based feature selection (CFS) was used to select the best features for neural network training. Then, tool wear prediction and tool wear state classification models were trained and validated by several network configurations. After that, the method of remaining useful life estimation was proposed.

Chapter 8 introduces the concept of 'spindle noise' which is a novel feature identified and extracted from the cutting sound signal discussed in Chapter 6. The power spectrum magnitude of spindle noise frequency and its cumulative value correlates remarkably well with tool wear at the variations of cutting speed and feed. Additionally, this feature was utilised in a drilling process to monitor the drill bit wear.

Chapter 9 presents the key findings and conclusions from the studies and gives recommendations that could be considered to build on this work. The publications and contributions of this thesis are listed and stated.

Chapter 2

General Background Knowledge I

High Value Manufacturing

Manufacturing and Machining Processes

Tool Wear in Machining Processes

This chapter describes the fundamentals of cutting processes which are common in manufacturing. The general background of machining such as tool geometry, chip formation, type of chips, cutting tool materials and cutting fluids, process parameters, and machinability are introduced. After that, tool wear in machining is described, including wear mechanisms, wear parameters, a typical tool wear curve, and the tool life equation.

2.1 High Value Manufacturing (HVM)

Recently, mass production has migrated to the economically developing regions. The manufacturing plants of many companies have moved, or been established, in lower cost-base countries such as China, India and Thailand. This causes unemployment problems in high-cost base countries e.g. the USA, the UK and other developed economies.

As a result, China and India have a growth of their GDP about 10% yearly. Both countries have developed their technological potential and have big advantages in manufacturing costs due to low wages and working conditions. They are fast adopters in technological competitiveness and productivity by implementation and imitation of knowledge. Those countries also have lower investment costs in terms of land, water, and electricity. They also open (deregulated in) the labour market and have good global logistics and communication services. For example, Japanese and South Korean manufacturers of electronic components, who are the leaders of the world market manufacture their products in countries such as Thailand and Vietnam. These are the main reasons of moving the production to such countries. However, there are also negatives such as political and economic stability, customer desire to purchase 'homegrown' products and issues with communication that make development of new products and maintenance of existing quality challenging.

Developed economies, such as the USA and UK aim to maintain or preferably grow the contribution of manufacturing to their GDP by enhancing and 'adding value', to manufacturing technology and the production system. This is called *"High Value Manufacturing"* or HVM. For example, as the UK will not be able to produce goods on high volume due to the high cost of productive resources so a practical strategy that can be implemented is adding value to the manufactured goods in terms of either component or processes.

In general, manufacturing processes, particularly machining processes are a major part of production. Most of the researches and technological breakthroughs centre on enhancing machining processes in several aspects for adding the value. The main objectives of HVM in machining processes include optimal tool preparation, reduction of tool change time, shorter machining time, higher material removal rate and extended tool life.

Therefore, this thesis aims to adopt the HVM concept to obtain the added-value to machining process by developing the in-line tool performance monitoring system to prevent the production losses caused by using the worn cutting tools.

2.2 Manufacturing Processes

The manufacturing process is the group of operations used to transform workpiece materials into final products by changing the geometry and properties of the raw material. The manufacturing processes can be broadly classified as: casting, forming, machining, joining, and surface treatment (finishing and heat treatment).

Casting or moulding processes are widely used to primarily produce parts which quite often need other following processes, such as machining to finish the product. A mould cavity is filled with molten metal and the metal retains the desired shape as the mould cavity after solidification. Casting is the term used for metallic material, while moulding is the common term used for plastic materials.

Forming or deformation processes are used to modify or change the size and shape of the material. In general, the materials generally pass through the series of forming operations, which are done in both hot and cold conditions. The workpiece material is often heated to the temperature below the melting point. The forming process can be divided into bulk metal forming process (rolling, forging and extrusion) and sheet metal forming process (blanking, coining, stamping, bending, and spinning).

Machining or Cutting, a group of metal removal processes, is a process of removing unwanted material from original workpiece in the form of chips to obtain a desired shape or finish. The seven traditional machining processes are turning, drilling, shaping, milling, sawing, broaching, and abrasive machining (grinding). Other metal removal processes are known as non-traditional processes because they use other media such as lasers, water jet, electron beams, chemical erosion, electric discharge and electrochemical energy to remove material instead of using cutting or grinding tool.

Joining is the process used to combine or assemble the machined parts or semi-finished parts to be the final product, including mechanical fastening, soldering, welding, press or snap fittings, adhesive bonding, and assembly processes.

Finishing processes or surface processing operations are performed for cleaning (chemical and mechanical), removing burrs (deburring), or providing protective surfaces on the workpiece (painting, coating, plating, buffing, galvanizing, and anodizing). These are done to prevent corrosion and enhance the component geometry before joining to other components.

Heat treatment is the process used to improve the metallurgical and mechanical properties of the metal for the specific purpose without changing its shape. This is

about heating and cooling of the metal to obtain the desired properties such as hardness, toughness, brittleness.

In recent years, a family of emerging additive manufacturing processes have been developed. These processes produce the first or prototype components quickly by using specialised machines controlled by computer-aided design that usually build up components layer by layer. The resulting components often still need further post-processing that uses the traditional manufacturing processes.

Machining is a major manufacturing process because:

(1) various materials can be machined by machining processes,

(2) various part shapes and geometric features can be made,

(3) machining processes can produce the components to close tolerances,

(4) machining is able to create very smooth surface finishes,

(5) the chips from machining operation can be usually recycled.

Although machining operations can be time-consuming, they are normally used to produce the final geometry, dimensions, and surface finish.

In Figure 2.1, there are several sorts of machining operations (turning, milling, drilling, boring, planning, shaping, broaching, sawing, grinding, polishing), each of which can generate certain part geometry. The most common types of machining process mentioned in this thesis consist of turning, milling, and drilling.

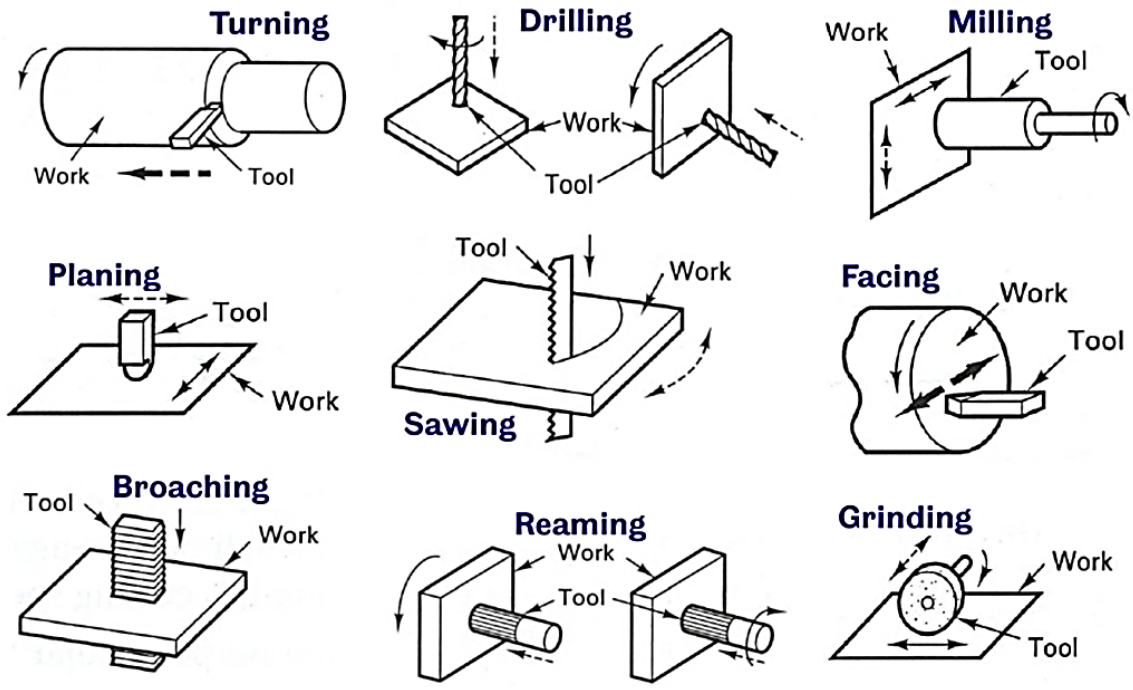

Figure 2.1 Basic machining process (adapted from [1])

In turning, a single cutting edge tool is used to remove material from a rotating workpiece in order to generate cylindrical shape. The spindle motor and gear set are used to speed the rotating workpiece, and cutting tool moves slowly in parallel direction to the rotating axis. Drilling process is used to produce a round hole with two cutting edges of a drill bit rotating around the rotating axis. The drill bit is fed in the parallel direction of the axis of rotation into the workpiece to crate the round hole. In milling, rotating tool which has multiple cutting edges is moved slowly to the workpiece to generate the plane or surface. The feed direction is perpendicular to the axis of rotation. Face milling and peripheral milling are the two basic forms of the milling process. The fundamental knowledge of machining process will be elaborated in following sections.

2.3 Fundamental of Machining Processes

2.3.1 Tool Geometry

The cutting tools used in machining processes can be separated into two main groups: single-cutting-point and multiple–cutting-point tools.

Single-cutting-point tools have only one effective cutting edge and are usually used for turning process, such as cylindrical turning in Figure 2.2 below. When the cutting edge is perpendicular to the feed direction, it is called *orthogonal cutting*. *Oblique cutting* is defined when the cutting edge is inclined to the direction of the feed. *Multiple cutting point tools* or multi-point tools are defined as the tool has more than one cutting edge such as twist drill, milling cutters, broaching tools, as well as abrasive wheels.

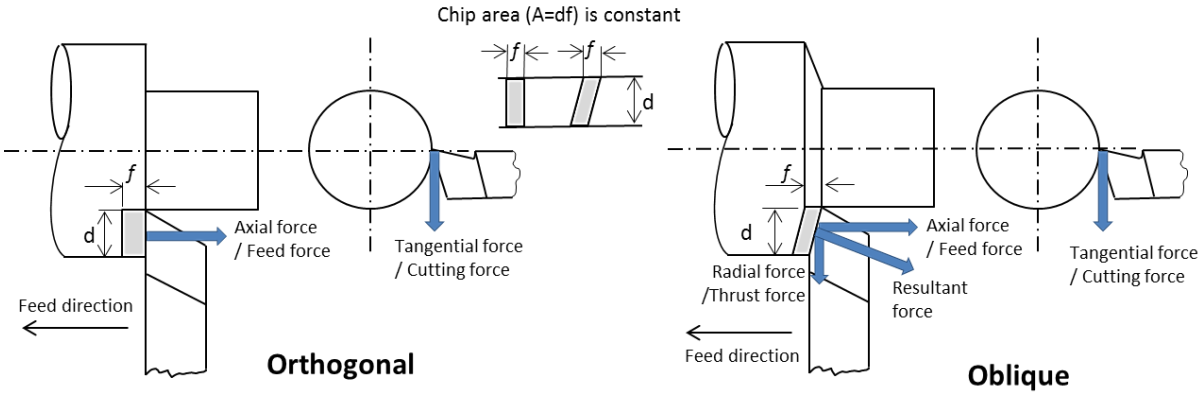

Figure 2.2 Orthogonal cutting and oblique cutting (adapted from [2])

All cutting tools have common shape features: clearance angle (α), wedge angle or cutting angle (β), and rake angle (γ) as shown in Figure 2.3.

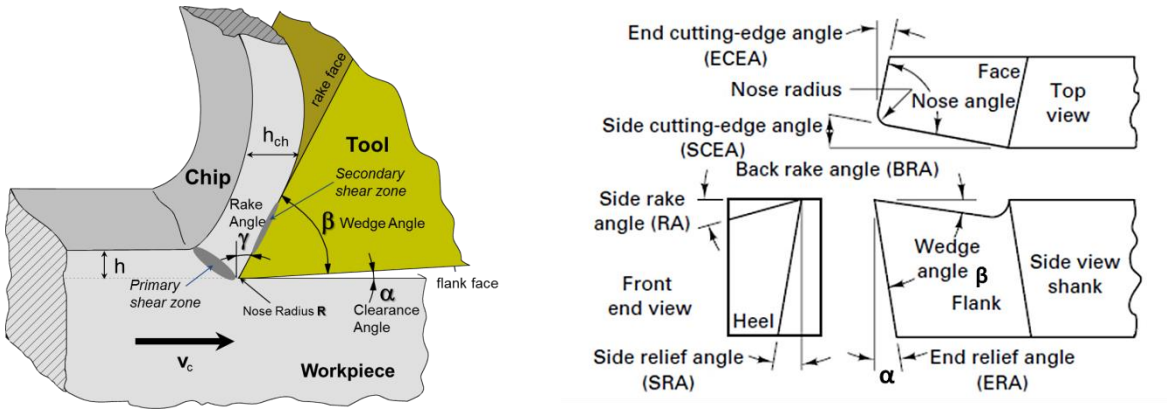

Figure 2.3 General cutting tool geometry (adapted from [1])

Clearance angle (α) or relief angle is measured on the flank side which provide a clearance in order to avoid the contact between the machined surface and the flank of cutting tool which would increase friction and the likelihood of damage to the just-machined surface.

Wedge angle (β) or lead angle is the cutting angle of the tool. Wedge is made up of two faces: a rake face and flank face. The greater wedge angle can make the tool stronger and to prevent tool overheat in order to prolong the tool life. It however, needs more cutting force to make the tool penetrate to the workpiece.

Rake angle (γ) is the angle between a rake face and a plane which is perpendicular to workpiece surface. The rake face is where the chip runs off. The tool-chip contact area where the chip is raked has lot of friction and high temperature due to rubbing between removing chip and tool surface.

2.3.2 Chip Formation

To understand the mechanics of machining, orthogonal cutting (two-force system) simplified cutting tool geometries from oblique model (three-force system), is used to describe the chip formation.

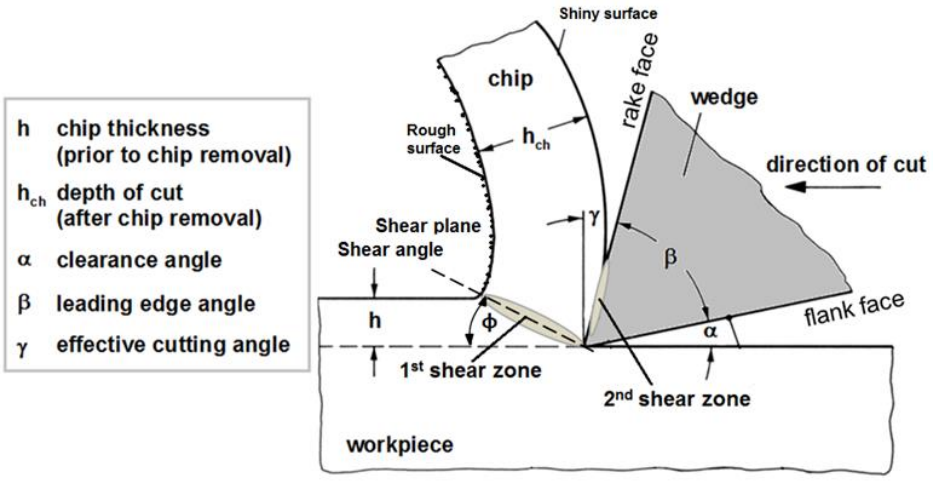

Figure 2.4 Chip formation (adapted from [3])

Figure 2.4 shows the idealised model of chip formation process by two-dimensional cutting model. A cutting tool with wedge angle (β) moves to the left into the workpiece at a constant velocity, and cutting depth (h). A chip with thickness (h_{ch}) is produced ahead of the tool by plastically deforming and shearing the material continuously along the shear plane in primary shear zone. The chip begins to flow and removes the tool via the rake face. During chip removal on rake face, the shear force due to tool-chip interface friction reacts in the secondary shear zone to against the moving chip, resulting in the tool-chip side of the chip being shiny surface while other side is rough.

2.3.3 Type of Chips

Chip formation is an important aspect of the machining process. According to [4], the chip formation can be categorised into four main types: continuous, discontinuous, serrated as shown in Figure 2.5, and built up edge (BUE) in Figure 2.6.

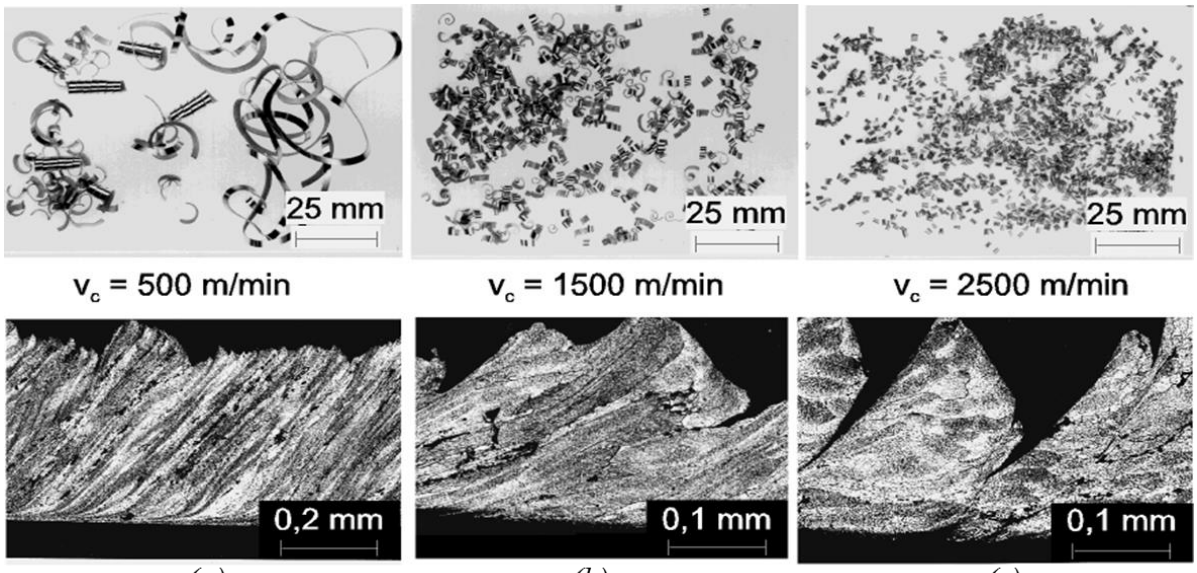

Figure 2.5 Chip morphology: *(a)* continuous, *(b)* discontinuous, and *(c)* serrated or segmented (reproduced from [3])

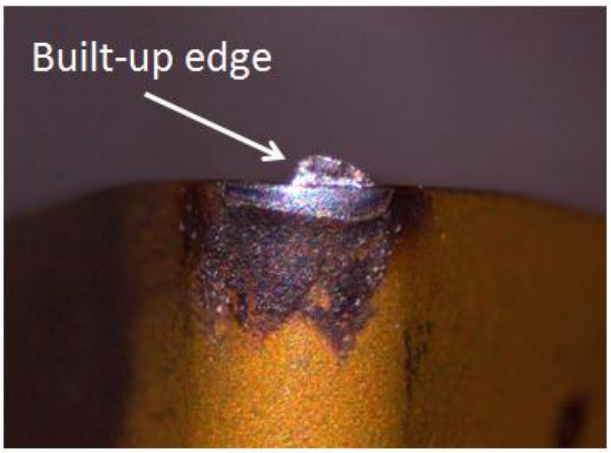

Figure 2.6 Built up edge on the rake surface

Continuous chips:

These take the form of long ribbon-like chips. They can be found when ductile materials (i.e. low-carbon steel, copper, and aluminium) are machined or in machining with high cutting speed or high positive rake angles. Although continuous chips generally produce a good surface finish, they are problematic for CNC machines because the chips may entangle with tool holder or jig and fixture or bring about stopping process to remove them if the chips are continuous and too long. This can be mitigated by using chip breakers (a design feature of the tool) or changing cutting parameters and using cutting fluids to reduce the resistance in tool-chip contact area.

Discontinuous chips:

This type is characterised by a continuous breaking of the removed material into uneven length chips. They may be randomly long or short. They are normally found when machining brittle materials, when the workpiece material has impurities or hard inclusions, or the use of very high or low cutting speeds, a large cutting depth, or low rake angle. The formation of these chips leads to variation of cutting forces that has an effect on surface finish and contributes to the onset of self-excited vibrations (chatter). It can also promote premature tool wear and adversely affects the dimensional accuracy of the machined part.

Serrated chips:

Serrated chips, or segmented chips, resemble a sawtooth which can be formed during the machining of low thermal conductivity metals and those with strength that decreases rapidly with temperature. Serrated chips consist of chip segments that are initially separated in the shear plane and then fuse together. They are often found during cutting of brittle materials like cast iron and can be formed at very low cutting speeds (V_c = 1-3 m/min).

Built-up edge:

Built up edge (BUE) stems from gradually growing of particles of metal from the chips attaching to the cutting tool tip because of high friction force between the chip and the rake face. This leads to increased friction force and heat at the cutting edge. BUE also changes the geometry of the cutting tools and has a direct effect on the surface finish. It can cause a rough surface on the workpiece if the particles of built-up material flake away weld themselves to the workpiece surface. It can also be considered as a protective surface, therefore it can reduce tool wear on the rake face if stable and thin. BUE formation can be reduced by increasing the cutting speeds and the rake angle, decreasing the cutting depth, and using effective cutting fluids.

2.3.4 Cutting Tool Materials and Cutting Fluids

Appropriate selection of tool materials is a major concern in defining a machining process. The important properties needed in a tool material include; high toughness (strength and ductility) to resist flank wear, high hardness at hot temperature to resist deformation of cutting edge, and wear resistance. Furthermore, the cutting tool material should be chemically stable to avoid oxidation and diffusion, resist to sudden thermal changes and be non-reactive with the workpiece material.

There are various tool materials used in machining processes such as carbon steels, alloy steels, high speed steels (HSS), cemented carbides, coated carbides, ceramics, and synthetic diamond each with different characteristics and uses. The cutting tool material must be matched to the workpiece material being cut and the cutting conditions selected. The general characteristics of tool materials are as follows.

High carbon steels with carbon content about 0.87-1.2 percent are mainly used for hand tools because the hardness is rapidly reduced when the temperature of the material significantly increases as often occurs in machine tools. Consequently, various alloy tool steels have been developed to improve the cutting ability of carbon tool steels.

High-speed steel (HSS) is widely used for tool material in several cutting applications such as drills, reamers, milling cutters, turning tools, planning and shaping tools. Tungsten (W) and cobalt (Co) are used as a main alloying content in order to retain the hardness of the tools under working in high temperature. The strength and toughness of the tool steel, so that it can be used to resist the cutting force in cutting of high-strength alloy materials, can also be improved in this way.

Cemented carbide and *ceramic* tools can be used in higher temperature than high speed steel. They are much more resistant to abrasion. However, such materials are relatively weak in tension and also more brittle. Ceramic tools are harder and more brittle than carbide but brittle. Therefore, they are normally used in high-speed finishing cuts with fine feed when the high surface finish is required.

Cutting tool materials are frequently coated with a layer of hard material such as titanium nitride (TiN) and titanium carbide (TiC) in order to enhance their efficiency and wear behaviour. *Coated tools* often provide a lower friction coefficient resulting in no BUE on the rake surface and reducing of cutting temperature, and promoting a longer tool life when compared with uncoated tools.

Industrial diamonds are mainly used for finish machining, such as grinding, which requires good surface finish and dimensional accuracy. Diamond tools are suited to cutting light, heavy and precious metals, hard and soft rubber, glass, plastic and stone. Due to limitation of cutting edge dimensions, it is difficult to use the diamond in large depths of cut and feeds. They can be used only with very fine feeds to minimise cutting force on them although they are very hard.

At the cutting point (Figure 2.7), the total energy input to the in the primary cutting zone is converted into heat, which is about 98% on tool-chip interface area and on the chips and workpiece surface about 2% [1]. This high temperature can reduce the tool life, and cause the accuracy problems with the workpiece due to the thermal expansion effect. To address these problems, cutting fluids are normally applied to the machining operation to cool down the temperature (coolants) and lubricate the chips removing pass through the cutting tools (lubricants). Using cutting fluids can reduce frictions (tool-chip and tool-work interfaces), total heat (shear zone and friction zone), cutting forces, and power consumption, and prolonging tool life.

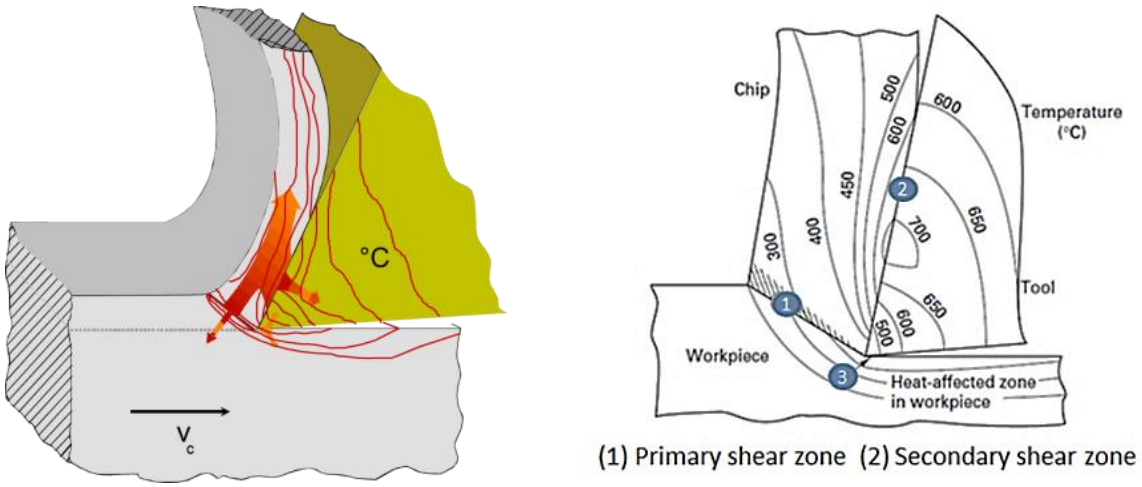

Figure 2.7 Temperature distribution in cutting point (adapted from [1])

There are several types of cutting fluids: petroleum oils, semi-synthetic, full synthetic, each with different characteristics. The machine operator should choose the proper type with right amount, directed in the right direction. The cutting fluids can be directed by hand in manual machine and by flooding or a high pressure jet over the cutting zone adjusted by programmed nozzle in a CNC machine. One important concern is disposal the old fluids which is costly and can cause pollution. Cutting fluids become contaminated with various substances such as chips, tramp oil, mould, fungi, and bacteria when they are used over time. This leads to odours and health hazards. Management of using the proper filtering system and frequently changing the fluid is a major concern to prolong the lifetime of the cutting fluids.

2.3.5 Process Parameters in Machining Processes

In machining processes the three important cutting parameters, used as dependent variables, are cutting speed, feed, and depth of cut.

Cutting speed (V_c) (also called surface speed) is the relative speed at which the tool passes through and removes the workpiece material or the distance of the workpiece which is cut in one minute. It is expressed in meters per minute (m/min).

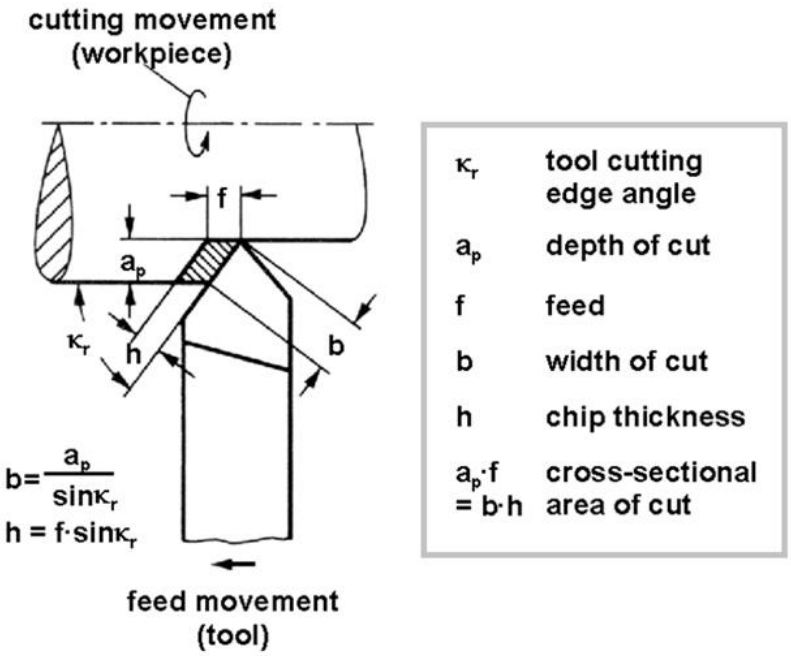

Figure 2.8 Process parameter in turning process (adapted from [3])

Feed (*f*) is the distance of cutting tool moves in the feed direction (perpendicular to cutting speed vector) through the workpiece material per a spindle revolution (mm/rev, in turning). Feed rate (V_f), distance of cutting tool moves through the material per minute (mm/min), is normally used when the workpiece does not rotate (e.g. in milling).

Depth of cut (a_p) is the distance at which the tool digs into the workpiece and expressed in millimetre (mm).

These three parameters have a direct influence on cutting forces, cutting power, temperature, types of chip, surface finish, tool life and cutting time. For example, an increase of feed and/or depth of cut increase the chip thickness, which then needs more cutting force/power. Using higher cutting speed reduces cutting time as increase the volume of workpiece removed in a period of time (Material Removal Rate, MRR) and this leads to having a shorter useful lifetime of the tools.

2.3.6 Cutting Force and Power Consumption

To simplify the cutting force, oblique cutting (three-force system) is selected to easily understand the forces in turning process. In Figure 2.9, *feed force* (F_r) acts in the direction of tool feed parallel to the axis of rotating workpiece in turning, also called axial force. *Passive force* (F_p) or radial force would gradually push the tool off the workpiece. It acts in a direction normal to the cutting speed. *Cutting force* (F_c) or sometime called tangential force which is major cutting force. F_c acts in the direction of the cutting speed (V_c). These three forces produce the *resultant force or machining force* (F). In general, the relationship between cutting forces and cutting parameters is shown in Figure 2.9.

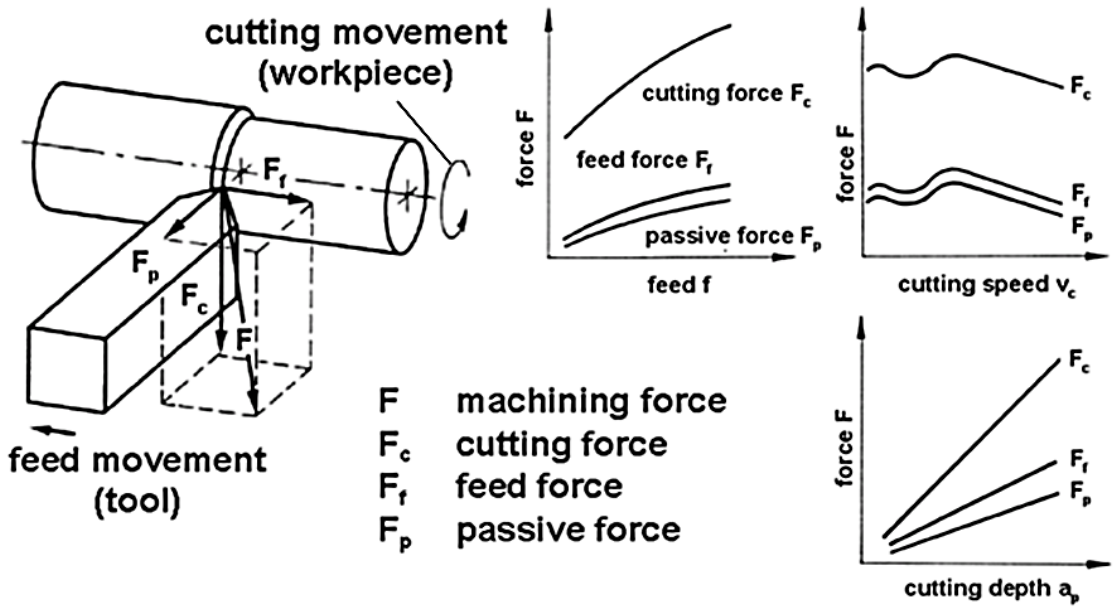

Figure 2.9 Forces acting on a cutting tool in turning (reproduced from [3])

Cutting power at the cutting point can be calculated by the product of cutting force and velocity ($P = F_c \cdot V$). This power is dissipated in both primary shear zone (shearing the workpiece) and secondary shear zone (tool-chip friction). In metal cutting machine, cutting force and power is necessary information to design the machine. Adequate power should be available to drive the spindle and feed movement to remove the material from the workpiece.

In tool wear monitoring, cutting forces are typically monitored by a dynamometer or load cells mounted on the cutting tool holder (in turning) and on workpiece table (in milling and drilling), while power consumption of main spindle motor is monitored by power monitoring system or wattmeter. These measurements allow the inference of tool wear as the force and power required to maintain cutting increase as the tool wears. Besides, current sensor is also applied to measure the power consumption of cutting process. Sensing techniques of cutting forces will be mentioned in Chapter 3.

2.3.7 Machinability

The machinability of a material is a method of characterising the difficulties a given material poses to cutting operations. It depends on a material's composition, mechanical properties, and microstructure. In general, four criteria are used to describe good machining properties: longer tool life, good surface quality, low machining force and power consumption, and having good chip control. In practice, machinability is normally represented by tool life and surface roughness of machined parts.

2.4 Tool Wear in Machining Processes

As tool wear is inevitable, it is important to maximum usage through the use of tool wear compensation and wear rate control techniques. As tool wear can cause an out of tolerance workpiece dimension, the tool position must be automatically compensated. To obtain longer tool life, cutting parameters (e.g. feed, speed, depth-of-cut) have to be controlled by adjusting feeds and speeds to suppress chatter, or increase the depth-of-cut to compensate. The following sections focus on the tool wear in the turning machining process.

2.4.1 Wear Mechanism in Turning Processes

In turning process, three major wear mechanisms are *abrasion* between the cutting tool and workpiece which is the main cause of wear, *adhesion* of chips to cutting tool, which can remove the cutting tool material, and *diffusion* of cutting tool atoms to the chips or workpiece. These mechanisms typically occur together and manifest themselves in the following characteristic ways:

Crater wear: this wear stems from abrasive wear mechanism between chip flowing out from the cutting zone and rake face. Crater wear occurs on the tool face that directly contacts the chips. Consequently, the contact area on the rake face wears out as shown in Figure 2.10. Crater wear can increase the rake angle, resulting in lower cutting force, but it will be consequently weaken cutting edge strength as wedge angle is reduced.

Flank wear: flank wear originates from the abrasive mechanism of the main cutting edge against the machined surface on flank face (Figure 2.10). This wear has a direct effect on the accuracy of the workpiece dimension and the quality of the surface finish. Therefore, the monitoring of this type of wear is required to prepare for tool changing, avoid production scrap and also adapt the cutting parameters to control tool life.

Notch wear: this is the combination of flank wear and crater wear. It normally occurs at the main cutting edge where contacts to the workpiece surface or both the rake and flank faces at the depth of cut line (Figure 2.10). This wear predominately affects the surface finish of the workpiece.

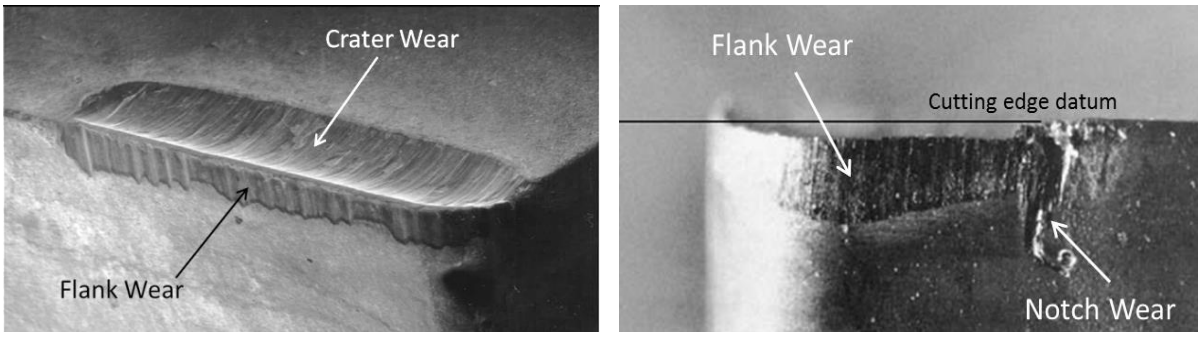

Figure 2.10 Wears on major cutting edge (adapted from [5])

Thermal cracking: this failure can be developed by temperature variation during machining when the temperature at the cutting edge changes rapidly from hot to cold or through inconsistent use of cooling liquids. The thermal cracks may appear perpendicular to the cutting edge (Figure 2.11). Thermal effects can also be a result of thermal fatigue of the cutting tool. The tool materials on the cutting edge will be pulled-out or broken when the crack propagates to a critical size.

Chipping (breakage): chipping at the cutting edges generally originates from discrete or intermittent cutting operations and it also can occur when the cutting edge first engages or disengages the workpiece. The breakage is the result of using too high feed and depth of cut, built-up edge, vibration or excessive wear on the cutting insert.

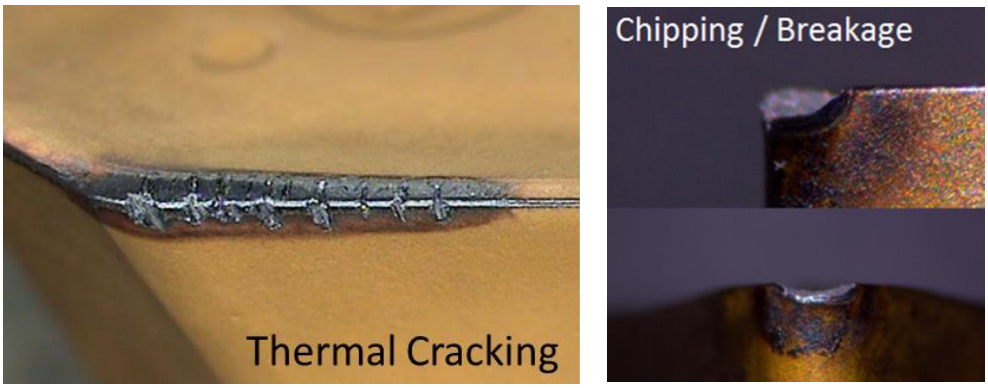

Figure 2.11 Thermal cracking and chipped cutting edge

Plastic deformation: This can found in the cutting edge when the tool material is softened by excessive temperature in cutting zone due to lack of coolant supply. This changes the geometry of the tool and thus its performance.

2.4.2 Determination of Wear in Cutting Tool (Wear Parameters)

The general practice of the standard for tool wear is defined in ISO 3685-1977, which considers reference workpiece/tool materials, tool geometries, cutting fluids, cutting conditions, tool life criteria, and tool wear measurement. The most common wear mechanisms monitored in cutting tool wear are crater wear and flank wear. The diagram of wear parameters is shown in Figure 2.12.

Crater wear: occurs at tool-chip interface area on the rake surface. Due to ISO-3685, crater depth (KT) and the location (KM) are normally used as a wear parameter in tool wear research or crater ratio K = KT / KM is sometimes used.

Flank wear (V_b)*:* is the width of wear land of the flank face which gradually forms. The wear land (Figure 2.12) is divided into three regions: C, B, and N. Zone C is the curved part of cutting edge corner, while the width of zone N is a quarter of a worn cutting edge length *b* farthest side of the corner. Notch wear, represented by (V_{Bn}) usually occurs in zone N. The remaining length of cutting edge between zone C and N is used to represent flank wear.

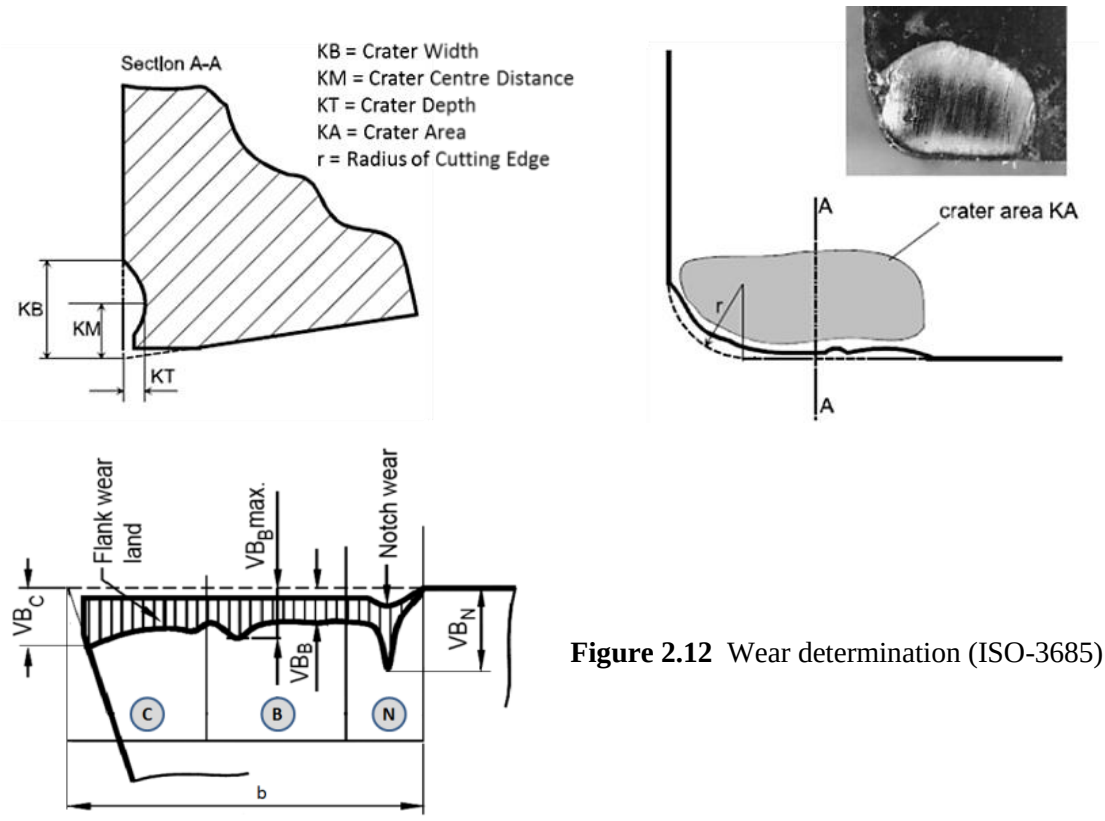

Figure 2.12 Wear determination (ISO-3685)

The flank wear limit in zone B is recommended at the average flank wear land VB_B=0.3 mm, in case of regular worn, and the maximum flank wear width VB_{max} = 0.6 mm, if the flank wear land is not considered to be regularly worn. Furthermore, other standards such as ISO 3685, ISO 8688, ISO 883, ISO 3364, ISO 6987 and ISO 9361, also provide guidance on tool wear evaluation and suggest the wear limits as reference values for replacing the new tool [6].

The quantities mentioned above are measured at different cutting times from the beginning until the cutting tool worn or catastrophic failure by optical microscope or other optical methods directly. Direct methods are generally more reliable but they are inconvenient for in-process use. Therefore, indirect measuring methods are normally used to correlate the tool wear. The details will be mentioned in Chapter 4.

2.4.3 Tool Wear Curve

Although recent developments in cutting tool materials and optimisation of machining process parameters have allowed longer tool life, the tools still wear out when used over extended periods of time. The typical relationship of tool wear versus cutting time is illustrated in Figure 2.13.

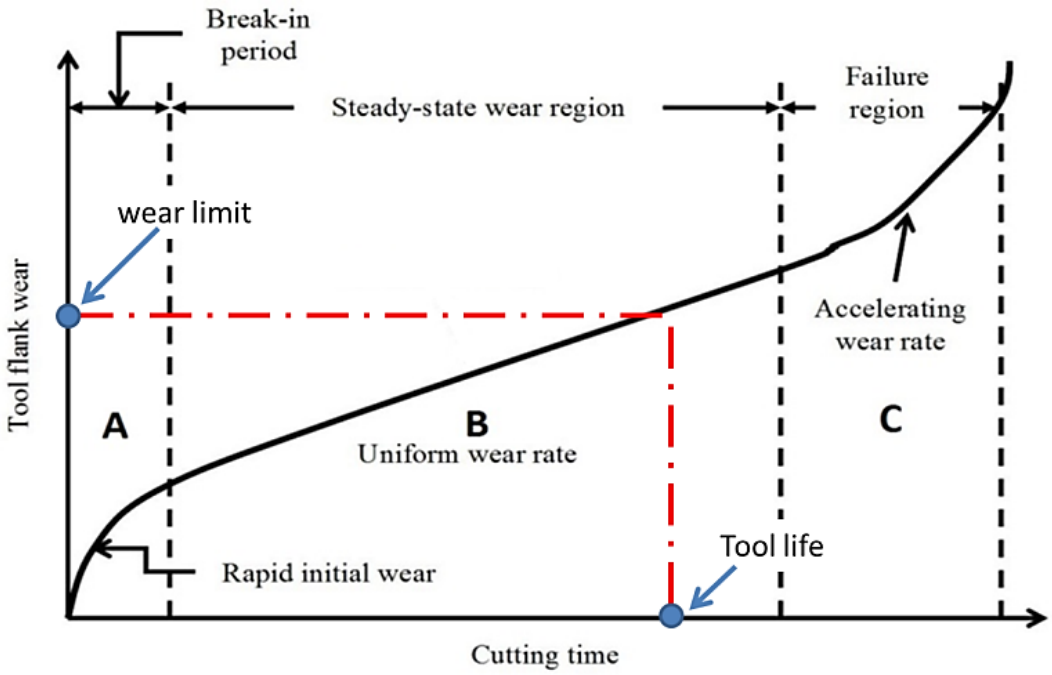

Figure 2.13 Tool wear curve and tool life (adapted from [5])

Three states of tool wear can be obviously separated. Zone **A** is break-in period as the initial flank wear is rapidly established. It will take a couple minutes from start cutting with the new tool. Zone **B** is then where wear develops steadily rate and zone **C** is where the wear occurs at a significant increasing rate (failure region). Machining beyond this region will cause tool failure or tool breakage. The *tool life* or *tool lifespan* could be defined as the time from the beginning of its use to it becoming worn out or blunt. According to ISO-3685, the cutting tools should be replaced when the flank wear on the main cutting edge exceeds 0.3 mm (wear limit) during normal use.

The slope in steady-wear region is also known as *wear rate* which is affected by workpiece material and cutting conditions. Hard workpiece material can encourage tool wear quickly, consequently, wear rate in steady region increases significantly. Increasing cutting speed, feed, and depth of cut has a similar consequence. Several wear curves with different cutting speeds is compared in Figure 2.14. It is generally observed that wear rate increases as cutting speed is increased. Higher cutting speed can reach the limit point in less time.

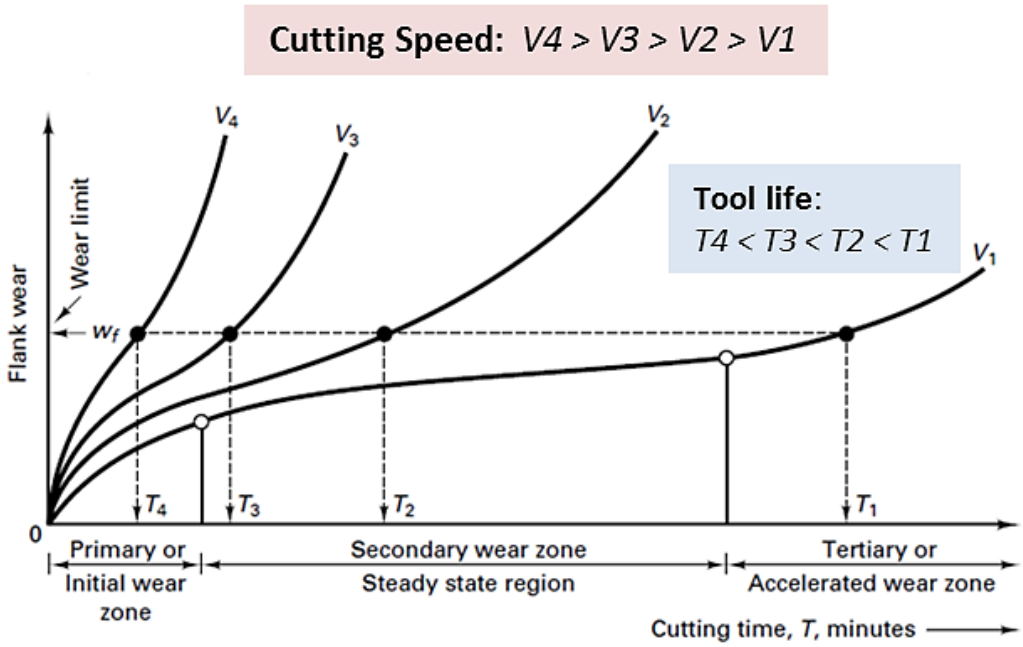

Figure 2.14 Flank wear curve of different cutting speeds (adapted from [1])

2.4.4 Tool Life Equation

Tool life (T), is one of the significant parameters used in characterising the machinability of workpiece materials. Tool life is the time in minute in which a cutting tool performs cutting operation from the first cut to the point which it becomes unserviceable or failed (0.3 mm due to ISO 3685). Long–run machining tests conducted on machine tools are generally performed to determine tool life values under various cutting conditions. There are several criteria used in considering tool life, such as measurable tool wear (flank wear, crater wear), all measurable workpiece data (change of roughness) and all measurable parameters of the cutting process (change of cutting power, chip temperature and form).

If the tool life values for the four wear curves in Figure 2.14 are plotted on a log-log scale of cutting speed and tool life, as a result, the outcome relationship is a straight line as shown in Figure 2.15. This linear relationship of tool wear is used to develop the tool life equation.

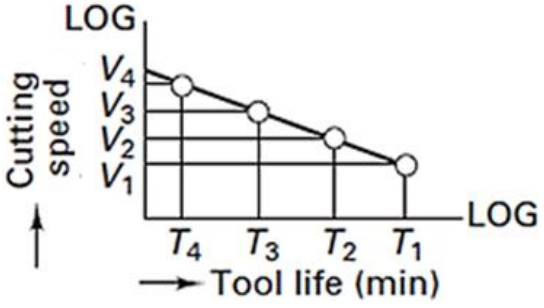

Figure 2.15 Relationship of cutting speed and tool life (log-log plot) (adapted from [1])

The tool life can be estimated by using tool wear equation [1, 5], developed by F.W. Taylor, and known as Taylor's tool wear equation as shown in Equation 2.1. This basic equation is capable of estimating over wide range of cutting conditions.

$$VT^n = C \tag{2.1}$$

T is the tool lifetime, V is cutting speed, C and n are determined constants which related to feed and depth-of-cut and need more tests to determine these extra coefficients. C depends on cutting tool, workpiece materials and cutting condition, while n relies on a given tool material.

C and n can be obtained from the log-log graph in Figure 2.15. The intercept on the speed axis represents C value, while n is the slope of the straight line. In practice, C and n can be looked up on the standard table (examples are found in [1, 5]).

From previous mention, cutting speed and feed are important variables associated with tool life. Therefore, from basic Equation 2.1, expanded version of the tool life equation, including feed, and cutting depth is determined by Equation 2.2.

$$VT^n d^x f^y = C \tag{2.2}$$

Where d is the depth of cut and f is the feed in mm/rev. The exponents x and y can be obtained from the experiment for each cutting condition.

In conclusion, it is generally viewed that increasing the cutting speed and feed reduces the process time and cutting costs. However, this also increases the rate of tool wear or reduces tool life which need more frequent times to replace the new tool. This leads to a loss in productivity. To obtain the minimum production costs, the operating conditions in machining need to be optimised in order to balance these influences.

Chapter 3

General Background Knowledge II

Tool Condition Monitoring

Tool Wear Sensing Signals

Sensor Fusion

This chapter is organised as follows: general methodology of an intelligent monitoring development is first mentioned. Then, currently-used sensors in the recent monitoring systems are summarised, with their outstanding characteristics, advantages and drawbacks. Next, the most effective signal processing techniques are concluded and frequent sensory features applied in the machining modelling process are discussed. Later, the sensory feature extraction methods for the relevant information are described. After that, commonly-used AI techniques are introduced. Last, the Design of Experiment (DOE) for modelling the machining operation and system verification are summarised.

3.1 Condition Monitoring

3.1.1 The Concept of Condition Monitoring

The condition monitoring system is an important aspect of several applications which seeks to prevent unplanned stops or failures that might lead to economic losses and safety issues. The consequences of failure may be inconvenience, the expense of repair, or a possible accident due to total failure. For example, shaft and turbine blades are used to convert hydropower to electricity in water power plants and a defective shaft may cause the system to break down leading to expensive ramifications in terms of both the cost and time required to effect repairs. Furthermore, shaft failure will not only have direct effects, but may also cause other parts to fail. In some applications, it is very important to be able to identify faults in systems, such as crack monitoring in aircraft structures. Since such cracks can cause catastrophic failures, they must be detected as early as possible.

Condition monitoring is based on the recording of measurements to predict the condition of the equipment. In general, condition monitoring system procedures can be separated into five stages as shown in Figure 3.1. Data or information is acquired from the systems by sensors or measuring devices. The acquired data is then analysed to extract the information sets as extracted features. Then, a selection process is used to find the best set of features from all candidate features which are good indicators of faults in the structure. Finally, the selected features are interpreted in a decision-making step to identify any faults in the system [7].

The objective of a condition monitoring system is to evaluate the condition of a structure or machine from measured data. Fault estimation can be achieved through the five stages shown in Figure 3.2.

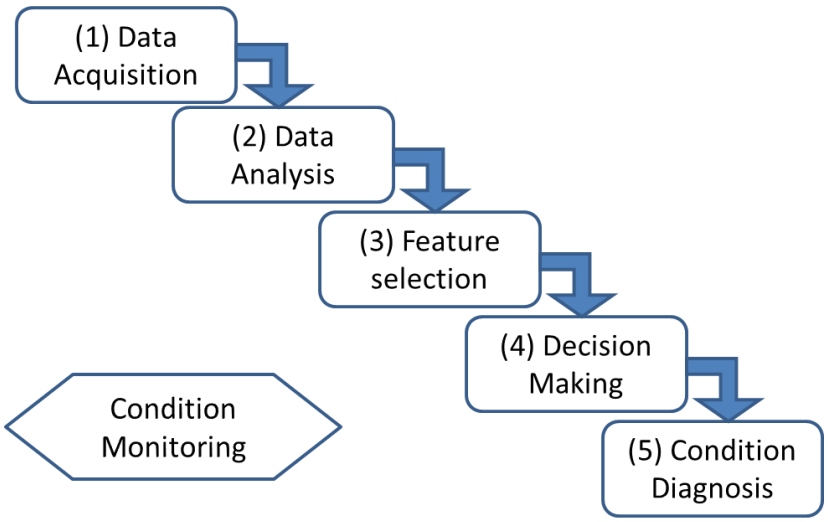

Figure 3.1 General procedure of condition monitoring (adapted from [7])

Figure 3.2 The stages of condition monitoring (adapted from [7])

The first stage of monitoring is the detection of the presence or absence of faults. Any abnormalities can be detected by the monitoring system, which normally provides binary results, such as good or not good, normal or abnormal. For example, in tool wear monitoring, a worn tool can be detected by an abrupt change in the root-mean-square (RMS) value of acoustic emission (AE) signals. The system can then detect a worn tool when the RMS values exceed a threshold value.

After detecting something unusual, the monitoring system can classify the faults, thus providing more detail about the nature of the problem. For instance, spectrum in the frequency domain from sensors can be used to classify the types or characteristics of the unusual or the states of anomaly occurred.

The next stage in the monitoring process is to determine the location of the faults. For example, in recent car monitoring systems, various sensors have been attached to monitor different locations in the engine. If an abnormality occurs somewhere, the sensor can initiate an alert, locating where the fault is.

Next, faults need to be evaluated to know their magnitude (severity). For example, the signal amplitude from an accelerometer attached to the machine structure can display the vibration levels of the machine structure.

In the last stage, an estimation of the remaining life of the component is necessary in order to know when the parts should be replaced because unplanned part change or part breakdown should be avoided.

3.1.2 Condition Monitoring in the Machining Process

Condition monitoring in machining processes can be applied in many ways, such as monitoring of cutting tools, quality of machined parts and machine-working conditions. Sensor-based monitoring systems are currently used to monitor machining processes, predominately by measuring power consumption of a running machine. The main concept of a condition monitoring system in the machining process is illustrated in Figure 3.3.

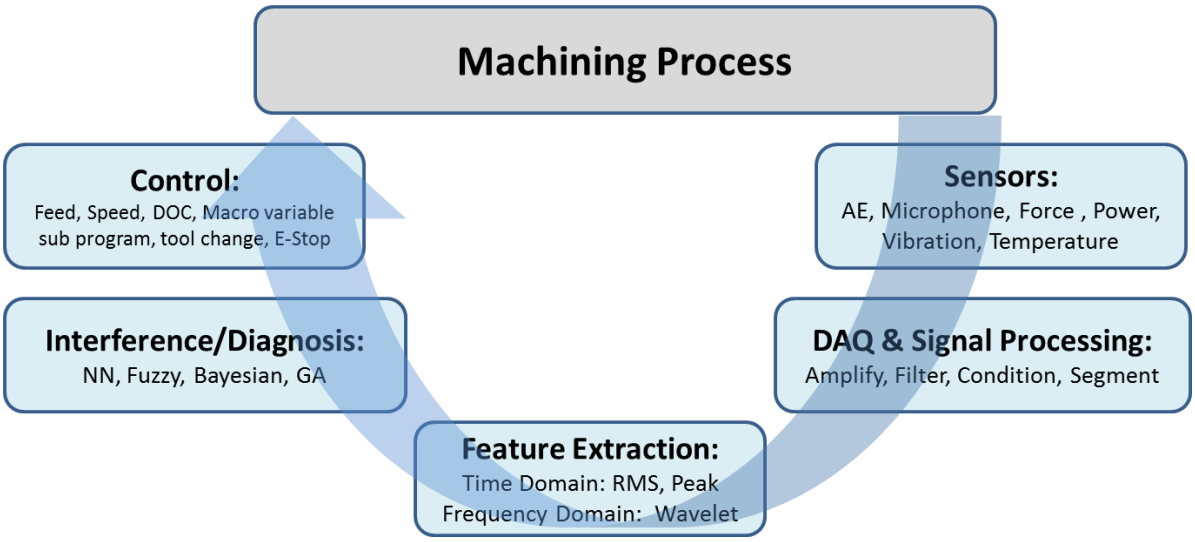

Figure 3.3 Condition monitoring in the machining process

Sensors such as for acoustic emission, force, vibration and temperature are also widely used to collect sensor signals from the machining process and transmit it to a computer via a Data Acquisition system (DAQ). These sensors transform a physical property into electrical signals. After that, some signal conditioning processes such as amplification and filtering may be required to improve the signal quality so as to be suitable for subsequent processes. Several sensory features of such signals are extracted both in time and frequency domains. To obtain robust and reliable models for monitoring, it is vital to use the features that describe the machining process in the most meaningful way. Then, the most sensitive features are selected by algorithms for use in the interference or pattern recognition processes. Several artificial intelligence techniques, such as neural networks and fuzzy logic, may be used to train the models with selected features and targets in order to obtain a prediction model through a supervised training scheme. In a tool wear monitoring system, artificial models can be used for tool wear state classification and tool wear value estimation. Finally, the machine control systems use the wear state or wear value automatically to adapt the cutting parameters such as feed and speed so as to maximise the tool life, or change the cutting tool before its failure.

3.1.3 Tool Condition Monitoring

Using worn cutting tools has a direct effect on the surface finish of a workpiece, part accuracy, and machine condition. Furthermore, using worn or broken tools significantly decreases productivity through un-planned stops for tool changes, produce scrap parts, and may injure the operators. Also, a tool breakage detection system is necessary for fully automated machining and must detect failure instantly so as to prevent workpiece damage. Furthermore, such a system needs to be reliable in order to avoid downtime due to false alarms. The competitiveness of the machining processes can be increased by increasing the utilised tool life and decreasing instances of part damage from excessive tool wear or tool breakage. Tool Condition Monitoring (TCM) is, therefore, a key component in many condition monitoring systems in machining processes, as has been reviewed in [8-10].

There are two different methods for monitoring the machining process. *Direct methods* are based on direct measurement, and are concerned with measuring the actual tool wear by using optical sensors, radioactivity and lasers. These techniques are used to measure flank wear in terms of material loss from the tool or by observing the worn surface using optical methods. These methods have the advantage of high accuracy and reliability, but cannot be used for online measurement since they are difficult to apply in the real machining process environment. They are also still very expensive. For example, *InfiniteFocus Real3D* (Alicona) measures tool geometries and cutting edges of every perspective. That costs many hundred thousands of pounds. Measurement of steep-sided flanks by *Infinite Focus SL 3D Surface* (Alicona) may cost more than £65,000.

In contrast, *indirect methods* are based on sensor technology, and although these provide less accuracy, they are more suitable for practical applications, and are more economical. Presently, sensor technology is being continuously developed to be more accurate, precise, and easy to calibrate or compensate the sensing signals. As a result, indirect methods are robust, cheap, easy to use, and can be used for online monitoring [9, 10].

TCM manipulates the sensor measurements in order to determine the tool states and to detect process anomalies. This could be gradual tool wear, tool breakage, or excessive chatter or vibration. Generally, four sensors are used in tool condition monitoring: dynamometers, accelerometers, AE sensors and electric current sensors [10]. The reliability, cost, and characteristics of each sensor should be considered in order to ensure the best fit for a given monitoring purpose, as is explored further in the following section.

3.2 Tool Wear Sensing Signals

TCM has been extensively developed over a period of time. Concurrently, it has parallel developments in electronic instruments, transducers, computer and software. This increases the development of TCM by using sensing features extracted from multiple sensors. As mentioned previously, TCM can be performed by direct and indirect measurement. Several sensors commonly used for indirect method (Figure 3.4) are mentioned in this section.

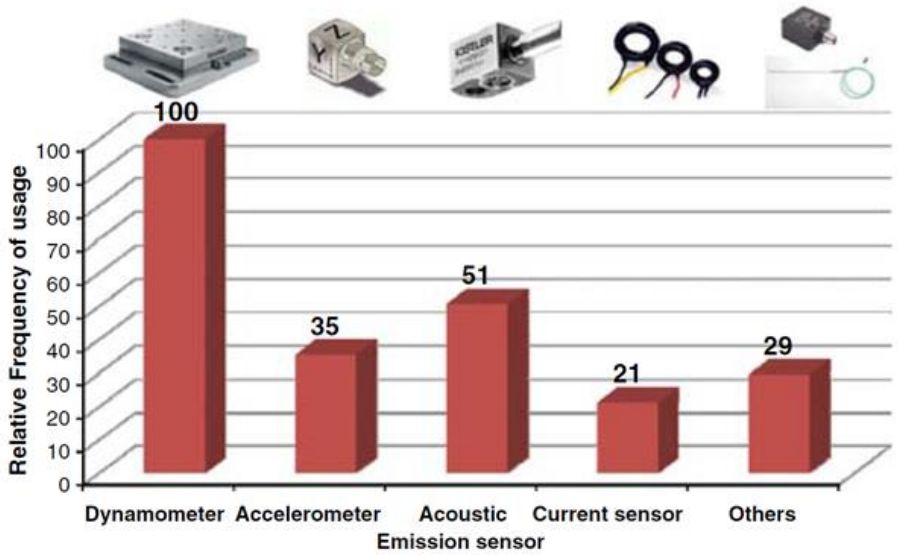

Figure 3.4 The percentage of sensors used in condition monitoring (reproduced from [10])

3.2.1 Dynamometer

In machining, cutting forces measured by a dynamometer are one of the best sensing methods in the machining process. It is commonly used for tool wear monitoring because friction forces increase if the cutting tool edge is dull or loses cutting ability. The cutting forces generally increase with flank wear because of an increasing in the contact area between wear land on cutting tool and workpiece. However, an increase of cutting force can be caused by other reasons such as types of wear, cutting condition, cutting tool and workpiece materials. Cutting forces can be related to surface roughness due to chip formation and built-up edge (BUE) which might be dependent on cutting force, and in the case of BUE may be desirable. Furthermore, excessive cutting forces can reduce the part accuracy as they cause the deflection of the actual tool path away from the intended path. Chatter frequency is often higher than cutting-force frequency, therefore, dynamometers can also be utilised for chatter detection if their bandwidth covers the chatter frequencies. However, the cost of multi-axis dynamometers are relatively expensive (~£10,000 up to £100,000) and impractical to apply in the industry because they need overload protection and are limited by their frequency response [11].

3.2.2 Accelerometer

The vibration signal measured by an accelerometer is mainly utilised for prediction of surface roughness since vibration generates an undesired displacement of the cutting tool. It has been used to monitor cutting tool wear because vibration amplitude has significant change during machining due to the progressive flank wear. The most commonly used method to analyse the vibration signal is using the Fast Fourier Transform (FFT) because unusual changes in vibration frequencies possible due to the tool wear. When a new tool is started to use, line contact between tool and workpiece offers a small resistance to oscillate the tool and workpiece and causes less vibration. In contrast to worn tool, the frictional damping is increased because of larger contact area between tool and workpiece leading to an increase of tool vibration. The vibration analysis has been applied to tool breakage detection by setting a threshold value [11]. Compared to other methods, such as AE sensor and dynamometers, this vibration system is easy to set up, low-cost, and more reliable. However, it is limited to non-vibrated machine parts and the location of vibration sensor has a direct effect on the signal amplitude.

3.2.3 Acoustic Emission

In this context, AE results from the strain energy released from chip formation, fracture, friction, tool breakage, thermal reaction, etc. The AE signals in cutting process consist of continuous and transient signals depending on the sources of signals. Continuous signals are generated by shearing in the primary shear zone and wear on the tool flank face, while transient or burst AE signals result from tool fracture or chip breakage [12]. AE is considered as the one of the most effective methods for sensing tool wear because the frequency bandwidth of AE (10 kHz-10 MHz) is higher than machine vibration and environmental noises (<1 Hz-10 kHz) [10]. AE signals have been applied to diagnose the wear of cutting tool and detect the tool breakage. For example, the amplitude of the continuous-type AE signal can be used for tool wear monitoring. Additionally, other AE parameters such as peak count, RMS voltage, and rise time can be used to evaluate tool wear. AE sensors are inexpensive and easy to install, but they have to be carefully calibrated. However, sensor location affects AE signal quality and parameters of AE signals have to be adjusted according to machining condition being used at any one time.

3.2.4 Microphone

Machining sound sometimes can be heard by humans in some circumstances. An experienced machine tool operator can easily detect a dull tool by simply listening to the sound generated during the machining process. The vibrations being excited in the cutting zone during machining often is in the range at which they can be heard by the operator, and therefore be recorded by a standard audio microphone. Several studies have used microphones to monitor the machining processes because microphones,

being a non-contact sensor, are very easy and flexible to install in the machine and there are a wide variety of inexpensive models with different performance characteristics [13]. Microphones have also been used extensively for chatter detection, and have been used on occasion to monitor tool wear in machining processes by analysing the audio signature of the cutting process to extract features which are sensitive to tool wear.

3.2.5 Current and Power Consumption

Motor current is also used to monitor the tool condition. Motor current used to generate torque in DC motors is proportional to the cutting forces, in turn. Therefore, to measure the motor current can be used for sensing the machining force indirectly. However, the current sensor behaves nonlinear characteristic which requires proper compensation and calibration [14]. This sensor can also be used in the low-frequency components of cutting force. It is suitable only for detecting slow spindle speed, such as in drilling and milling processes.

Alternatively, power consumption of the spindle motor which indirectly represent current consumption is measured by power sensors or power monitoring systems. The use of power sensors has the same limitations as in current sensors and also is dependent on the relative magnitudes of the power consumption of the machine and of the process. Threshold values are normally used to set the maximum current/power consumption values. Consequently, the thresholds will vary as the cutting condition changes. Although power sensors are not as accurate as other, more precise sensors, they are economical and easy to install and normally used for detecting tool breakage and diagnosing tool wear.

3.2.6 Other Sensing Signals

Temperature sensors, optical sensors, and ultrasonic sensors are also variously used to monitor machining process.

Temperature sensors such as thermocouples, thermal resistant elements usually measure the temperature in cutting tools. They can be a good indicator of the cutting process because the cutting temperature varies as the tool wears due to its ability to cut and changes in tool geometry [14]. Cutting temperature also has an effect on surface roughness and the acceleration of tool wear, which increases diffusion and weakens the tool. To reduce extremely high variation of cutting tool temperature, coolants are normally applied to extend cutting tool life as mentioned in Chapter 2. However, the accuracy of cutting temperature measured by the sensors can be variable, therefore, average temperature around the cutting tool is usually monitored for tool condition monitoring.

Optical sensors are based on a beam of light that is reflected from the machined surface and whose intensity can be correlated with the surface quality [15]. In a

machine vision system, the light source illuminates the machined surface and acquires an image by a digital camera. It is also used to evaluate the surface roughness in machining processes. The optical technique is normally faster than traditional profilometer method in surface roughness measurement. However, this technique has some limitations in the monitoring in-process implementation because the system can be affected by machining environment such as the presence of cutting fluids and chip removal. Also, the optical sensors must use in the harsh machining environment and they are sensitive to different light sources with various light configurations. They also are sensitive to steep angles between surfaces (i.e. near perpendicular adjacent surfaces) in geometry.

3.2.7 Comments on Tool Wear Sensing Techniques

A major challenge in TCM is the lack of robustness of sensors. For example, sensors can be mounted at a specific location, and when they change to another location far away from previous place, they do not provide sensing information. Another difficulty is using one sensor to cover a wide range of cutting conditions. As different sensor signals have different correlation efficiency and their effective, only a robust sensor may not be able to make a reliable result for all the cutting conditions. Thus, the use of multiple sensing signals permits the combining of sensory features from different sensors (sensor fusion) so that the resulting prediction is more compete, more accurate and reliable than the sensing signals are used separately.

Due to very high cost and mounting problem, the robust sensor such as dynamometer is inappropriate to use in the shop floor. Therefore, this study attempts to develop a low-cost tool wear monitoring system which is acceptable to the industry. The use of less robust sensors (i.e. cheaper ones) in a fusion sensing setup both allows for redundancy of sensors and potentially using sensors as a consumable (i.e. it does not matter if they get damaged).

3.3 Signal Processing

Due to the fact that the interference of mechanical, electrical, and environmental noises makes the signal inappreciable to process, this needs a proper signal processing to improve the signal quality before extracting sensory features. In general, the signal processing scheme for TCM can be divided into five steps as shown in Figure 3.5 [10].

Step 1: *Analogue filtering and signal sampling* are important parts of the scheme, particularly to obtain the proper signals within the frequency response of sensors (without aliasing) so as to prevent signal distortion during signal acquisition. The Nyquist-Shannon sampling theorem states that the sampling rate (*fs*) should be more than the frequency response of the selected sensor by at least twice ($fs > 2S_b$ where S_b is signal bandwidth). To prevent or reduce aliasing, the rate of sampling can be

increased and anti-aliasing filter is used to restrict the bandwidth of the signal. However, the use of a very high sampling rate leads to some limitation as it may cause memory problems during acquiring the sensor data and needs more space of data storage.

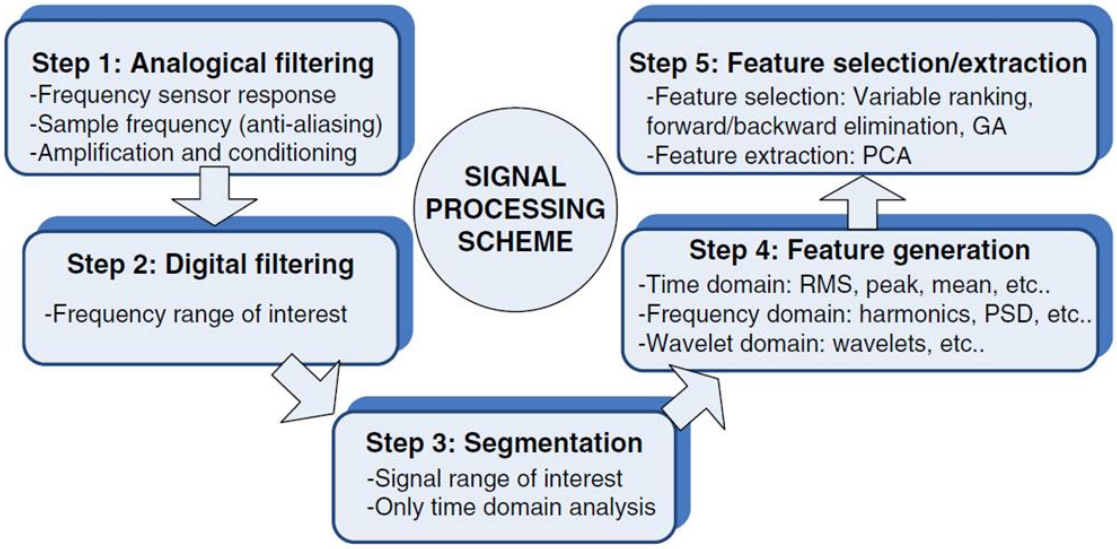

Figure 3.5 General signal processing scheme (reproduced from [10])

Step 2: *Digital filtering* is used to maintain the sensor information correlation to the process variables. In general, the acquired signal is filtered in order to prevent unwanted signal frequencies such as high frequency from interfering noises and low frequency from the oscillation of transient mechanical events. Several filter types (e.g. high-pass, low-pass, band-pass, and band-stop) can be applied to remove unwanted frequency of the main signals. The level of acquired signals is extremely low in some applications such as AE signal. Also, very long connecting cable might cause signal attenuation. Thus, signal amplifications are practically used to gain more signal level before the subsequent processing steps.

Step 3: *Signal segmentation*, an optional step, may be performed to select only the specific part of the whole signal to extract the information. In the context of machining, the raw sensor signals are typically collected from the entire cutting cycle, including time before and after cutting. The raw signal will be selected only in the region containing the information of the tool wear condition and surface roughness generation, for example, the part of the signal when the cutting tool is removing metal steadily (stable cutting).

Step 4: *Feature extraction* comprises a generator module transforming the digital signal into various sensory information known as features. There are several methods applied for feature extraction in the time, frequency and wavelet domains. For example, average and RMS values are normally used as a descriptor of the most signals such as cutting forces, vibrations, and AE signals. Other statistical values such

as standard deviation, skew, peak, and kurtosis are also used as the process features in the time and frequency domain analysis. These features will be variously discussed in Sections 3.4.1.

Step 5: *Feature selection* is required to select the most effective features from the total features extracted in the Step 4, leading to accurate prediction model and most reliable monitoring system. It could be not to use all features for monitoring system since it has some limitation of process characteristics and monitoring system. This leads to elimination of insignificant features in certain particular conditions and usage of the suitable features in the monitoring system. Section 3.4 briefly describes the feature extraction and selection.

3.4 Feature Extraction / Selection

3.4.1 Feature Extraction

Several sensory features are extracted by the signal processing techniques (Section 3.3) in order to be used as inputs of the prediction models. Those features can then be roughly divided into four categories: features in time domain, features in frequency domain, features in time-frequency domain, and features in statistical domain [16].

Time domain features are firstly used as raw data acquired by DAQ systems are measured in the time domain. The most commonly used features in the time domain are average values (the magnitude) or effective values (RMS) in specific time intervals, the change in signal level (increments, or decrements, also differential values), and ratio value (e.g. crest factors, the ratio of the peak value to the RMS value).

In frequency domain, the *spectral features* are often computed by means of a Fourier transform. Some regions in the spectrum are sensitive to tool wear in which the shift of relevant spectral bands can represent the tool wear evolution. The frequency of the highest peak in the spectrum (peak frequency), power spectrum density (PSD) is example, features extracted from the frequency domain of the signals.

Frequency domain data transformed by FFT only illustrates the frequency components of stationary signals. However, some types of fault have a non-stationary characteristic. Therefore, *time-frequency domains* such as Short-Time Fourier Transform (STFT) and Wavelet Transform (WT) have been used when the time localisation of the spectral components is needed. STFT is used to calculate the FFT within a small time window. The time window is shifted to a new time position and then Fourier transform is recalculated. As a result, a time-frequency spectrum is obtained. The limitation of using STSF is the frequency resolution depending on the length of the window, while WT is based on small wavelet with limited duration and it was developed to overcome the resolution problems of STFT.

Sensor signals in time and frequency domains are also computed as *statistical features* as they are assumed to have a probabilistic distribution and to be stationary during the short time interval. It is often found that the changes of tool wear can be indicated by the changes of statistic features [7]. Mean, variance, standard deviation, skewness, kurtosis are normally used to describe the probability distribution of the random process (stochastic). These features used in the current study will be detailed in Chapter 4.

3.4.2 Feature Selection

Feature selection is used to select the most significant of all the features in order to reduce the dimensionality of the feature space, and therefore increase algorithm speed. It also removes the redundant, irrelevant or noisy data, resulting in the improved data quality which, in turn, increasing the accuracy of prediction results or minimising the prediction error [16].

Feature selection can be performed by using a ranking technique and a subset selection technique [10]. In feature ranking, a matrix is used to rank the features and eliminate the features that do not meet the qualified score. This method is very practical and easily scaled or weighted. In contrast, in subset selection method, feature extraction is used to search the set of possible features for optimum subset. The common subset selection techniques are forward selection, backward elimination and genetic algorithms. The forward method starts with no variables and adds them one by one. The backward one starts with all variables and removes them one by one. The criteria of these methods are error changes in each step. Search algorithms such as Genetic Algorithms (GA) have been used as a searching procedure to obtain the best feature subset before pattern recognition process.

3.5 Sensor Fusion

Sensor fusion is defined as the use of more than one sensor signal in a complementary manner to provide more robust prediction and evaluation. It is more useful to use several sensor signals instead of only single sensor signal in order to increase the reliability of the sensor under varying machining conditions [17]. The implementing fusion strategies are broadly comprised of two approaches (Figure 3.6). In centralised fusion approach, the information of each sensor was extracted at a central feature extraction, while pattern-level fusion approach the feature extraction is performed for each sensor independently.

Sensor fusion systems need algorithms to combine and fuse the sensor information at the pattern recognition stage. The algorithms commonly used to fuse the information can be classified into two major approaches: statistical and artificial intelligence (AI) approaches.

The statistical model is obtained from multi-variable regression of machining process variables, while AI uses complex non-linear model such as neural networks and Bayesian networks to find relation between sensor data and machining process variables. The final stage is decision making which may be performed under computer control or interactive action of human. In machining, existing literature (reviewed in Chapter 4) pays attention to a sensor fusion system based on AI approaches in different purposes, such as tool wear diagnosis, tool breakage detection, surface roughness evaluation, and prediction of dimensional part accuracy.

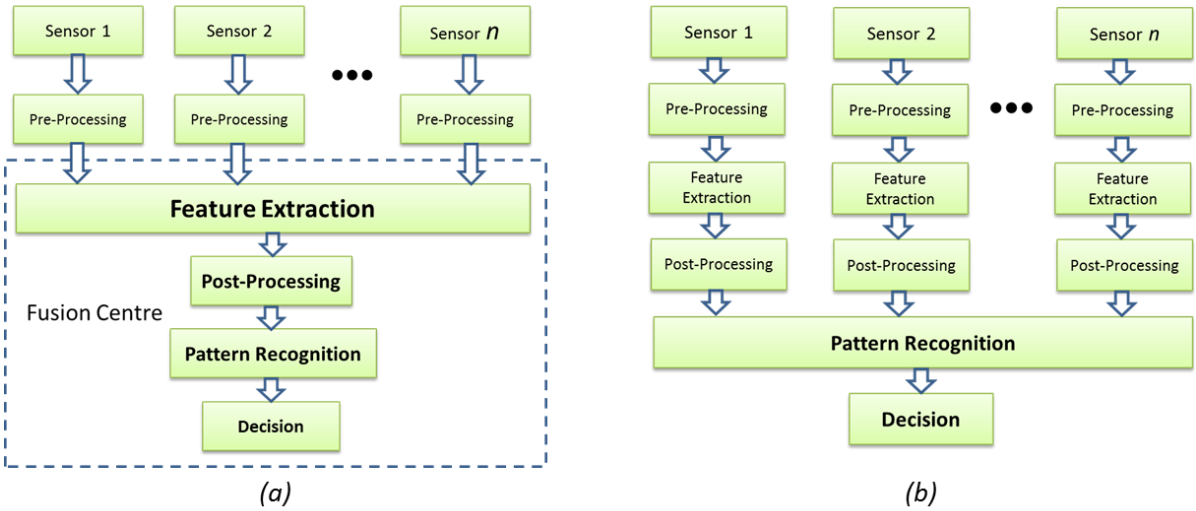

Figure 3.6 Sensor fusion strategies: *(a)* centralised fusion and *(b)* pattern-level fusion (reproduced from [17])

3.6 Artificial Intelligence in Tool condition Monitoring

In the survey of Abellan-Nebot and *et al* [10], very often, artificial neural networks (ANNs), fuzzy logic, a hybrid combination of both are used to develop tool condition monitoring systems. Generally, they are used to model the non-linear dependencies between tool conditions and extracted features of measured signals in various cutting conditions. Other AI techniques such as hidden Markov model [18-20] , Bayesian network (BN) [21-23], support vector machine (SVM)[24, 25] have been less applied.

3.6.1 Artificial Neural Networks

The artificial neural networks (ANNs) imitate a form of biological neurons and their interactions, which pass information through the network connections. This information is transformed by algorithms and mathematical models. ANNs can be broadly classified as: supervised networks, unsupervised networks, radial-basis function (RBF) networks, competitive or self-organising networks, and recurrent networks which are extensively reviewed in [16, 17, 26].

ANNs are used in several problems such as function approximation, classification, unsupervised clustering, forecasting, and control systems because they are able to generalise information, learn data collection, recognition patterns, classifying data, prediction and estimation functions, and filtering signals. To generalise information, the neural networks need to be trained in order to find the weights of each neuron. The training procedure aims to minimise the error between the prediction outputs of the target values [26]. Feed-forward neural networks (Figure 3.7) trained by backpropagation training algorithm are commonly used to develop tool condition monitoring system for machining processes. Many studies have used them to model nonlinear relationship between machining process parameters (feed, cutting speed, cutting depth) and tool wear (*Vb*) [8, 9, 16, 27] and will be highlighted reviewed in following chapters.

However, data training is time-consuming process depending on the amount of training data and network structure. If the process condition changes, the network requires retraining. The use of ANNs provides the capability for developing the model without requiring physical process knowledge [28]. It is defined as a black box which is unable to offer any physical meaning [29]. This means they are impractical to extract information or knowledge from the created model.

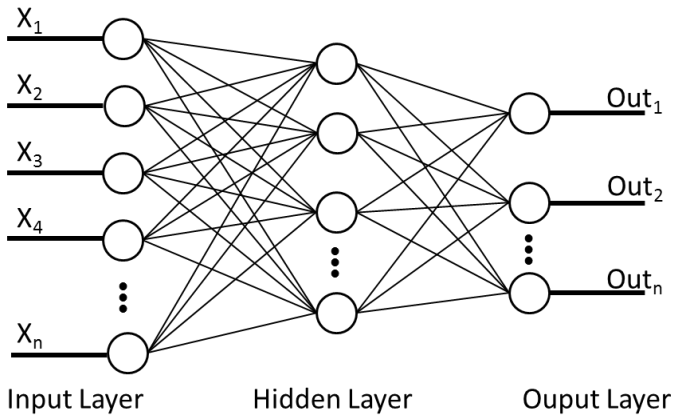

Figure 3.7 Generic architecture of feed forward neural network

3.6.2 Fuzzy Logic

Fuzzy logic is based on natural language leads to an easily understood model. Fuzzy logic is used to map an input space to the output space. The formulating process of the mapping from the given input to an output using fuzzy logic is defined as fuzzy inference. The fuzzy inference comprises of membership function, fuzzy logic operators, and IF-THEN rules [30]. Membership functions (triangular, trapezoidal, bell-shaped, etc.) are a curve that defines how each point in the input space is mapped to a membership value between 0 and 1 as shown in Figure 3.8. Then, the decision can be made by considering the mapping output. However, there are no standard methods to transform human knowledge into fuzzy model. It needs the experience of the experts to

set the rules and has some limitation of the number of input parameters fed into the model.

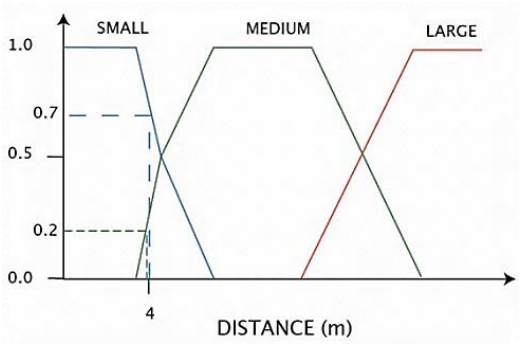

Figure 3.8 An example of IF-THEN rules of fuzzy logic used trapezoidal membership function

3.6.3 Neuro-fuzzy inference system

Adaptive Neuro-Fuzzy Inference Systems (ANFIS) from a group of hybrid technique that takes advantage of both neural network and fuzzy logic, achieving the simplicity of modelling (neural networks), while providing knowledge expressed in a set of conditional rules [29]. Neural networks with good learning capabilities can be used to learn the decision rules of the fuzzy system, while the fuzzy system provides expert knowledge to be used by the neural network [28]. Although the neural network can learn from data and feedback, understanding the knowledge or pattern learned from it has been difficult. On the other hand, fuzzy logic models are easy to understand because they use linguistic terms in the form of IF-THEN rules [31]. Therefore, some level of skill and expert knowledge is necessary to develop the fuzzy rules. Figure 3.9 shows the generic architecture of ANFIS where the network has a feed forward structure with all signals propagate from left to right. The operation of ANFIS was summarised in [17].

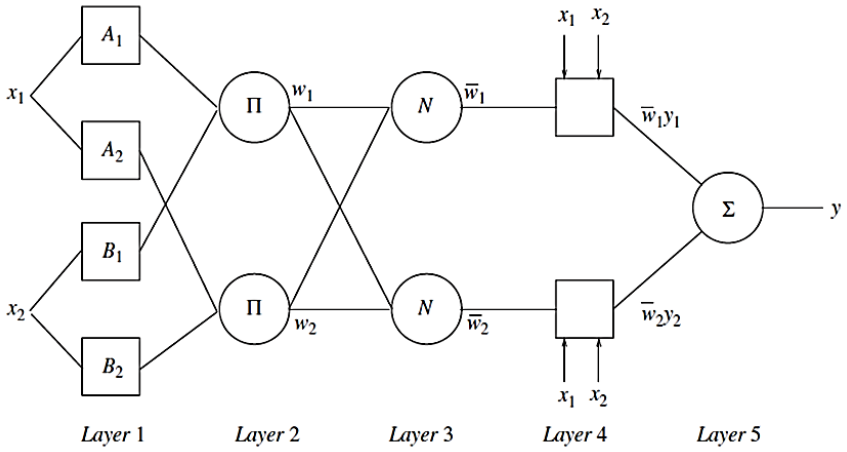

Figure 3.9 Architecture of Adaptive Neuro Fuzzy Inference System (Reproduced from [17])

3.7 Experimental Design and System Validation

3.7.1 Design of Experiment

Since machining experiments are costly and time-consuming, it is essential to perform an effective experiment with as few runs as possible in order that the most relevant factors of machining variable could be found quickly. Previously, several methods have been used to quantify the influence of cutting parameters (cutting speed, feed, and cutting depth, etc.) and process variables such as tool wear, vibration, temperatures, etc (for example in [32-35]).

One of the preferred methods is Design of Experiment (DoE) of factors being studied. This full factorial design of two-levels require 2^k factorial runs or test cases for performing the experiment. However, the number of runs required also increases rapidly when the number of factors increases. It is often unfeasible to run all cases because it is time-consuming and use lots of experimental resources.

Therefore, *fractional factorial designs* where the subset of the run is tested are used. The fractional factorial designs collect data from a specific subset and it only requires 2^{k-q} runs, where q is selected according to the desired design resolution. Fractional factorial designs are capable of determining which factors and their combinations have significant effects on the response variable [36].

Similarly, *Taguchi's orthogonal arrays* apply new concepts to parameter design and tolerance design. The factors are divided into two groups: control and error factors. The levels of control factors may be controlled in both laboratory and in actual production, while error factor levels may be controlled in the laboratory only. This method is able to determine which levels of the control factors have a little effect on the performance variable [35, 37, 38].

The response surface design is used to examine how important factors affect the response of an experiment. This leads to the development of polynomial models (1^{st} and 2^{nd} order) that include both the parameters under consideration and their statistical significance [36].

3.7.2 System Verification

As machining operations may change at any time, a tool condition monitoring system should be periodically verified in order to detect the change in the machining system. The model trained by AI techniques may need re-training to fit the new machining conditions and maintain accuracy. The preferred indicators to verify the change are two statistical tests: *the equal variance test* and the *two-sample t-test*.

The equal variance test checks the different variance value between the present prediction error (σ_2) and the error after monitoring system was implemented (σ_1). The null and alternative hypotheses are defined as Equation 3.1 and 3.2.

$$H_0 = \sigma_1^2 = \sigma_2^2 \quad (3.1)$$

$$H_a = \sigma_1^2 \neq \sigma_2^2 \quad (3.2)$$

The equal variance test statistic is:

$$F_0 = \frac{s_1^2}{s_2^2} \quad (3.3)$$

F distribution is used with degree of freedom (DOF) n_1-1 and n_2-1, where n_1 and n_2 are the sample size. The variable $s_1^2$and s_2^2 are the variances of each sample. The null hypothesis is rejected if:

$$F_0 < f_{\left(1-\frac{\alpha}{2},n_1-1,n_2-1\right)} \quad or \quad F_0 > f_{\left(1-\frac{\alpha}{2},n_1-1,n_2-1\right)} \quad (3.4)$$

where $f_{\left(1-\frac{\alpha}{2},n_1-1,n_2-1\right)}$ is the value of the F distribution at a significant level of α.

The two sample t-test is used to check whether the mean of the present prediction error (μ_1) is statistically equal to that obtained after monitoring process was set up (μ_2). The null and alternative hypotheses for two sample t test are defined as Equation 3.5 and 3.6:

$$H_0 = \mu_1 = \mu_2 \quad (3.5)$$

$$H_0 = \mu_1 \neq \mu_2 \quad (3.6)$$

The two-sample t test statistic is:

$$T = \frac{\overline{Y_1} - \overline{Y_2}}{\sqrt{\frac{s_1^2}{n_1} + \frac{s_1^2}{n_2}}} \quad (3.7)$$

where $\overline{Y_1}$ and $\overline{Y_2}$ are the sample means. The null hypothesis is rejected if :

$$T < -t_{\left(\frac{\alpha}{2},\upsilon\right)} \quad or \quad T > -t_{\left(\frac{\alpha}{2},\upsilon\right)} \quad (3.8)$$

where $t_{\left(\frac{\alpha}{2},\upsilon\right)}$ is the value of the t distribution at a significant level of α

$$\upsilon = \frac{(\frac{s_1^2}{n_1} + \frac{s_2^2}{n_2})^2}{\frac{(s_1^2/n_1)^2}{(n_1-1)} + \frac{(s_2^2/n_2)^2}{(n_2-1)}} \quad (3.9)$$

The results of both tests can indicate whether there is any change in the machining process. As a result, a decision can be made whether to continue using this monitoring system or to re-train process to reduce prediction error of the modelling.

In summary, this introductory chapter provides a brief overview of the condition monitoring system for monitoring tool wear in machining processes. It begins by the concept of an intelligent monitoring development. Then, several sensors normally used in the tool condition monitoring system are summarised and signal processing techniques are concluded. Later, the sensory feature extraction/selection methods for

the relevant information are described. After that, commonly-used AI techniques are introduced and the experiment design and system verification are summarised.

The following chapter includes the general methodology used for developing the proposed monitoring systems to monitor tool wear on the cutting tools. The general background of magnetisation and Barkhausen noise are summarised. Also tools and equipment used in this study are described. Previous attempts of tool condition monitoring system are then reviewed. More importantly, the design of multisensor fusion-based tool wear monitoring system in turning and required component involved in the system are elaborated. The measuring system and data acquisition used in the experiments are also introduced. The data processing by artificial neural network used for modelling tool wear prediction and tool wear stat classifications are described.

Chapter 4

General Methodology

Background and Development of Barkhausen Noise Measurement System and Tool Wear Monitoring in a Turning Process

This chapter begins providing the background and development of a Barkhausen noise system. In-house equipment such as preamplifier and power amplifier was built. The experimental setup and test cases were explained. As for tool wear monitoring, some currently-published studies have been reviewed and the sensor fusion concept was applied in this case study. Tools, workpiece, equipment and experimental setup were stated. Finally, the background of data processing used are detailed.

4.1 Background and Development of Barkhausen Noise System

Traditional destructive methods such as micro-hardness profiling and metallography are normally used to evaluate the depth of hardened layer and/or coated layer in cutting tools; however, they are considered destructive, expensive, time consuming, and not suitable for real-time process control. Therefore, several non-destructive methods for measuring the depth of hardened layer have been developed. Several methods exploiting the magnetic properties of materials have been attempted to evaluate hardness and case depth such as magnetic hysteresis properties, Barkhausen noise effect, and magnetoacoustic emission (MAE).

4.1.1 Characteristics of Ferromagnetic Materials

Any ferromagnetic material consists of magnetic domains in which all atomic magnetic moment vectors are aligned in parallel and the adjacent magnetic domains are separated by 180° or 90° domain walls. Normally, all the domains are randomly oriented when the material is in demagnetised state. When this material is subjected to an external varying magnetic field, the magnetisation of the material increases in the direction of applied magnetic field. The cyclic magnetisation process is comprised of domain nucleation, domain wall movement and domain rotation. The irreversible movement of magnetic domain walls makes the major contribution to the magnetisation process, which is influenced by microstructural features, such as grain boundaries, dislocations, phase precipitates, and stresses.

Ferromagnetic materials have particular magnetic characteristics. Magnetic moments are uniformly oriented in areas at the temperature lower than the Curie-temperature and no external magnetic field. These areas are called magnetic domains or Weiss domains as shown in Figure 4.1*(a)*. The moment's arrangement is caused by the interaction between interconnection force and the disoriented heat motion. Figure 4.1*(b)* shows connection of two domains, which are separated by a tiny wall, called Bloch wall, which rotates the magnetic vector of the domains. The rotation is from one area to another and it is performed orthogonally on the plane of the wall.

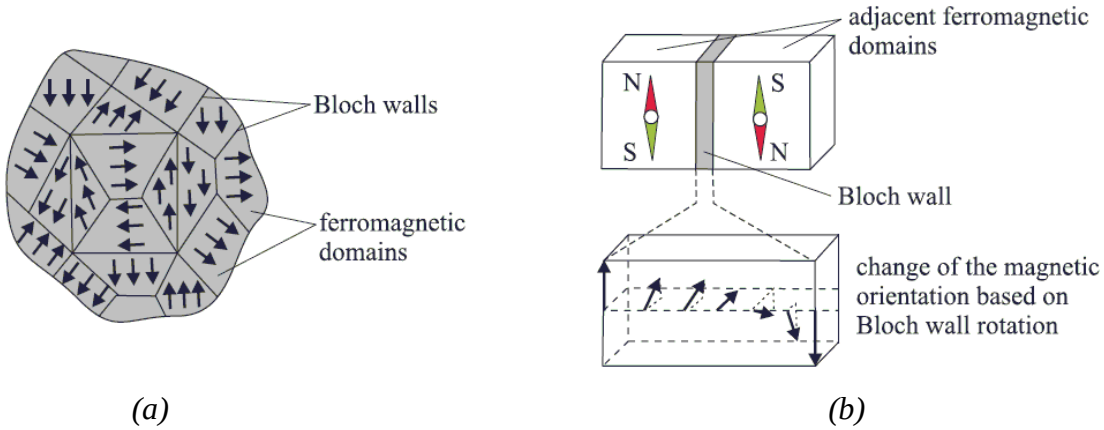

Figure 4.1 Magnetic domain and Bloch wall (reprinted from [39])

One of the important properties is the magnetic hysteresis loop or a B-H curve. This curve illustrates the relationship between the magnetic field strength (H) and the magnetic flux density (B), as shown in Figure 4.2. An external magnetic field initiates the orientation of the Weiss domains in the line of least resistance, where unfavourable magnetic orientation increases over the areas with an unfavourable orientation. The increase occurs by the movement of the Bloch walls and the increase is stepwise. The course is discontinuous like stairs, resulting from the irregular changes of the magnetisation in the elementary movement and the discontinuous jumps can be made audible. The discrete changes in magnetisation induce electric voltage pulses in a pick-up coil placed near the surface of ferromagnetic material. These noise-like voltage pulses were first observed by Barkhausen [40] and the phenomenon is known as magnetic Barkhausen noise (MBN). Most of MBN applications have been focused on magnetisation characteristics and hysteresis loop (B-H curve) as seen in Figure 4.3.

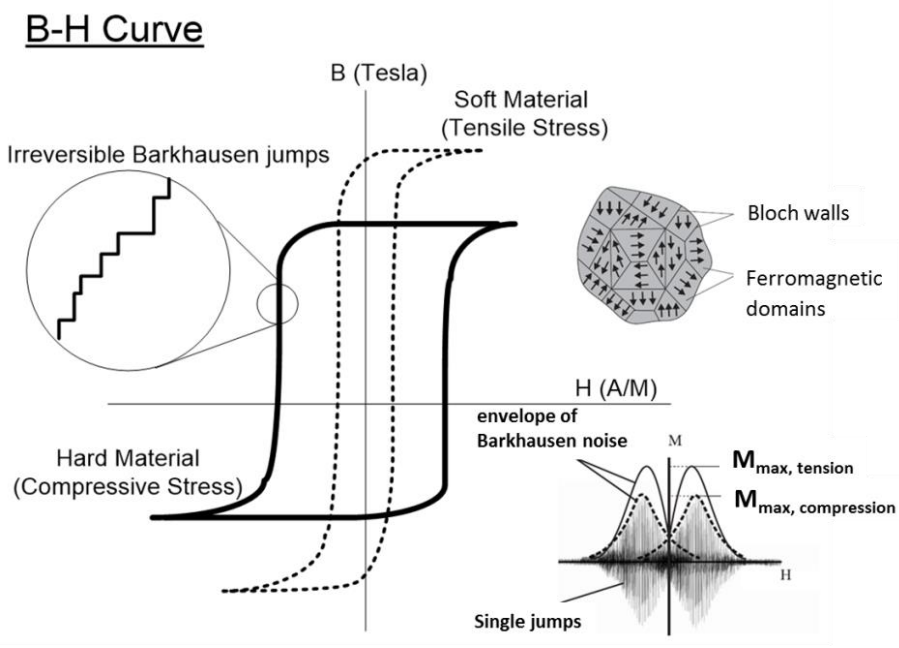

Figure 4.2 Hysteresis loop characteristics (modified from [39])

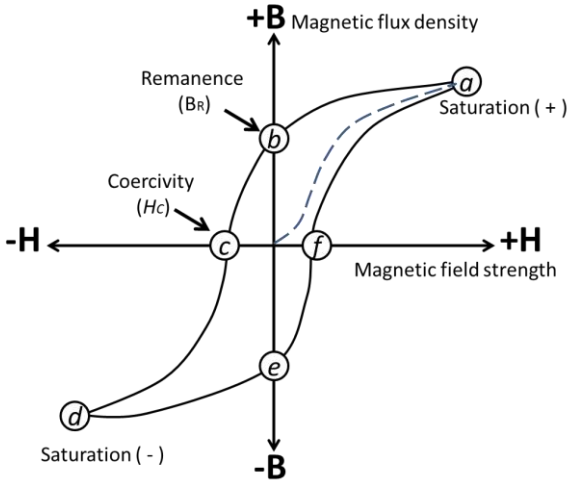

Figure 4.3 Typical of B-H loop for ferromagnetic material (modified from [39])

The B-H loop is created by measuring of magnetic flux density (B) during the change of magnetic field strength (H). Flux density of completely-demagnetised ferromagnetic material will increase, following the dashed line, as H is increased from zero to a positive direction. At point "*a*", all of the magnetic domains are aligned. Consequently, an increase in H produces a slight increase in B. At this stage, the material has almost reached magnetic saturation, called saturation point. When H is reduced to zero, the curve reaches point "*b*". Some magnetic flux remains in the material even though H is zero. This is known as the state of remanence denoted as B_R. This is caused by domain walls being pinned by impurities. The point "*c*" will be arrived after H is reversed, which is known as the coercive point, H_C, where the flux has been reduced to zero. The saturated state, point "*d*", will be reached in the negative direction. Reducing H to zero brings the curve to point "*e*" which will have a level of remanence equal to that achieved in the other direction. Increasing H along the positive direction will return B to zero. From point "*f*", the curve will back to the saturation point where the loop will be completed. The Enclosed Area of the loop is directly proportional to the energy loss in the material per unit volume per magnetisation cycle. This is often referred to as hysteresis loss.

General magnetic properties of a material can be determined from the hysteresis loop. *Remanence* is the magnetic flux density that remains in a material when the magnetic field is zero. It is the value of B at point "*b*" in Figure 4.3 and represented by B_R. *Coercivity* is the amount of reverse magnetic field applied to a magnetic material to make the magnetic flux density to return to zero. It is the value of H at point "*c*" in Figure 4.3. It is also known as the coercive field and is denoted as H_C. *Permeability* is the ease at which magnetic flux is established in a material defines the permeability of that material. Permeability (μ) is used to define the relationship between B and H as Equation 4.1.

$$B = \mu H \qquad (4.1)$$

Magnetic hysteresis curve and its parameters are affected by changing microstructure of steel parts. For example, in hard material, the B-H curves become wider, providing higher H_C and hysteresis loss, and lower B_R values. On the contrary, the curve of soft materials is steeper, providing lower H_C and hysteresis loss, higher B_R values as can be seen in Figure 4.2.

4.1.2 Principle of Barkhausen Noise Technique

The magnetic Barkhausen emission (MBE) is a non-destructive testing (NDT) method used for microstructure and stress evaluation in ferromagnetic steels. Barkhausen noise (BHN) signal results from the discontinuous movement of magnetic domain walls within materials when it is excited from the external varying magnetic field as previously described in Section 4.1.1. In Figure 4.4, when a ferromagnetic material is subjected to magnetic excitation, the magnetisation is obtained in the form of discrete jumps due to domain walls interacting and overcoming barriers in their path. Train of pulses induced in the primary coil changes magnetisation in the workpiece material via a yoke. BHN receiver consisting of air coil with or without ferrite core measures the remnant magnetic fields. Sudden changes in magnetisation yield electromagnetic and acoustic signals and these can be detected by a pick-up coil or an AE sensor [41]. The typical BHN signal is shown in Figure 4.5 which can be read out by oscilloscope or data acquisition.

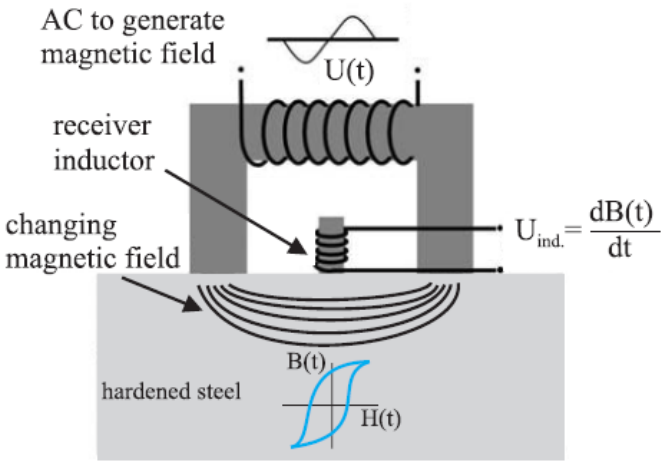

Figure 4.4 Principle of Barkhausen noise (reprinted from [39])

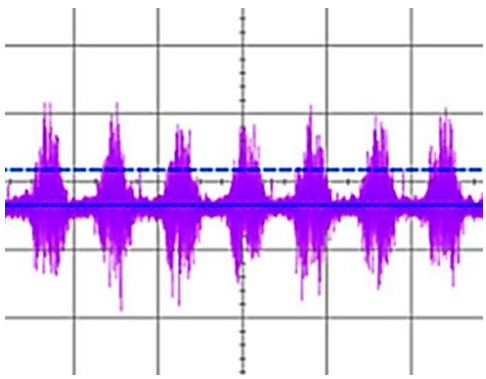

Figure 4.5 Typical pulse-train of Barkhausen noise

The MBE technique is broadly used for assessing the characteristics of ferromagnetic steels due to no need of surface preparation, portability of equipment, faster measurement, and capability to measure complex component like gears. One limitation of this technique is *skin-depth* (depth below the surface it can reach) which depends on the frequency used and material properties.

The penetration depth of the magnetic field in a material is limited by the skin effect. The skin depth (δ) is defined as the distance in which the wave amplitude decreased by a factor of e^{-1} (about 37%). The skin depth can be calculated by Equation 4.2, where f is the frequency of electromagnetic wave (Hz), μ is magnetic permeability (H/mm) and σ is electrical conductivity (%IACS).

$$\delta = \frac{1}{\sqrt{f\pi\mu\sigma}} \tag{4.2}$$

From Equation 4.2, the skin depth reduces as the frequency of applied wave increases. As a result, the high frequency excitation means the magnetic field occurs at the near surface and low frequency offers a greater depth but decrease in sensitivity. A study suggests that MBE propagates through the material with the maximum measurement depth about 1 mm [42].

An alternative method used electromagnetic for stimulation the structure in order to produce AE signal for analysis is well-known as Electromagnetic Acoustic Emission or Magnetoacoustic Emission (MAE). The measurement depth of MAE is much greater than MBE. For instance, the maximum measurement depth of ferritic stainless steel was about 7-8 mm for MAE, and only 0.1 mm for MBE.

The BHN signal is directly influenced by the variations of material properties, especially residual stress and material hardness. For example, when the mechanical stresses are applied to the material in the elastic region, the BHN signal amplitude is high under the tensile stress and low in case it is under compressive stress as shown in Figure 4.6 [43].

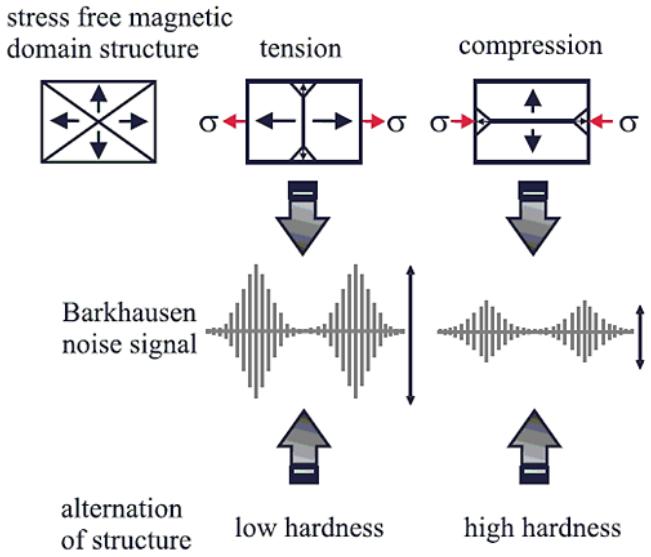

Figure 4.6 Effect of residual stresses and material hardness on BHN signal (reprinted from [39])

With regards the material hardness, the BHN signal amplitude increases when the material structure is low hardness (soft material) due to low carbon content, while the amplitude decreases when the material structure is high hardness (hard material).

4.1.3 Previous Attempts of Barkhausen Noise in Manufacturing

Typically, Barkhausen noise is used for various applications such as hardening depth evaluation, residual stresses and fatigue monitoring, wear and surface integrity evaluation, phase transformation and precipitation.

4.1.3.1 Case-Depth Evaluation

The case-depth evaluation with BHN measurement is based on the hardness difference of the harden case and the soft core. The measurement is usually achieved by using low magnetising frequencies to enable deeper penetration of the magnetic field into the ferromagnetic sample. Dubois *et al* [41] used BHN to evaluate case-depth of carburised steels (AISI 8620 and 9310) and nitride tool steels (AISI P20, D2, and H13). The results showed good correlation between BHN and harden depth values on the order of 100 and 1000 μm for carburised steels and 25 and 200 μm for nitride steels. This technique, however, was limited by the surface permeability which reduces the skin depth value.

Zhu *et al* [44] examined BHN measurement in case-hardened steels. Two case hardened carburised steel disks were used as test specimens. To vary case depth, grinding was used to remove the harden layer on the specimens. Barkhausen measurements were repeated to detect any changes stemming from the material removal. They summarised that the level of BHN signal increases as material was removed and the remaining case depth decreased.

According to Lo [45], hysteresis measurement can be used for quantitative evaluation of case-depth in surface hardened steel component. A series of induction hardened steel rods with various case-depths were tested by magnetic hysteresis properties and Barkhausen techniques. The depth profiles of magnetic properties such as coecivity and RMS value of BHN signals were found to be very close to the hardness profiles which measured from the strip samples cut from the rods. Hysteresis loop was used to characterise the case-depth between two regions (case, core) in the rods due to different magnetic properties of soft and hard materials. These estimated depths by hysteresis measurement were in good agreement with the nominal case depths. These authors all agreed that it is possible to measure subsurface hardness using BHN which suggests that relative measurements taken during the use of a tool could be used to infer the rate of tool wear or to infer the remaining thickness of coating layer in coated tools.

BHN technique was used to evaluate hardenability of SAE 4140 and SAE 6150 steels after Jominy test as found in the study of Franco *et al* [46]. Several BHN features were compared with hardness measurement and microstructure analysis. It was found that

BHN features follow the cooling gradient have linear correlation with hardness measurements.

Wilson *et al* applied Magneto-Acoustic Emission (MAE) and BHN to measure case depth in EN36 gear steels [42]. The correlation between BHN and MAE profile features and domain activity within soft core and case hardened layer have been drawn. The outcomes of their study showed that the overall amplitudes of both BHN and MAE have a good correlation with case-depth.

Suvi Santa-aho *et al* [47] investigated the Barkhausen noise magnetising sweeps technique to measure the case-depth in hardened steels. The results from magnetising voltage sweeps (MVS) were analysed and compared to the case-depths from conventional method. Induction and carburising hardened samples were determined by MVS and the residual stress state of the sample surface was also studied by X-ray diffraction.

4.1.3.2 Residual Stresses and Fatigue Monitoring

The applications of BHN technique for residual stress measurement and fatigue monitoring have been shown to be successful as reported by many authors. Lindgren *et al* [48] applied BHN to continuously monitor fatigue failure of mild steel and high strength steel specimens when the specimen were under tensile and bending test. It was found that in comparison with AE signals, the changes in BHN signals could be used to indicate crack initiation and growth for both specimens. Stewart *et al* [49] used the characteristic values of the BHN signal (peak high, peak width, peak position, skew) to characterise the difference between tension and compression stresses on steel (AS1548-7-460R) at different levels. They also measured the stress concentration caused by welding and found the correlation between stress concentrations and the distances from the edge of the weld.

The use of high and low frequency BHN technique to evaluate residual stress alteration in case-carburized EN36 steel was demonstrated by Moorthy *et al* [50, 51]. They found that the results obtained from high and low frequencies are correlated to residual stress-depth profiles measured by x-ray diffraction. For the samples subjected to varying grinding damage levels, the high frequency BHN is more suitable to evaluate the residual stresses on a surface whereas the low frequency BHN is more useful to evaluate the residual stress at much larger depth

4.1.3.3 Wear and Surface Integrity

The bulk of what work has been carried out attempting to use BHN as a wear detection method has been in monitoring grinding processes. This process may cause damage to the workpiece surface due to high cutting temperature and cause the workpiece to become softer or harder, and induce micro cracking. Several studies have reported that BHN can be used in detecting these grinding 'burn'.

Moorthy *et al* [50, 51] used BHN to detect grinding burn by low and high frequency measurement. They found that a single peaked BHN profile can be found in high frequency measurement, while a double-peaked profile can be observed in low frequency measurement. They concluded that the stress changes due to grinding burns correlated with the height of BHN profile in the high frequency measurements.

Karpuschewski *et al* attempted to find possibility to use BHN technique for quality inspection of gear manufacturing process [39]. Due of heat-effected zone from grinding process, the mechanical properties of gears such as reduced hardness, residual stress, is changed leading to easily develop of surface fatigue and gear breakdown. They measured the change in residual stresses and material structure by using BHN analysis. The results showed that this technique can detect thermal damages on workpiece surface effectively. Some studies used laser to make artificial grinding burns [52]. Santa-aho *et al* [53, 54] produced calibration blocks for grinding burn detection by using laser processing to produces artificial grinding burns and BHN were used to evaluate them. They concluded that the change in BHN features can indicate the changes in the material properties of calibration blocks due to the laser processing.

Moreover, surface integrity of grinded gear was studied by BHN technique. Vrkoslavová *et al* [55] used *Rollscan300* by varying magnetising frequency sweep (MFS) and magnetising voltage sweep (MVS) to measure the depth profile of grinded gears. Magnetoelastic parameter (MP) obtained by software *Viewscan* was used as evaluator and to find the correlations between conditions of grinding, residual stress, and MP.

However, there are some downsides that the sensitivity of BHN method is varied by changing heat treatment, material used and manufacturing processes as the BHN signal has been found to be very sensitive to material properties. Therefore, the proper calibration of the BHN measurement system is necessarily required for each particular material.

4.1.4 Barkhausen Noise System and Equipment

Many studies used a commercial BHN system produced by Stresstech Company [39, 55-60] since it was comfortable to use and not always easy to develop the BHN system. *Rollscan 300* (or series 300) in Figure 4.7 is the favourite analyser which is designed for surface quality control and testing of near-surface defects such as grinding burns, heat treatment defects, as well as changes in stress and microstructure. Others have attempted to develop their own BHN systems by design of a measuring probe and signal processing in order to use in their experiment [41, 42, 44, 46, 61-64]**.** These systems are based on the BHN theory presented in section 4.1.2 (Figure 4.4)**.**

Figure 4.7 The system commonly used in Barkhausen noise studies

In a real application, BHN technique, however, requires attaching the sensor close to the workpiece surface to prevent air gaps which could make some errors in measured value. Variation in material properties and heat treatment can cause the change in BHN signal. Furthermore, cracks, remnant magnetisation of the workpiece, and the external electromagnetic field also have an effect on the signal, therefore accurate calibration is required.

4.1.5 Development of BHN Equipment

The BHN system used in the present work is shown in Figure 4.8 and has similar features to those used in most studies mentioned in Section 4.1.2.

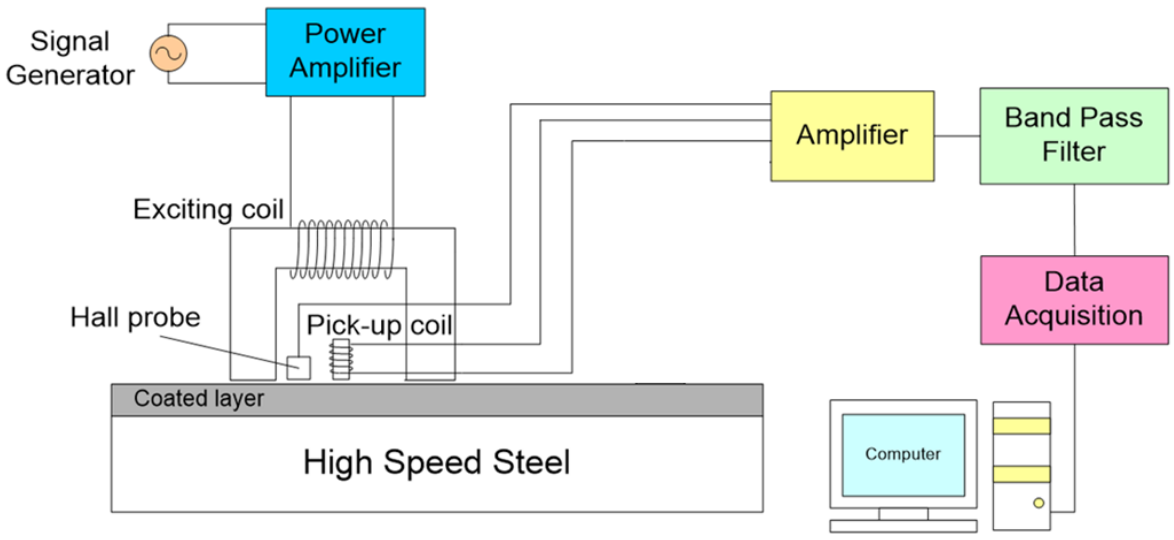

Figure 4.8 The Barkhausen noise system used in the experiment

The current signal used for magnetising the specimen was generated by analogue output module of National Instruments NI-USB 6212 and low frequency at 1-3 Hz of sinusoidal signal was supplied. This signal is then magnified by a power amplifier to provide current signal about 1 A to the exciting coil made from copper wire wound around the ferrite core. This magnetising current was monitored by a current probe.

The magnetic flux from the exciting coil flows through the specimen and magnetic flux density on the surface of the specimen is measured by a linear hall sensor (A1302). A search coil or pick-up coil picks up the BHN signal from the specimen. The very low level of BHN signal was gained by signal amplifier to be proper level for signal processing. All signals are gained and filtered before processing the signals via a computer which are interfaced by National Instruments NI-9223 put in a USB chassis cDAQ-9171.

To keep within the concept of low cost monitoring systems as the commercial laboratory equipment used is relatively expensive such as bipolar power amplifier and signal amplifier. Therefore, some dedicated equipment used to perform the experiments in this work has been developed with the support of a colleague from KMUTNB, Thailand.

4.1.5.1 Bipolar Power Amplifier

The function of this (Figure 4.9) is to drive the exciting coil in order to generate electromagnetic flux into the specimen. The current required in this study is approximately 1-2 A. A sine wave (about 1-2 Hz) generated by analogue output is magnified to the exciting coils by high power monolithic operational amplifier giving gains to input signals from low to high ampere up to 10 A peak.

Power amplifier was tested by amplifying sine signal from waveform generator to obtain high current output up to 5 A. In this experiment, only 1-2 A current output will be used to stimulate exciting coils in the experiment. Therefore, this amplifier was continuously tested by amplifying sine wave at 1 Hz and current output of 2 A for 10 minutes as shown in Figure 4.10. The test result shows the amplifier can work effectively and ready to use in the BHN experiment.

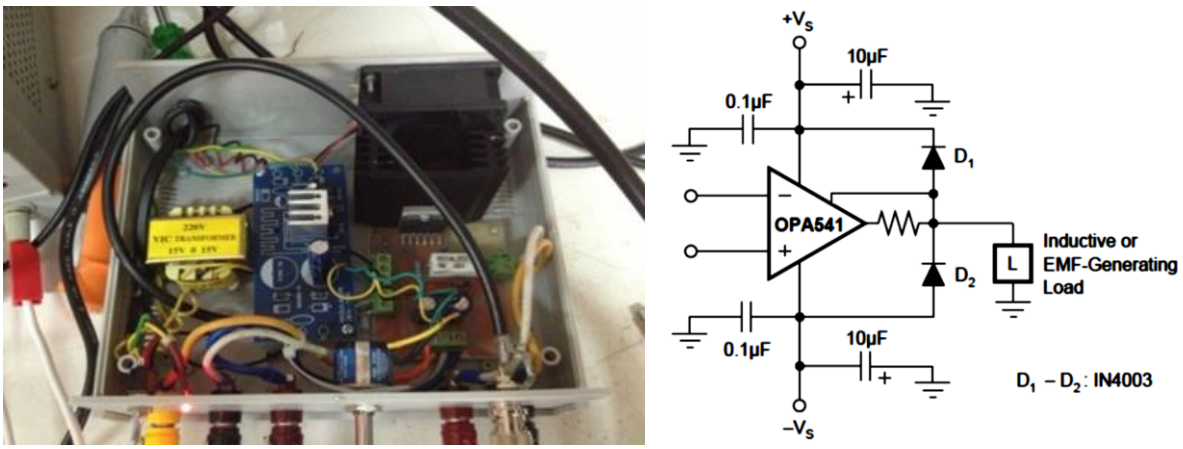

Figure 4.9 In-house bipolar power supply and equivalent circuit of OPA541

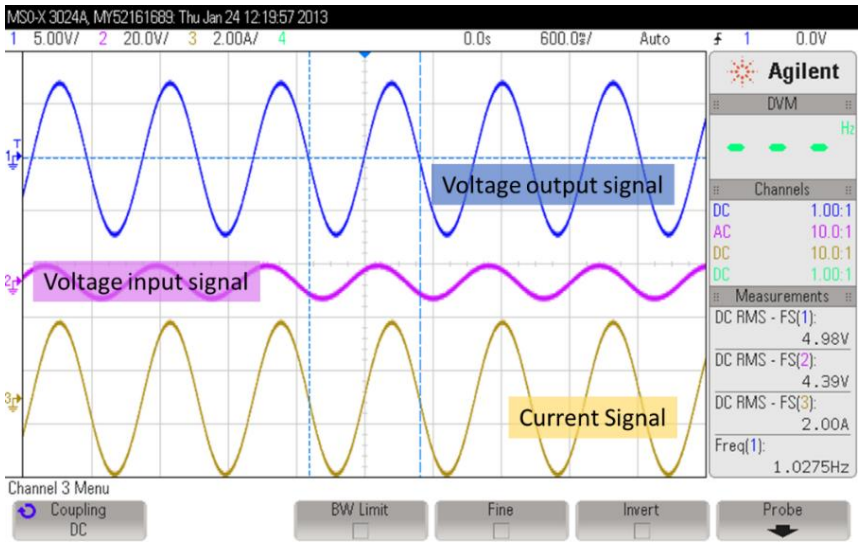

Figure 4.10 The test result of power amplifier used to generate 2 A at 1 Hz

4.1.5.2 Signal Amplifier

A 2-channel signal amplifier was built and used to gain the signal from pick-up coil to have a desired signal level before signal processing (Figure 4.11). This amplifier comprises of a low power instrumentation amplifier offering excellent accuracy and a further amplifier used to increase the output signal from the first amplifier. To gain BHN signal, amplifying gain needed to acquire the signal is about 60-70 dB.

The two channel signal amplifier was tested by an input sine wave with varying frequencies at low amplitude, 4.82 mV. The gain resistor (R_G=50 Ω) was used for the instrumentation amplifiers (INA-128) to magnify 1000 times of the input signal and operational amplifiers (LM-218) were set as a voltage follower circuit at gain output equal 1. Figure 4.12 illustrates the comparison between input and output signal which can amplify sine wave with amplitude 4.82 mV to 4.07 V.

Figure 4.11 Two-channel signal amplifier

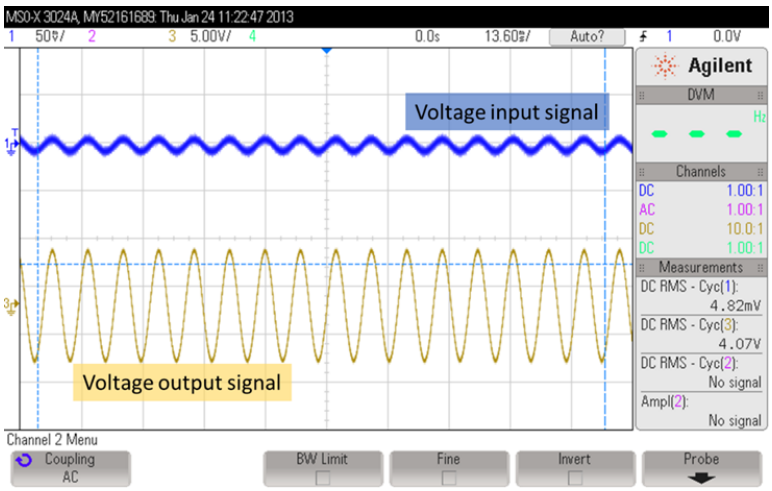

Figure 4.12 Input and output signal from in-house signal amplifier

4.1.5.3 Preliminary Tests of Barkhausen Noise system

In Figure 4.13, sine wave was generated at 1 Hz by a function generator then amplified to obtain a 1 A output to exciting coil. The C-shape laminate core (Figure 4.14) wound by copper with 200 turns was attached on the ferromagnetic material workpiece. The output voltage of a hall sensor attached at centre of magnetic yoke was recorded to observe the voltage changed before and after inducing the current to the coil. A pickup coil (Figure 4.14), copper wire wound onto a ferrite core, was used to receive the BHN signal from the magnetisation area.

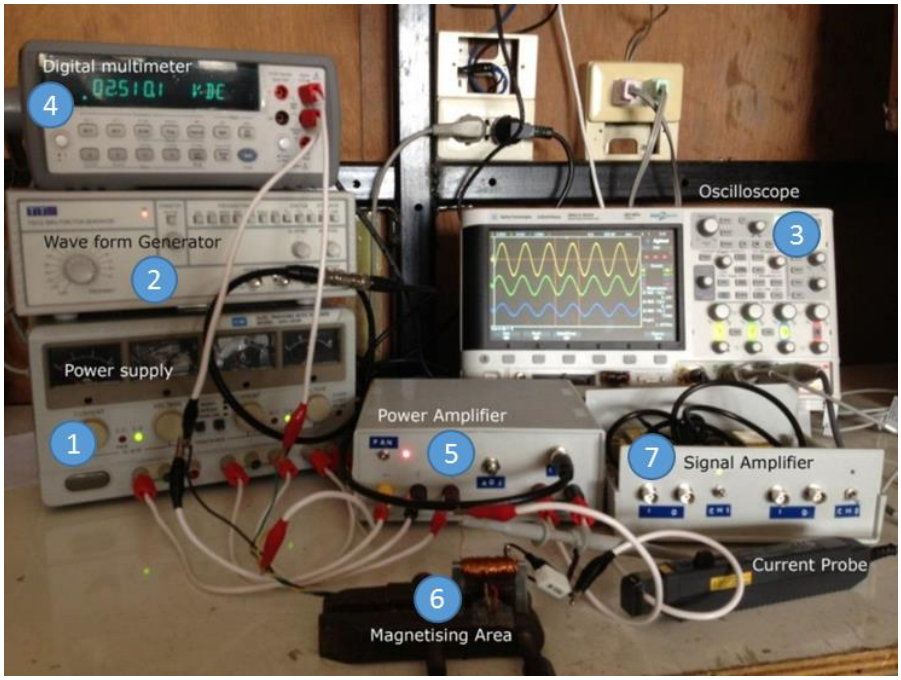

Apparatus:

1. Dual Power Supply (GW model GPC-3030)
2. Waveform Generator (TTI model TG310)
3. Oscilloscope and Current Probe (Agilent Tech: model MSO-X3024A)
4. Digital Multi-meter (Agilent Tech model 34401A)
5. Bipolar Power Supply (In-house power amplifier)
6. Exciting Coil, Pickup Coil and Hall sensor IC #A1302
7. Signal Amplifier (in-house amplifier)

Figure 4.13 Experimental setup for preliminary test of BHN

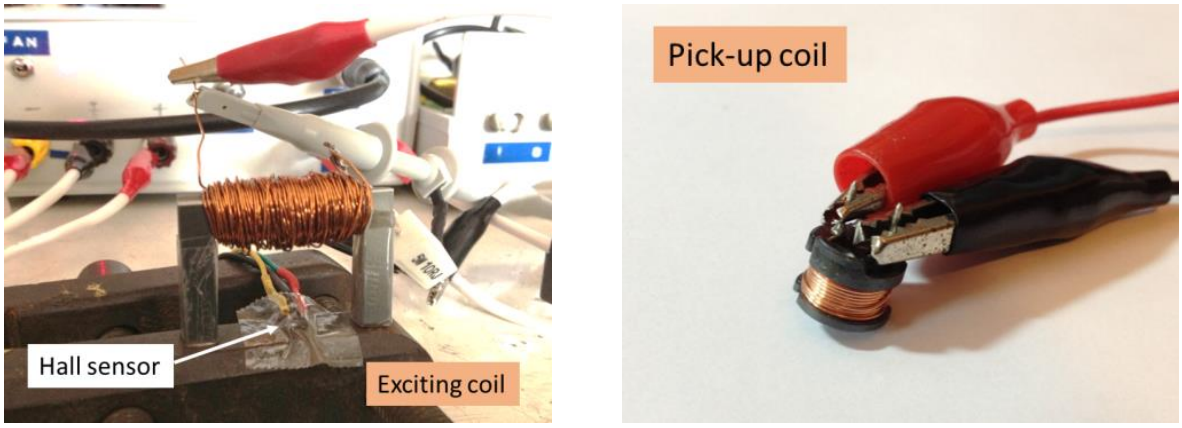

Figure 4.14 Exciting coil and pick-up coil used in the BHN measuring system

The resulting Barkhausen noise received from the pick-up coil can be seen in Figure 4.15.

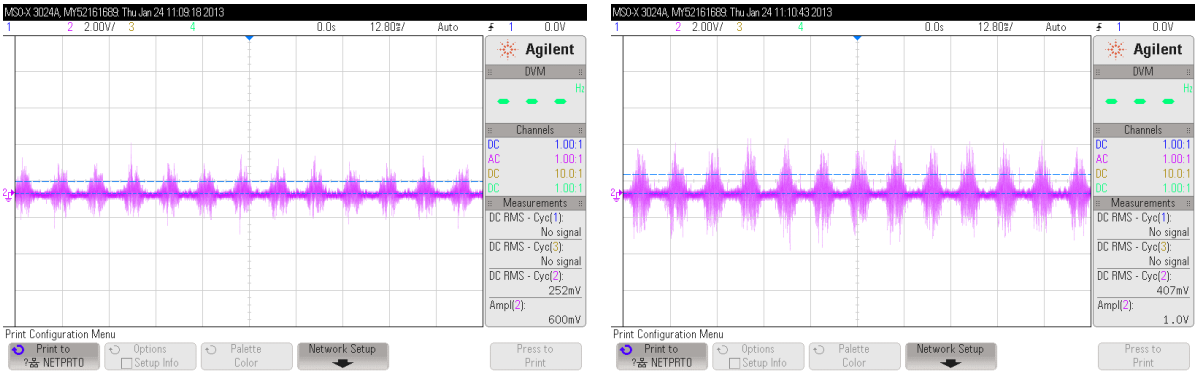

Figure 4.15 Barkhausen noise (RMS) from pick-up coil with two different magnetic fields

The pulse trains of noises which have different amplitude due to the different magnetic field intensities are compared in Figure 4.15. The significant parameters such as RMS, peak amplitude or number of peaks in one complete cycle are used to calculate to show the effect of different magnetisation in ferromagnetic materials.

These preliminary results show that this equipment is cost-effective and has potential to be used for BHN experiments. In Chapter 5 of this thesis the equipment developed here was used to generate low frequency signal to the magnetising coil and to acquire the noise signal from the pickup coil in order to extract the sensory features for evaluating coating-depth layer of coated HSS specimen.

4.1.6 Magnetising Coils and Pick-up Coils

The BHN measuring probe comprises of an electromagnetic yoke for excitation (also known as the magnetising or driving coil) and a pick-up coil for sensing the BHN signal. There are several concerns for making a measuring probe.

BHN measurement can be divided into two categories: low or high exciting frequency [65]. Measurement using the low frequency is usually performed at magnetising frequency f < 10 Hz and the BHN signal is analysed in the range of 0.5-100 kHz, while

the high frequency uses the higher excitation frequency f > 10 Hz and the pick-up noise signal is analysed in 2-1000 kHz.

The low frequency measuring system requires higher applied magnetic field strengths, leading to a larger electromagnetic yoke (typically covering an area of about 50 mm x 25 mm with the pole gap of 20 mm). The spatial resolution of measurements for low frequency excitation can be considered to the ferrite core diameter of the pick-up coil. On the contrary, the high frequency measurement involves lower applied magnetic field strength and the measuring probe can be smaller and easily pick the BHN signal from complex geometry such as gear teeth.

4.1.6.1 Exciting Coils

The number of turns of copper wire wound around the U-core and exciting current have an influence on the maximum magnetic field strength (H). According to Equation 4.3, a larger number of turns (N) and higher exciting current (I) will give a higher applied magnetic field strength. Deeper field penetration (skin depth) and higher magnetic field strengths can be attained at lower excitation frequencies due to skin depth calculated by Equation 4.2. As it delivers a high current (>1.5 A) relative to the typical diameter of wire used, the heating of magnetic yoke and copper wire will limit its use for long-term continuous measurement. The current delivered and number of turns should be optimised so that the BHN probe will have an optimum size, life and it is suitable for the application.

$$H = \frac{NI}{L} \tag{4.3}$$

To produce the exciting coil used here, copper wire (AWG19, Ø 0.870mm) with 300 turns was wound around the laminated U-shaped core made of Fe-Si electrical steel. This lamination steel has a low hysteresis loss and high permeability in order to enhance the magnetic flux generated. The stripes of laminations were cut by wire EDM and spot welded together. The pole face of U core should be smooth and has a good contact with the surface of the specimen to minimise the air gap effect. This is the cause of demagnetisation and accordingly minimising this is important to maximise the magnetic field penetration. This electro-magnetic yoke generates an applied magnetic field with a maximum strength of 4-5 kA/m. Before winding the coils, polyester film also called mylar was used to prevent contact contacting between the U-core frame and coils. The dimension and semi-finished core are shown in Figure 4.16 and Figure 4.17 shows the finished exciting coil used in this study.

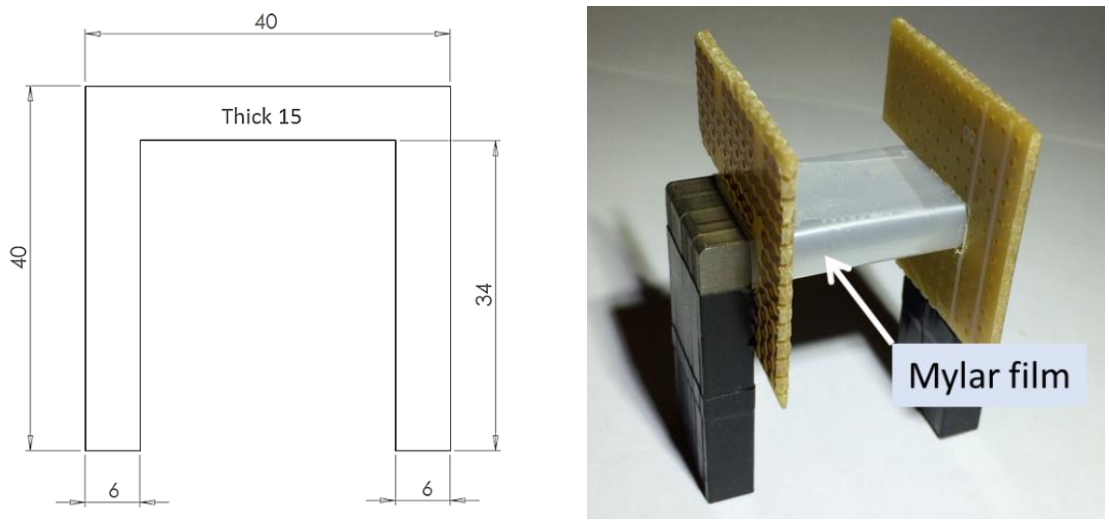

Figure 4.16 Dimension of Fe-Si laminated core for the exciting coil

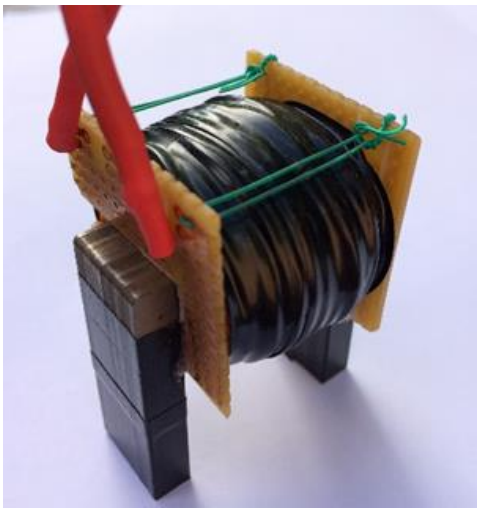

Figure 4.17 The finished exciting coil

4.1.6.2 Pick-up Coils

The number of turns of the pick-up coil has an influence on the sensitivity and frequency response of the BHN signal. Signal sensitivity increases (higher BHN peak amplitude) if the number of turns in the pick-up coils increases [65]. With a high exciting frequency, the higher induced voltage level can be acquired in the coils as the higher rate of change of magnetisation and the frequency response of the BHN signal will be high in direct proportion to the exciting frequency. This results in it being easy to detect the signal by pick-up coil with a smaller number of turns.

In the case of a low magnetising frequency, the rate of magnetisation is lower and the induced voltage level in the coil is low as well. The majority of the BHN signal will be in the low frequency range (< 50 kHz) and it is necessary to wind more turns of copper wire around ferrite rod for detecting enough BHN signal and receiving the signal generated from the deeper subsurface. In consequence, the pick-up coil for low

frequency measurement will normally bigger than that for high frequency measurement. In order to achieve high sensitivity with smaller size of the pick-up coil, it is possible to wind the thin copper wire around the ferrite rod.

The copper wire (AWG-43, Ø 0.063 mm) was used for making the pick-up coils which wound around ferrite rods (material grade 4B1) as shown in Figure 4.18. The dimension of ferrite rods and the number of turns were detailed in Table 4.1. The number of turns was chosen randomly relevant to other studies.

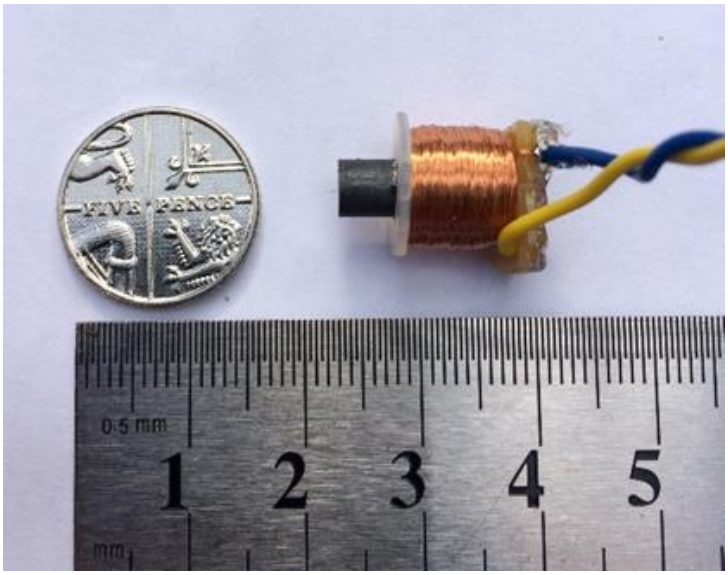

Figure 4.18 Pick-up coils made by copper wire wound round a ferrite rod

Table 4.1 Information of pick-up coils used in this study

Probe No.	Rod dimension	Number of turns
P-01	Ø 5 x 16 mm	2,000
P-02	Ø 5 x 16 mm	3,000
P-03	Ø 5 x 16 mm	4,000

The pick-up coil is normally placed on the surface of the test pieces between the poles of electromagnetic yoke in order to receive the BHN signal (Figure 4.19). The acquired signal is then magnified by the signal amplifier (Section 4.1.5.2) in order to a gain of approximately 60 - 70 dB. According to Moorthy, the signal is usually filtered by a 1 kHz high-pass filter [65]. Chapter 5 will describe the experimental setup, the signal features used, and results of the BHN measurement system found in this study.

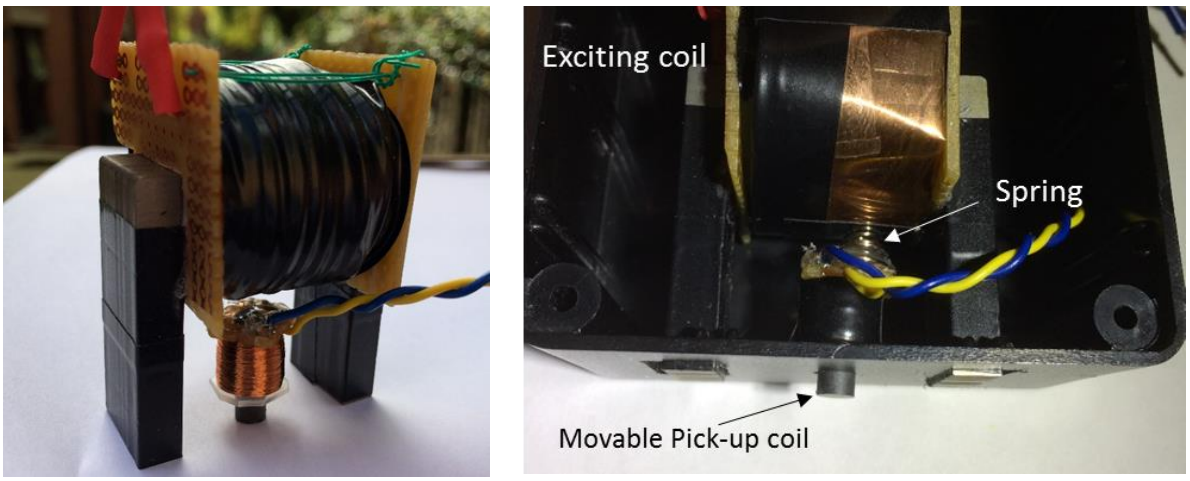

Figure 4.19 Magnetic Barkhausen noise probe in the enclosure box

4.2 Background & Development of Fusion Sensing Tests

A review of the previous tool wear monitoring system based on sensor fusion techniques and proposed monitoring system in this study are presented. As the indirect measurement is favourite methods normally used in automated machining system, the literature surveys in following sections centre on using multiple sensors to obtain the process signals of machining operation indirectly and modelling the selected sensory features to predict the tool wear value or the state of wear.

4.2.1 Machining Process Monitoring Methods

Tool wear monitoring systems aim to classify the tool wear state and current wear values in order to estimate the remaining tool life and as a result it can reduce or avoid the production waste. As discussed in Chapter 3, current sensing techniques can be categorised into two basic types: direct and indirect methods. The *direct method* is the most accurate measure for determining tool wear, however, the production have to be stopped due to off-line measurement. On the contrary, *indirect method* can be used continuously while machining operation.

Direct method

Direct method or direct measurement is concerned with measuring tool wear by using optical sensors, radioactivity and lasers. These methods directly measure tool wear in terms of material loss from the cutting tool or sometime observing the worn surface optically.

Machine vision is widely applied to measure the worn tool. Digital image processing (DIP) is used to assess the tool condition. This imaging technique is typically used to assess the tool wear by two methods. Cutting wear images are analysed by DIP to calculate the wear parameters such as flank wear width (V_b), crater wear, and nose

wear [66-68]. Alternatively, the surface finished of machined workpiece can refer to the condition of the tool [69, 70]. These methods can be used independently or complementary to each other.

Kurada *et al* summarised the computer vision techniques used for applying to tool condition monitoring [15]. They also attempted to use a CCD camera and digital image processing techniques to assess tool wear images based on image grey level [71]. This computer vision technique can be used to quickly obtain the wear profiles but it is sensitive to ambient light variations and vibration of the machine structure. Similar to the study of Kurada, a vision system was used by Kerr *et al* to measure tool wear using a CCD camera [66]. The wear image was analysed by image processing technique in order to assess the wear states and remaining useful life. Jurkovic *et al* [67] developed a vision system for tool wear measurement using CCD camera and LED. They recommended that this vision method is capable of measuring 3D images of relief surface and is possible to measure many tool wear parameters by image technique without any other device. Compared to the result of other works, this study applied the similar vision system to measure 2D profile, and the crater depth of the surface was also obtained by the light scattering measurement using a laser diode. However, to measure many wear parameters as they claimed, it is necessary to do the measurement at least two sides (flank face and relief face), and it is not practical to arrange the camera and light scattering system normally fixed at a specific location on the machine to do all measurements.

Shahabi *et al* studied several issues that they used an image processing technique to make an evaluation of tool wear especially in turning process. They assessed the flank wear and nose radius wear from a workpiece roughness profile in turning operation [68]. The wear profiles were measured using the machine vision method. The subtraction method between the unworn and worn tool image profile were used to calculate the amount of worn nose. The two binary images before and after machining were subtracted pixel-by-pixel. They also attempted to apply this technique to calculate build-up edge from 2D image [72]. They suggested the proposed image processing methods succeeded in determining the tool wear. However, this optical sensing method can be used only between cutting cycles which are not on-line measurement.

Flank wear can be monitored by radioactive techniques. For example, the remaining of radioactivity on the cutting tool or chips is traced. Some studies such as [73] used this technique to develop tool wear monitoring system as can be found in a review paper of Cook [74]. They all suggested that this radioactive methods are very accurate, but time-consuming, mostly used offline, and not safe for practical use. In almost last three decades, there is no cited use of this technique in tool condition monitoring.

Although direct methods provide high accuracy and reliability, they cannot be used for online monitoring and they are not suitable for practical application and inconvenient

to apply in machining process environment. It seems that optical methods are suitable to use, image distortion, light variation, formation of built up edge, and chip and coolant are the major challenges of this optical technique.

Indirect method

Online monitoring systems are commonly applied by indirect method. Several signals deriving from physical phenomena such as cutting force, acoustic emission, and vibration are indirectly correlated with the evolution of tool wear and widely used in tool condition monitoring. Besides, the temperature in cutting zone varies as the progression of tool wears due to changes in the tool geometry and its cutting ability as found in several studies [80-83]. They all suggested that the tool wear progression was associated with an increase in the tool temperature measured by thermocouples, thermal elements and infrared thermovision. However, it is difficult to access the cutting zone to measure the exact temperature. The average temperature around the cutting tool is commonly used for tool condition monitoring.

The general characteristic of each signal were discussed in Section 2.3 (Chapter 2) and in this chapter, previous attempts of using several sensing techniques in tool condition monitoring are summarised as follows.

4.2.1.1 Dynamometer

A dynamometer is used to measure the cutting forces and torque which are significantly correlated with the tool wear. It is generally viewed that the cutting forces used to remove the materials increase as the tool gradually wears due to the increasing friction between tool and workpiece. Cutting force measurement is considered as the reliable and accurate method for tool wear monitoring [75] and is the most common method to obtain the information about tool wear [76].

Several studies applied cutting force measurement methods to use in tool wear monitoring. Various force measurement methods were reviewed by Dan *et al* [77], Dimla [78] and Sick [16], but it is difficult to draw conclusions across these studies due to the complex relationship between cutting forces and mechanisms causing tool wear and because forces also related to cutting conditions. Teti *et al* [79], in reviewing current sensor technology, signal processing, and decision making strategy for tool condition monitoring system, and Sikdar *et al* [80] in measuring cutting forces and flank wear surface from three areas concluded that the greater flank wear value bring about large contact area at the flank. Consequently, the interface area between the flank and workpiece increases, and then the friction between them increases significantly, resulting in high cutting force. It is suggested by Cakir *et al* [81] that the force measurement techniques were most sensitive and suitable for detecting the chip formation and breakage than using vibration and motor current based signals.

The table dynamometer, such as those made by Kistler, are widely used [82], however, the cost of multi-axis dynamometers are relatively expensive (multiples of £10k) and impractical to apply in industry. Scheffer *et al* [83] concluded that most systems developed and presented in the literature were only used in the laboratories but not suitable to use on the shop floor.

4.2.1.2 Accelerometer

Accelerometers are commonly used to measure the vibrations in machine structures and are relatively inexpensive (up to several £100) and easy to use. Vibrations generated by a machining process can provide information about the state of cutting tools. The use of vibration measurement techniques for monitoring tool wear has been discussed by Dan *et al* [77], Sick [16], Teti *et al* [79] and it can be concluded that vibration amplitude has significant change during machining due to the progressive flank wear. The most basic analysis transforms the time domain signal to the frequency domain using the FFT to detect unusual changes in vibration frequency.

Several vibration techniques were applied to monitor flank wear such as by Lu *et al* [84] and Alonso *et al* [85]. Dimla [86] analysed vibration signal both in time and frequency domains to monitor the tool wear and found that the features in the time domain were more sensitive to cutting conditions, while frequency features correlated with tool wear. Salgado *et al* [87] used vibration signals to successfully predict the surface roughness from a turning process using a support vector machine (SVM). Where cutting conditions, tool geometry, and features extracted from the vibration signals were used as inputs. Ding *et al* [88] developed a prediction model between tool wear states and cutting tool vibration signals, AE signals, current signal of the spindle motor. The proposed model appears to be able to estimate tool reliability assessment effectively.

4.2.1.3 Acoustic Emission

Several AE techniques have been proposed to monitor tool wear [9, 79] and more generally, AE has been used in process monitoring and quality control in several applications such as the crack of storage and pressure vessels [89].

Li [12] suggested that AE can be used for sensing tool wear effectively as the frequency respond of AE sensor is in the range of 10 kHz - 10 MHz. This bandwidth is much higher than environment noises and machine vibrations. Generally, AE signals from metal turning consist of continuous and burst types (or transient). Continuous AE signals are generated from shearing in the primary shear zone and wear on tool face and flank. Burst type signals result from either chip breakage or tool fracture.

AE methods are able to detect most of the phenomena during machining such as tool wear, tool breakage and chipping, and chip formation detection due to wide sensor dynamic range [82, 90]. For example, peak to peak amplitude is able to detect the tool

breakage [91]. Chip formation effect on tool state using AE in turning was studied by Bhuiyan *et al* [92]. Several works reported that the amplitude of the continuous-type AE signal could be utilised to monitor the wear of cutting tool. Many AE parameters such as peak count, RMS voltage, and rise time can be used to characterise of tool wear state [12]. Rangwala *et al* [93] used AE with other signals for tool condition monitoring. The mean RMS of AE signal can be used to evaluate flank wear in cutting tool during machining operation as it is sensitive to flank wear. Some studies (such as Chungchoo *et al*) attempt to develop models for flank wear and crater wear prediction by using AE parameters. The average accuracy of developed models for flank wear and crater wear estimation is reported to be fairly accurate [94].

AE signals have been combined with other sensing signals. Sharma *et al* [95] and Gajate *et al* [96] used AE, vibration, and force signals to monitor the tool wear in turning process. It also was observed that peak count or ring down count of AE signals showed a significant increase with the tool wear. Jemielniak [97] extracted several features from cutting force, AE, vibration sensors to estimate the tool condition in turning process.

AE has some limitations because of signal attenuation and multi-path distortion is heavily dependent on the mounting location of AE sensor [98]. Kulandaivelu *et al* [91] suggested that the best locations of AE sensor to detect flank wear and crater wear are the side and the top surface of tool holder, respectively since flank wear emits surface wave which travel along the side of the tool holder and crater wear emits the wave along the top surface of the tool holder.

Effective data acquisition and signal processing is required to collect and process data as the sampling rate of data acquisition is relatively high and needs large data storage space for saving data. This makes AE technique costly and unpractical to use in the shop floor compared to other methods.

4.2.1.4 Microphone

Although microphones are inexpensive and flexible to set up, very few studies have used them to record the machining sound due to issues with robustness [27]. Teti *et al* [79], reported that various sound measuring techniques were used successfully to measure flank wear in turning [84, 99], milling [13, 100, 101] and drilling [102], but almost all studies performed the machining experiment in dry cutting condition.

Kopac and Sali [103] used a microphone to monitor the cutting sound from turning lathe machine and the sound signal was analysed in frequency domain to build a model for tool wear monitoring. They concluded that an increase of sound signal amplitude correlates with an increase of tool wear. Similar to [104], Raja *et al* monitored the sound signal which has different tool wear states: fresh, slightly worn and severely worn tools. The results suggested that the sound pressure amplitude measured from cutting operation increases with an increase of with flank wear.

Tekiner *et al* [105], attempted to determine the best cutting condition for turning stainless steel (AISI 304) by using the sound signal recorded by a microphone and concluded that the best cutting parameters could be determined depending on the cutting sound. Lu *et al* [84] used a microphone to develop a tool wear monitoring model which used the sound emitted from a turning process to model the main effect of tool wear on system dynamics during stable cutting.

4.2.1.5 Current and Power Consumption

As a worn tool requires more cutting force to maintain a particular cutting condition than a sharp tool, the machine tools have to increase the power used for motor rotation. Thus, cutting forces can be measured indirectly in terms of current and power consumption of spindle motor for detecting the tool wear and tool breakage [14, 106, 107].

Bhattacharyya *et al* [106] estimated the tool wear by using spindle motor current and input power. Also, Szecsi [107] monitored the cutting tool condition by using current and speed sensors. The system was trained by a genetic algorithm based fuzzy rule set. They summarised that the current of the main motor can be used to classify the tool condition during turning. Siva *et al* [108] used spindle current signals along with vibration, force and sound signal to develop a tool wear monitoring system. They concluded that spindle current exhibited a strong correlation with flank wear. Several studies [10, 79], used current signals to monitor tool wear. Power consumption, indirectly representing current consumption, is also used to monitor the tool wear.

Renones *et al* [109] diagnosed the tool breakage of multitooth tools by using electrical power analysis. As complexity of cutting tool, power consumption of the tool drives represents the best signal among noise, vibration, temperature. It can be used to perform online detection of tool breakage.

There are several aspects to consider when the current and power consumption sensors are used in tool condition monitoring. As spindle motors normally increase and decrease rotational speed before and after cutting, they need higher power used to accelerate and to stop the rotation of spindle than that used for stable cutting. Therefore, to represent tool wear, spindle current and power consumption signals should be considered under stable cutting without acceleration and deceleration of the spindle [107]. Furthermore, as it behaves a nonlinear characteristic, the current sensor requires proper compensation and calibration [14].

It appears from the literature that because power sensing techniques are not as accurate as others (e.g. AE and dynamometer), they are commonly used for detecting tool breakage and tracking tool wear in a general sense. A basic review of the market also suggests that these sensors are commonly installed as standard in many designs of machine tool.

4.2.2 Combing These Sensors Together ('Fusion Sensing')

As discussed in Chapter 3, different sensing signals have different characteristics and their own limitations (e.g. robustness, cost). Consequently, it is proposed that using multiple sensors to obtain the signals from different sources is used to provide more information for the monitoring or control tasks and improve accuracy in the classification of tool wear states. Sensory features extracted from multiple sensor signals are combined together and this known as fusion sensing.

The major advantages of fusion sensing over other methods are: potential for higher statistical confidence, reducing ambiguity and obtaining a robust tool condition monitoring system, and improved precision. Additionally, using a sensor such as dynamometer to monitor tool wear can be inappropriate to use on the shop floor due to a very high cost and difficulties with location. A low cost tool wear monitoring system, using less robust and inexpensive sensors could be a better solution for industry.

4.2.3 Previous Attempts at Fusion Sensing

Attempts have been made to consider various sensory features extracted from multiple sensors fused by several methods such as pattern recognition, neural networks and fuzzy classifications, in order to make a decision for tool condition monitoring system.

The most commonly used sensors are dynamometer, AE, and vibration [9, 79]. The algorithms commonly used to fuse the information can be classified into two major approaches: statistical and artificial intelligence (AI) approaches. The AI method widely used in tool condition monitoring consist of artificial neural network (ANN), fuzzy logic, a hybrid combination of both (neuro-fuzzy) [10].

Silva *et al* [108] used multiple sensors including spindle current, force, vibration, and sound) to develop tool wear monitoring system. Statistical features based on frequency spectra of these sensors were extracted to classify the tool wear state and fused by neural networks and expert system. Lo *et al* [110] considered using temperature, load current, vibration, acoustic emission and cutting force. However, it was only the last two of these that showed useful information in terms of tool-failure condition. Consequently, only these two signals were used as input parameters in the Adaptive Neuro Fuzzy Inference System (ANFIS) model in order to evaluate the tool wear states. It was concluded that tool wear state from ANFIS was successful in classifying the tool condition.

Sharma *et al* [111] selected acoustic emission (ring down count), vibration, cutting force, and time usage as input parameters into ANFIS in off-line training when considering turning operations on EN24 with an uncoated tool for various cutting conditions. This model can estimate the wear rate of cutting tool and provide actual and predicted tool wear values. Cuneyt *et al* [102], measured force, vibration and machine AE signals in turning and several sensory features were used to develop a fuzzy-logic-base sensor fusion method for estimating the cutting tool wear. In this

study, the tool wear condition was determined according to the decision by the two-stage fuzzy logic system which can classify the state of tool into three regions: sharp, workable, and dull.

Malekian *et al* [112] determined the factors affecting tool wear and a tool wear monitoring method. Various signals, from accelerometers, force, and AE sensors were fed through the neuro-fuzzy method (ANFIS) in order to determine if the tool is worn. The outputs of selected sensors, across several cutting conditions, were applied to a fuzzy logic model to advise the operator which of the three states: good, average, and bad, the tool was in.

Tangjitsitcharoen *et al* [113] applied sensor fusion for tool wear and cutting state monitoring using cutting forces, sound, vibration, and AE. These signals were fused via the back propagation neural network and integrated via the pattern recognition technique in order to monitor tool wear and detect the change of cutting states. Formation of continuous chips, broken chips and the onset of chatter can be classified by proposed signal features with the high accuracy and reliability.

Segreto *et al* [114] used cutting force, AE, and vibration signals for tool wear state classification during turning of Inconel 718. Principle Component Analysis (PCA) was used to reduce dimension of sensory data and extract significant feature for neural network to classify tool wear state. Jemielniak *et al* [97] used various sensory features extracted from cutting forces, AE, and vibration in order to monitor tool wear in rough turning of Inconel 625. Numerous features were extracted from time, frequency domain signals and wavelet coefficients (time-frequency domain). The best features combination was determined by efficient method and the selected feature set were used for tool wear estimation. Zhang *et al* [115] adopted multiple sensor fusion to monitor tool wear in turning by using AE and cutting sound signals. Sensory features of two sensors to train the classification and regression models based on support vector machine (SVM). They concluded that combined decision of two sensory results is better than using individually.

This recent literature suggests that ANFIS would be the best methods for fusion sensing as it takes advantage of easy learning ability from neural network can be used to learn the fuzzy decision rules very well. Also, it is suggested that ANFIS can provide very high accuracy results in tool condition monitoring. Nevertheless, one limitation is the number of inputs used for training data. The number of decision rules immensely increases as the number of feature inputs increases. Similar limitations have been found in fuzzy logic method.

4.2.4 Development of Tool Wear Monitoring System Based on Sensor Fusion

This machining experiment was supported by the Advanced Manufacturing Research Centre (AMRC). They provided facilities for conducting the experiment including; CNC machine, tool inserts, EN24 workpiece, sensors and DAQ system. These are described as follows.

4.2.4.1 Machine Tool and Cutting Inserts

MORI SEIKI (NT4300 DCG), the multi-axis mill turn centre used for milling and turning was used for machining EN24 with DNMG 150608-PM (DNMG 442-PM) coated cutting tool.

4.2.4.2 The Sensors and Data Acquisition Used in the Experiment

The tool wear monitoring system in this study used three sensors: AE sensor, microphone, and power sensor to obtain the motoring signals from the machining process as several studies in the literature suggest that AE sensor responds to wide dynamic range and can detect of most of the activities in machining [9]. Also, the size of AE sensor is small and it mount easily near the source of AE signal compared to other sensors. Besides, using microphone and power monitoring system is relatively low cost method. These three sensors used in this study could be a good combination for developing a cost-effective monitoring system.

The installation of the wide band AE sensor (Kistler 8152B111) is shown in Figure 4.20, and was used for measuring AE signals above 50 kHz to 400 kHz. The AE signals from the sensor were first filtered and magnified by Kistler coupler 5125B used as a pre-amplifier and band pass filter (50 kHz and 1 MHz).

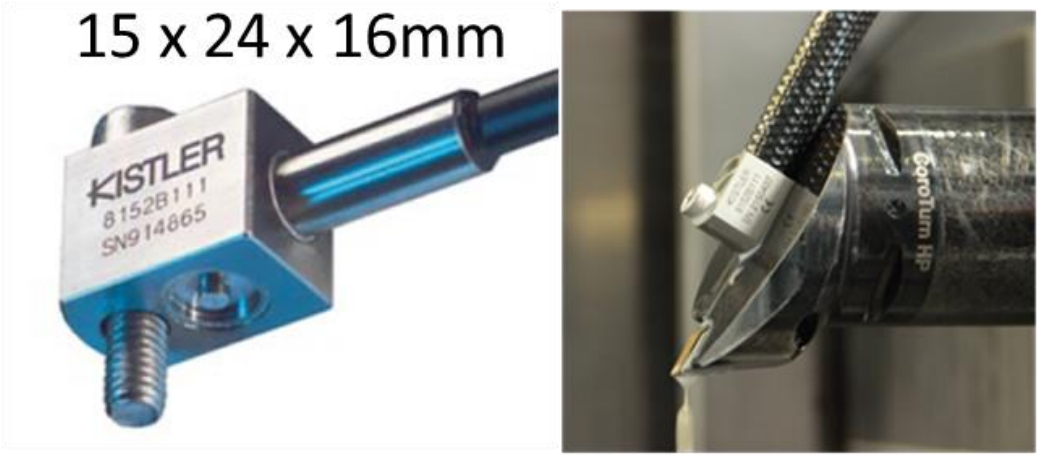

Figure 4.20 AE sensor mounted by M6 x 25mm on the tool holder

AE sensor was connected to a National Instruments NI-9223 data acquisition system. The scan rate must be chosen carefully because the down-sampled analogue signals are imprecise, while over-sampling for a long duration time, the size of data files becomes

relatively large. As the frequency response of AE signals in cutting process is about 100-300 kHz. According to Nyquist's theorem, sample rate should be 600 kS/s for this study.

A PCB Piezotronics 130E21 microphone with built-in preamplifier was used to record the sound during turning process as shown in Figure 4.21. The frequency response of this microphone is 100 to 4000 Hz at ±1 dB and 20 Hz to 20 kHz at -2 to +5 dB. It can be also used to identify noise near field of AE signal. The microphone signal was acquired by a National Instruments NI-9234 at a sample rate of 50 kS/s.

As the power consumption of the spindle motor is related to the tool condition, a Load Controls Portable Power Cell PPC-3 power monitoring system was used to measure the power consumption of the spindle motor. The system was connected to a National Instruments NI-9201 DAQ and the output signal from this system was sampled at 50 kS/s.

Figure 4.21 PCB130E21 microphone for measuring sound pressure

4.2.4.3 Signal Acquisition and Processing

All sensors connected to different analogue input modules mentioned previously. They were combined by National Instruments NI-cDAQ 9174 chassis which has the ability to simultaneously convert analogue to digital signals with different sampling rate (600 kS/s for AE, and 50 kS/s for microphone and power consumption signals). National Instruments LabVIEW software was used to develop the acquisition program to acquire the sensor data and perform post-signal processing. The acquisition program concurrently receives three sensor signals, post-signal processing was performed to extract several features both in time and frequency domains.

4.2.4.4 Tool Wear Measurement and Validation

During the machining, a portable microscope was used to acquire images after each cutting cycle to observe any flank wear developed on the cutting edge. As machining was in a wet cutting condition, it was necessary to protect the camera system from the spreading coolant that might cause damage to the camera and lighting system. A waterproof camera box and LED light source were held by a flexible magnetic stand and fixed on auxiliary spindle located at the machine tailstock (Figure 4.22).

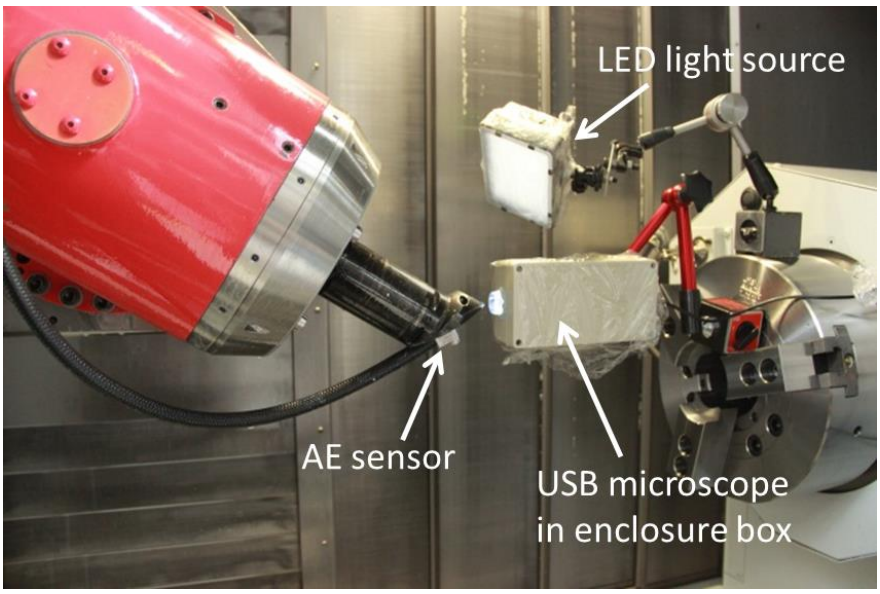

Figure 4.22 USB microscope attached to the machine by a flexible-magnetic stand

To calibrate USB microscope, the width of flank wear was periodically removed from the tool holder and measured by a high resolution bench-top optical microscope and used as reference values for training the neural networks. The neural network training and image processing were performed by MATLAB.

4.3 Background & Development of signal processing

4.3.1 General Background of Signal Processing for Machining Data

As described in Section 3.4.1, significant sensory features which correlate with tool wear were extracted by signal processing techniques in order to be used as inputs of the prediction models. These features can be roughly divided into four categories: features in the time domain, features in the frequency domain, features in the time-frequency domain, and features in the statistical domain. According to Siddhpura [9], the most widely used features are extracted from time domain, frequency domain, and statistical domain, while few works succeeded in using time-frequency domain.

4.3.1.1 Time Domain

In Sharma *et al* [111], AE (ring down count), vibration (acceleration), cutting forces along with time, and time usage were selected to be input parameters into ANFIS in off-line training. Lo [110] selected only two signals (AE, cutting forces) to extract five significant features in time domain (average AE RMS, maximum AE amplitude, average AE amplitude, mean main force, and ratio of feed force and main force). Those features then were trained by the ANFIS for tool wear state classification in turning. The classification model produced successful classification (100% of correct rate) for tool state with respect to only two classes (normal or failure).

Also, Malekian *et al* [112], the RMS value of cutting force, and acoustic emission signals were used to train the ANFIS for monitoring tool wear. Regarding to Segreto *et al* [114], RMS of cutting forces, AE, and vibration were extracted and Principle Component Analysis (PCA) was used to select significant features for neural network training in order to classify the tool wear states. Dimla [86] used time and frequency domain features of vibration signal during turning of EN24 to correlate with tool wear and suggested that the vibration features were effective for use in cutting tool wear monitoring and wear qualification. Therefore, the favourable time domain features such as RMS value, maximum amplitude will be used to extract the sensory features for tool condition monitoring system proposed in this study.

4.3.1.2 Frequency Domain

Fang *et al* [116] used cutting forces and vibration signals to sense tool wear during finish turning of Inconel 718. The Fast Fourier Transform (FFT) and Discrete Wavelet Transform (DWT) were used to process the vibration signals and it was found that DWT is more effective for indicating the variation of cutting vibrations across wide range of frequency bands. It appears that the increase of vibration amplitude due to tool edge wear progression can be indicated by the change of DWT. Tangjitsitcharoen *et al* [113] used power spectral density (PSD) of sound, and AE signal to estimate the tool wear via the neural network. They used standard deviation of AE signal and PSD of both sound and vibration signal to identify the broken chip. The energy spectral density (ESD) of the three sensors used was proposed to estimate the tool wear, identify the cutting states of chip formation and chatter. In this study, only the FFT will be used to transform the sensor signals from time domain to frequency domain and several time domain features used in this study are mentioned in Section 4.3.2.

4.3.1.3 Statistical Domain

Cuneyt *et al* [102] used statistical features such as RMS, standard deviation, mean and maximum values derived from experimentally measured force, vibration and AE signals to estimate the tool wear based on fuzzy inference system. However, the estimation model was not satisfactory and they suggested using more sensors could increase the tool wear estimation accuracy. Silva *et al* [108] used statistical features (Mean, absolute deviation, kurtosis and skewness) and frequency domain features (FFT) of spindle current, force, vibration, and sound signals to train the neural network and expert system for developing tool wear monitoring system. They found that the statistical features did not correlate with the tool wear progression as it may because of unexpected variations in their machining experiment. However, some statistical domain features (mean, standard deviation, kurtosis, skewness) will still be used in this study and will be described in Section 4.3.2.

4.3.1.4 Time-Frequency Domain

Zhang *et al* [115] adopted multiple sensor fusion by using AE and cutting sound to monitor tool wear in turning. They used time-frequency features of two sensors to train the classification and regression models based on support vector machine (SVM). They concluded that combined decision of two sensory results is better than using individually.

The combination of feature domains can be adopted as found in Jemielniak *et al* [97]. They used various sensory features extracted from cutting forces, AE, and vibration in order to monitor tool wear in rough turning of Inconel 625. The features were extracted from time, frequency domain signals and wavelet coefficients (time-frequency domain). The best features combination was determined by efficient method and the selected feature set were used for tool wear estimation.

4.3.2 Feature Extraction

This section describes the statistical features used in this study. Sensing features were extracted both in time and in frequency domains these will be further discussed in detail in Chapter 7. The general feature definition and calculation are given in short here.

4.3.2.1 Root Mean Square (RMS)

RMS as described by Equation 4.4 is used, unless otherwise stated, to calculate the average value of overall discrete signals in time domain.

$$RMS(x) = \sqrt{\frac{\sum x_i^2}{N}} \qquad (4.4)$$

where N is the number of data points and x_i represents the signal from each data point.

4.3.2.2 Mean

This feature is the standard statistical mean value of the signal. In contrast to RMS, the mean is reported only for rectified signals because in raw time signals, this value remains zero.

$$\overline{x} = \frac{\sum_{i=1}^{N} x_i}{N} \qquad (4.5)$$

4.3.2.3 Maximum or Peak value

This feature is simply the maximum value of signal amplitude.

$$Peak = \max(x_i) \qquad (4.6)$$

4.3.2.4 Peak-to-Peak (Range)

Peak-to-peak value or range is the difference between maximum and minimum signal amplitude.

$$Peak\ to\ Peak = \ Range = \max(x_i) - \min(x_i) \qquad (4.7)$$

4.3.2.5 Kurtosis and Skewness

Kurtosis is a measure of 'peakedness' and is a normalized form of the fourth-order moment about the mean. Kurtosis is defined in Equation 4.8 and is the ratio of the fourth moment to the square of the second moment (or variance).

$$Kurtosis = \frac{(N-1)\sum_{i=1}^{N}(x_i - \overline{x})^4}{\sum_{i=1}^{N}(x_i - \overline{x})^2} \qquad (4.8)$$

Skewness is a measure of symmetry and is a normalized form of the third-order moment about the mean. Skewness is defined in Equation 4.9.

$$Skewness = \frac{1}{N-1}\sum_{i=1}^{N}(x_i - \overline{x})^3 \qquad (4.9)$$

where $\overline{x}$ is the mean value.

Kurtosis and skewness are extracted from two statistical moments used to describe the shape of the distribution curve of signal data.

4.3.2.6 Standard Deviation (SD)

$$SD = \sqrt{\frac{1}{N}\sum_{i=1}^{N}(x_i - \overline{x})^2} \qquad (4.10)$$

4.3.2.7 Frequency Domain Features

To extract sensing features in frequency domain, Fast Fourier Transform (FFT) is normally used to obtain the frequency spectrum of time domain signal. The FFT of *x(t)* can be calculated by Equation 4.11 and the inversion of Fourier transform of *X(f)* can be calculated by Equation 4.12, where *t* stands for time, *f* stand for frequency, *x* denotes signal in time domain, *X* denotes the signal in frequency domain.

$$X(f) = \int_{-\infty}^{\infty} x(t)e^{-2j\pi ft}\,dt \qquad (4.11)$$

$$x(t) = \int_{-\infty}^{\infty} X(f)e^{2j\pi ft}\,df \qquad (4.12)$$

In this study, some statistical features used in feature extraction were summarised as follows:

-*Mean Frequency* is defined as the average frequency content in the discrete time.
-*Maximum Frequency (magnitude)* is the frequency content having the maximum magnitude or peak magnitude or the highest point of the spectrum.
-*Peak Magnitude* is the highest magnitude or the magnitude of maximum frequency.
-*Maximum per Mean Magnitude Ratio* is the ratio between maximum and average magnitude in the discrete time.

4.3.3 Feature Selection

Based on the literature it appeared that the techniques mostly likely to be suitable to evaluate the best feature set to be used for training the neural network were as follows

4.3.3.1 Feature Selection Based on Correlation Coefficient

Using correlation coefficient (R), sometimes known as cross-correlation, is a simple way used to select the features. This value represents the linear relationship between two variables; inputs and targets. The R value lies on from – 1 to + 1. Generally, a correlation which is greater than 0.8 is defined as strong, while a correlation less than 0.5 is generally described as a weak or non-linear relationship. The plus sign refers to positive correlation, i.e. y increase while x increases, and negative correlation means that y decrease while x increases.

To evaluate the relationship between extracted features and flank wear width, their correlation coefficients are calculated and ranked in descending order. The features having low correlation level with the flank wear should not be used as feature input of network training as they have no linear relationship or weak relationship between features and the flank wear. This correlation coefficient was used to select a feature set for tool wear classification and regression which is discussed in detail in Chapter 7. Typically, the correlation coefficient between a selected feature x and a tool wear value y can be expressed in Equation 4.13.

$$R = \frac{n\sum xy - (\sum x)(\sum y)}{\sqrt{n(\sum x^2) - (\sum x)^2}\sqrt{n(\sum y^2) - (\sum y)^2}} \qquad (4.13)$$

A previous study used the correlation coefficient in feature selection to find the features that can best characterise tool wear conditions [117]. The result showed that the network trained by the features having high correlation coefficient had rate of success in tool wear detection about 96%. Therefore, this coefficient will be used in this study in order to select the best correlated feature set for training the neural networks in Chapter 7.

4.3.3.2 Correlation Based Feature Selection (CFS) by WEKA

Correlation-based feature selection (CFS) is a well-known algorithm used to determine feature sets that are highly correlated with the class. WEKA is an open source software which is developed by machine learning group at the University of Waikato, New Zealand [118]. WEKA offers a collection of machine learning algorithms for data mining tasks. The algorithms can be easily directly applied to a dataset or called from the Java code. It provides several tools for data pre-processing, classification, regression, clustering, association rules, virtualisation and feature selection.

The selection methods and search methods available in WEKA are shown in Table 4.2, Searching algorithms can be used to provide possible feature sets and to test their performance and the software suggests the selected attributes that have a high correlation with the class. In this study, *cfsSubsetEval* was used as an evaluator and four searching schemes including greedy step wise, genetic search, evaluation search, and linear forward selection were chosen to find the best feature set for training the neural network. The results of this simulation are further discussed in Chapter 7.

Table 4.2 Attribute Evaluator and Search methods for Feature Selection [118]

	Name	Function
Attribute Subset Evaluator	*CfsSubsetEval*	Consider the predictive value of each attribute individually, along with the degree of redundancy among them
	ClassifierSubsetEval	Use a classifier to evaluate the attribute set
	ConsistencySubsetEval	Project training set onto attribute set and measure consistency in class values
	CostSensitiveSubsetEval	Makes its base subset evaluator cost sensitive
	FilteredSubsetEval	Apply a subset evaluator to filtered data
	WrapperSubsetEval	Use a classifier plus cross-validation
Search Methods for Attribute selection	*BestFirst*	Greedy hill climbing with backtracking
	ExhaustiveSearch	Search exhaustively
	GeneticSearch	Search using a simple genetic algorithm
	GreedyStepwise	Greedy hill climbing without backtracking; optionally generate ranked list of attributes
	LinearForwardSelection	Extension of *BestFirst* that considers a restricted number of the remaining attributes when expanding the current point in the search
	RaceSearch	Use race search methodology
	RandomSearch	Search randomly
	RankSearch	Sort the attributes and rank promising subsets using an attribute subset evaluator
	SubsetSizeForwardSelection	Extension of *LinearForwardSelection* that performs an internal cross-validation in order to determine the optimal subsetsize

4.4 Background & Development of Data Processing

This section discusses the use of artificial intelligence for tool condition monitoring, including; its use in tool condition monitoring, the typical neural network structures and training parameters used, and the methods used to train, validate and evaluate the tool wear prediction and tool wear state classification models in this study.

According to Siddhpura [9], AI techniques used for decision making in tool condition monitoring system (TCMS) consist of Artificial Neural Networks (ANN), fuzzy logic, neuro-fuzzy, Hidden Markov model, and Support Vector Machine (SVM). The first three techniques are widely used in TCMS and were alreaday discussed in Chapter 3 (Section 3.6). Also, some of literatures have been reviewed previously in Section 4.2.3 and 4.3.1. Further extensive reviews can be found in [10, 79]. Some of the previous attempts of neural network for TCMS are discussed in the next section.

4.4.1 Previous Attempts of Neural Networks for Tool Condition Monitoring

Broadly, network training can be classified into supervised and unsupervised learning methods. The supervised neural networks are used to present the network trained by teaching them with input patterns and expected output patterns. The error between actual and predicted outputs is used to modify the weight of the connections between neurons. Unsupervised neural networks are used to classify the data without prior knowledge of the classes involved. Only input patterns are fed during training and the neural network automatically clusters them in groups with similar features.

In supervised learning, backpropagation (BP) neural networks, which are multiple-layered feedforward neural networks, have been often used in TCM for various machining processes as can be seen in the reviews of Teti and Siddhpura [9, 79]. This neural network is a multilayer perceptron (MLP), which is trained by using backpropagation method [26]. The term backpropagation refers to the way that the error computed at the output side is propagated backward from the output layer to the hidden layer and to the input layer in finally.

The applications of neural networks in TCMS can be applied for two broad categories. First category is function approximation, or regression, including time series prediction and modelling, which is used for tool wear prediction. Second is classification, including pattern and sequence recognition, which is used for tool wear state classification and decision making.

Many studies used neural network for classify the tool wear state. For example, Silva *et al* [108] used an unsupervised neural network (self-organising map and adaptive resonance theory) and expert system to fuse statistical features based on frequency spectra of spindle current, force, vibration, and sound sensors to classify the tool wear state in turning operation. Dimla *et al* [119] used a neural network based tool condition monitoring system to classify cutting tool states in turning process. The training

features were extracted from cutting force and vibration and were fed into MLP neural network with different number of node in hidden layer (1-100). The proposed system was found to be able to classify tool state in excess of 90% accuracy but deteriorated when the cutting conditions were significantly changed. Segreto *et al* [114] developed tool wear state classification in turning by using a neural network. The significant features of cutting force, AE, and vibration which were selected by principle component analysis (PCA) were fed into the feed-forward back-propagation neural network to classify the state of tool wear. They suggested that the highest success rate in tool wear classification obtained from the sensory feature of three sensors. This was in agreement with the studies of Silva *et al* and Dimla *et al* [108, 119] that using features from multiple sensors can improve the classification accuracy.

In the case of tool wear prediction, Zhou *et al* [120] monitored flank wear of a CBN tool in precision hard turning by the use of artificial neural network. The passive force level, the frequency energy and the accumulated cutting time were used to train the neural network in order to predict tool flank wear. They claimed that the developed monitoring system is robust and good consistent for tool wear monitoring in precision hard turning. Similarly, Natarajan *et al* [121] used back-propagation feed forward neural network for tool life prediction. They used cutting speed, feed, depth of cut, and flank wear were taken as inputs and tool life as an output parameters. They proposed the evolutionary technique (particle swarm optimisation) to predict tool life and the results of these two methods matched very well.

Some authors have applied neural network techniques to develop the artificial model for both flank wear estimation and wear state classification purposes. In the study of Tangjitsitcharoen *et al* [113], back propagation neural network was used to fuse the sensory features from cutting forces, sound, vibration, and AE in order to estimate the tool wear and detect the change of cutting states (continuous chip, broken chip and the chatter). The neural network model can be effectively classified by sensor features. Lui *et al* [122] applied neural network to develop tool wear monitoring system for automated boring machine. They used counterpropagation neural network (CPNs) with the cutting force data and the output was tool wear state and the value of tool wear. Several network structures were tested to find the best network structure for real-time recognition of tool wear states and real-time measurement. They claim that their network can be able to predict tool wear state with 100% of accuracy, while tool wear value prediction can meet a minimum error about 8.5%. It is assumed that their model can successfully achieve 100% because only two classes (usable and worn-out tools) were used for tool state recognition, and only 48 training data was obtained from the machining experiment and other data for training comes from linear interpolation.

Other authors have applied neural networks for surface roughness estimation in turning process. Wilkinson *et al* [123] used a back-propagating neural network from five input features to predict the tool wear states. The input features were extracted

from the AE signal and physically measured surface profiles that were produced during the machining of EN24 steel. The surface finish features can be obtained from either an off-line profilometer measurement or on-line during machining operations by using a high resolution microscope camera. They classified tool wear into three states: light, medium and heavy wear. Other utilisation of neural network in surface roughness estimation can be found in the work of Asiltuerk *et al* and Risbood *et al* [33, 124].

An interesting survey of artificial neural networks (especially used in turning) was reviewed by Sick [16] in year 2002. This review paper has been published the almost two decades. It review paper evaluates the 138 publications which are based on indirect, continuous monitoring, and use neural networks for tool wear monitoring. Several methods applied in monitoring tasks were compared and the methodologies used to select certain methods, to carry out the simulation experiments, to evaluate and present results also were suggested.

4.4.2 Development of Neural Network for Tool Condition Monitoring

The application of neural networks in the work presented in this thesis can be grouped into two categories: tool wear prediction and tool wear state classification. Using a supervised leaning scheme, the neural networks have trained by the training data which are sensory features extracted from the sensor signals and the flank wear values. Figure 4.23 shows the diagram of the off-line training procedure to obtain prediction and classification models.

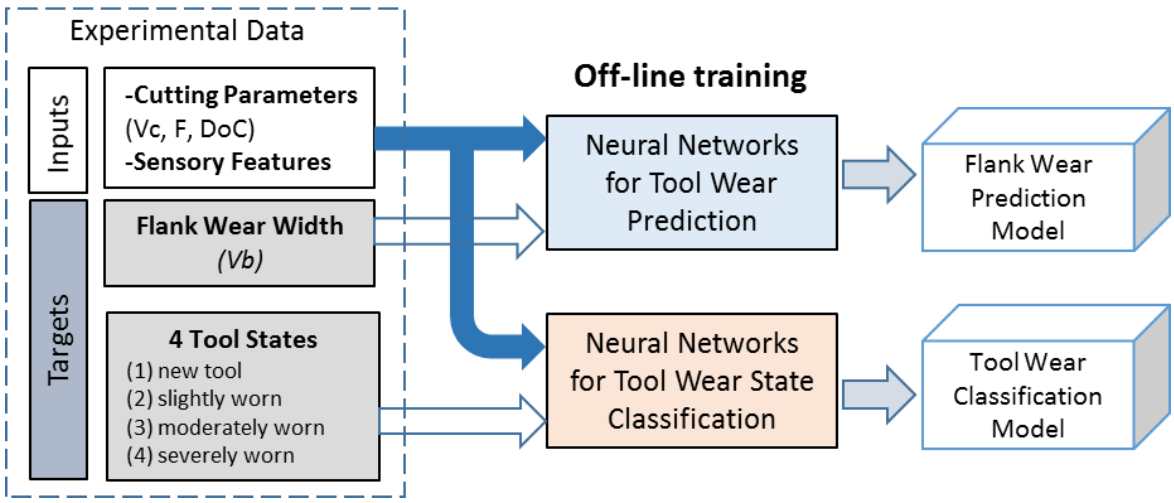

Figure 4.23 Diagram of off-line neural network training procedure for flank wear prediction and classification

The input vector and the target vector, both experimentally measured values obtained from the machining experiment, will be fed into the feed forward neural networks for training. With respect to the network targets, tool wear prediction is categorised in the fitting or regression problem that the targets used for training the network should be a

numeric value (i.e. flank wear width, V_b), while the targets for training the classification model could be a numeric or character value (i.e. class 1-4).

The tool wear prediction and classification models are used on-line during machining operation to monitor the progression of flank wear and the current tool wear state, and the decision is then made (Figure 4.24).

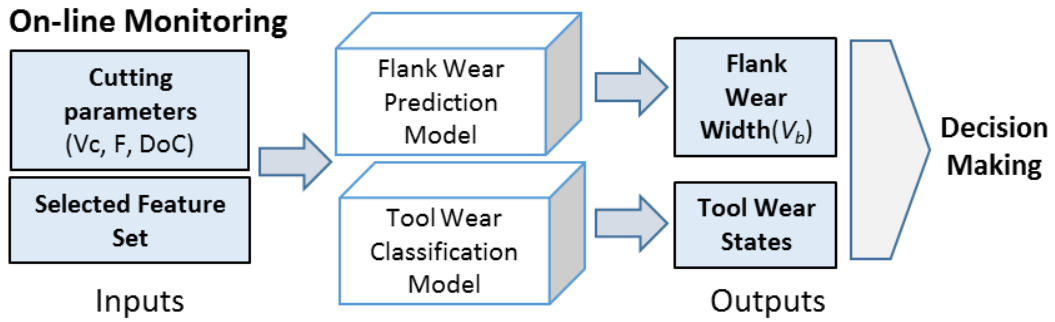

Figure 4.24 Diagram of on-line tool condition monitoring

The inputs to the models are the features obtained from the sensor signals and cutting conditions. The prediction and classification models can then determine both the current flank wear values and the tool wear state at different rotational speeds and feed rates. After that, remaining useful life can be estimated. This will be further discussed in more detail in Chapter 7.

According to Basheer *et al* [26], there are several types of artificial neural network available for performing the monitoring task. In this study, the backpropagation (BP) network, which is the multilayer perceptron (MLP), was applied to fuse the selected-input features and its output predicts both tool wear state and current wear values as this type of neural network is favourable and widely used for data modelling and classification. This network also provides great performance with a short training time.

The typical architecture of MLP neural network (single hidden layer) is shown in Figure 4.25.

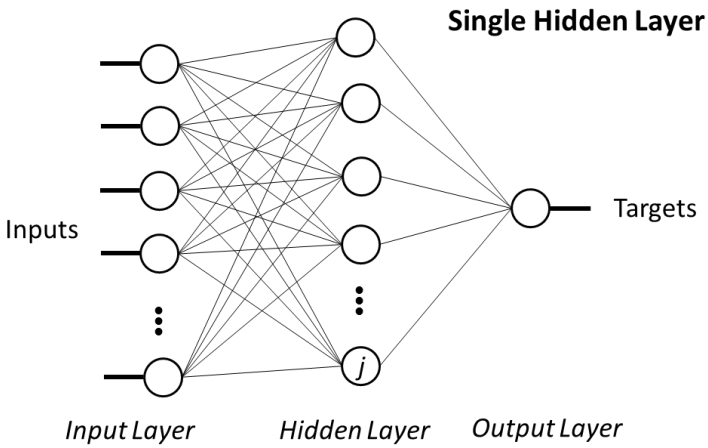

Figure 4.25 Architecture of multilayer perceptron neural network

It consists of an input layer, one or more hidden layers, and an output layer. The nodes in hidden layer, known as hidden nodes, process the information received from the input layer and pass them over the output layer. In this network, the data are fed forward into the network without feedback. The number of input nodes is equal to the number of selected input features; the output layer has only 1 node. In this study, both single and double hidden layers are used and the number of nodes in hidden layers will be varied. The configuration of neural networks used in this study will be described in Chapter 7.

The network was trained off-line by training patterns. Multifold-cross validation (Section 4.4.3) was performed in order to obtain the highest performance network structures in tool wear prediction, while 70/30 training and testing ratio was used for data training in tool wear state classification.

To determine the best network configuration, several neural network architectures were created by changing the network parameters. The neural networks with different activation or transfer functions and training algorithms were used to produce the artificial models for flank wear prediction and tool wear classification.

Comparison between the actual tool wear and the predicted results from neural networks was verified statistically e.g. mean absolute error (MAE), root mean square (RMS) error, and sum square error (SSE). After evaluating the combinations of several networks, the neural network with the lowest error was chosen.

As for the classification model, the performance of tool wear state classification was examined by percent of classification accuracy. Considering the confusion matrix is commonly used to evaluate the accuracy of the classification model. These network performance evaluators will be described in Section 4.4.4.

For the work presented in this thesis all of the neural network design and development was carried out using the Neural Network toolbox in MATLAB.

4.4.3 Multifold Cross-Validation Method

This study has a relatively limited amount of data for training and validation, total of 506 cycles of cutting from seven cutting conditions, multifold cross-validation have been adopted for training the network, in regression problem of flank wear width prediction, to obtain better generalisation training error. The training data set was applied as a validation data set. This method used where the network was trained K times. The training data set with N samples was grouped into K partitions.10 folds are commonly used in network training. In Figure 4.26, all data sets are evenly distributed into 10 folds. Nine folds or 90% of all data sets are used for training the network, apart from that (10%) is used for validation.

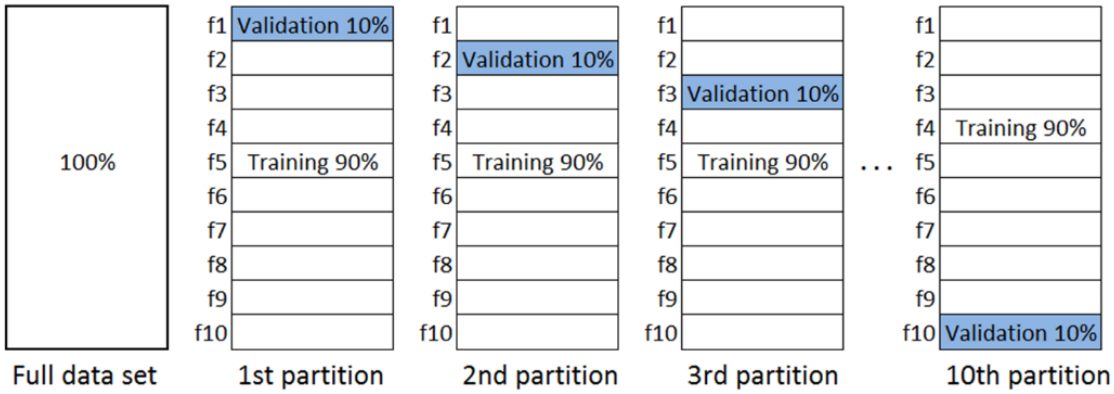

Figure 4.26 The 10-fold cross validation scheme

The network was firstly trained with the data from f2 to f10 which is therefore defined as the training set and excludes the validation set (f1). The training process was repeated ten times by leaving out the validation set.

The performance of the resultant network was evaluated by averaging the mean squared errors or classification error over all ten training partitions. It is also called leave-one-out training process if k is equal to 1. This technique is used when the amount of data is inadequate. However, several studies advise that the multifold cross-validation method performs better performance than the leave-one-out method in terms of approximating generalisation errors. This multifold cross validation method was also implemented in the present work in the part of the flank wear prediction.

4.4.4 Performance Evaluation of the Prediction models

4.4.4.1 Prediction Accuracy of Tool Wear Value Estimation

After training, the performance of the neural networks used for flank wear prediction was tested with a new set of input features against an expected tool wear value. The predicted wear values are then compared with this expected or actual target to find the representative network with high accuracy for tool condition monitoring system.

In tool wear prediction, three criteria calculated by Equation 4.14 - 4.16 were used to compare the accuracy of prediction models where y_i' and y_i are predicted value and actual value of the tool wear, respectively. N represents the number of observations.

Root Mean Square Error (RMSE)

$$RMSE = \sqrt{\frac{\sum_{i=1}^{N}(y_i' - y_i)^2}{N}} \tag{4.14}$$

Mean Absolute Error (MAE)

$$MAE = \frac{\sum_{i=1}^{N}|y_i' - y_i|}{N} \tag{4.15}$$

Sum of Square Error (SSE)

$$SSE = \sum_{i=1}^{N}(y_i' - y_i)^2 \tag{4.16}$$

4.4.4.2 Classification Accuracy of Tool Wear State

The performance of tool wear state classification can be also evaluated by three criteria mentioned in Section 4.4.4.1 where the classification task is a numeric prediction. It can also be determined by confusion matrix. In a multiclass classification, the result of a test set is often shown by two dimensional confusion matrix with a row and column for each class. The example confusion matrix is shown in Figure 4.27, where the rows show the predicted class (output), and the columns show the actual class (target).

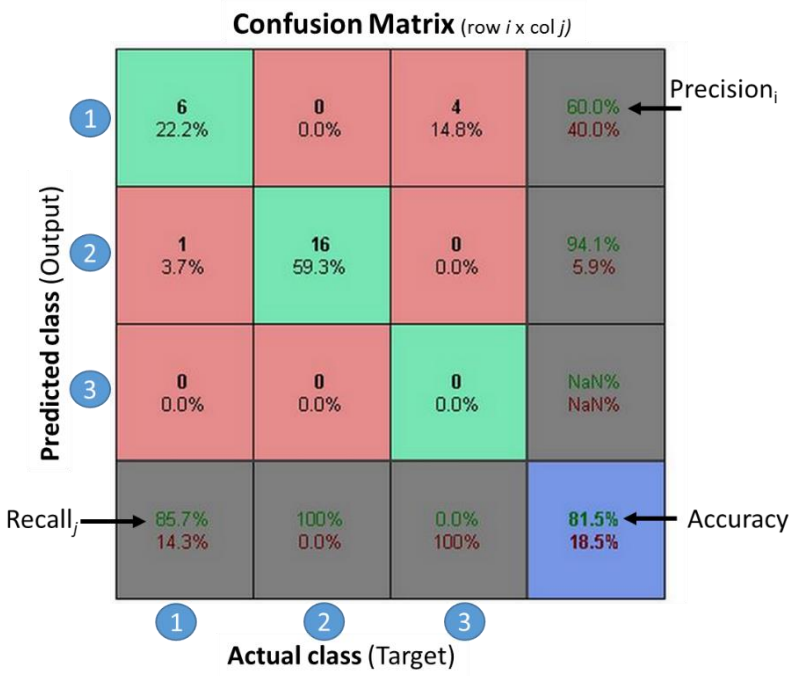

Figure 4.27 An example of confusion matrix used to determine the accuracy of the classification

In confusion matrix evaluation, a good result corresponds to large numbers down the main diagonal and small off-diagonal cells. From the matrix in Figure 4.27, the test set has 27 instances (the sum of the nine numbers in the matrix), and 6+16+0 = 22 of them are predicted correctly, and the percentage of correctly classified instances or overall accuracy is 81.5 %. From the confusion matrix (m x n), four basic evaluators of classification performance can be calculated with Equation 4.17 - 4.20.

$$Accuracy = \frac{\sum_{i=1}^{n} M_{i,i}}{\sum_{i=1}^{m}\sum_{j=1}^{n} M_{i,j}} \tag{4.17}$$

$$Precision_i = \frac{M_{i,i}}{\sum_{j=1}^{n} M_{i,j}} \tag{4.18}$$

$$Recall_j = \frac{M_{j,j}}{\sum_{i=1}^{m} M_{i,j}} \tag{4.19}$$

$$F = \frac{2 \times precision \times recall}{precision + recall} \tag{4.20}$$

Accuracy is the fraction of correct predictions. The diagonal cells of confusion matrix show where the actual class is equal to predicted class and the off diagonal cells show instances where the classifier has made incorrectly. The column on the right hand side shows the accuracy for each predicted class, while the row at the bottom shows the accuracy for each actual class. The cell at the bottom right shows the overall accuracy (81.5% of correct and 18.5% incorrect classification).

Precision is the proportion of instances predicted to this class that are correctly classified. It is calculated as TP / (TP+FP) where TP and FP are the number of true positive and false positive predictions for the considered class (*i*) and (TP+FP) is the sum of the instances in the corresponding row *i* (excluding the TP).

From confusion matrix in Figure 4.27, precision of predicted class 1, 2, and 3 are determined as bellows.

$$\text{Precision}_1\ (\%) = TP_1 / (TP_1 + FP_2 + FP_3) = 6 / (6+ 0+4) = 60\%$$

$$\text{Precision}_2\ (\%) = TP_2 / (TP_2 + FP_1 + FP_3) = 16 / (1+16+0) = 94.1\%$$

$$\text{Precision}_3\ (\%) = TP_3 / (TP_3 + FP_1 + FP_2) = 0 / (0+0+0) = \text{NaN}\ \%$$

Recall (also called sensitivity) is the proportion of actual instances of this class that are correctly classified. It can be calculated as TP / (TP+FN) where TP and FN are the number of true positive and false negative predictions for the considered class (*j)* and (TP+FN) is the total number of instances of the considered class (i.e. the sum of the column *j*)

$$\text{Recall}_1\ (\%) = \text{Sensitivity}_1 = TP_1 / (TP_1 + FN_2 + FN_3) = 6 / (6+1+0) = 85.7\%$$

$$\text{Recall}_2\ (\%) = \text{Sensitivity}_2 = TP_2 / (TP_2 + FN_1 + FN_3) = 16 / (16+0+0) = 100\%$$

$$\text{Recall}_3\ (\%) = \text{Sensitivity}_3 = TP_3 / (TP_3 + FN_1 + FN_2) = 0 / (0+4+0) = 0\%$$

In some circumstances, having the precision and recall can make it difficult to compare classifiers. For example, that one classifier has better precision and the other has better recall. To make comparison easier, precision and recall are sometimes combined into single value such as *F* value in Equation 4.20.

In conclusion, these evaluators mentioned previously will be used to determine the best tool wear prediction and tool wear state classification models and will be discussed in Chapter 7.

Chapter 5

Coating-depth Evaluation Using Barkhausen Noise Technique

This chapter describes an offline measuring technique which can use on the shop-floor in order to measure the thickness of the remaining coating layer of a coated cutting tool. The chapter is organised as follows: firstly, details about the hob cutter used in the gear cutting process and previous studies focusing on case-depth evaluation are introduced. Then, the measuring system and experimental setup are described followed by the results and conclusions

5.1 Introduction

Gears are commonly employed as components machine drive trains of all sizes and applications. They are primarily produced by a machining process known as hobbing which produces externally toothed cylindrical gears. The hobbing process plays a key role in gear manufacturing because of its high efficiency. An example of a gear hob is shown in Figure 5.1.

Figure 5.1 TiN-coated cutter for hobbing process

There is a wide range of cutting tool materials used in machining processes as discussed in Chapter2. These tool materials have different characteristics and use. Hobbing tools are typical produced from high speed steel (HSS) due to the relatively low cutting speed requirements of the process. They are usually coated for reasons of tool life and scope for increased cutting speeds (10%-20%) over uncoated HSS if desired. Commonly used coating materials are titanium nitride (TiN) (Figure 5.1), titanium carbide (TiC), titanium carbonitride (TiCN), and aluminium oxide (Al_2O_3). The coated layer of the tool is typically 2-15 microns in depth. The advantages of coated HSS tools over plain HSS are reduced tool wear, higher hardness, and lower coefficient of friction against typical workpieces [125].

Figure 5.2 Breakage of hob cutter

The coating material can improve the effective hardness of the HSS tools. Normally, the hardness of coated cutting tools is about R_c 80-85 compared to R_c 65-70 for uncoated HSS tools. Consequently, abrasion wear is reduced. As TiN has relative inertness, adhesion processes driven by chemical affinity between chips and cutting tools could also be reduced, which results in longer tool life. The reduction in coefficient of friction can allow an increase in the shear angle, which results in reducing in the cutting forces, spindle power, and heat generated by the deformation processes during machining.

TiN coated tools provide good cutting performance at higher cutting speeds and feeds. Flank wear of coated tools is significantly lower than uncoated tools [126, 127] and flank surface can be reground when it is dull. However, in the case of low cutting speeds, the coated tools do not perform well because the coating can be worn off by chip adhesion [1]. Cutting fluids are needed to reduce the effect of this adhesion.

It is generally viewed that reduced tool wear means longer tool life and leads to less material removal during tool regrinding. Hobs are repeatedly re-ground and the dimensions of the individual teeth gradually reduced significantly. Teeth eventually fail by brittle fracture after excessive wear (Figure 5.2). As a TiN coated hob cutter can cut 300 gears per sharpening, but an uncoated tool cut only 75 gears [1], the use of coatings is clearly important to maintaining productivity. Problems arise as the hobs are getting close to the end of their life (i.e. nearly all of the coating has been removed) because operators cannot easily tell the life remaining by a visual check. This leads to the hob failing during the process.

Traditional destructive methods such as micro-hardness profiling and metallography are used to evaluate the depth of coated layer; however, they are destructive, expensive, time consuming, and not suitable for in-line or in-process monitoring. It is therefore, a desire of this industry to have some cost-effective tools or equipment to monitor the coated layer of hob cutter.

Recently, several non-destructive methods have been developed in attempts to characterise a material below its surface. For ferrous materials, techniques aiming to make use of the differential permeability and saturation magnetization in the material, particularly, were studied to find its relationship to the depth of case hardening. Many magnetic methods have been attempted to evaluate hardness and case depth such as a Barkhausen effect, magnetic hysteresis properties, and magnetoacoustic emission. These methods are discussed in Section 4.1.1 - 4.1.3.

It is proposed in this study, that a novel magnetic measuring system based on BHN technique could be developed in order to measure the coated layer of high speed cutting tool as in a similar fashion to the use of magnetic methods to measure case hardening.

This study focuses on measuring the thickness of the coated layer of high speed cutting tools by using BHN techniques. Firstly, the characteristic of pick-up coils was identified to find the most sensitive one for use in this study. Three pickup coils varying the number of turns were used to receive the BHN signal from the induced material surface and then were compared. Additionally, the effect of exciting frequency was studied in order to find the influence of exciting frequency on BHN signal. Finally, coated high speed steels with different coated materials and thickness will be tested by the proposed BHN measuring system. Some useful signal features such as Root-Mean-Square, maximum peak amplitude, peak count, skewness, kurtosis, and signal energy were used to correlated with the thickness of coated layer.

5.2 Literature Reviews

As discussed in Chapter 4, Barkhausen noise (BHN) can be applied to certain applications, such as material deformation, fatigue, grinding burn evaluation, and case-depth evaluation. It has been found that BHN activity (peak amplitude and signal energy) increases significantly with tensile stress, and decrease under compressive stress [128]. As also found in Moorthy *et al*, Vincent *et al*, and Lindgren *et al* [48, 128, 129], they confirm that the BHN technique can be used to classify the different stages of fatigue and can also be applied in grinding burn detection [42, 50, 58]. They used low and high frequency measuring systems to detect grinding burn. A single-peaked BHN profile obtained by high frequency measurements can be well used to be correlated with the residual stress change due to grinding burn.

The surface condition of the workpiece has a direct effect on the fatigue life of the materials. Heat treatments such as carburising and induction hardening are normally used to create a hard and a wear resistant layer on top of the softer interior. These processes can change the metallurgical properties of the workpiece at certain depth below the surface. This hardened layer depth can be used to evaluating the life. The methods such as metallographic analysis, micro-hardness measurement at the cross-

section, and direct carbon content evaluation by chemical or spectrographic methods, are normally used to evaluate the case-depth [130]. These are destructive methods, are very time-consuming, and cannot be used on-line. This increases the need of a reliable and non-destructive method for the case-depth measurement.

Generally, the evaluation of case depth can be performed by BHN measurement which is based on the hardness difference of the hardened case and the soft core of the material [60]. Several studies concluded that two-peaked BHN profiles are obtained when the hardening depth is measured by BHN technique [131-133]. It is found that the first peak at a lower applied field strength corresponds to the soft core and the second peak corresponding to the hardened case. The ratio of these two peaks can be used to represent the case-depth. The two peak profiles are not always found as reported in Dubois *et al* and Moorthy *et al* [41, 132]. Moorthy *et al* observed that the second peak cannot be found if the case depth is too deep and they suggested that the two peak profiles can be found when the case depths up to 1 mm, and then case depth can be determine by the ratio of two peak heights [132]. To increase sensitivity of BHN profile, Blaow *et al* suggested that an increase of the excitation field strength can increase the height of both peaks. The peak at a higher field increases significantly compared to one at lower field [134].

Possibly, the hardened surface undergoes a decarburising process where the surface layer softens. Conversely, a single-peaked profile transforms into a two-peaked one where decarburisation occurs as reported in Blaow *et al* [61]. Also, the height of the second peak at higher applied field strengths increased with increasing depths and the peak position shifted to lower field strengths. According to Stapakov *et al* [135], the RMS value first increases, then followed by a decrease with an increasing depth of the decarburised layer.

The case-depth of many steel types treated by carburising and nitriding was studied by Dubois *et al* [41] and they confirmed a success of harden depth evaluation by using BHN technique. The case depth measurement in EN36 gear steels were studied by Wilson *et al* [42]. They concluded that the peak amplitude of BHN decreases with an increase of case depth. Santa-aho *et al* [47] observed the same relationship between the RMS value and the case depth. They also proposed a new approach to detect the case depth by using voltage and frequency sweeps to evaluate the thickness of the surface layer. The BHN magnetising sweeps technique was used to measure the case-depth in hardened steel. It is observed that the ratio of two voltage sweeps with different frequencies produces a good estimation of the case depth. Drehmer *et al* [64] applied BHN measurement for estimating the case depth of SAE 1020 steel. They used RMS barkhausen pulse envelope and the FFT to estimate case depths successfully, and the normalised power index (NPI) was proposed to estimate case depths if the properties of the surface layer and core are considerably different.

This study aims at investigating the suitable methodology for measuring coated layer depth of coated cutting tool based on BHN measurement. However, this subject has not been well studied in literature and thus it is great interesting to find feasibility to use BHN technique for monitoring coated layer in coated high speed cutting tool.

5.3 Experimental Methodology

5.3.1 Specimen Preparation

The specimen used in this study is HSS (M2) and the composition of HSS (M2) is shown in Table 5.1. The HSS, dimension 25 x 50 x 5 mm, were coated with two coating materials: chromium nitride (CrN, silver colour) and titanium nitride (TiN, gold colour) as shown in Figure 5.3.

The coated specimens were prepared by electron beam plasma assisted physical vapour deposition (EBPAPVD). The Tecvac/Wallwork IP70 was used to coat TiN and CrN on the HSS specimens. The process temperature was about 450 °C and 10 x 10^{-3} mbar of process pressure. The thickness of coated layer was measured by Fischerscope XRF. Three levels of coating thickness are approximately 5, 10, and 15 μm as listed in Table 5.2.

Table 5.1 Composition (% by weight), HSS(M2)

	Fe	C	Si	Mn	P	S
HSS (M2)	balance	0.78/1.05	0.20/0.45	0.15/0.40	0.03	0.03
	Cr	Mo	Ni	W	V	Cu
	0.20/0.45	4.50/5.50	0.3	5.50/6.75	1.75/2.20	0.25

Table 5.2 Coated HSS specimens used in this study

Coating Materials	Depth (micron)
CrN-5u	5.1
CrN-10u	10.9
CrN-15u	14.4
TiN-5u	5.0
TiN-10u	10.9
TiN-15u	14.4

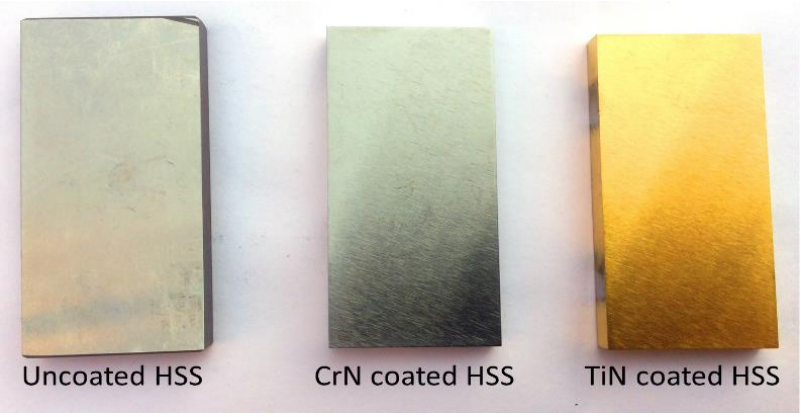

Figure 5.3 CrN/TiN coated Specimens with varying case-depth layer

Note: The CrN/TiN coated-HSS specimens were prepared by a third-party company.

5.3.2 Tools and Equipment

The BHN signals are processed and evaluated electronically as shown in Figure 5.4. Tools and equipment used in the BHN measuring system are described previously in of Chapter 4. In-house electronic equipment was designed and built specifically for these experiment to maximise the chance of success (Section 4.1.5). Also, the design of exiting coil and pick-up coils is also described in Chapter 4 (Section 4.1.6). The experimental setup of the BHN measuring system is shown in Figure 5.5.

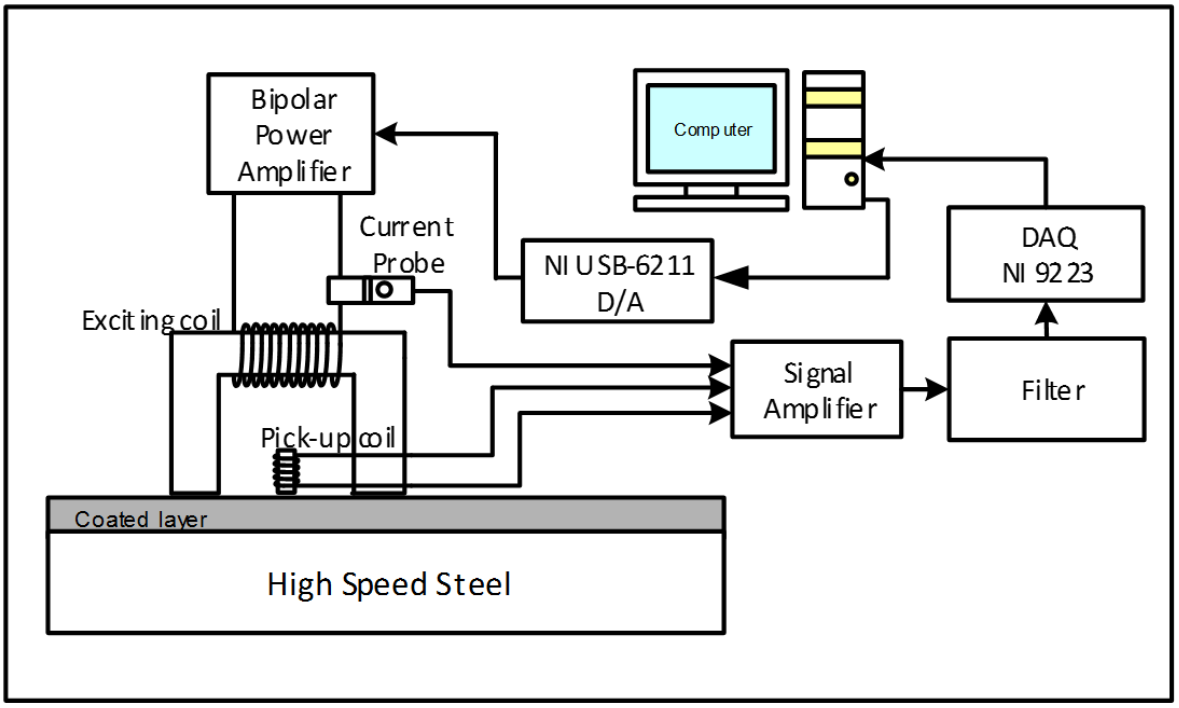

Figure 5.4 Experimental setup

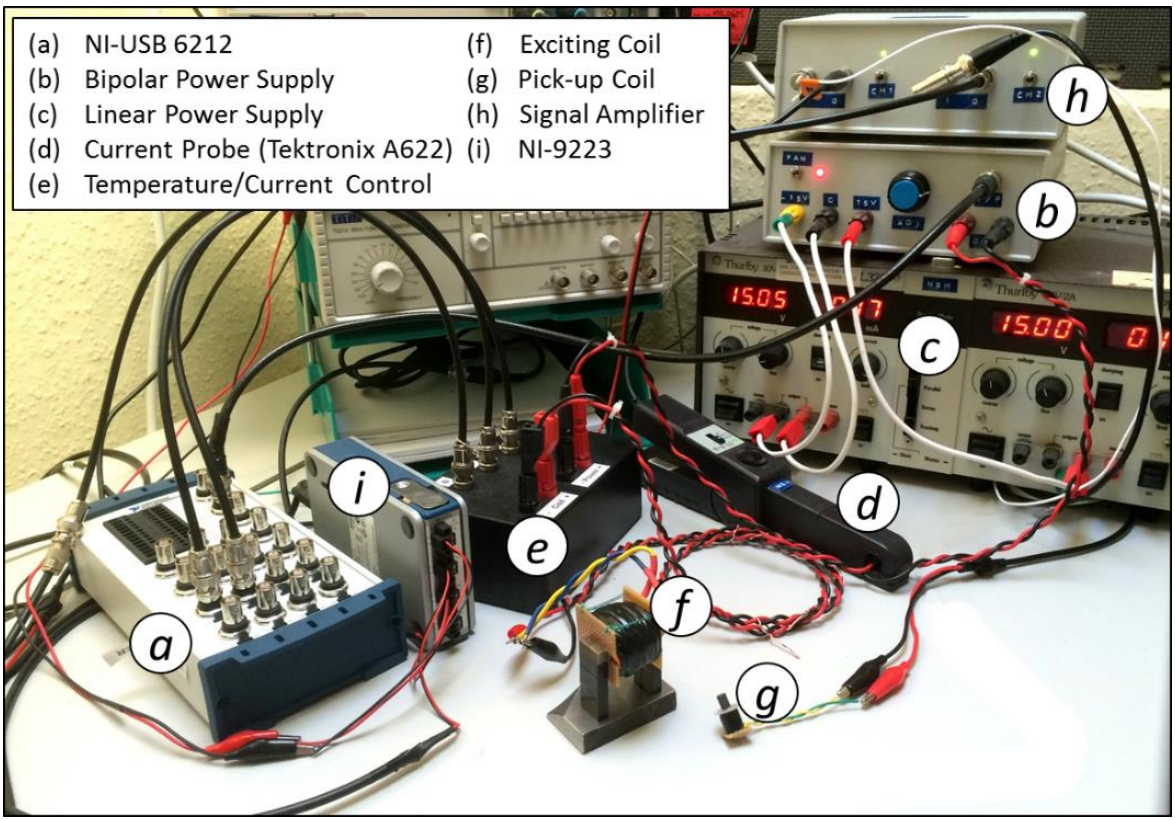

Figure 5.5 The BHN measuring system used in this study

In Figure 5.5, a National Instruments-USB 6212 (*a*) was used for generating the exciting current signal to a magnetic yoke (*f*) at specific exciting frequency (f_e) controlled by LabVIEW. This exciting signal was then magnified by a bipolar power amplifier (*b*) to gain current signal up to 1 A for the exciting coil (*f*) made from copper wire wound around the Fe-Si lamination core. A current probe (*d*) was used to monitor the magnetising current, the actual current in the exciting coil to calculate the magnetic field strength (H) to the workpiece, and also for damage prevention due to over current.

The magnetic flux from the excited coil flows through the specimen via the yoke's poles. A search coil or pick-up coil (*g*), picks up the BHN signal from the specimen. The relatively low level of BHN signal was amplified by custom design signal amplifier (*h*) to a suitable level for subsequent signal processing. All signals were amplified and filtered before processing the signals via a personal computer interfaced by a National Instruments-9223 put in the cDAQ-9171 (*i*). Post signal processing and feature extraction was performed by MATLAB (described in Section 5.3.3).

5.3.3 Signal Processing and Feature Extraction

The BHN signal was sampled at 200 kS/s with 70 dB of amplification gain. The raw signal was first filtered by high-pass filter at 1 kHz of the cut-off frequency to remove unwanted frequency. The signal of each measurement was collected for five seconds. For sensory feature extraction, the signals generated within two complete magnetising

cycles were used in the calculation; however, to eliminate a contamination of other unexpected noises at the beginning of a measurement, only signals collected after one second were selected.

The typical BHN signal (in the time domain) received from the pickup coil is shown in Figure 5.6*(a)* and the frequency bandwidth of the BHN signal is in the range of 0.5 – 6 kHz as shown in Figure 5.6*(b)* where the exciting frequency = 5 Hz.

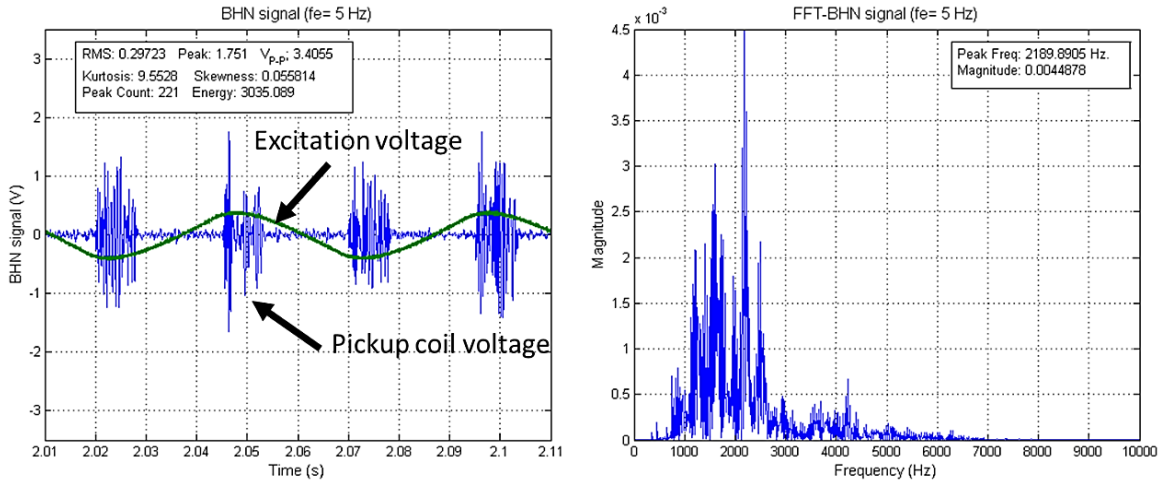

(a) *(b)*

Figure 5.6 *(a)* Typical excitation voltage and the MBN signals in time domain, and *(b)* typical frequency spectra of MBN signals acquired using pick-up coil in 1-6 kHz range.

In this study, only time-domain and statistical features were extracted from the selected signal, such as RMS, peak amplitude, peak-to-peak voltage, skewness, and kurtosis. Peak count and signal energy (area under peaks) were also used in this chapter as they could be useful to indicate the intensity of burst signal like BHN signal.

The peak count and signal energy were calculated from the absolute signal amplitude as shown in Figure 5.7*(a)*. The peak points of the BHN signal in Figure 5.7*(b)* were counted if they are higher than the predefined threshold value and defined as 'peak count'. This feature was also used in the studies of Vashista *et al* [136] but they defined it as an 'event' and they used it to make an assessment of residual stress in surface ground component.

Signal energy, the area under peaks of the absolute BHN signal amplitude over the fixed period, as shown in Figure 5.7*(a)* and it can be calculated by graphical calculation method which also proposed by O'Sullivan *et al* [137]. However, it can also be easily determined by trapezoidal numerical integration function in MATLAB and it was this numerical method used in this study.

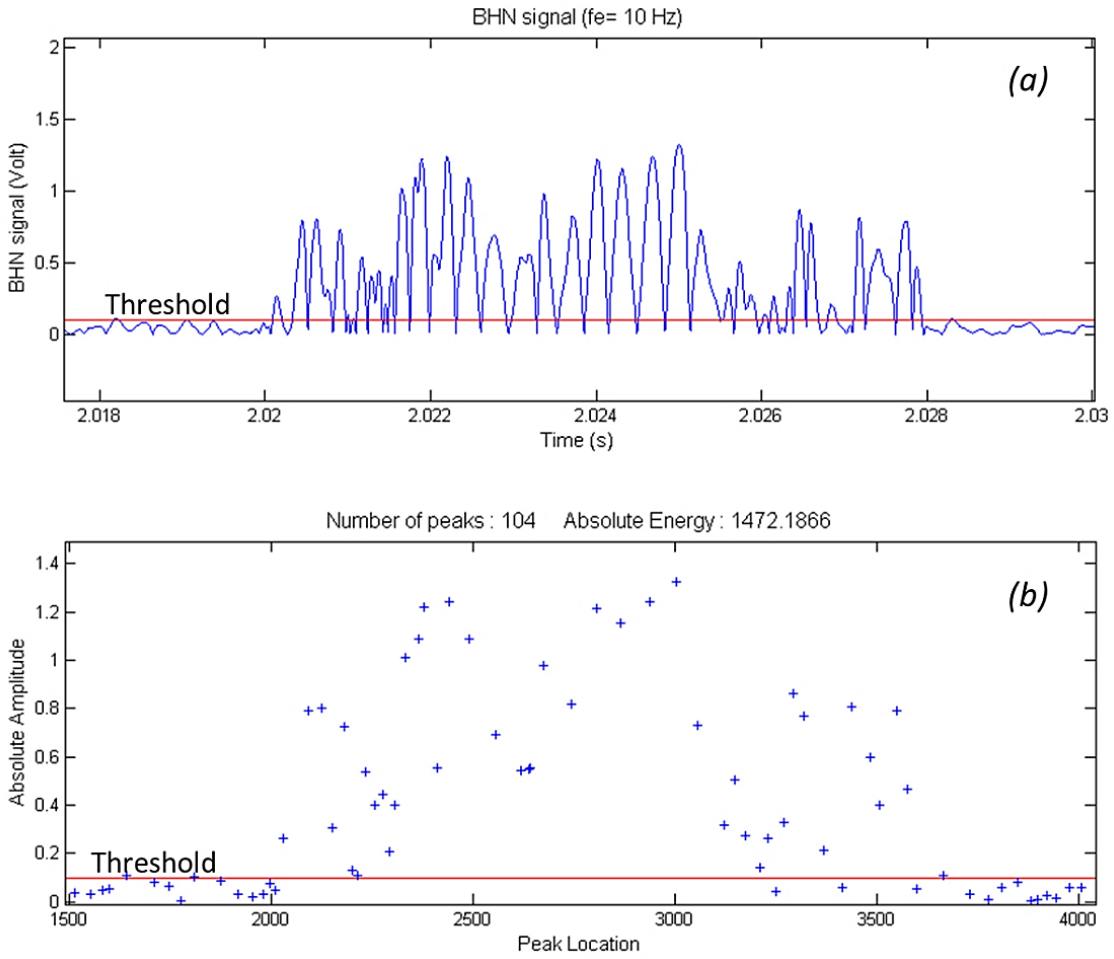

Figure 5.7 Typical BHN signal of one burst: *(a)* absolute amplitude, *(b)* the location of peaks over threshold value

5.3.4 Barkhausen Noise during Current Excitation

In this study, the applied current to magnetic yoke was varied from 0.1 A to 1 A to induce different magnetic field strengths (H) to pass through the specimens being examined. In general, the RMS value of the BHN signal received by the pickup coil first increases, and is then followed by a decrease with the an increase in applied current as shown in Figure 5.8. There are three clear regions, therefore it can be easily divided into three states: (I) background noise, (II) weak BHN, and (III) strong BHN.

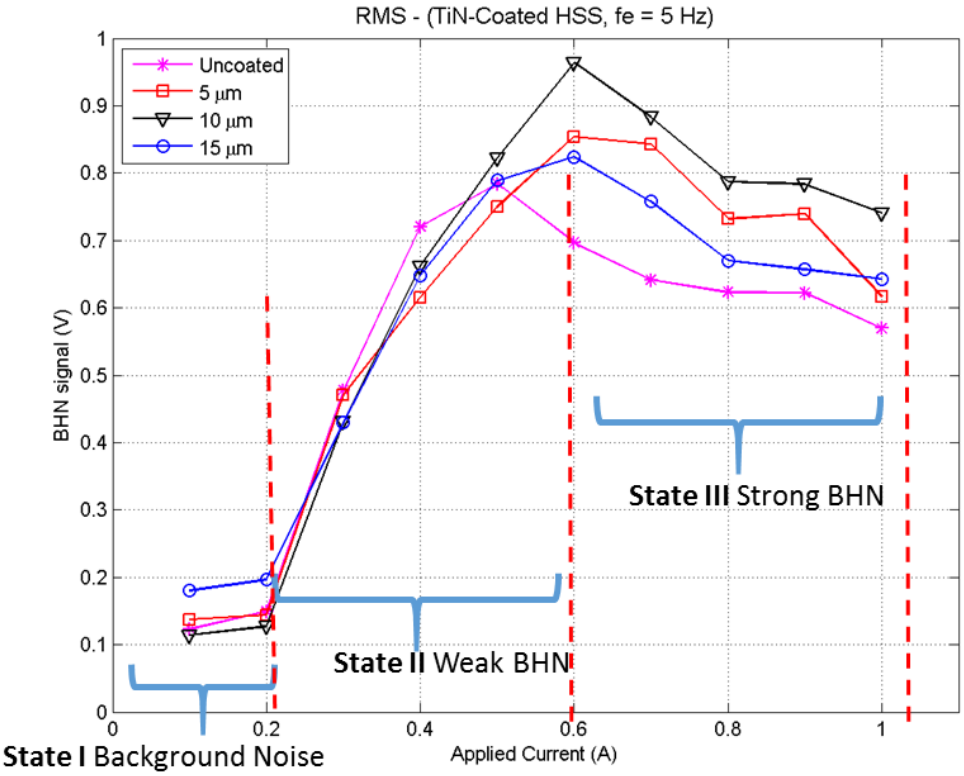

Figure 5.8 Typical RMS values of BHN signals during the experiment

Considering the signal from an uncoated HSS specimen (asterisk/purple), in the first state, the RMS values are low as only background noise received from the pickup coil as shown in Figure 5.9. It is assumed that the exciting current is not enough to move the magnetic moment vector in magnetic domains. The BHN signal emerges from the background noise where the applied current is greater than 0.2 A and Figure 5.10 shows the BHN signal in this state. During State II, the amplitude and width of the BHN signal increases significantly as the magnetic flux intensity (B) increases due to an increasing of exciting current. As a result, the magnetic moment vector alters more frequently. Consequently, the amount and amplitude of BHN signal can be found increasingly. The RMS value increases continuously and reaches a peak RMS value where the applying current is about 0.5 A. After that, the BHN signal in State III slightly changes to be steeper as shown in Figure 5.11. Consequently, the RMS value slightly decreases while the magnetisation in the workpiece becomes saturated. Finally, the BHN signal disappears when the applied exciting current is greater than the saturation point.

It is expected that the BHN signal in State II and State III will be useful to characterise the material properties, especially the thickness of the coating layer in coated HSS.

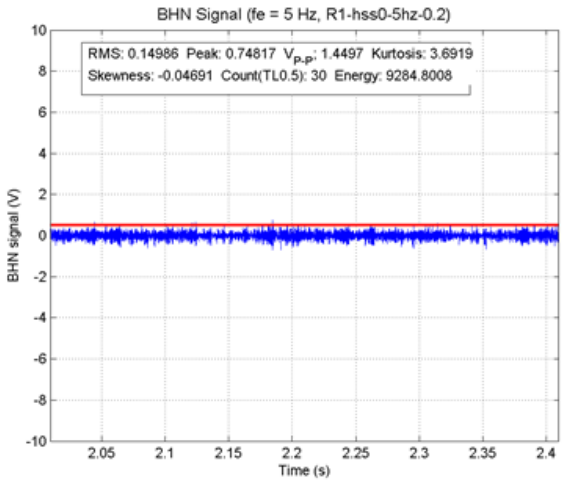

Figure 5.9 Barkhausen noise in state I (background noise)

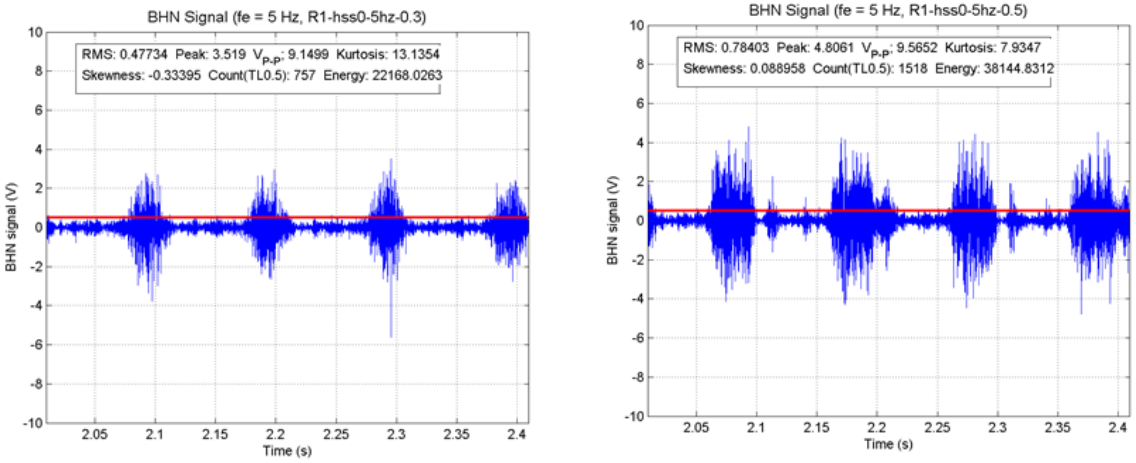

(a) *(b)*

Figure 5.10 Barkhausen noise in State II: *(a)* applied current = 0.3 A, *(b)* applied current = 0.5 A

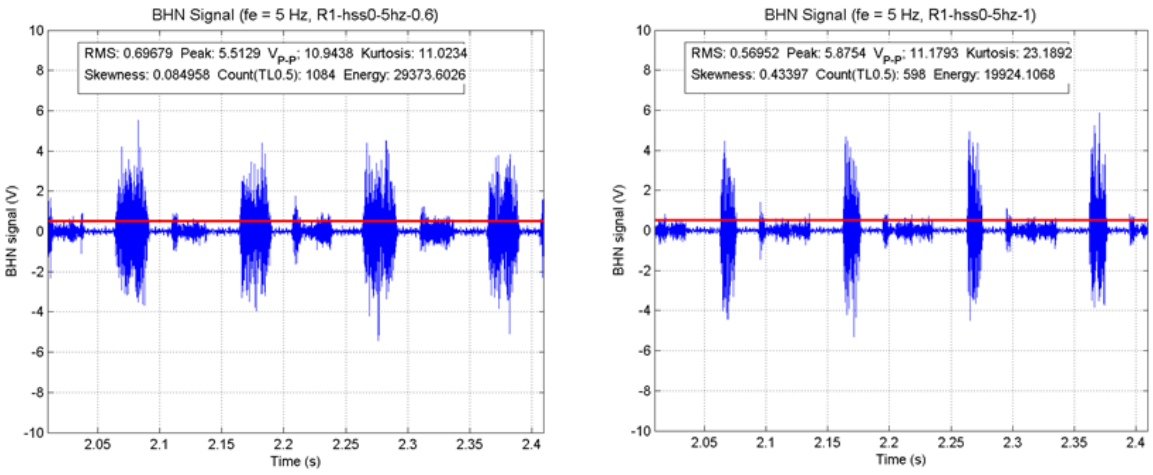

(a) *(b)*

Figure 5.11 Barkhausen noise in state III: *(a)* applied current = 0.6 A, *(b)* applied current = 1.0 A

5.4 Magnetic Probe Characteristics

In this section, the characteristic of the proposed BHN system was evaluated. Three pickup coils with different number of turns were used to sense the BHN signals. The BHN signal received by these coils was then compared in order to find the most sensitive and effective one for use in other studies. Also, the operating condition used in setting up the BHN system for measuring the coating depth in HSS was identified.

5.4.1 The Influence of Number of Turns

The pickup coils with different number of turns (2000, 3000, and 4000 turns) were made as described in Chapter 4. To obtain the coil sensitivity and frequency response, a sinusoidal waveform was used to excite the magnetic flux into an uncoated HSS specimen and the BHN signals acquired from three pickup coils were then compared under the constant frequency of exciting current (f_e = 1, 5, and 10 Hz). The current applied to the exciting coil was varied from 0.1 - 1.0 A. The Figure 5.12 to Figure 5.14 compares RMS values for three pick-up coils for each excitation frequency.

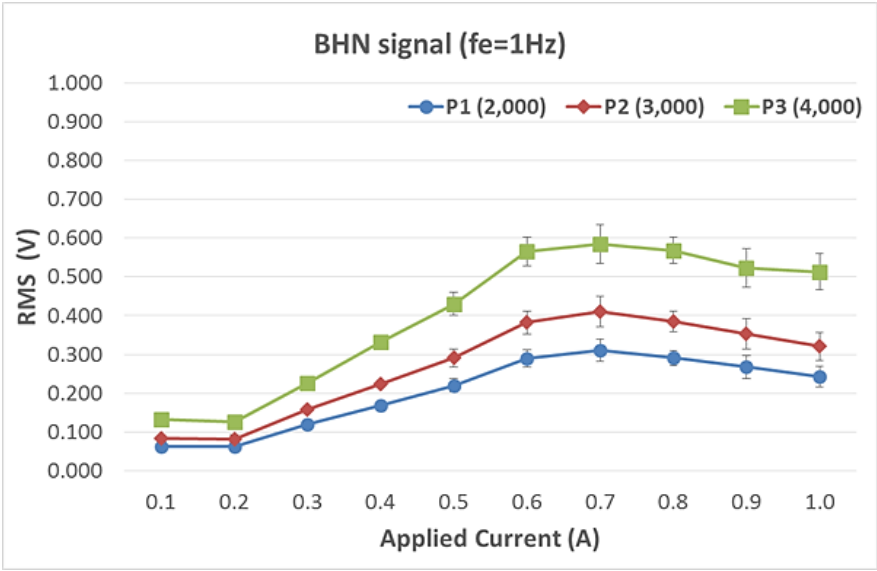

Figure 5.12 RMS value of BHN signal compared by different pickup coils (f_e=1Hz)

In Figure 5.12, the BHN signal of all pickup coils slightly increases after 0.2 A and it is noticed that the complete shape of BHN signal have been formed after this exciting current value. The RMS value continuously increases and reaches the maximum RMS around 0.7 A, and then decrease gradually. Obviously seen that the RMS value of three pickup coils separates clearly and the pick-up coil (P3, 4000 turns) produces the highest BHN signals. The results indicate that an increasing of number of turns in the pick-up coil increases its sensitivity, which is in agreement with the finding of Vashista *et al* [138]. Similarly, these results can also be found in 5, 10 Hz of exciting frequency as presented in Figure 5.13 and Figure 5.14

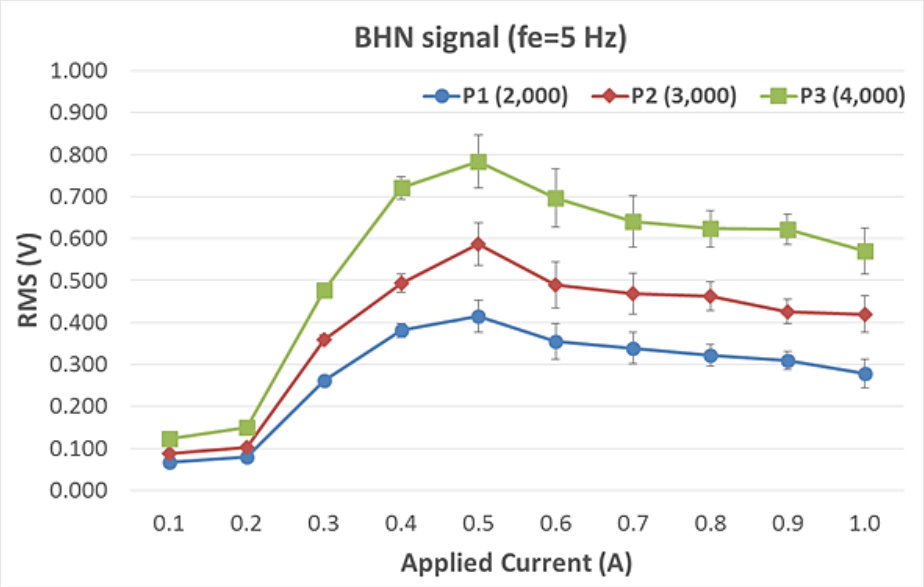

Figure 5.13 RMS value of BHN signal compared by different pickup coils (f_e=5Hz)

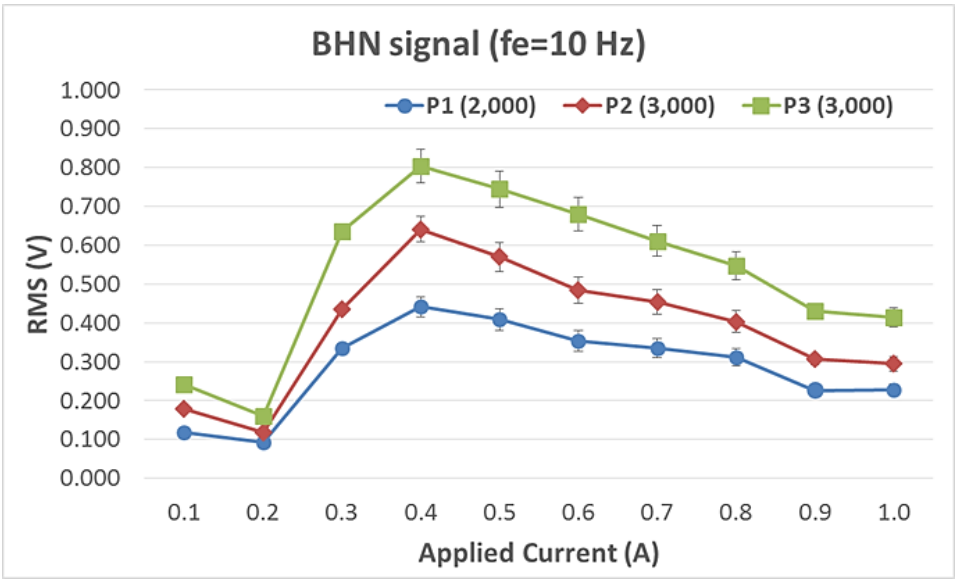

Figure 5.14 RMS value of BHN signal compared by different pickup coils (f_e=10Hz)

Comparing to three different exciting frequencies, it can be observed the peak of RMS values well correlates with the exciting frequency. Similar to the earlier studies that the positions of the peak RMS values are shifted from high values of applied current to low ones by an increasing of the exciting frequency [46, 138]. For example, the peak values or RMS profiles were found at 0.7 A for 1 Hz, 0.5 A for 5 Hz, and 0.4 A for 10 Hz.

The RMS profiles of lower exciting frequencies are flatter than those in higher exciting frequency. This means the lower exciting frequency provides a wider measuring range of BHN signal (state II) as described in Section 5.3.4. Furthermore, the BHN signal received in low magnetising frequency is, however, lower signal amplitude (i.e. RMS value) than in high frequency. These results are consistent with the finding of other

studies [46], in which the high exciting frequency produces higher BHN signal level than lower exciting frequency.

In conclusion, the pickup coil should have a high number of turns for obtaining high sensitivity. Consequently, the pickup coil with 4000 turns was used in other measurements for this study as it provides the highest sensitivity. Also, exciting frequency has an influence on BHN signal amplitude and the range of measurement and the effect of exciting frequency will be described in following section.

5.4.2 The Influence of Magnetising Frequency

As the exciting frequency has a direct effect on the amplitude and measuring range of BHN signal, an appropriate exciting frequency needed to be identified for the HSS material used in this study. A sinusoidal current at varying frequencies was applied to induce the magnetisation in the uncoated HSS specimen (described in Section 5.3.1) using the 4000-turned pickup coil. The sensory features extracted from the BHN signal are presented in Figure 5.15 to Figure 5.17.

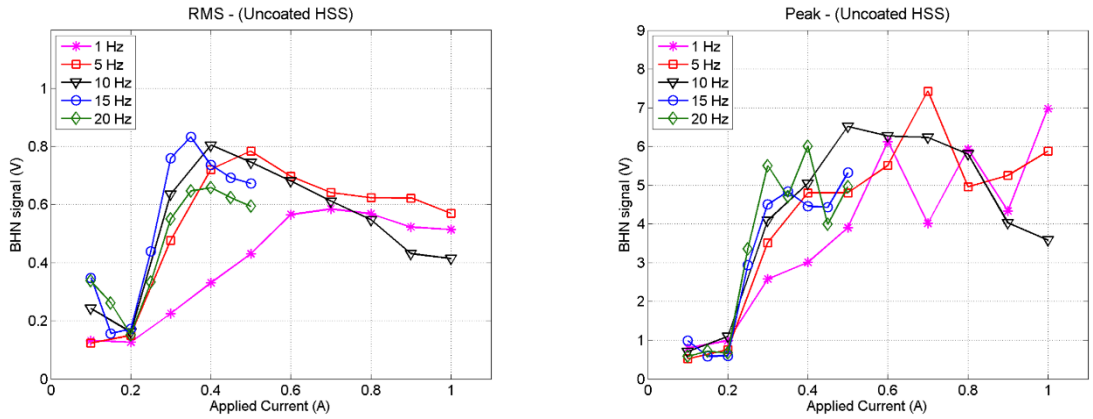

(a) *(b)*

Figure 5.15 BHN signal under different exciting frequency: *(a)* RMS, *(b)* peak amplitude

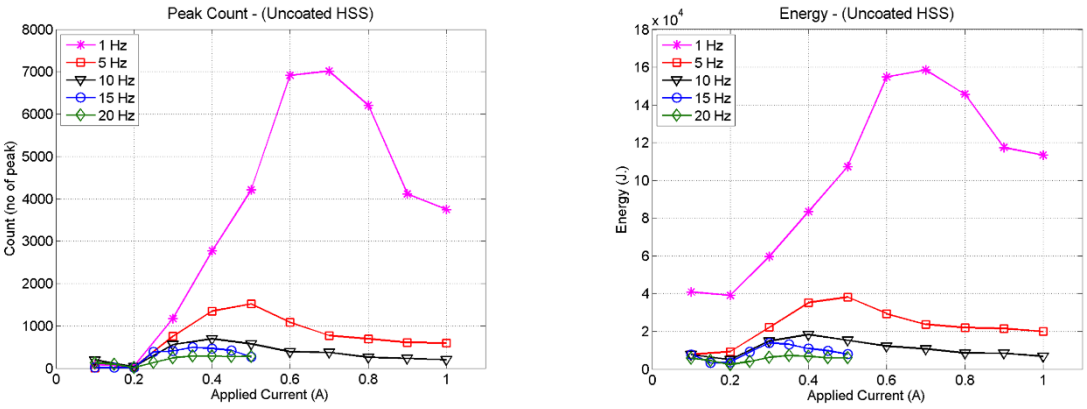

(a) *(b)*

Figure 5.16 BHN signal under different exciting frequency: *(a)* peak count, *(b)* signal energy

It is seen from Figure 5.15 the BHN signal induced by the higher exciting frequency offers the higher signal amplitude, which is represented by RMS and peak amplitude

values. This is due to higher rate of change in magnetisation and hence higher induced BHN voltage level. Conversely, a low exciting frequency produces low rate of magnetisation and accordingly low induced voltage level received by the pick-up coil. This result can be found only in the second state of BHN signal (referred to Section 5.3.4). Clearly, the peak positions of the RMS profiles in Figure 5.15*(a)* change to lower values of applied current due to an increase of the exciting frequency.

In BHN state III, the RMS value shows the clearly-separated trend, while the peak amplitude has a fluctuating pattern. This oscillating trend of peak amplitude may be due to the interfering noises caused by unexpected events which contaminates to the main BHN signal such as a malfunctioning of the electronics.

Interestingly, the completely-separated curve of BHN signal can be presented by the peak count and signal energy features (Figure 5.16). Clearly seen the BHN signal can be easily found where the HSS specimen is induced by low exciting frequency. The large number of peaks and signal energy can be found in 1 Hz excitation although the BHN voltage level is low due to previous explanation. The completely-formed BHN (BHN state II) can also be found between 0.2 - 0.7 A which is the largest range compared to other higher frequencies. It is suggested that this exciting frequency might be useful for indicating the difference of coating depth in HSS.

In Figure 5.17*(a)*, the kurtosis representing the peakedness of BHN signals shows an increase of BHN amplitude during the BHN state II from 0.2 - 0.3 A. Then, the kurtosis slightly decreases as the BHN amplitude decrease. After that, it rapidly increases as the BHN signal has been changed into steeper shape in state III.

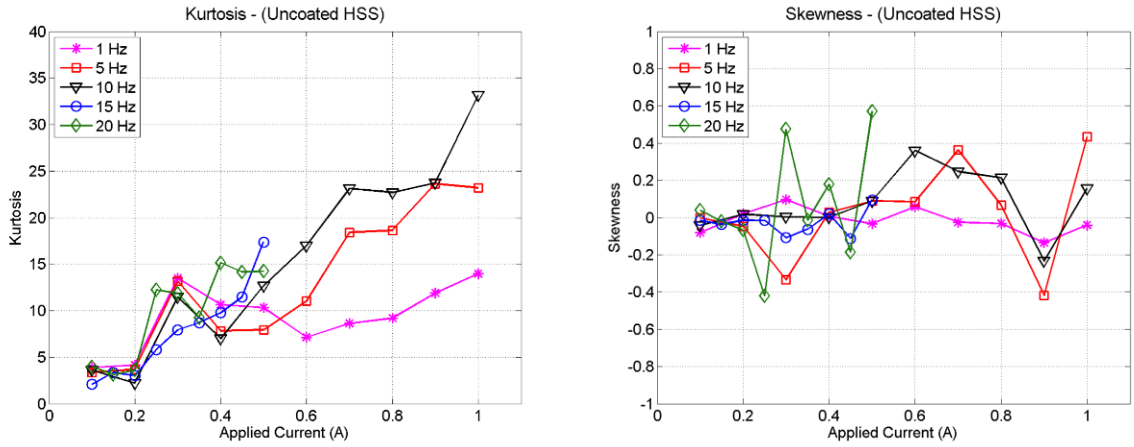

(a) *(b)*

Figure 5.17 BHN signal under different exciting frequency: *(a)* kurtosis, *(b)* skewness

Skewness representing the symmetry of the BHN signal can also be used to show the shape of BHN signal. The zero skewness shows the symmetrical shape of BHN, positive skewness represents right-tailed shape, and negative represents left-tailed

shape. From the Figure 5.17*(b)*, a good BHN shape can be found where the HSS specimen was excited at 1 Hz as the skewness lies on zero.

5.4.3 Selection of Key Features

In conclusion, the most useful features used for indicating the coating depth could be RMS, peak count and signal energy as they can determine the difference of BHN signal both in state II and III, while peak amplitude can indicate only BHN signal in state II. Although kurtosis and skewness do not have a correlation with exciting frequencies, these features can be used to represent the shape of BHN during electromagnetic excitation.

5.5 Barkhausen Noise on the Coated High Speed Steel

In reviewing the literature, no study was found on the use of BHN technique to associate with the coated HSS material. Thus, this section aims to study the relationship between BHN features and the coating layer depth in HSS specimen as this is an important issue for future research on tool condition monitoring. Chromium nitride (CrN) and titanium nitride (TiN) were used as coating materials and the preparation of those specimens has been described in Section 5.3.1.

Firstly, the CrN/TiN coated HSS with highest thickness of coating layer (15 µm) was measured to ensure that the BHN signal from coated HSS specimens can be picked up by the proposed measuring system. The BHN features of CrN and TiN coated HSS are descrbied in Section 5.5.1. After that, the comparison of BHN features due to different coating layer depths of each coating material are summarised in Sections 5.5.2 and 5.5.3.

5.5.1 BHN Signal on Coated HSS

It is necessary to first examine the BHN signal response to the different property variations in HSS specimen. In this section, the coated HSS specimens were measured by the proposed BHN system to assure the BHN measuring system can be applied to take the measurement on the coated HSS. The CrN/TiN coated HSS specimens with the thickest depth were first studied and several exciting frequencies were performed.

5.5.1.2 BHN Signal on Chromium Nitride Coated HSS

To begin with CrN coated HSS, the sensory features extracted from the BHN signals are illustrated from Figure 5.18 to Figure 5.20.

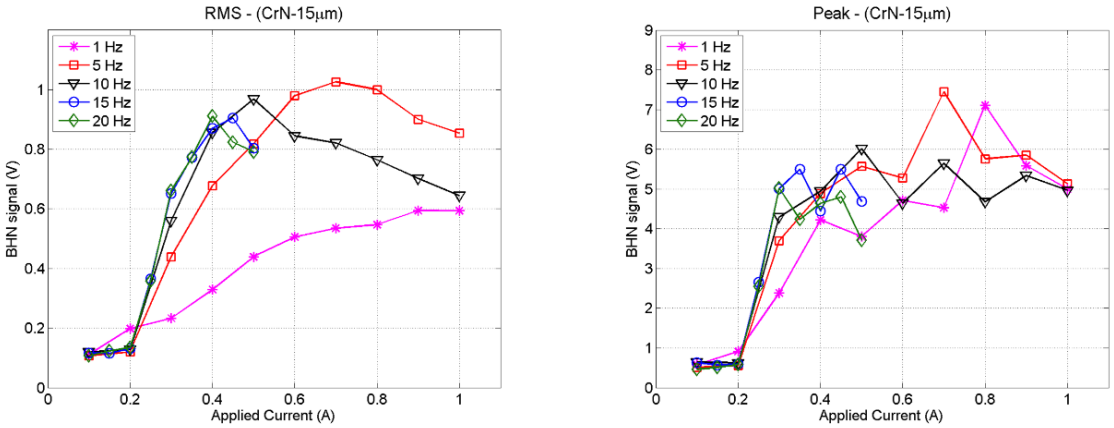

(a) *(b)*

Figure 5.18 BHN signal of CrN HSS with 15 μm thick: *(a)* RMS, *(b)* peak amplitude

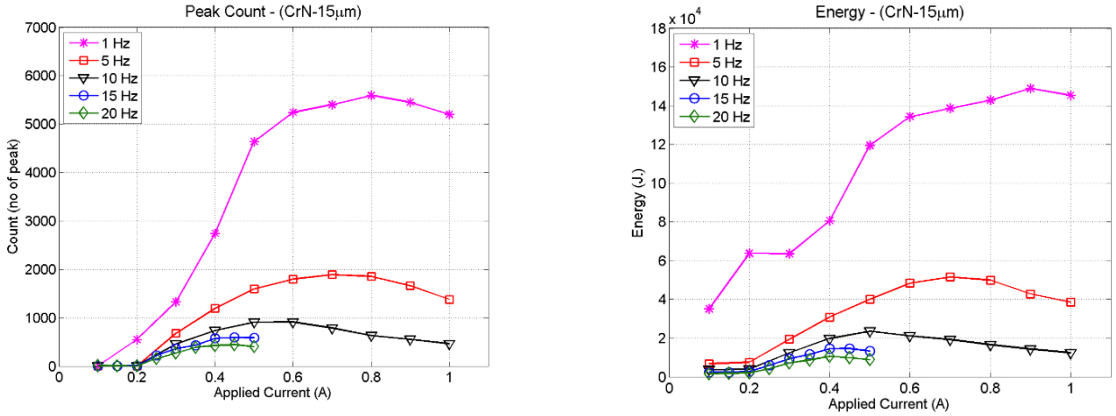

(a) *(b)*

Figure 5.19 BHN signal of CrN HSS with 15 μm thick: *(a)* peak count, *(b)* signal energy

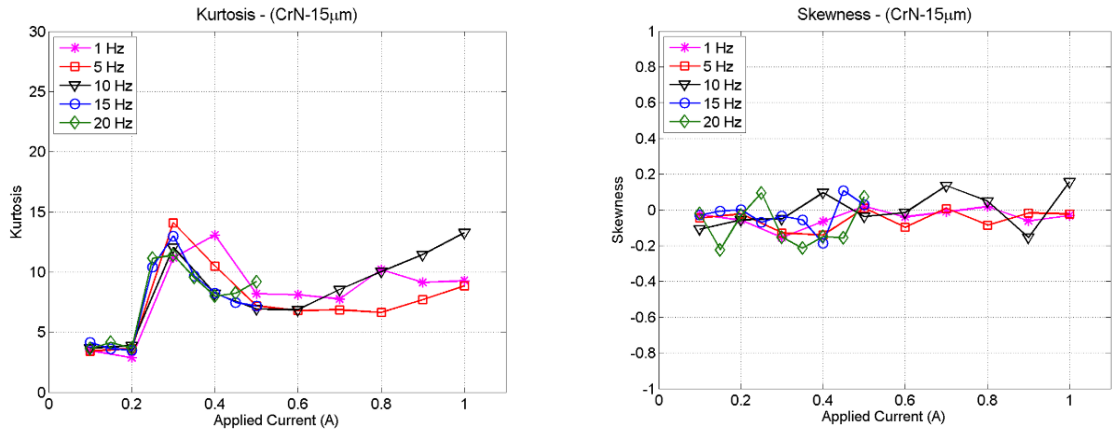

(a) *(b)*

Figure 5.20 BHN signal of CrN HSS with 15 μm thick: *(a)* kurtosis, *(b)* skewness

From the figures, the existing of signal features confirms that the BHN signal in CrN-coated HSS can be detected by the BHN measuring system. Interestingly, these results are able to indicate the differences between the uncoated (Figure 5.15 to Figure 5.17, Section 5.4.2) and the coated HSS, such as, the value of features, the maximum value of each feature in particular frequency, and the positions of those maximum values. As regards kurtosis and skewness, these two features in Figure 5.20 presents a good evolution of BHN signal and the symmetrical shape of BHN signal throughout the range of applied current as previously described in Section 5.4.2.

5.5.1.2 BHN Signal on Titanium Nitride Coated HSS

For the TiN coated HSS material, the BHN features extracted from the acquired signal are presented from Figure 5.21 to Figure 5.23. These results are similar to those in the previous sections (Section 5.42 and 5.5.1) where RMS, peak count, signal energy are the most useful features to indicate the variations of material properties in coated HSS. These features tend to have generally different values that can be distinguished from ones in case of uncoated HSS specimen.

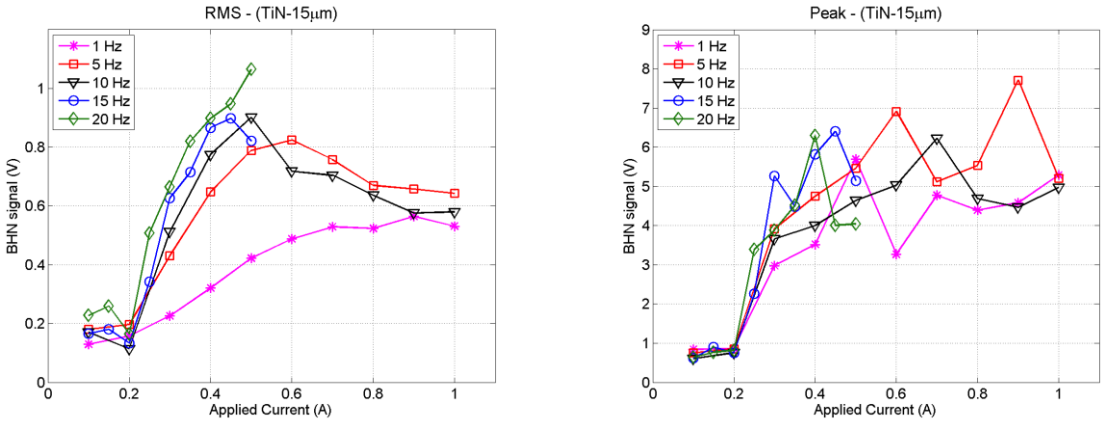

(a) *(b)*

Figure 5.21 BHN signal of TiN HSS with 15 μm thick: *(a)* RMS, *(b)* peak amplitude

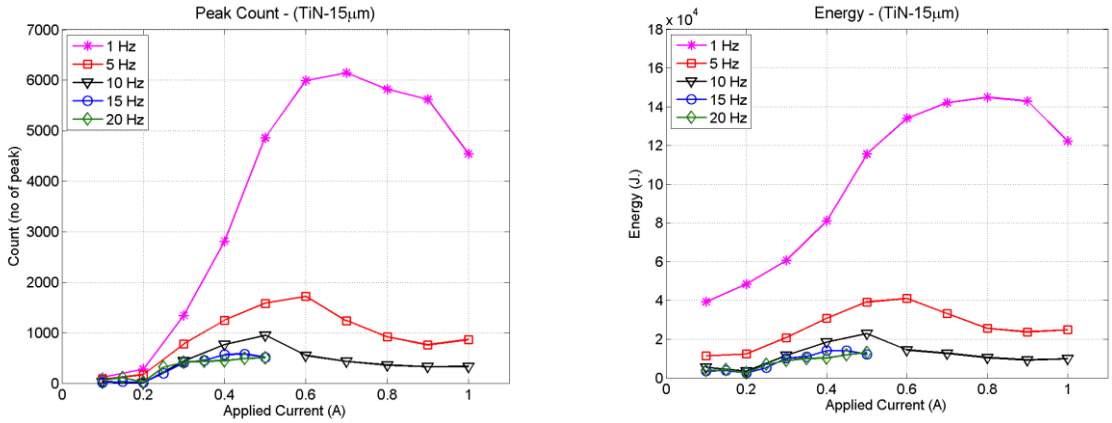

(a) *(b)*

Figure 5.22 BHN signal of TiN HSS with 15 μm thick: *(a)* peak count, *(b)* signal energy

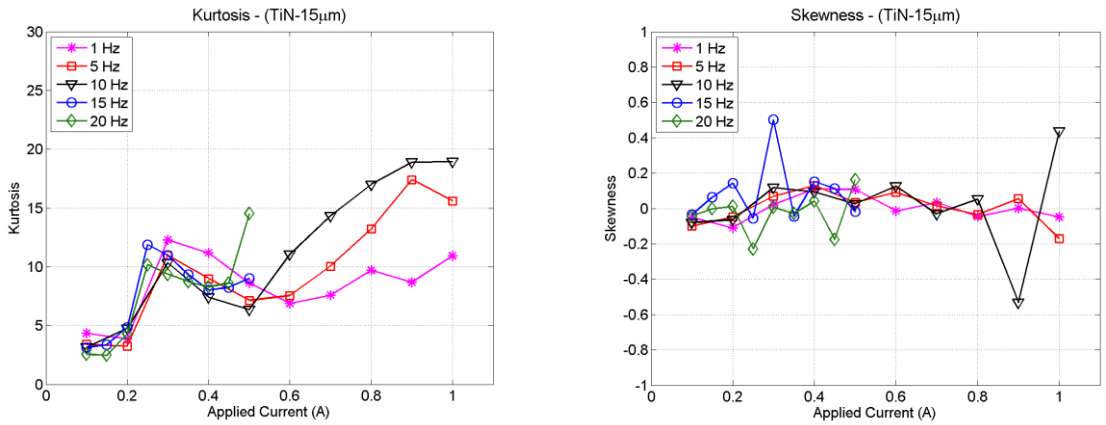

(a) *(b)*

Figure 5.23 BHN signal of TiN HSS with 15 μm thick: *(a)* kurtosis, *(b)* skewness

In conclusion, it appears that the RMS, peak count, and signal energy can be used very well to indicate the differences between uncoated and coated HSS for each particular exciting frequency. The variations of those features can probably indicate the thickness of coating layer. It is concluded that the proposed BHN system can be applied for measuring the coating layer thickness of the CrN/TiN coated HSS.

5.5.2 Comparison of Coating Depth Layer on CrN HSS

As the RMS appeared to be one of the most useful features to indicate the different thicknesses of the coating material on HSS, four levels of coating thickness at different exciting frequencies were first evaluated by the RMS values and the results are shown in Figure 5.24.

The BHN signal of all exciting frequencies can be found after 0.2 A of applied current and the RMS values increase significantly until reach the maximum point (defined as BHN state II). The slope of the curve in this state correlates with the exciting frequency in which low exciting frequency in Figure 5.24*(a)* provides low degree of slope (flatter), while high frequency (e.g. Figure 5.24*(e)*) have a steeper slope. However, the curve in this state cannot be used to indicate the coating thickness because the RMS values of each coating thickness are quite close together.

In BHN state III, the curves are clearly separated and significantly oriented which could be used to indicate the thickness of coating layer for exciting frequency *fe* = 5, 10, 15, 20 Hz. It is clearly seen the thicker coating layers have higher RMS values and thinner layers have lower RMS. Most importantly, the exciting frequency has an influence on measurable range of the BHN signal. For example, the RMS feature can be used to indicate the coating thickness where the applied current varied between 0.6 and 1.0 A for the exciting frequency = 5 Hz, while it can be only used from 0.5 to 1.0 A in case of 10 Hz. In Figure 5.24, the proper exciting frequency is 10 Hz because this frequency provides the largest measuring range (0.5 - 1.0 A) that can be used for

coating depth measurement in CrN coated HHS, and the RMS curves have more linearity than those in 5 Hz which offer the same measuring range.

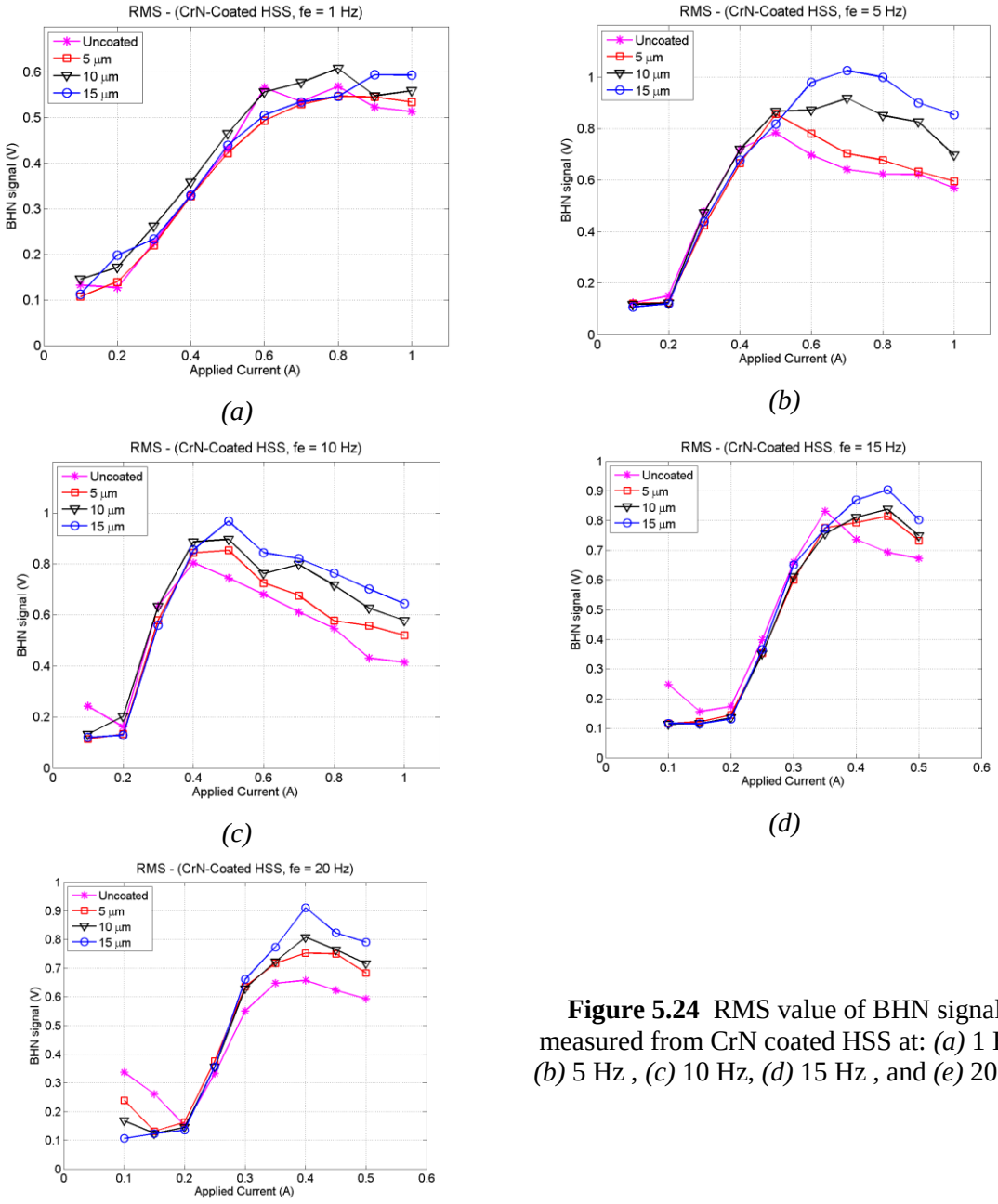

Figure 5.24 RMS value of BHN signal measured from CrN coated HSS at: *(a)* 1 Hz, *(b)* 5 Hz , *(c)* 10 Hz, *(d)* 15 Hz , and *(e)* 20 Hz

Likewise, the results in Figure 5.25 confirms that peak count and signal energy features of 10 Hz can also be used to indicate the coating depth layer, while the peak amplitude in Figure 5.26 is unusable for indicating the difference of coating thickness due to unexpected noise. (The results of other exciting frequency are summarised in Appendix A).

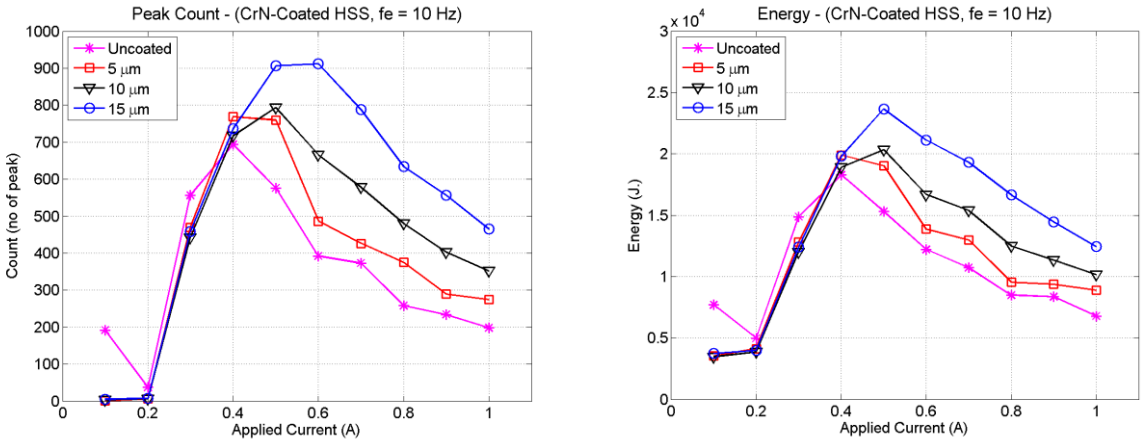

(a) *(b)*

Figure 5.25 BHN signal of CrN coated HSS: *(a)* peak count, *(b)* signal energy

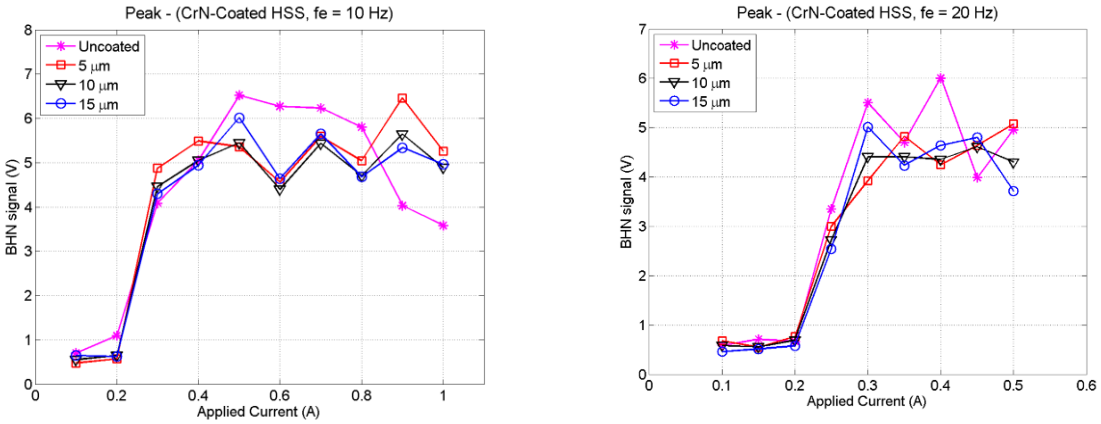

(a) *(b)*

Figure 5.26 Peak amplitude extracted from BHN signal of CrN coated HSS at exciting frequency: *(a)* 10 Hz, *(b)* 20 Hz

In conclusion, the effective magnetising conditions used for the propose BHN system in order to indicate the thickness of coating layer in CrN coated HSS are 10 Hz of exciting frequency and the applied current from 0.5 to 1 A. The effective features used to indicate the thickness of coating layer are RMS, peak count, and signal energy. Besides, the kurtosis and skewness are likely used to investigate the shape of BHN signal.

5.5.3 Comparison of Coating Depth Layer on TiN HSS

With respect to TiN coated HSS, Figure 5.27 compares the RMS of BHN signal of each exciting frequency. Similar to CrN coating material, it is seen that the RMS values separate in BHN state III, where the exciting frequency is greater than or equal to 5 Hz, but the separation is not in the correct order except for f_e = 20 Hz.

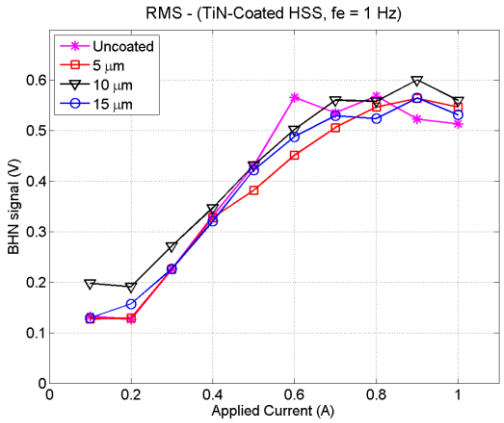

(a)

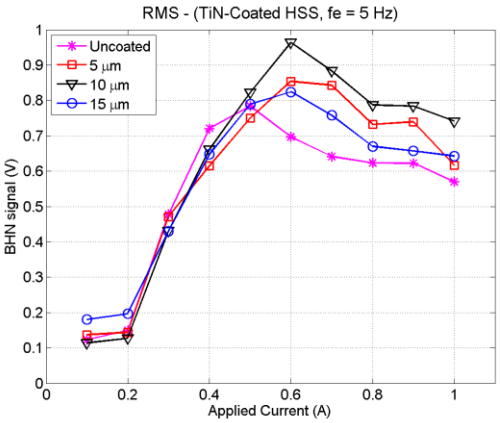

(b)

Figure 5.27 RMS value of BHN signal measured from TiN coated HSS at: *(a)* 1 Hz, *(b)* 5 Hz

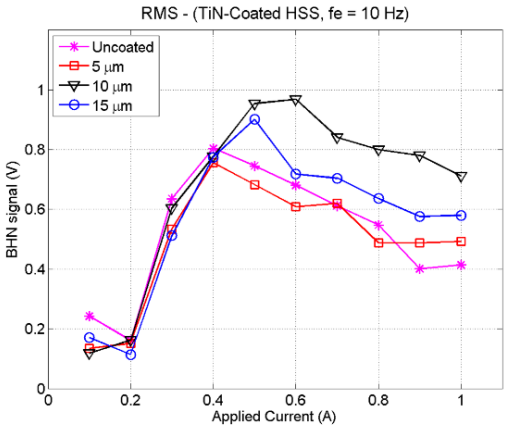

(c)

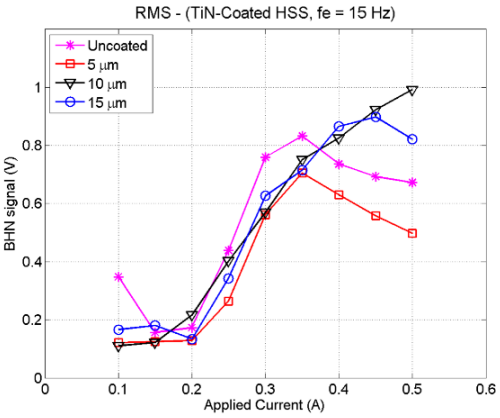

(d)

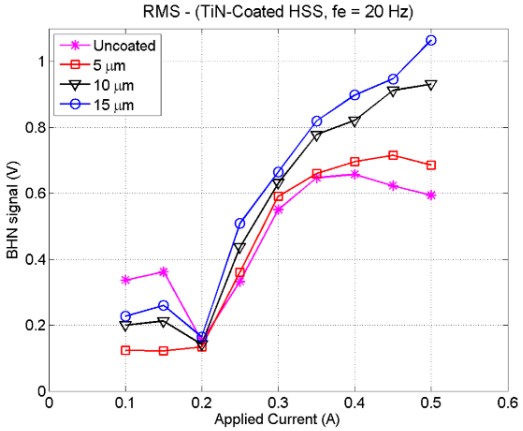

(e)

Figure 5.27 (cont.) RMS value of BHN signal measured from TiN coated HSS at: *(c)* 10 Hz, *(d)* 15 Hz, and *(e)* 20 Hz

Interestingly, the RMS values of each thickness in Figure 5.27*(e)* have the correctly-ordered separation both in state II and state III. It can be confirmed by the peak count and signal energy features in Figure 5.28 that this exciting frequency can be used to indicate the different thicknesses of TiN coated HSS. Cleary seen that the effective range of TiN coating depth measurement is in the condition that applied current varies

from 0.3 to 0.5 A and the exciting frequency is equal to 20 Hz. A possible explanation for this might be that BHN signal in high exciting frequency have an effect on the near surface according to skin depth Equation in Chapter 4. Consequently, the slight change in the thickness of TiN layer would make the BHN feature separated which can be used to indicate the change of coating layer.

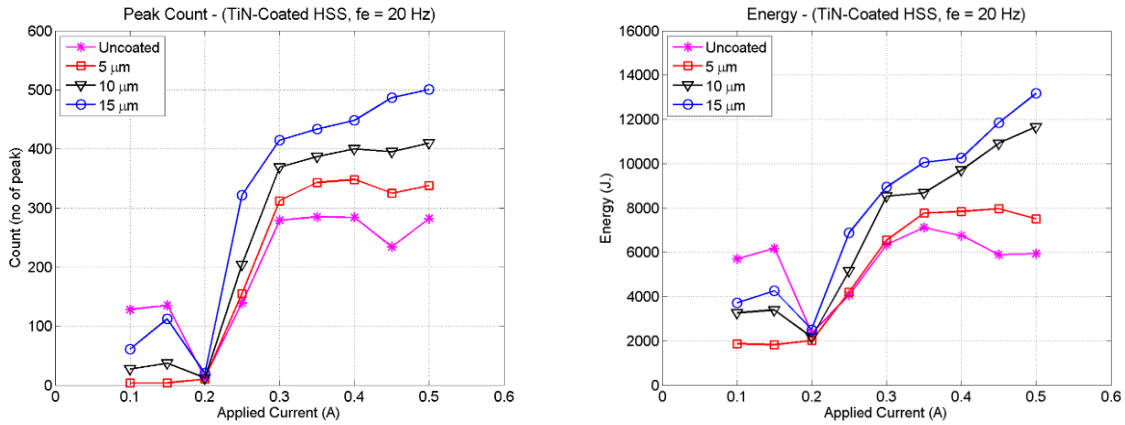

(a) *(b)*

Figure 5.28 BHN signal of TiN coated HSS: *(a)* peak count, *(b)* signal energy

In conclusion, it can be concluded that the high exciting frequency offers very sensitive to near surface properties as offering a shallow skin depth due to the effect of lower magnetic field penetration and higher attenuation. Consequently, the coating layer will have strong effect on the field penetration and the BHN signal, and accordingly the BHN signal which has good correlation with the coating depth can be detected in this case.

In case of low frequency excitation, a thin coating layer would not significantly affect the BHN signal level since low frequency excitation induces deeper skin depth. Therefore, the variation in near surface properties does not have a significant effect on the BHN signal generation.

5.6 Utilisation of BHN Technique on Tool Condition Monitoring

From the experimental result, it is shown that the Barkhausen noise technique could be used for measuring the coating depth layer on coated HSS cutting tools, especially gear hob cutters which commonly made by TiN coated HSS.

The simplest method is using the BHN measuring technique to monitor the tool coating conditions. Firstly, the thickness of coating layer has to be defined into classes. For example, the coated tool having ≥15 µm of coating layer depth is classified as new tool, 10 - 15 µm as moderately used, 5 - 10 µm as highly used, and <5 µm as weaken tool. Then, the three sensory features of BHN signal in the effective range are monitored both before and after use the cutting tool to know the coating condition. It is

helpful for the operator to be aware when the tool is in highly-used condition and avoid using the weaken tool.

Furthermore, the remaining depth of the coated HSS tools can also be estimated by using regression model or data fusion concept, such as neural network, fuzzy logic, or other artificial intelligence algorithms. For example, supervised artificial neural network favourable use for data fusion, can be applied in order to obtain the prediction model by training the network with given data. The sensory features of the BHN signal (RMS, peak count, signal energy) are used as inputs and the actual coating depth measured by other reliable methods are used as targets for the neural network training. However, the sufficient data is required for training and the precise measurement of actual value is necessarily required. In practical application, the feature values measured from the workpiece are fed into the trained neural network model; the coating thickness will be then obtained.

Due to the large probe size, this makes the BHN technique difficult to measure the coating layer on the main cutting edges of small cutting tools (i.e. turning and drilling tools). It may be only used for monitoring the coating depth of hob cutters which is the original objective of this study. However, as gear hob cutters have a complex shape and geometry, the challenge of using BHN technique to measure the coating depth layer is how to make a probe accessible to the flank surface of the cutters. The compact BHN probes could be designed as shown in Figure 5.29. Importantly, the geometry of the gear hob cutter has an influence on the BHN signal. For instance, the BHN signal on a flat bar specimen and gear tooth flank which is made with the same material and properties will be different because of the different geometry and measurement set-up. Some limitations of using BHN system and the comments on utilisation are discussed in following section.

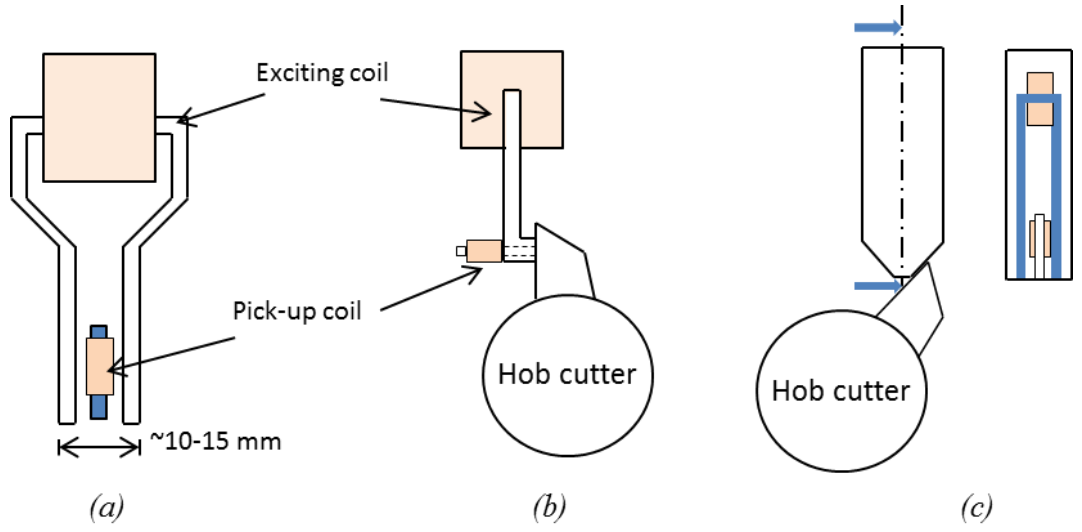

Figure 5.29 The compact design of a BHN probe for measuring the coating thickness of hob cutters

5.7 Comments on BHN measuring system

Design and Probe Size

One major concern is the size of measuring probe consisting of an exciting coil (electromagnetic yoke) and pick-up coil. This probe should be suitable for a given geometry and component because smaller probes may be necessary for restricted space. However, the proper design of exciting coil has to take into consideration since the maximum magnetic field strength (H) relies on the number of turns of the coil and the current applied into the coil. A larger number of turns and higher current provides higher applied magnetic field strength, and deeper field penetration at lower excitation frequencies, but this makes the size of exciting coil relatively large. Therefore, the optimised number of turns and current is necessary for making smaller yoke suitable for the application. Also, the geometry of workpiece and accessibility of the measuring probe pose a limitation on the size and design in some application such as round bar specimen. Furthermore, it is necessary to make smaller size of pick-up coils with large number of turns by using very thin copper wire to obtain higher sensitivity and have high spatial resolution, but they are likely to have small variations in life-off which have an effect on the BHN signal.

Temperature Effect

From the experiment, the temperature of the magnetic yoke increases if the measuring probe was used for low frequency excitation with high applied current and taking a long measurement sequence. Moreover, the temperature has a major influence on the stability of electronic hardware. It is practical to leave the electronic equipment turned on for a period before taking a measurement to allow the electronic device to be in thermal equilibrium.

Most importantly, a shunt resistor in magnetic circuit easily overheats when it is used for high current and low exciting frequency. The measurement should halt for a period if the BHN measuring system has been used for a long period. Alternatively, the temperature of the shunt resistor have to be monitored to prevent overheat effect that might cause the error on the current measurement. Also, the compensation will be required to obtain the accurate value of the circulating current on the exciting coil.

Besides, the workpiece temperature is one of thermal effects that may cause a slight drop in the magnetic flux density in the workpiece surface because the resistivity of the workpiece increases with the temperature. Consequently, the skin depth is reduced by increase of workpiece temperature. In summary, the temperature variations of electronics, probe, and workpiece should be controlled to a few degrees so that these sources of error will be small.

Accuracy and Calibration

In most applications, the BHN measurements can be reliably used for the qualitative and qualitative assessment. In case of quantitative assessment, this technique requires an extensive calibration and the BHN system must be calibrated to every particular test for validation and obtaining an accurate result. However, unexpected variations of background noise or malfunctioning of the electronics in the measurement system would result in variations of BHN signal. Also, an air gap (lift-off) which results from error in the placement of BHN probe on the test component would effect on variations of BHN signal level. These errors can be identified by measuring on previously measured workpiece or the standard workpiece used as a reference signal. It is quite important to perform calibration for each workpiece geometry, material and measurement parameters for obtaining the high accuracy of quantitative evaluation.

5.8 Concluding Remarks

In this study, several set-up of BHN measuring system were tested in order to achieve the maximum sensitivity for coating depth measurement on coated HSS specimen. The variation of coating layer can be correlated to different BHN features extracted from the BHN signal generated during the magnetisation cycle.

The proposed BHN system can successfully indicate the thickness of CrN coated HSS where the exciting frequency is equal to 5, 10, 15, and 20 Hz, while only 20 Hz excitation can be used to indicate the thickness of TiN layer coated on HSS specimen. From the experimental results, the most significant BHN feature used in this study are RMS, peak count, and signal energy, which are extracted from the BHN signal in state III. These features can be used individually to indicate the thickness of coating depth very well. To increase more reliable result, the use of multiple BHN features can improve the result accuracy, which is the key component of the data fusion concept.

Although the BHN measuring technique has initially been developed to be performed off-line, this non-destructive and very short time-measuring method can reduce the production costs due to rejected parts caused by tool breakage, and can reduce the time from un-planed tool replacement during the production. The application of BHN technique for coating depth evaluation will be an important issue for the future research on tool condition monitoring.

Chapter 6

Tool Condition Monitoring in Turning Process

Data Acquisition

Data Collection

Tool Wear Measurement

A short contextual review of on-line tool condition monitoring in turning process is presented and then details of the specific experimental setup, materials and methods are described. The results, particularly of the sensing of tool wear, are presented and the effect of cutting parameters on the sensing signals is also discussed. These are combined in order to compare the sensory features with flank wear progression.

6.1 Introduction

Tool condition monitoring (TCM) plays a key role in the quality enhancement of the finished products in automatic machining. Tool wear and failure are undesirable. The unplanned tool replacement can cause machine downtime leading to economic loss. Tool life depends upon machining conditions, workpiece materials, cutting time and cutting tool material. Worn tools also have a direct effect on the productivity of the process and the surface finish of the workpiece. They can also produce unwanted forces, sound, vibration, and other parameters, leading to machine downtime, product rejection and damage to the machine. To avoid this, tool wear condition monitoring systems have been developed which can warn the operator of the condition of the tool.

This study overcomes the TCM problem from multi-sensor fusion perspective. Multiple layer perceptron neural network has been applied to fuse the selected sensory features (input vector) and flank wear width (output/target) and four tool wear states to warn of the cutting tool conditions.

6.2 Context

In the past decade, research on tool condition monitoring has been often conducted using a turning process because its operation is very simple by having a single cutting edge and non-rotating cutting tools. Mostly, the tools are fixed in a tool holder and translated through a rotating workpiece. Therefore, in turning, the sensors can be mounted on the cutting tool directly and easily because of no rotation. It is much more difficult to use other processes, such as milling, drilling, and grinding, because the cutting tools usually rotate through a translating workpiece. The tool geometry used in turning also has a simplistic shape which facilitates easy wear measurement.

Dynamometers (force sensors) and acoustic emission sensors are often used for condition monitoring in turning. Cutting forces measured by a dynamometer are usually the preferred method of tool wear detection and tool breakage in turning [81, 139-141], while other cutting forces can be measured indirectly in terms of current and power consumption of spindle motor [14, 106, 107], as mentioned in Chapter 3 and 4. However, as spindle motors increase and decrease rotational speed before and after cutting, they need higher power to accelerate and to stop the rotation of spindle than is

required for stable cutting. Therefore, to represent tool wear, spindle current and power consumption signals should be considered under steady-cutting state without acceleration and deceleration of the spindle.

According to Rehorn *et al* [82], it can be summarised that AE signals are considered as an effective signal for detection of tool breakage, determine of tool wear and chipping. AE sensor has been used for developing the tool condition monitoring system in machining processes as previous chapters. AE-based tool wear sensing method developed for tool condition monitoring and process analysis were found in reviewed of [12, 89]. Some studies used statistical tools such as skewness, kurtosis for analysing AE signals in turning process [142, 143]. Bhaskaran *et al* used kurtosis and skewness of AE_{rms} extracted from AE signals for monitoring tool wear and failure during hard turning. They concluded that skewness becomes negative while tool wear increases and kurtosis grows up as the tool wear increase. AE sensors have also been used continuously for monitoring tool wear in hard metal [120, 143] and super alloyed workpieces such as nimonic C-263 super alloy [144]. It presumably means that AE signals travel well through the hard materials. In this study, an AE sensor was chosen for tool wear monitoring during machining EN24 which is classified as a hard material.

Audio microphones can also be used to monitor the tool conditions in turning as they are inexpensive and flexible to set up compared with other sensors. The microphone is normally fixed by a magnetic stand which easily move to the desired location. Although it has advantages over others, very few studies used the microphone to record the machining sound because few microphones which are robust enough to use in such an noisy environment. As a result, the signal-to-noise ratio of measured sound signal is quite low due to ambient noises.

Many studies concluded that sound signal amplitude increases as tool wear increases [103, 104, 105]. This can be used to monitor flank wear in machining operations. Lu *et al* used microphone for tool condition monitoring in turning [84] and they introduced tool wear monitoring model which used audio sound emitted from cutting process in turning to model the main effect of tool wear on system dynamics during stable cutting. Besides, the use of microphone have been found in other machining process such as milling [13, 100, 101] and drilling [102].

The use of multi-sensory signals and a sensor fusion approach have been adopted by several authors. Sensory data can be fused using AI algorithms such as neural networks [114, 120, 145], fuzzy logic [145, 146] and ANFIS [95] to increase reliability and robustness of the system. These AIs provide a decision-making system that can be used to fuse all sensory features in order to predict the tool wear state and estimate the tool wear value.

A multilayer perceptron (MLP) with backpropagation algorithm can be used for tool wear state classification and tool wear estimation. Tool wear state classification using

a MLP neural network was studied by Dimla *et al* [119] where cutting force and vibration signals acquired from the cutting of EN24, and the flank wear measured on cutting inserts were fed to the neural network trained to classify the states of tool wear. Balazinski *et al* [145] compared three AI methods used for tool wear prediction in turning including neural network, fuzzy decision support system, and neuro-fuzzy system. In data training of three methods, cutting forces and flank wear were used as inputs, and an output, respectively. They found that these methods gave similar and acceptable results, but the significant difference is the learning time. Segreto *et al* used signals of cutting force, AE, and vibration sensors to classify tool state in turning of Inconel 718. Sensor fusion approach based on the Principal Component Analysis (PCA) was used to extract the significant sensing features and these features were used as input to three-layer feed forward neural network (with backpropagation) for decision making on tool wear condition [114].

In terms of tool wear monitoring, Shahabi *et al* studied aspects of using an image processing technique to make an evaluation of tool wear, especially in a turning process. They assessed the flank wear and nose radius wear from a workpiece roughness profile from a turning operation [68]. The wear profiles were measured using the machine vision method. The subtraction method between the unworn and worn tool image profile were used in this study to calculate the amount of worn nose. The two binary images before and after machining were subtracted pixel-by-pixel. They also attempted to apply this technique to calculate build-up edge from 2D image [72].

6.3 Scope of the Study

The study presented here aims to extend the currently-published research for tool wear monitoring based on multiple sensor fusion in turning. In Figure 6.1, acoustic emission, the power consumption of spindle motor, and sound pressure were monitored during a turning operation. The machining of seven cutting conditions was conducted to collect sensor signals during turning operation. Sensory features of those signals were extracted and feature selection was performed off-line to obtain the representative features required for tool wear modelling by AI technique. The artificial neural network was used to classify tool wear states and estimate tool wear values for predicting remaining tool life by using selected features as inputs and flank wear values as outputs in the supervised training scheme. The outcome of this study is to provide guidance to the operator for changing the cutting tool before it fails. This system could also inform the automatic tool changer of a CNC machine to change the tool when it has worn to a predetermined level in order to increase machine productivity. Tool wear states would be used as information to the CNC controller to adapt cutting parameter properly to reach the maximum usage.

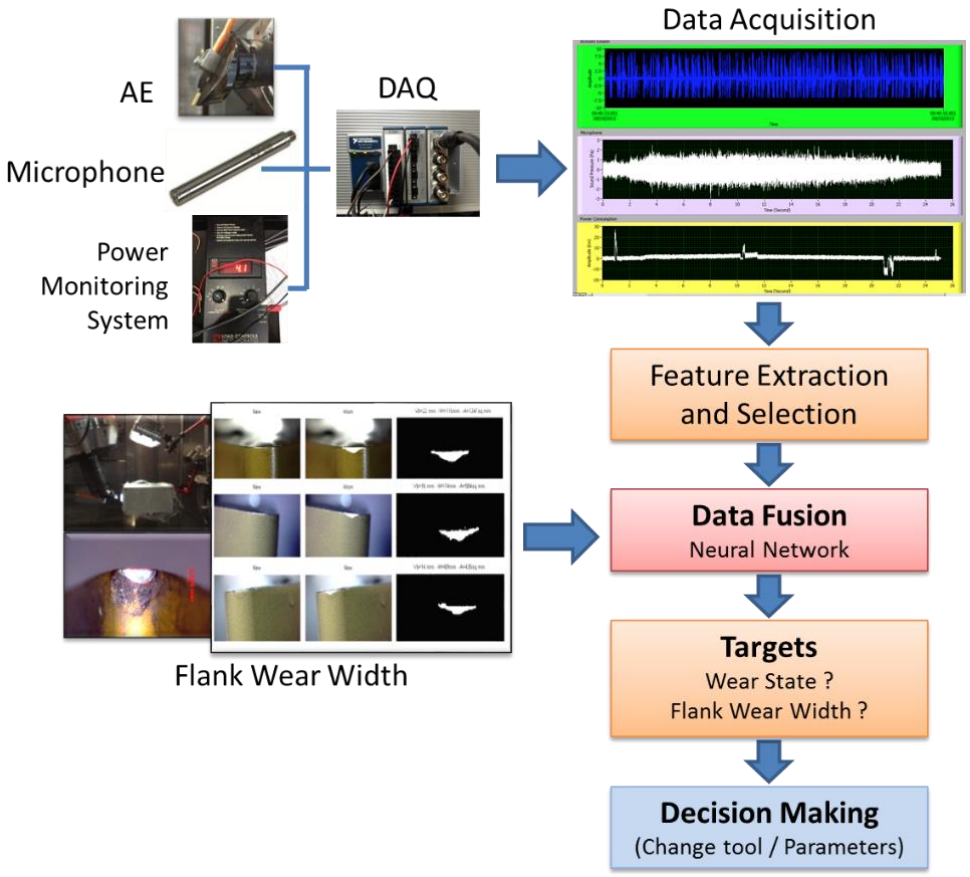

Figure 6.1 The concept of monitoring system

The study can be separated into two parts: data collection and system modelling as illustrated in Figure 6.2.

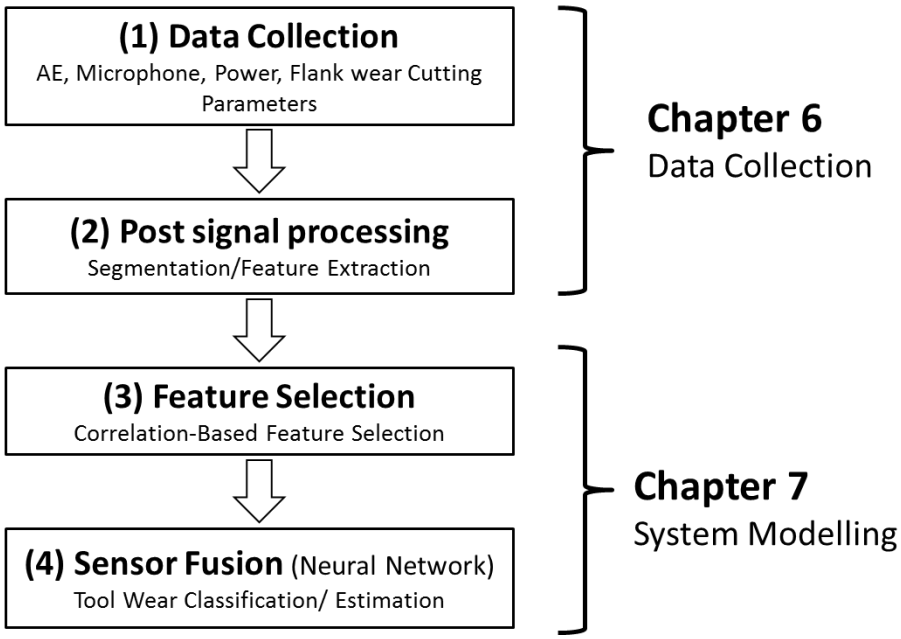

Figure 6.2 Procedures of the study

Chapter 6 explains the collection of machining data, including sensor signals and flank wear progression during machining. Then, post signal processing (e.g. signal segmentation) is described and off-line feature extraction is also discussed. Chapter 7 presents the details of the feature selection methods used to define feature sets as inputs for neural network training and then how tool wear classification and estimation are modelled by neural networks.

6.4 Experimental Setup and Methodology

6.4.1 Experimental Setup and Methodology

The experimental setup used for developing the tool condition monitoring system is shown in Figure 6.3. The sensors, data acquisition setup, tools and equipment used have been previously introduced in Chapter 4.

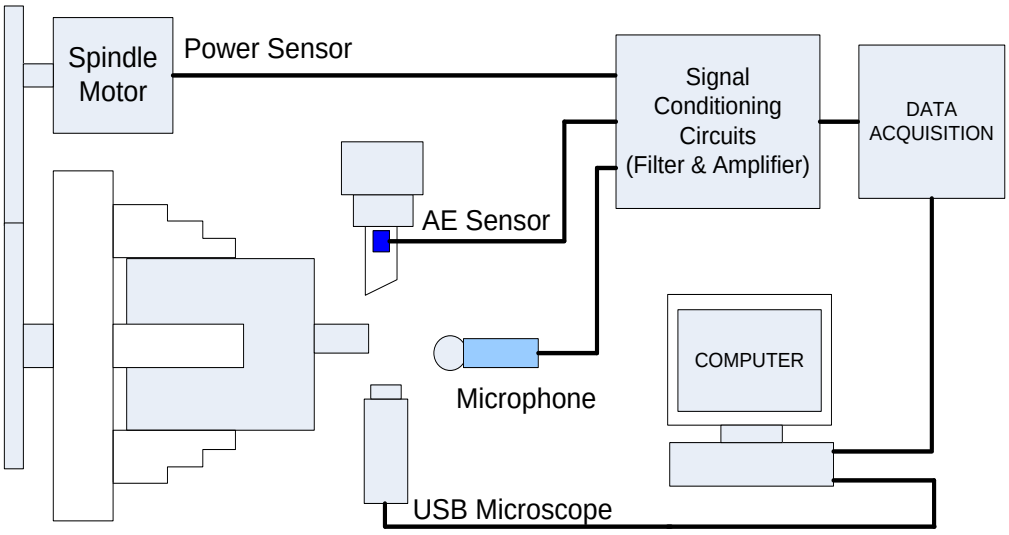

Figure 6.3 Experimental setup

From the diagram, the power monitoring system was used to measure the power consumption of the main spindle motor. An AE sensor was mounted on the tool shank by means of a M6 bolt in order to measure the AE signals in the primary cutting zone, and a microphone was used to record the cutting sound. A USB microscope camera in an enclosure box was used to record the tool wear evolution by taking images of cutting inserts at specific cutting cycles. This image acquisition system, including camera and extra light source, was fixed on the auxiliary spindle on tailstock (Figure 6.4).

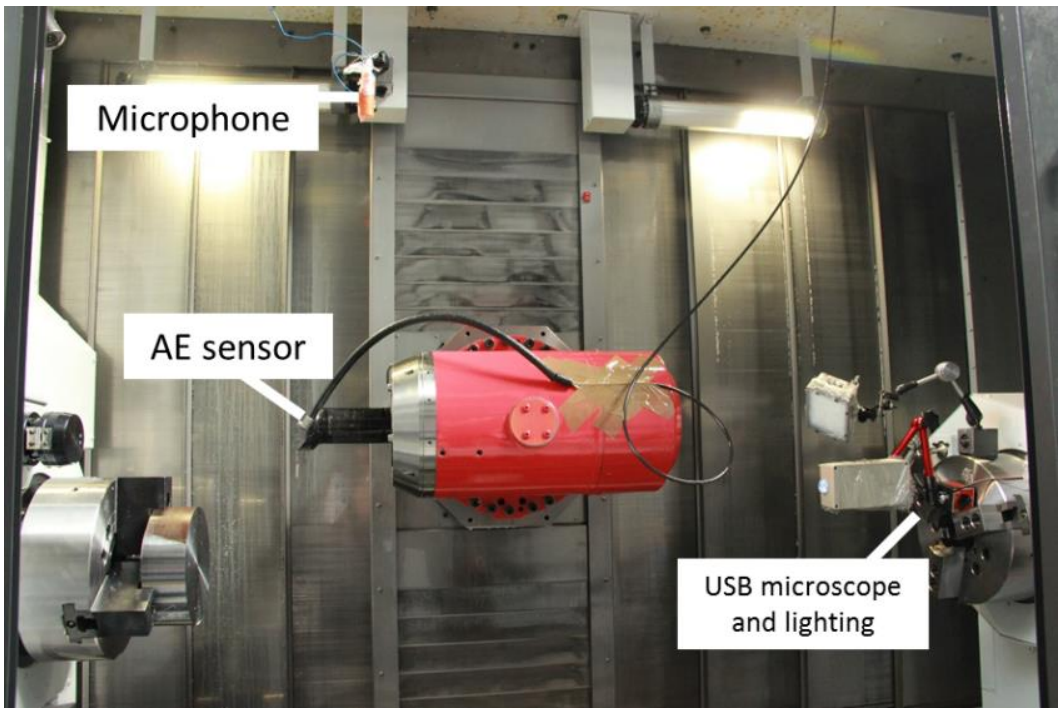

Figure 6.4 Working area of machining experiment

A PCB130E21 microphone with built-in preamplifier (Figure 6.5*(a)*) was used to record the cutting sound during the machining process. It was mounted on the ceiling of the machine by means of a magnetic stand, 1.2 m away from the cutting zone as shown in Figure 6.5(*b)*, and suitably enclosed to avoid damage from the coolant (Figure 6.5*(c)*).

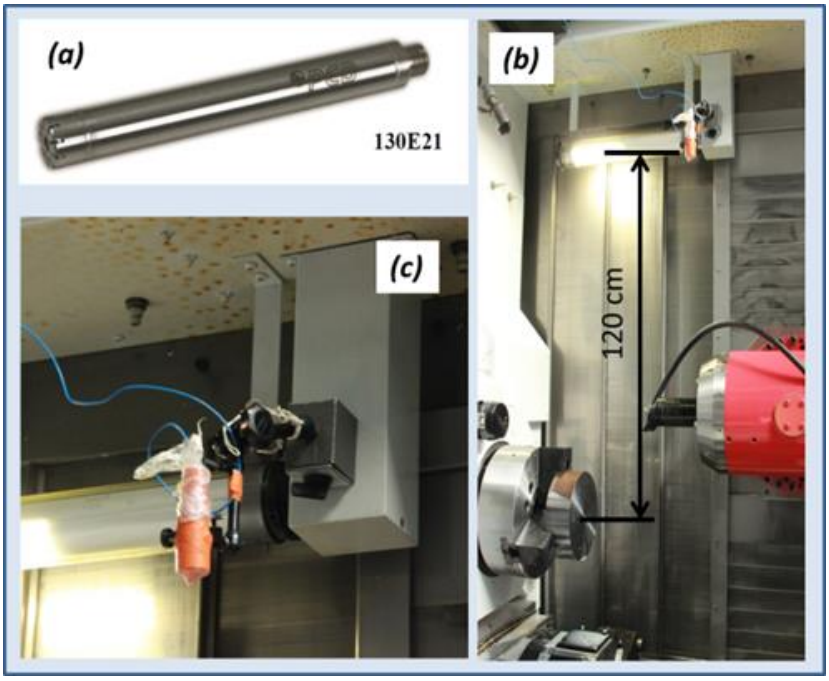

Figure 6.5 Arrangement of experimental apparatus showing the microphone (*a*) and its position in the machine tool (*b*, *c*)

6.4.2 Test Materials and Cutting Inserts

This study performed cutting experiments of EN24 being faced turned by a CNC lathe machine. EN24 is originally introduced for use in the automotive and machine tool industries for gears, pinions, shafts, spindles and similar components and has excellent machinability. The chemical composition of EN24 is shown in the Table 6.1. The cutting tool used in this study was a coated carbide cutting tool, DNMG 150608-PM (DNMG 442-PM). The cutting tool geometry and range of cutting parameters recommended are shown in Figure 6.6.

Table 6.1 The typical chemical composition of EN24 (% by weight)

C	Si	Mn	S	P	Cr	Mo	Ni
0.36/0.44	0.10/0.35	0.45/0.70	0.040 Max	0.035 Max	1.00/1.40	0.20/0.35	1.30/1.70

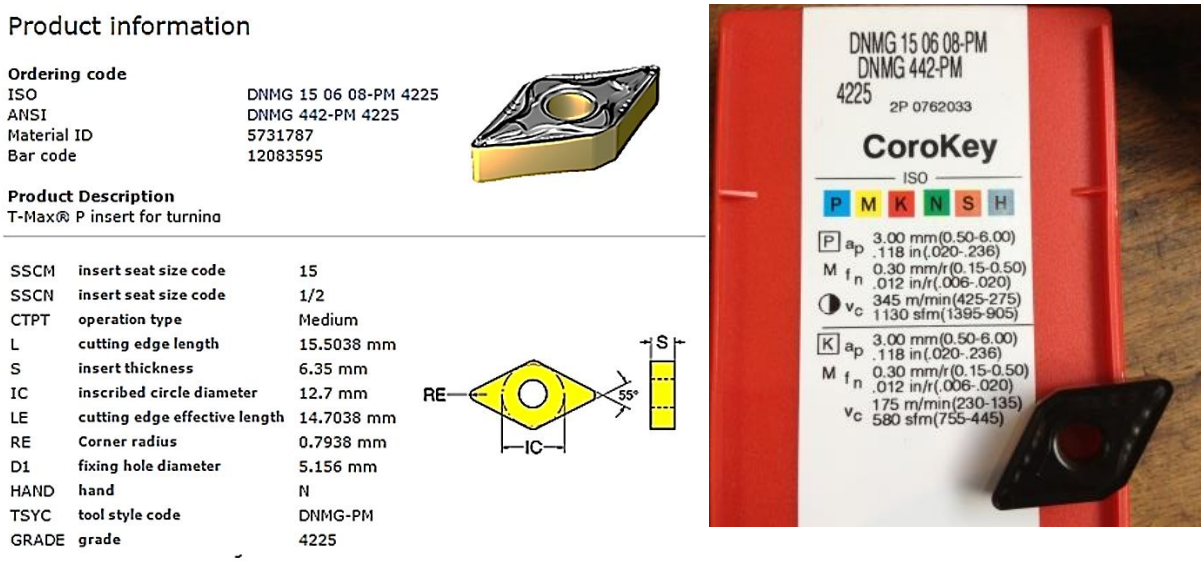

Figure 6.6 The product information of cutting insert used in this machining experiment

6.4.3 Experimental Trials

Typically, the cutting parameters used in the real turning process should be set according to the recommended range provided by the tool company (as found in Figure 6.6). To accelerate tool wear with few cuts, the machining experiments should be performed at higher values than recommended cutting conditions of the tool insert so as to save cost and time. However, this strategy may cause catastrophic consequences such as tool breakage. There is also a difference in the cutting state or the tool wear evolution between experiments and actual machining operation and this difference will affect the application of research findings when the monitoring system is used in a real machining operation.

Two process variables, the feed (F) and cutting speed (V_c), were varied. Three feed (F) were 0.30, 0.35, 0.40 millimetre per revolution and cutting speed or surface speed (V_c) were 280, 300, 320 metre per minute. The depth of cut (D) was constantly set at 0.5

mm in order to economically consume the workpiece. Seven cutting conditions are shown in Table 6.2, and Figure 6.7 illustrates the experimental matrix of seven cutting conditions.

Table 6.2 Process parameters used for performing machining trials

Condition	Cutting Speed (Vc) [m/min]	Feed rate (F) [mm/rev]	Depth of Cut (D) [mm]
1	300	0.30	0.5
2	300	0.35	0.5
3	300	0.40	0.5
4	280	0.35	0.5
5	280	0.40	0.5
6	320	0.35	0.5
7	320	0.40	0.5

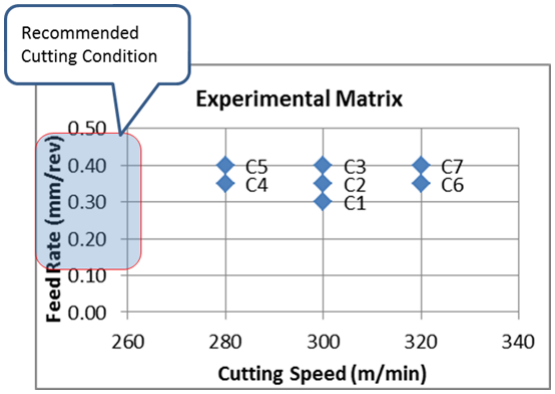

Figure 6.7 The machining conditions performed in this study

All machining trials were conducted in wet machining conditions (the cutting zone was flooded with Hocut795b coolant) until the observable flank wear width (FWW) on the main cutting edge exceeded 0.4 - 0.5 mm or the tools failed catastrophically. A machining trial, each corresponding to one of the seven sets of cutting conditions (Table 6.2) were each performed twice. This was to obtain a larger dataset to train and test the neural network to increase accuracy of the prediction model. For each condition, the inserts were removed from the tool holder and the flank wear width was measured optically (to ISO-3685) every 10, 20 and 30 cuts. The frequency of measurement was then increased as the wear limit was approached.

6.4.4 Signal Processing and Feature Extraction

As previously mentioned in Chapter 4, all sensor signals were acquired using a National Instruments cDAQ-9174 system which consists of three analogue input modules. Each module acquire the signals with different rate of sampling: 600 kS/s for acoustic emission signal, 50 kS/s for microphone and power consumption signals. LabVIEW software was used to acquire the sensor signals and performed data processing (i.e. signal segmentation and feature extraction). Sensory features from three sensors were extracted both in time and frequency domains as listed inTable 6.3. The definition of each feature has been presented in Chapter 4.

In Chapter 7, all 42 features (3 sensors x 14 features) will be selected using feature selection methods so as to obtain the selective feature sets used for training the neural networks. The results in this chapter show the trend of some interesting features compared to the width of flank wear. These are summarised in the following sections.

Table 6.3 The list of features extracted from the acquired signals

Time Domain		Frequency Domain	
Feature	**Feature Name**	**Feature**	**Feature Name**
XX_tRMS	Root Mean Squred value	**XX_fMean**	Mean Magnitude
XX_tMean	Mean value	**XX_fMax**	Magnitude at peak frequency
XX_tMax	Maximum amplitude	**XX_fPeakFreq**	Peak Frequency
XX_tP-P	Peak-to-Peak value	**XX_fMax-p-Mean**	Ratio of Max per Mean magnitude
XX_tKur	Kurtosis	**XX_fKur**	Kurtosis
XX_tSkew	Skewnesss	**XX_fSkew**	Skewness
XX_tSD	Standard Deviation	**XX_fSD**	Standard Deviation

XX = AE, MIC, POW

6.5 Results and Discussion

The analysis of the data obtained from the machining experiment can be separated into two main parts: signal evaluation (this chapter) and sensor fusion by neural networks (in Chapter 7). The first part of this chapter presents the flank wear progression during the turning process, the effect of cutting speed and feed on AE, power consumption, and also microphone signals. Additionally, the relationship of power consumption of main spindle motor is compared with flank wear progression. The typical results are discussed in this chapter and all extended results are summarised in Appendix B.

6.5.1 Flank Wear Progression during Experimental Trials

It is necessary to obtain the width of flank wear during machining to develop tool wear curve. Flank wear was monitored in three regions in this study. Three angle images of cutting inserts comprise flank wear width at nose radius (FWWN), flank wear width at right cutting edge (FWWR), flank wear width at left cutting edge (FWWL) as shown in Figure 6.8 and Figure 6.9.

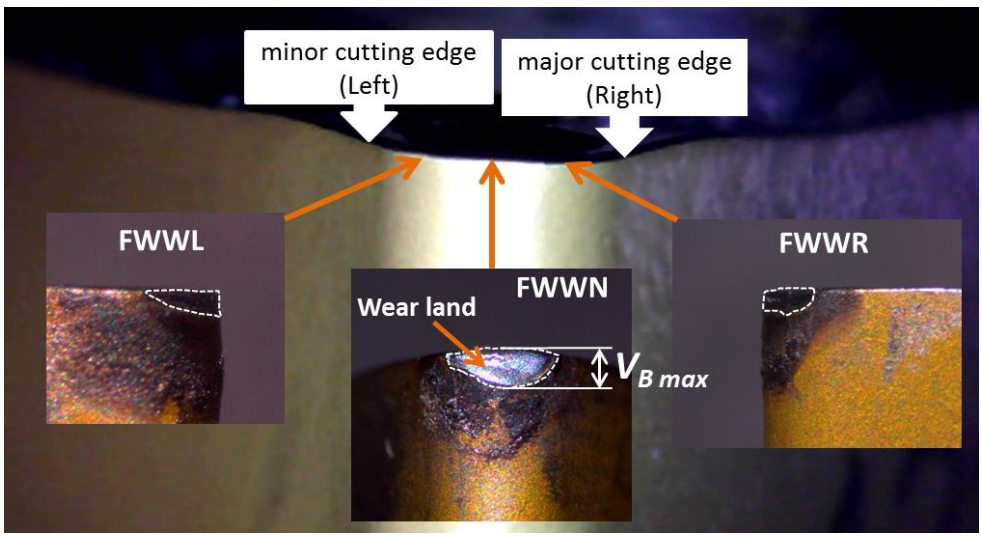

Figure 6.8 Definition of flank wear width on cutting insert

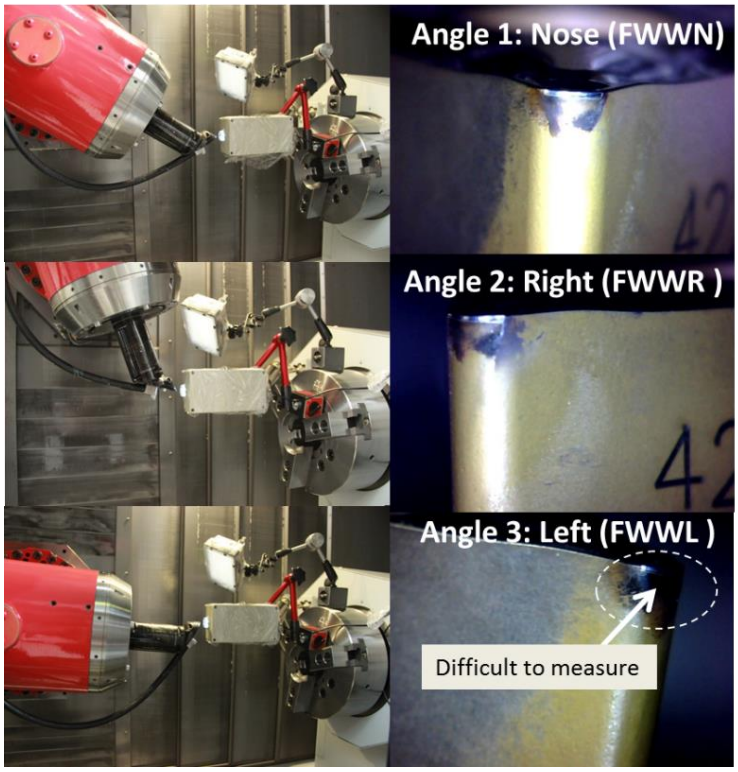

Figure 6.9 Three tool holder positions to capture flank wear of three cites during turning

Figure 6.9 obviously seen that the flank wear width on left side (angle 3) of cutting inserts could not be obtained because it was not practical to fix a USB microscope camera at one specific location to take the picture for all three angle images. Similarly, it was difficult to adjust the tool holder in order for it to be at well-adjusted position for obtaining a good quality image. Due to the arrangement of the apparatus in this study, it was not possible for the external light source to shine on the cutting edge perpendicularly. As a result, the image of left-side cutting edge (FWWL) was darker than any other angles that could not be useful. Fortunately, FWWN and FWWR are the major cutting edges and were used in this work for training the neural network (in Chapter 7).

6.5.1.1 Wear Images Taken by a USB Microscope

Traditionally, sensory features of actual sensor signals are used as inputs and fed into the AI algorithms to train the neural networks with the flank wear obtained by a microscope used as target of the network (Figure 6.10). It is time-consuming to interrupt the machining to remove cutting tools from a tool holder in order to measure tool wear on a microscope. Consequently, the first aim was to assess the feasibility to use an inexpensive USB microscope to take the tool wear images during a machining experiment (experimental details in Section 4.2.4). It is suggested that the flank wear width obtained by image processing technique can then be used as a reference for off-line wear measurement. This can reduce the experimental time and make online flank wear measurement by a machine vision approach a possibility.

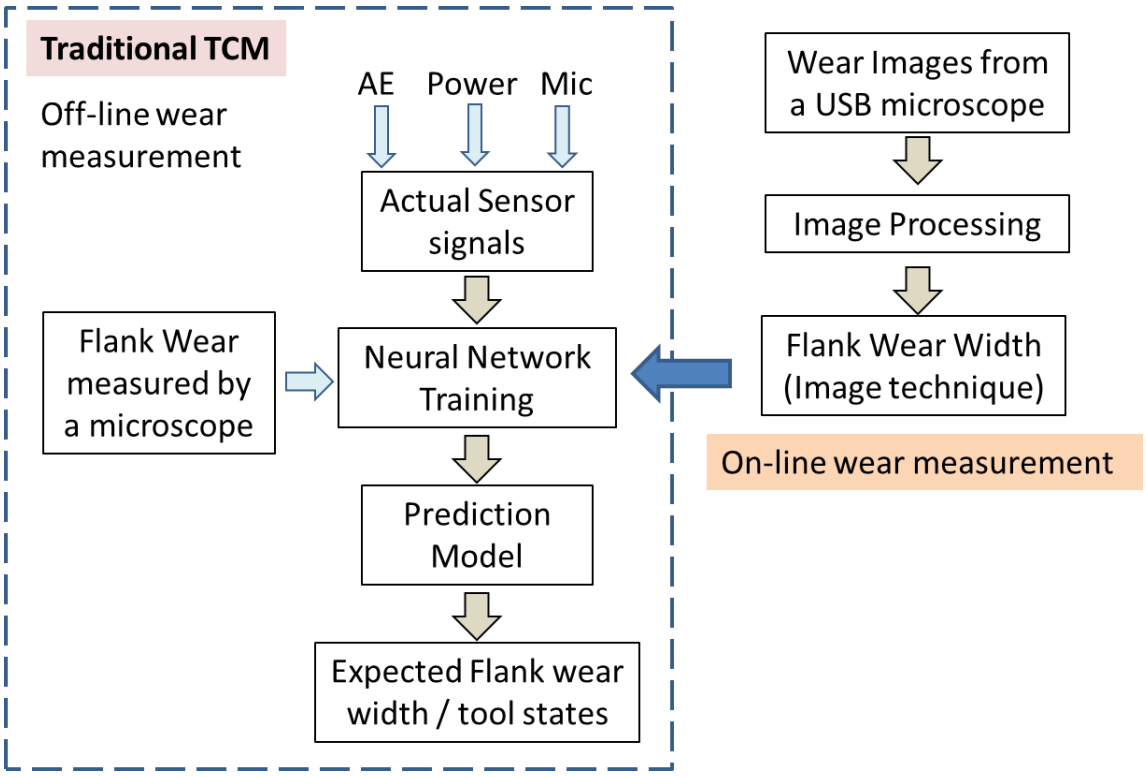

Figure 6.10 The concept of flank wear measurement

In this work, an image processing program has been developed using image processing toolbox in MATLAB to calculate the width of flank wear and wear area as shown in Figure 6.11. The wear images were captured from three angles as shown in Figure 6.9. Pre-image processing techniques such as filtering, rotating, and thresholding were then used to improve the image for flank wear calculation. The true colour images of the new cutting tool captured by the USB camera were turned into binary images before subtraction between the new tool images and worn tool images (retouched by adding white pixels). From the results, it looks feasible to use this image processing technique to do online flank wear measurement by the USB microscope when the proper calibration has been adopted.

In reality, there are several difficulties concerning the tool wear images taken by the USB microscope as illustrated in Figure 6.12.

Ambient light control: due to performing in a wet machining condition it is difficult to achieve consistent lighting of the tool. This is in contrast to the study of Shahabi *et al* [68, 72], who used a similar image processing concept to subtract unworn and worn tool images pixel-by-pixel, but their images were obtained from the turning process without using cooling liquid which enabled the ambient light to be more easily controlled. The outputs of designed image processing program where it used wear images from the machining experiment are displayed in Figure 6.13.

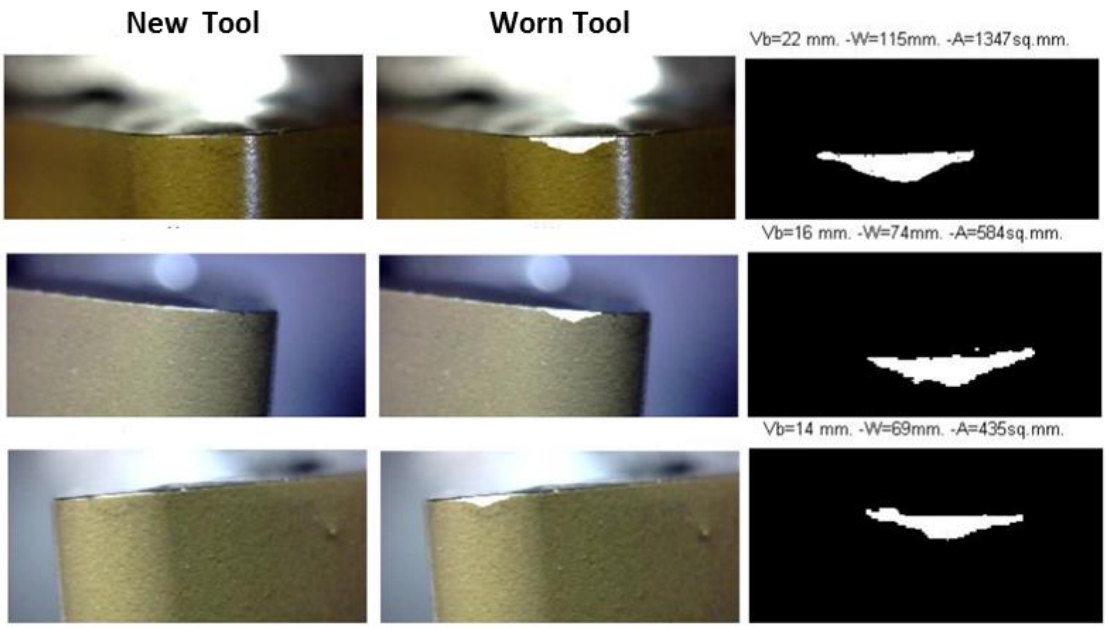

Figure 6.11 Subtraction technique used for determining flank wear on cutting edge

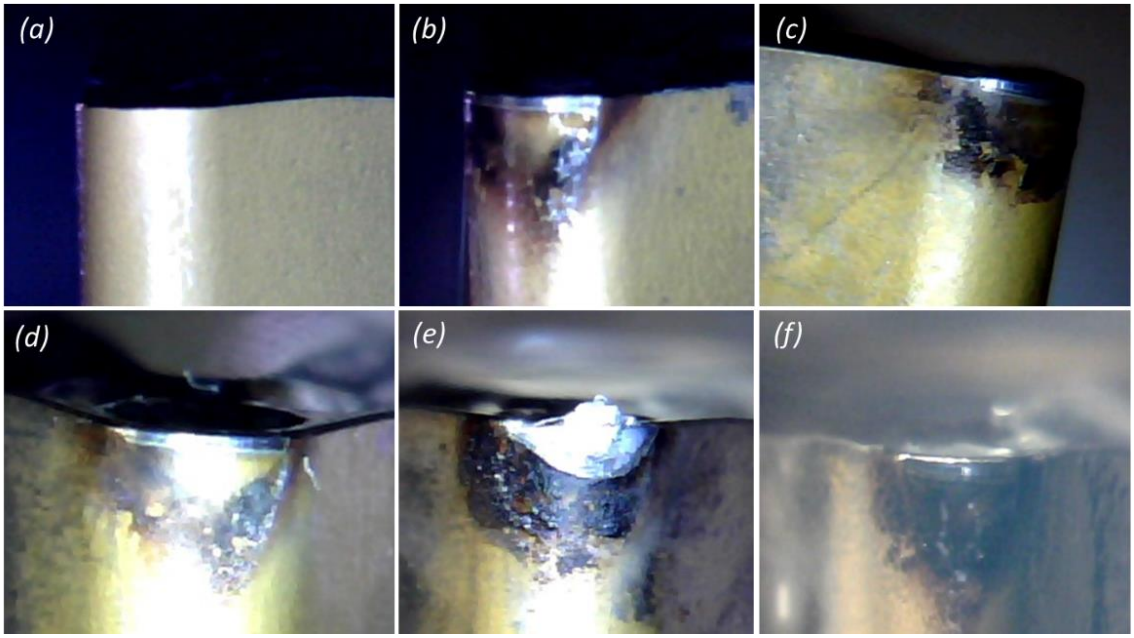

Figure 6.12 Example images taken from the USB microscope in real machining:
(a) new tool, *(b)* wet tool, *(c)* insufficient light, *(d)* undefined wear boundary,
(e) oxidation stain and BUE, *(f)* moisture image

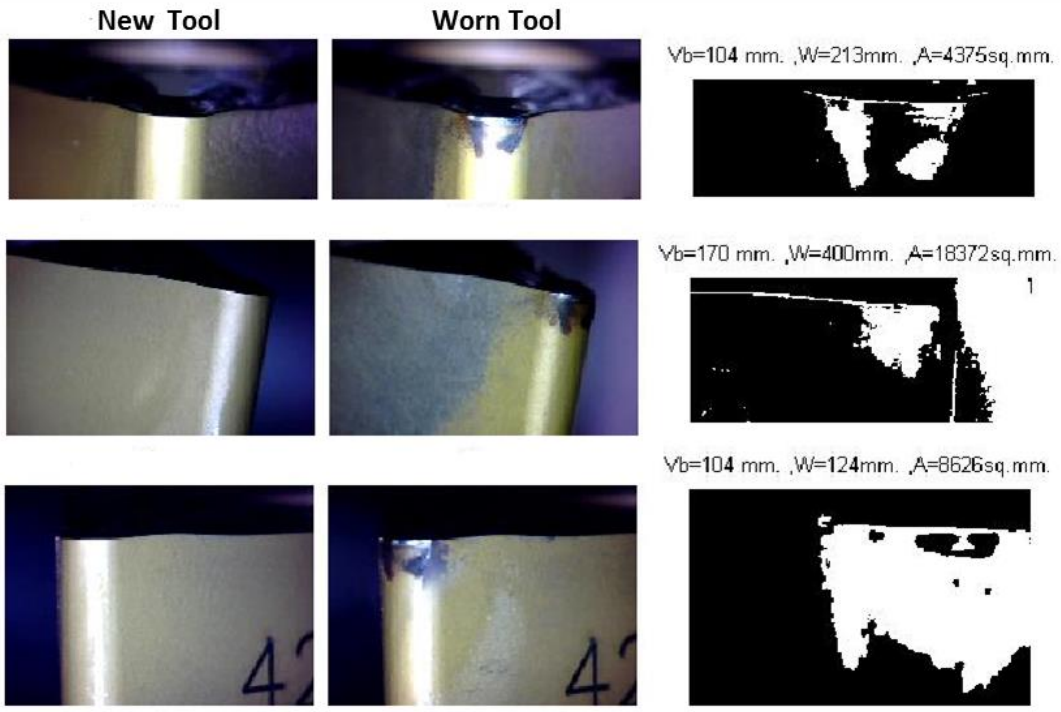

Figure 6.13 Output images where the real wear images of cutting tool were used

As shown in Figure 6.13, the tool was unable to extract the boundary of the wear area due to the oxidised surface, wet tool, and moisture.

Tool orientation: similarly, it is also seen in Figure 6.13 that the system is highly sensitive to the orientation of the tool, its magnification, and its effect on the ambient light. This is an issue because the worn surface is not normal to the direction that the USB microscope are taking the image from. Therefore, the image is seeing a projection of a plane which will have an adjustment to its area accordingly. In this case, the USB microscope should be normal to the tip of the tool, which will be approximately normal to the worn surface, and so that the tool images may not have the problem of the projection of a tilted plane.

Magnification of the image: it is important to consider and record the magnification settings of the camera. Any problems can be avoided by using the same zoom settings in all the images. If there is any change in magnification, it will need to measure the exact length/width of the tool insert in pixels and adjust the measured area accordingly. As for the lighting problem, although the microscope has a built-in light source around the lens, it also need for an extra light source. However, the acquired images were not good enough quality to process the images.

Depth of field and focus: the depth of field refers to the range of distance that appears acceptably sharp. It varies depending on camera type, aperture and focusing distance. The USB microscope camera used in this experiment provides a fixed large aperture (smaller F-stop number) and closer focusing distances which produces a shallower depth of field. Consequently, the edge of cutting inserts can be captured clearly in some

area which is in focus, while the other area is out of focus. Therefore, the image of the cutting insert is not sharp enough to detect all the areas of cutting edge.

6.5.1.2 Flank Wear Progression Measured by a Microscope

To obtain flank wear, traditional measuring method was used during machining experiment. Figure 6.14 shows examples of flank wear developed by cutting process which were captured by a microscope.

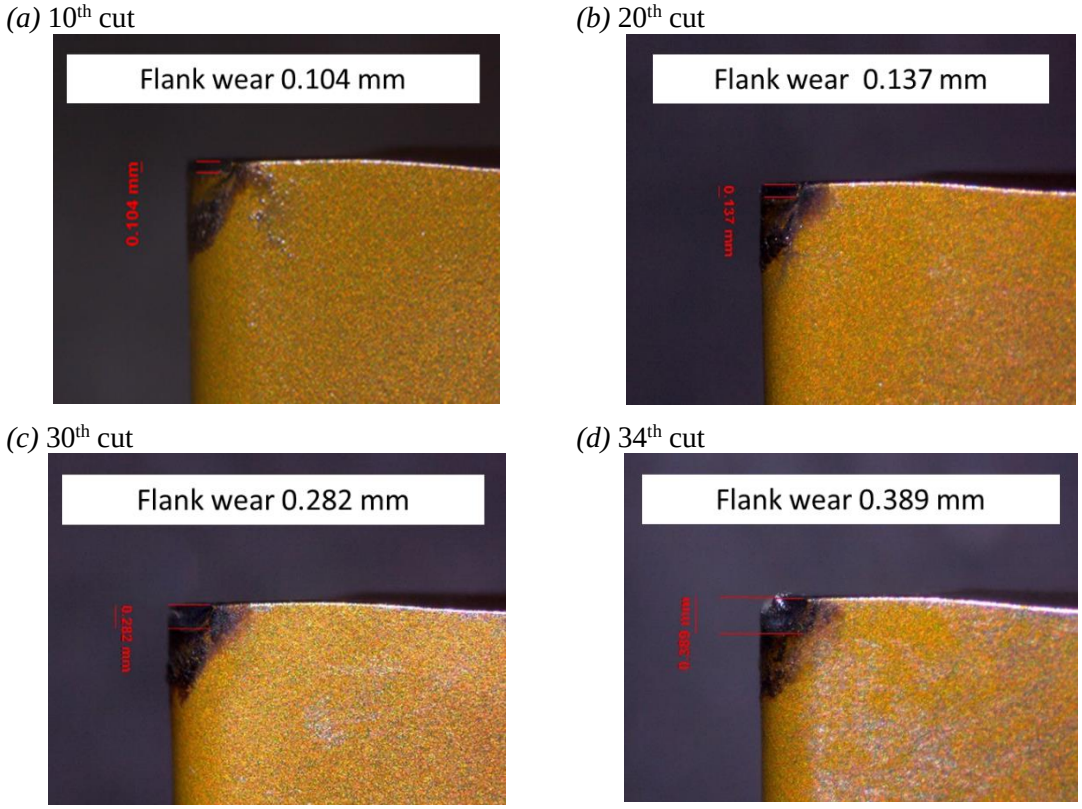

Figure 6.14 An example flank wear on cutting inserts under a microscope (Vc = 300 m/min and F = 0.35 mm/rev)

The flank wear progression of seven cutting experiments (replication 1) measured by the microscope are shown from Figure 6.15 to Figure 6.17, while the flank wear of replication 2 is summarised in Appendix B. In this study, x-axis of tool wear graphs represents the cutting time, or number of cuts in this case, while the y-axis represents the width of flank wear. From the experimental matrix (Figure 6.7), seven cutting conditions are grouped into three main combinations: at constant cutting speed (V_c=300 m/min), at constant feed (F=0.35 mm/rev), and at constant feed (F=0.40 mm/rev).

For the first combination, tool wear graphs of three cutting conditions (C1, C2, and C3) are shown in Figure 6.15*(a)* and Figure 6.15*(b)* which were performed at cutting speed (V_c) 300 m/min and feed 0.3, 0.35 and 0.4 mm/rev respectively.

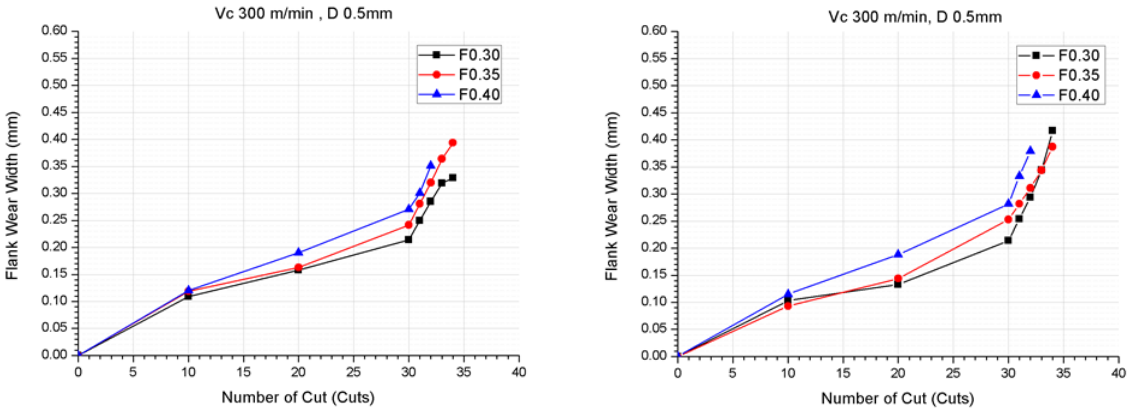

(a) *(b)*

Figure 6.15 Flank wear width at cutting speed 300 m/min on the main cutting edges (replication 1): *(a)* nose radius, *(b)* right side

At the beginning, the cutting edge wears rapidly. The first region occurs within the first few minutes of cutting (about 10 cuts). After that, the wear rate then increases uniformly in the steady-state middle zone. In this region, the 'curve' has a linear relationship. The slope of tool wear in second region is affected by cutting conditions. It can be concluded that using more cutting speed encourages wear rate. Finally, in the third region, tool wear increases sharply until it fails or it becomes severely worn to be effectively useless. In Figure 6.15, these wear curves display three states of tool wear, which are clearly in agreement with the tool wear curve presented Chapter 2 (Section 2.4.3).

For the second combination, Figure 6.16*(a)* and Figure 6.16*(b)* compare the flank wear width of three cutting conditions (C4, C2, and C6), which were machined at a constant feed rate 0.35 mm/rev and at three different cutting speeds.

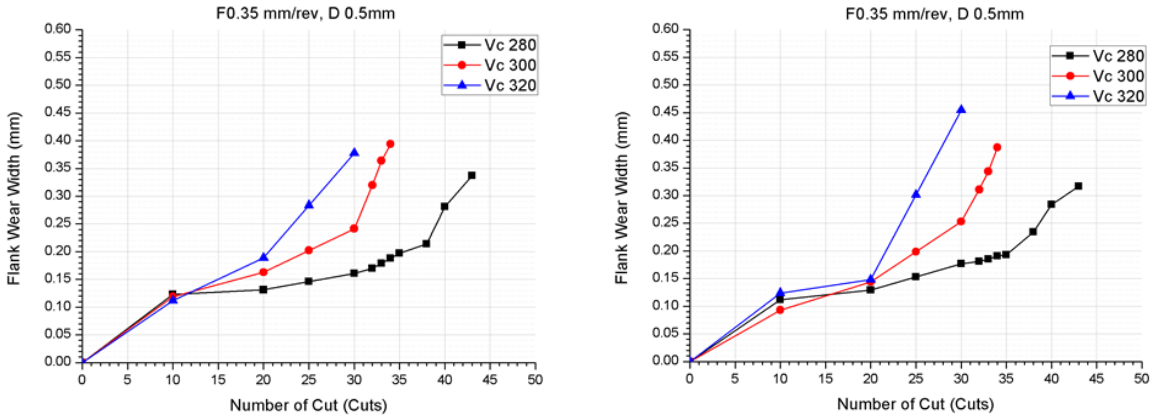

(a) *(b)*

Figure 6.16 Flank wear width at Feed rate 0.35 mm/rev on the main cutting edges (replication 1) : *(a)* nose radius, *(b)* right side

From Figure 6.16, it seems that cutting speed has a quite impact on flank wear. Tool life decreases with increase in cutting speed because cutting higher speed leads to high temperature at cutting zone so that tool wear is accelerated. Consequently, tool life is reduced.

Lastly, the flank wear widths of condition C5, C3, and C7 performed cutting at constant feed 0.40 mm/rev are compared and shown in Figure 6.17*(a)* and Figure 6.17*(b)*. Similar to before, the cutting at higher cutting speed encourage more wear rate representing shorter tool lifetime.

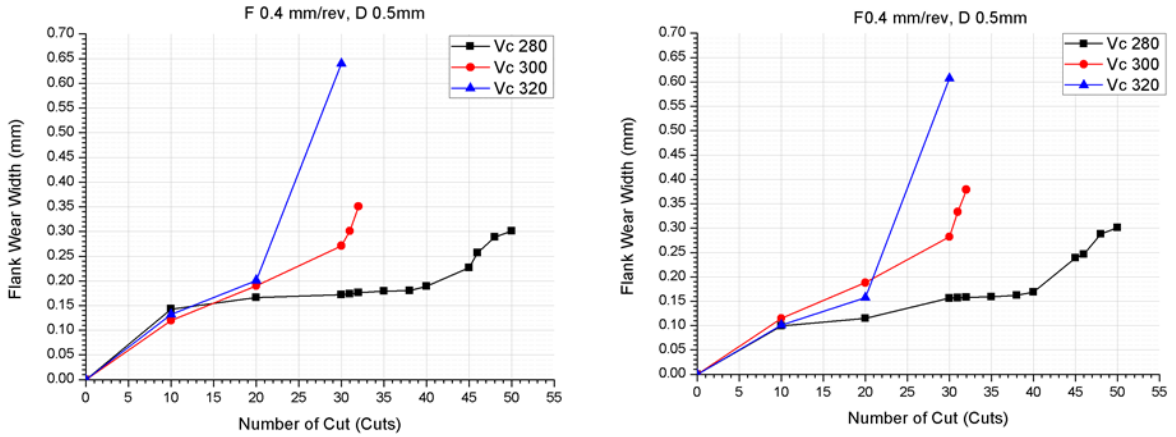

(a) *(b)*

Figure 6.17 Flank wear width at Feed rate 0.4 mm/rev on the main cutting edges (replication 1): *(a)* nose radius, *(b)* right side

In conclusion, the wear progression of almost all cutting trails is in good agreement with ideal tool wear curve described in Chapter 2. It is a nature of machining activities that it is not always possible to obtain the same results by using the same conditions. It is known from experience that wear on cutting tool is often not highly repeatable and this is also described in the study of Zhang *et al* [115]. This inconsistency of the result may be due to defect of material workpiece, inconsistency of cutting inserts, and setting-up arrangements.

However, the turning point between break-in period and steady state of wear cannot be defined exactly, as the first flank wear measurement was attained at the cut number 10, which might be a time after the transition state between the first and the second tool wear regions. To determine the turning point, flank wear should be measured more frequently during the first period.

Firstly, this study attempted to use a cheap USB microscope camera to monitor tool wear in turning process instead of very expensive monitoring system. The novel method takes the advantage of processing the images of tool tips captured by a camera, which, in turn, provides faster analysis and cheaper cost of operation compared to traditional methods. However, there are several problems obstructing the use of USB microscope in this study, as addressed in the previous section (Section 6.5.1.1). It is expected that tool wear evolution measured by this cheap camera can achieve similar

results to more expensive methods. As found in several studies [66-68, 71, 72], the image processing technique was successfully applied to tool wear measurement in which a high resolution CCD camera with external light source has been normally used. If the addressed problems in using a USB microscope camera can be tackled, its application for real industrial machining condition could be achieved. Therefore, although more research on this issue needs to be undertaken this part of the work contributes significantly towards the main goal of developing a tool wear monitoring system with cost effective equipment.

6.5.2 The Effect of Cutting Speed and Feed on Acoustic Emission Signals

As reported in the review of Siddhpura *et al* [9], the development of tool wear on cutting insert can be represented by acoustic emission signal both the time and frequency domain. Possible sources of AE during the metal cutting process summarised by Dronfield *et al* [89] are: *(a)* plastic deformation in workpiece and chip (primary cutting zone), *(b)* friction contact (between workpiece and tool flank face (flank wear) or *(c)* between the tool rake face and chip, *(d)* collisions between chip and tool, *(e)* chip breakage, *(f)* and tool fracture as shown in Figure 6.18.

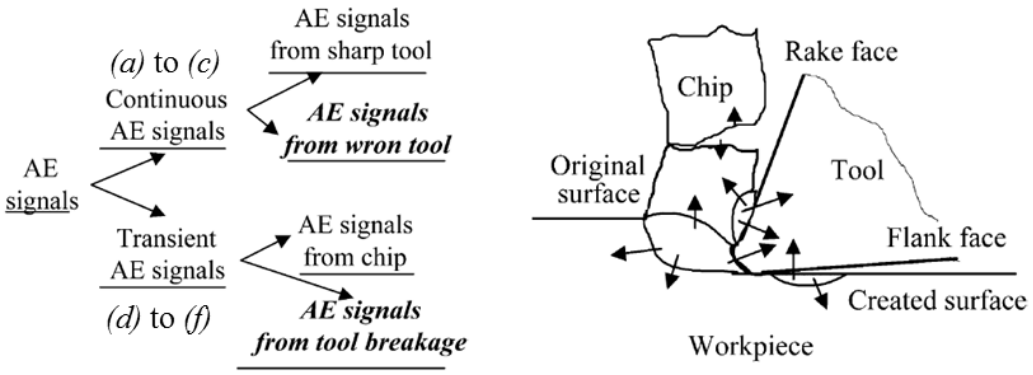

Figure 6.18 AE signal type in cutting process (adapted from [12])

Generally, acoustic emission signals from a cutting process can be classified into two types: continuous and burst (as shown in Figure 6.19). The continuous type represents the AE activity in the cutting zone (from (*a)* to *(c)*) and the burst type or transient signal comes from *(d)* to *(f)* [12]. Bhuiyan *et al* [92] reported that the frequency of chip formation in turning or continuous AE signal has been found between 68.3 kHz and 634.83 kHz and the maximum intensity was observed at 97.7 kHz, which is a relatively high frequency.

Compared to Figure 6.20, an example of the frequency spectra of AE signal obtained during the work performed for this thesis, it can be concluded that the high frequency AE signal (from 60 kHz to 140 kHz) originates from the continuous AE signal, and the burst type signal due to chip breakage is at about 20 kHz (low frequency). Therefore

the types of chips and cutting tool conditions have a direct consequence on AE signal characteristics.

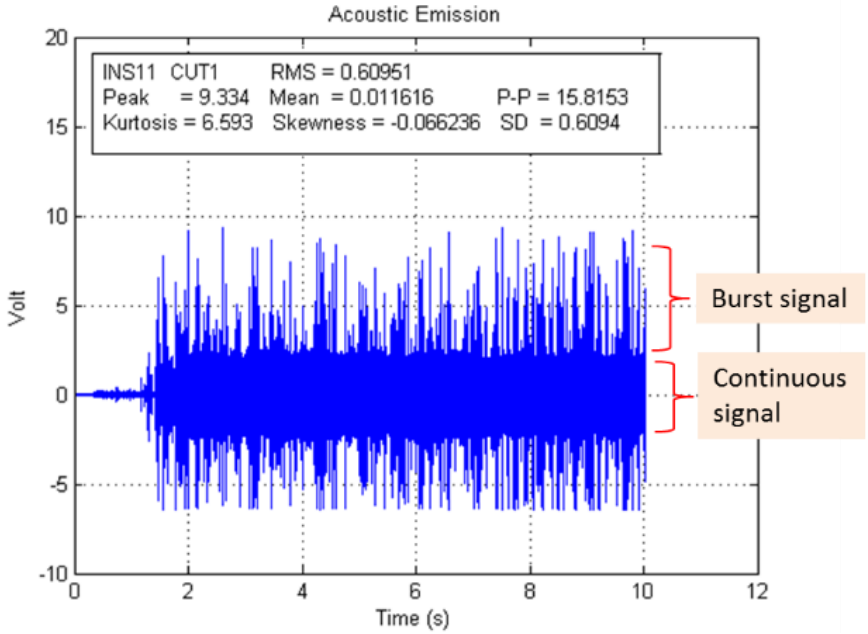

Figure 6.19 Typical AE signal in time domain from the turning process

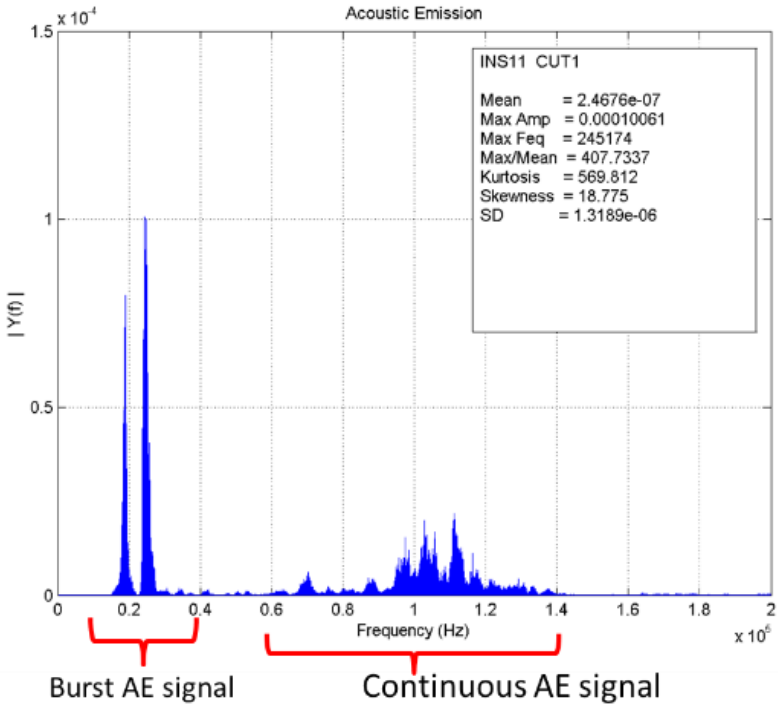

Figure 6.20 Typical AE signal in frequency domain from the turning process

6.5.2.1 Acoustic Emission Signal during Tool Wear States

In this section, the characteristics of AE signals during the three states of tool wear are illustrated through both time domain and frequency domain graphs. Figure 6.21 displays a tool wear curve from the cutting condition 1 (V_c 300, F0.3, D0.5) which can

be clearly defined three tool wear states. The first state (break-in) is defined from the start cutting to cut number 10, the second (steady-state wear) from cut number 11 to 30, and third the dramatic increase after cut number 30 (failure wear). AE signals in both the time and frequency domains can illustrate the point of signal change which is denoted by the number filled in the circles (1 to 9). Further graphs representing all of the recorded data can be found in Appendix B and the points of particular interest are illustrated here. Examples of AE signals in time and frequency domains are shown in Figure 6.22 (break-in), Figure 6.23 (steady-state wear), and Figure 6.24 (failure wear).

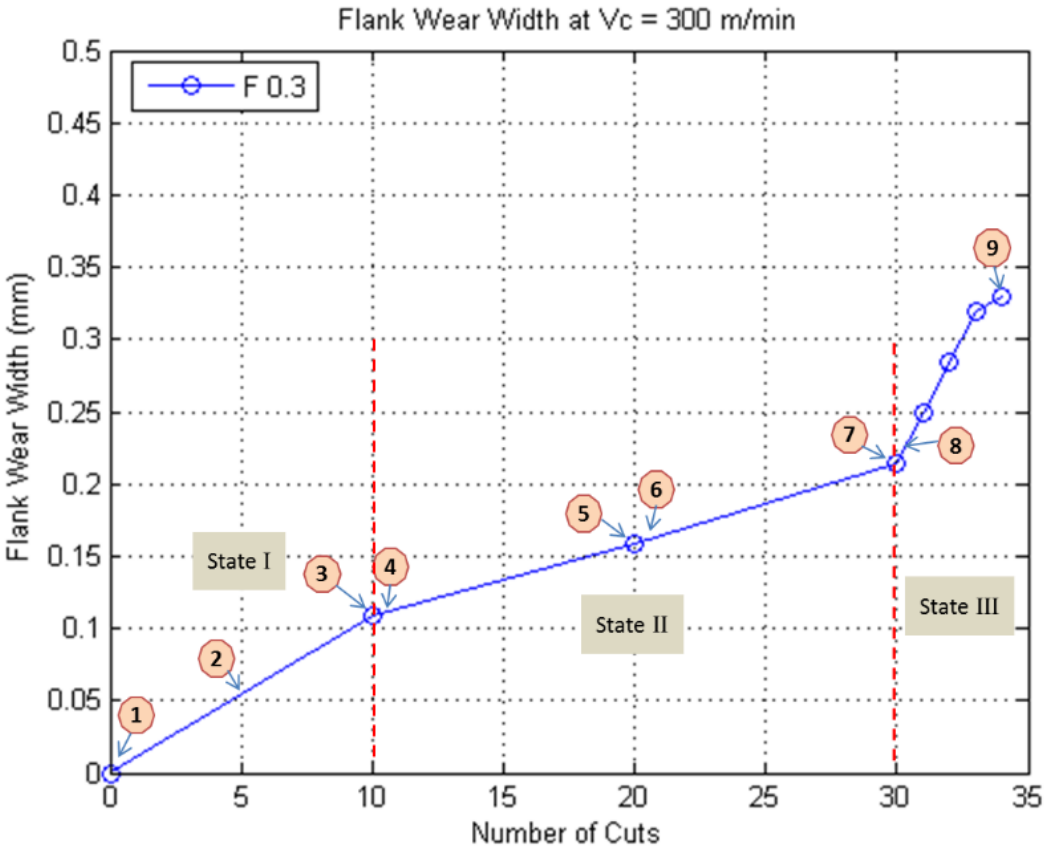

Figure 6.21 AE signals at different tool wear state performed by cutting condition 1 (V_c 300, F0.3, D0.5)

Figure 6.22 shows AE signals of cut numbers 1 and 10, which are in the break-in wear state. In cut number 1, there is significant AE burst type signal (representing chip breakage) but the magnitude of each frequency rarely is the highest. This means the new tool has a good cutting edge and ability to cut the workpiece.

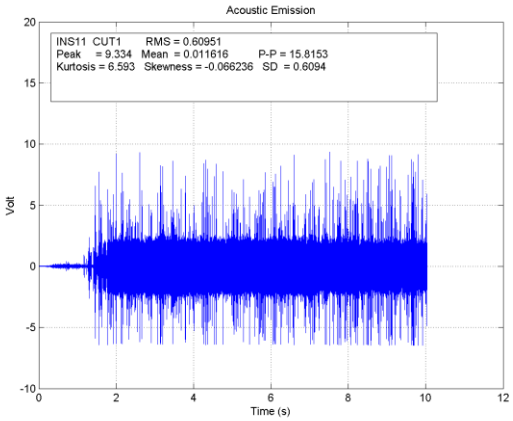

(a) Time domain of point 1, 1st cut

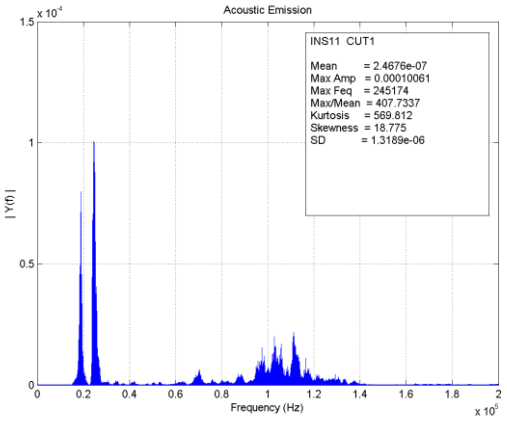

(b) FFT of point 1, 1st cut

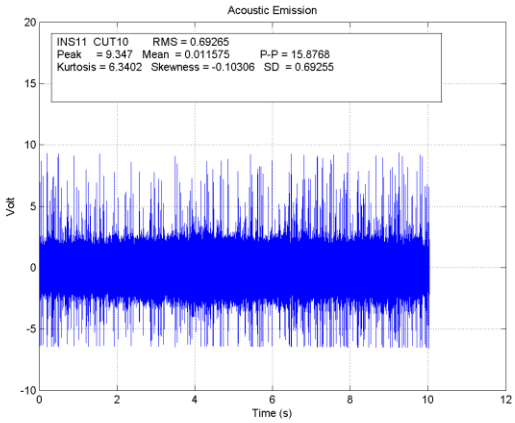

(c) Time domain of point 3, 10th cut

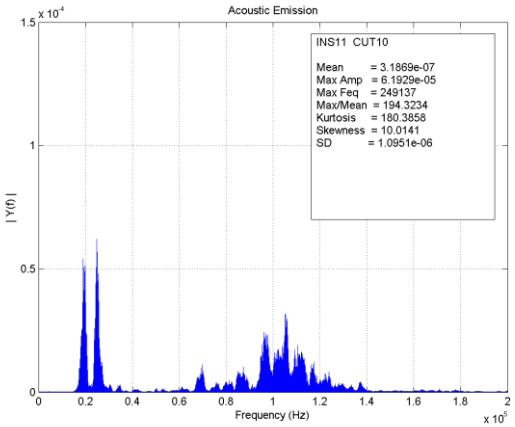

(d) FFT of point 3, 10th cut

Figure 6.22 Typical AE signal during break-in period (cut number 1 and 10)

In cut 11, as seen in Figure 6.23*(a)* and 6.22*(b)*, the AE signal in the time domain reveals that there has been fewer bursts so therefore fewer chip breakages than the first period. The FFT shows the frequency content of 30 kHz disappears, illustrating that the tool wear state has changed from breaking-in to steady-state wear as denoted in Figure 6.21 (point 4). This signal characteristic has continued until the middle of steady-wear state at about cut number 20. After that, in cut 21, there is a significant change both in time and frequency domain. This change can be used as a first warning signal representing half the tool life.

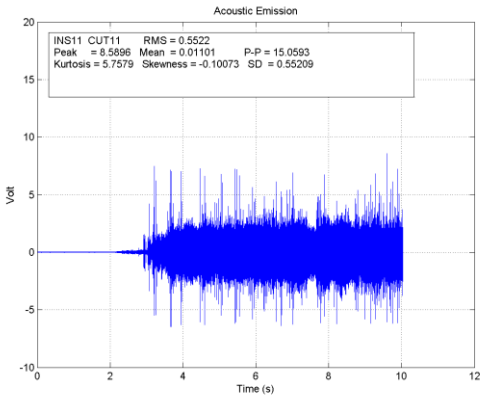

(a) Time domain of point 4, 11th cut

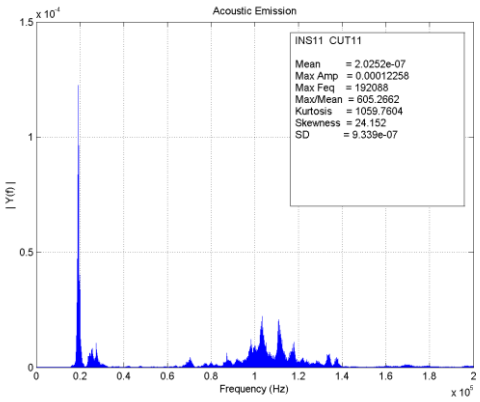

(b) FFT of point 4, 11th cut

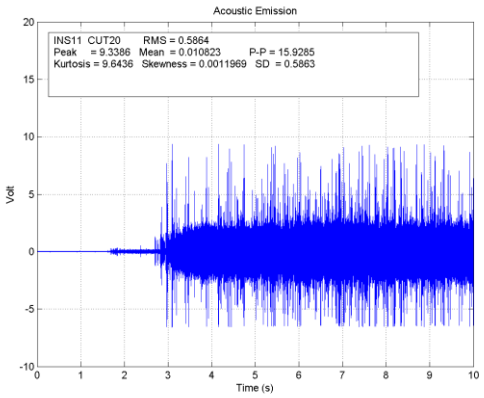

(c) Time domain of point 5, 20th cut

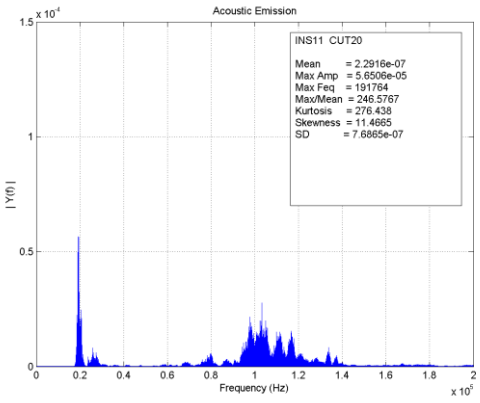

(d) FFT of point 5, 20th cut

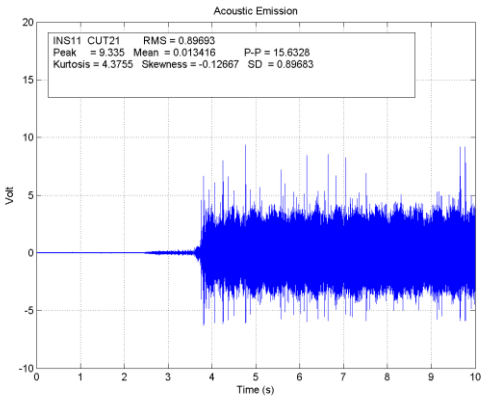

(e) Time domain of point 6, 21st cut

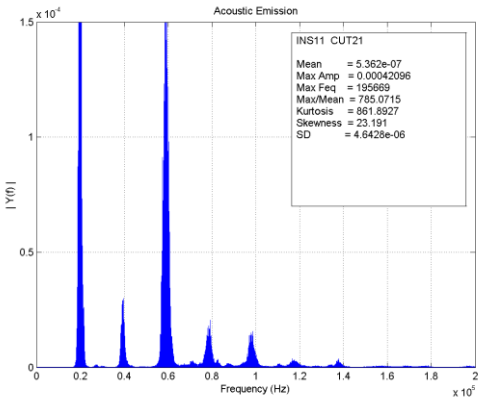

(f) FFT of point 4, 21st cut

Figure 6.23 Typical AE signal during steady-wear period (cut 11, 20, 21)

Figure 6.24 shows the AE signals in the final state of tool wear. The severely-worn tool has lost the ability to cut effectively and the number of chip breakages is extremely reduced. Consequently, the burst type signal of low frequency content becomes absent in FFT graph, while the amplitude of AE-continuous type increases significantly. The amplitude of the AE signals rapidly increases from cut 30 to cut 31, which can be defined as the transition state between the steady-wear and severe wear regions. It can be clearly seen that in cut 34 that AE signals in time domain have very high amplitude, as does the high frequency content.

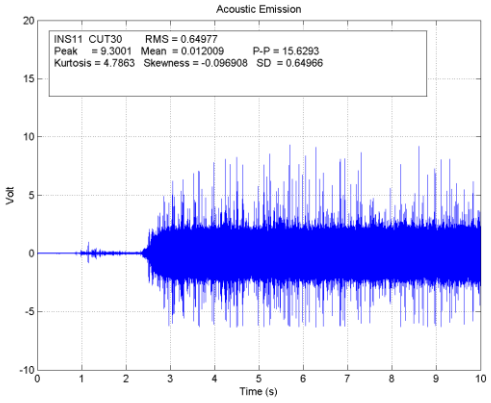

(a) Time domain of point 7, 30th cut

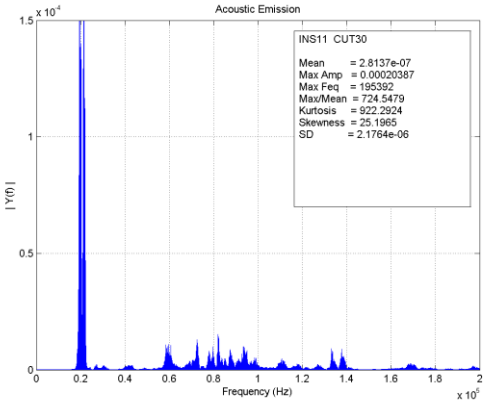

(b) FFT of point 7, 30st cut

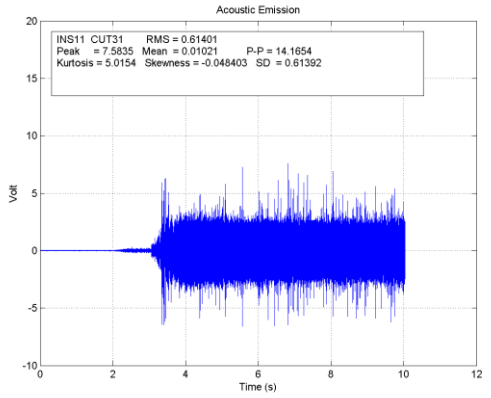

(c) Time domain of point 8, 31st cut

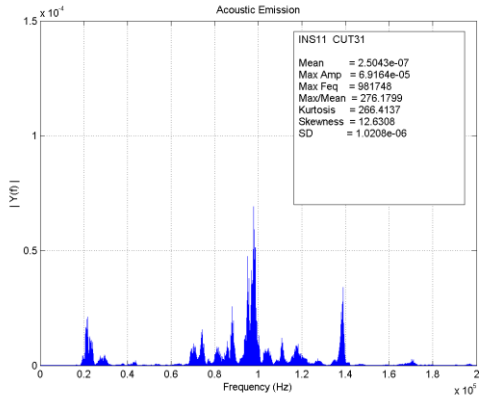

(d) FFT of point 8, 31st cut

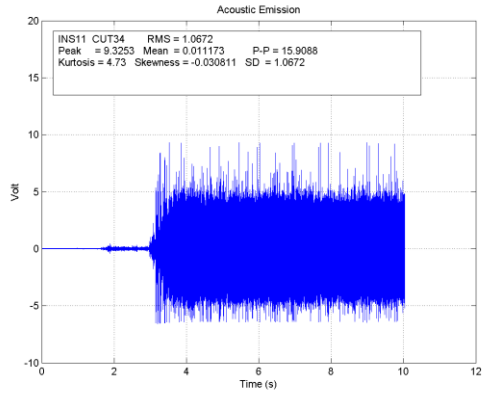

(e) Time domain of point 9, 34th cut

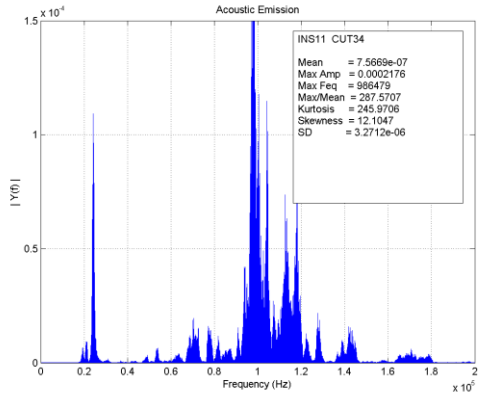

(e) FFT of point 9, 34th cut

Figure 6.24 Typical AE signal during wear out period (cut 30, 31, 34)

Figure 6.25 illustrates the example chips removed from the workpiece during the experiments for each of the three wear state regions. The chip produced when using a new tool (Figure 6.25*(a)* and Figure 6.25*(b)*) has good shape and colour characteristics (long, continuous, periodic break, and shine colour) as discussed in Chapter 2. The chip colour is a bright colour, especially in break-in wear region (Figure 6.25*(a)*) and becomes darker due to higher temperature as the chip-tool contact area increases as the tool is used (Figure 6.25*(b)*). Also, the cutting ability of the inserts is significantly decreased after the middle point of steady-state wear region (20 cut) shown in Figure

6.25 *(c)* by the reduced spiral radius and darker colour of the chips compared to the ones shown in Figure 6.25*(b)*. The long-ribbon like chips and darken ribbon in Figure 6.25*(d)* are produced in the final state wear region. Accumulation of this type of chip (Figure 6.26) is unwanted because they can cause damage to instrumentation related cables around the cutting point and the chips may entangle with tool holder or jig and fixture, and ultimately stop the process.

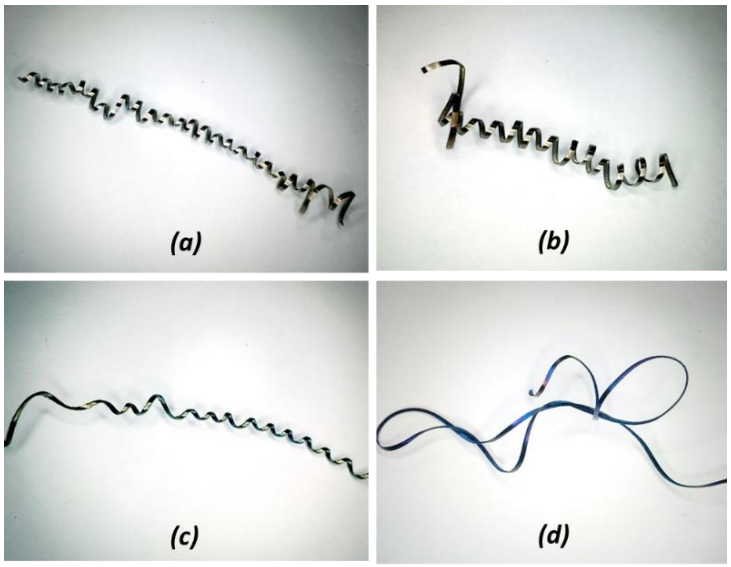

Figure 6.25 Chips removed from the workpiece: *(a)* 5th cut (break-in), *(b)* 15th cut (steady wear I), *(c)* 25th cut (steady wear II), and *(d)* 32nd cut (failure wear)

Figure 6.26 Chips removed from the workpiece in the failure wear state

6.5.2.2 The Effect of Cutting Speed and Feed on AErms and AEp-p

Continuous-typed AE signal representing tool wear can be monitored by the RMS value, while burst type signal representing chip breakage can be monitored by peak-to-peak ($AE_{p\text{-}p}$). These features extracted from all cutting conditions are grouped and illustrated only two combinations. All combination graphs are presented in Appendix B. Figure 6.27 combines three different cutting conditions where a constant 300 m/min of cutting speed was used. Similarly, experiments with at constant feed rate 0.35 mm/rev are shown in Figure 6.28.

In general, AE_{rms} of all conditions slightly increases during cut 1-15 and then significantly increase depending on feed. This significant change can be used as warning signal for when the tool becomes dull. According to several studies [9, 103, 120], the greater feeds result in the higher RMS level and the earlier the increasing of RMS level. Nevertheless, AE_{rms} of the highest feed (0.4 mm/rev) in Figure 6.27*(a)* lies at the middle place of the other two conditions and shows the significant increase of RMS value lately.

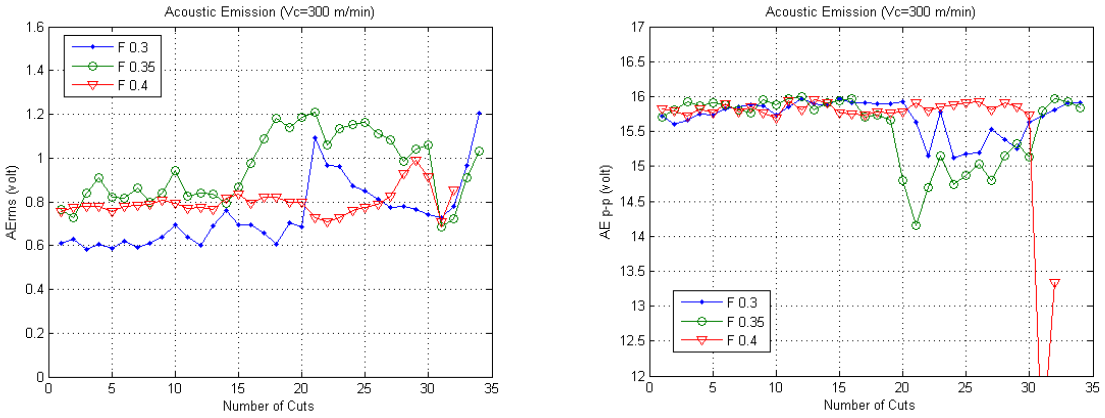

(a) *(b)*

Figure 6.27 RMS and peak-to-peak values of AE signal AE signals during machining at constant cutting speed 300 m/min: *(a)* AErms and *(b)* AEp-p

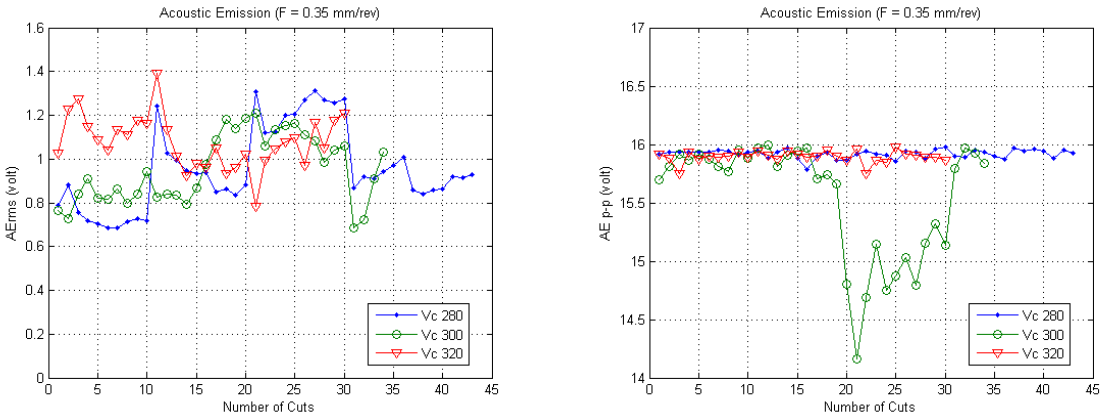

(a) *(b)*

Figure 6.28 RMS and peak-to-peak values of AE signals during machining at constant feed rate 0.35 mm/rev: *(a)* AE_{rms} and *(b)* AE_{p-p}

One possible explanation of these unexpected results might be that the RMS values in this graph were determined from AE signals without the separation of burst and continuous signal types. From the time domain graphs, a large number of peaks representing chip breakage were found towards the beginning of experiment and fewer later on. Thus, the number of peaks and their amplitude has a major consequence on variation of RMS value. It can be concluded that a high chip breakage rate was found in cutting with new tools, while low number of peaks represents a lower chip breakage rate as a result of using a worn tool.

Considering to the peak-to-peak amplitude (AE_{p-p}) in Figure 6.27*(b)*, the three conditions shows similar average AE_{p-p} up to the cut number 16, which represents the use of sharp cutting tool. Then, the values drop considerably from cut number 20 in the condition of feed 0.3 and 0.35 mm/rev. This result may be explained by the fact that the number of chip breakage was reduced as it lost cutting ability due to tool wear. Consequently, the amplitude of the burst AE signal was also decreased due to significant progress of worn tool. Interestingly, the condition of feed 0.4 provides

consistent chip breakage until a few cuts before its failure. This sudden change leads to a difficulty in detecting the warning signal. It may be that this cutting condition offers perfect chip removal, leading to consistent chip breakage while tool wear gradually increases.

It is difficult to explain the random pattern result in Figure 6.28*(a)* as the trend of each condition fluctuates. This partly due to the nature of research in machining because there are various factors in the machining process to consider as mentioned in Chapter 2. However, this inconsistency may be due to different chip formation in each condition. The result in Figure 6.28*(b)* is seen that almost all conditions have a consistent chip breakage until the end of usage, except condition V_c=300 m/rev which peak-to-peak values decrease after the 20th cut. It can be assumed that the chip length removed would be a key influence on the peak amplitude of AE burst-typed signals or longer chip length might emit higher magnitude of AE signal when the chip breaks. This is an interesting and important issue for the future research.

6.5.2.3 Relationship of AE_{rms} and flank wear

The relationship between typical AE_{rms} and flank wear of example conditions are shown in Figure 6.29 and also found in Appendix B. Clearly, AE_{rms} increases for most cutting conditions because of tool wear progression. This increase was frequently found in the steady-state tool wear period across all the different cutting conditions. However, some condition such as condition 6 has no correlation with tool wear.

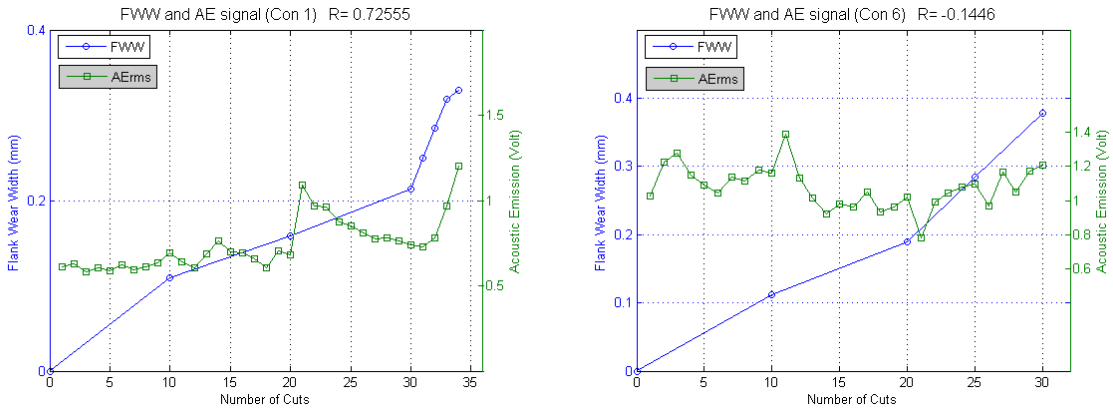

(a) *(b)*

Figure 6.29 The correlation of between AE_{rms} and flank wear from seven cutting conditions

6.5.2.4 Relationship of AE_{p-p} and flank wear

In Figure 6.30, AE_{p-p} representing the chip breakage slightly increase from the start to the middle of the second state wear region. Then, the peak-to-peak values clearly decrease as a number of chip breakages diminish due to tool wear. (Further results in Appendix B)

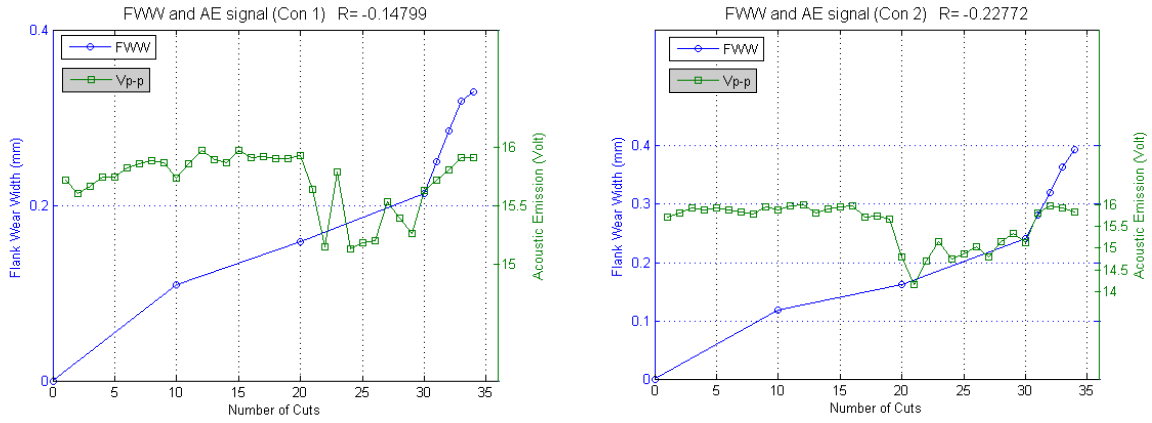

(a) *(b)*

Figure 6.30 The correlation of between AEp-p and flank wear from seven cutting conditions

In conclusion, although several studies suggest that tool wear monitoring using AE signal is potential method and popular use, this method has some variation and inconsistency which cannot be used to monitor tool wear on its own. This encourages the hypothesis of using multiple sensors to monitor tool wear to increase generalisation.

6.5.3 The Effect of Cutting Speed and Feed on Sound Pressure Level

Sounds emitting from the cutting zone during cutting process are often heard by the operator and, if they are experienced enough, can be used as a way of monitoring the process. The sound signal emitted during machining could therefore be related to the tool condition, particularly if a change in cutting condition has an effect on the feature of the noise. In this section, cutting sound was used to examine the possibility of in-process tool wear monitoring in turning. Compared to other sensors, a microphone, being a non-contact sensor, is very easy and flexible to install in the machine.

Note: in this section, unless otherwise stated, the 'noise' from a machine, component or process is taken to mean noise that is within the range of human hearing and can therefore be detected by a standard microphone typically used for voice or music recording.

6.5.3.1 Machine Background Noise

An important consideration in of using the microphone to record the sound in the machine shop is background noise. The background noise will always interfere the sound signal obtained by the microphone, unless complex physical filters are used which may hinder the process. Noises from a machine tool stem from vibration in cutting zone, vibration caused by machine tool drive systems, vibration of machine tool and shop floor, noise from driving control electronics, air leaks from pneumatic system and etc.

In this work, sound from the running machine tool without cutting occurring was recorded and identified as a reference noise for all seven cutting conditions. An example of machine background noise spectrum is shown in Figure 6.31 below.

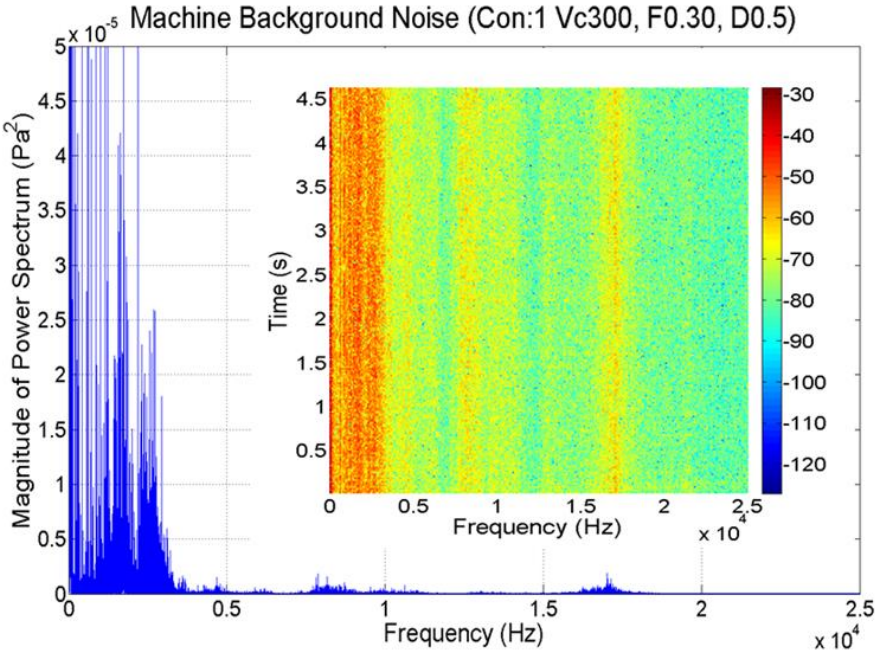

Figure 6.31 Background noise from the microphone without cutting occurring

In Figure 6.31, frequency content in 0 - 3 kHz can be inferred as surrounding noise from near-by machine tool, conveyors or traffic from outside, and some form of electronic noise and Kopac *et al* confirmed that surrounding noise has been identified in the range of 0 - 2 kHz [103]. Therefore, the sound generated by cutting process emits in the frequency range of 3-20 kHz, which is higher than the reference background noise.

Therefore, a high-passed filter was used to remove the background noise and the audible features were extracted from the filtered signal to obtain the most meaningful features for tool wear classification and prediction. In this Chapter, mean sound pressure is correlated with flank wear.

6.5.3.2 The Effect of Cutting Speed and Feed on Mean Sound Pressure

The average sound pressure of each cut was determined after filtering out the background noise. Basically, correlation coefficient (R) or sometimes called cross-correlation (described in Section 4.3.3) was used to evaluate the relationship between mean sound pressure and flank wear.

Previous studies [103, 104] were performed in dry machining where it is easier to record a clear cutting sound. In this experiment, the sound of high pressure of the cooling liquid ejecting to the cutting point could be a significant effect on the recorded sound. Figure 6.32 shows the summarised results from experiments using all cutting conditions (Section 6.4.3).

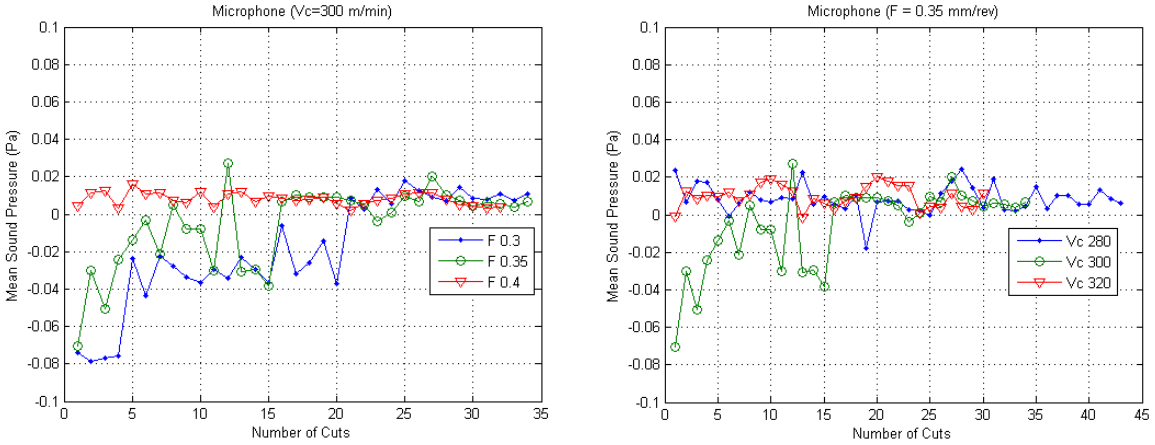

(a) *(b)*

Figure 6.32 Mean sound pressure at different cutting conditions: *(a)* at constant cutting speed (V_c =300 m/min), and *(b)* at constant feed rate (F=0.35 mm/rev)

The results in Figure 6.32 (above) indicate that an increase in flank wear width correlates with an increase in signal amplitude of recorded sound in the range of 3 and 25 kHz. Furthermore, an increase in feed resulted in increase of sound intensity. These findings agree with the results of other studies [103, 147], where sound pressure amplitude increases when tool wear increases. However, some cutting condition such as F=0.4 in Figure 6.32*(a)*, mean sound pressure level have no significant change and this is similar to those conditions in Figure 6.32*(b)*. These results are similar to AE_{rms} in Figure 6.27 and $AE_{p\text{-}p}$ in Figure 6.28 that the RMS and peak-to-peak values have no significant change during the experiment.

6.5.3.3 Relationship of Mean Sound Pressure and Flank wear

Figure 6.33 shows example results of cutting condition 1 and 5. Results from the other cutting conditions can be found in Appendix B.

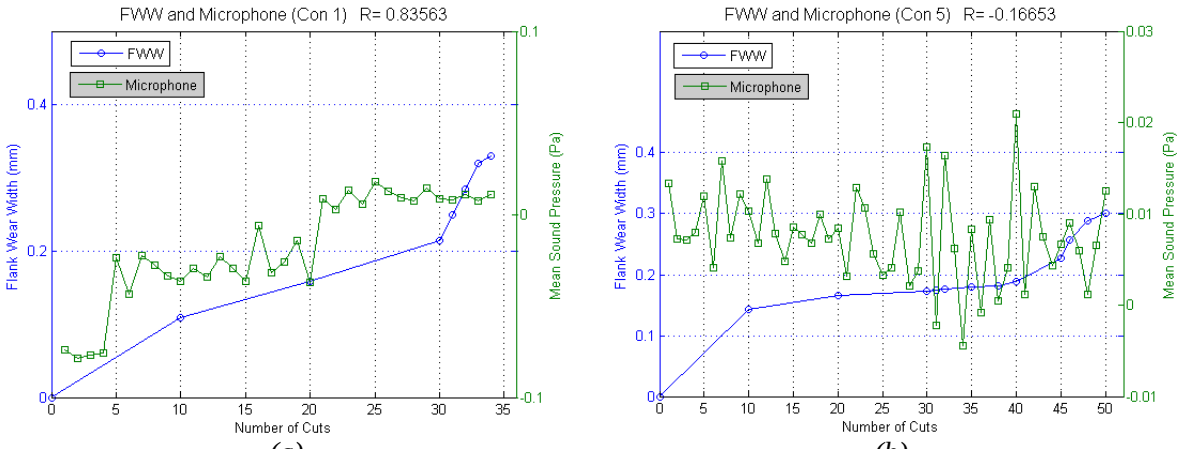

(a) *(b)*

Figure 6.33 Mean sound pressure of the microphone signal

From cutting conditions 1, 2 and 7, the sound pressure signal shows an upward trend similar to that shown in Figure 6.33*(a)* because sound amplitude slightly increases due to an increasing amount of tool wear. The mean sound pressure of these conditions provides a good correlation with tool wear compared by R value. These results match those observed in previous studies [103, 104] but considering to other cutting conditions (3, 4, and 6), they are difficult to explain the fluctuated and unpredicted trend and they have a low correlation coefficient as seen in Figure 6.33*(b)*.

One possible explanation for these results is that unexpected sound emitted from nearby working machines during machining operation which have higher frequency and higher sound intensity than normal background noise as isolated in Section 6.5.3.1. These large machines are located very close to the CNC lathe machine used in this experiment. They can occasionally, and unpredictably, emit a very loud noise different to their usual audio signature when operating. Consequently, the cutting sound recorded was mixed with near-by working machines. This may be constructive or destructive interference. In order to minimise any interfering noise, the isolating a machine from other noise, either physically or by turning all the other machines off, is required. However, turning off all the other machine can realistically only be done in a research environment as it is often impractical to use in the factory.

Finally, this study found an interesting feature extracted from the sound signal. It is named as 'spindle noise' which is a sound generated in the main spindle motor. The details of spindle noise are described in detail in Chapter 8.

6.5.4 The Effect of Cutting Speed and Feed on Power Consumption of Spindle Motor

Power consumption of spindle motor was also monitored throughout seven cutting conditions (Section 6.4.3). Figure 6.34 illustrates spindle power used in the spindle motor during one cutting cycle. The typical power consumption signal was captured from a cutting cycle of condition 1 (V_c =300, F=0.30, D=0.5) which took 30 seconds to complete the cutting.

The first peak signal on the left side resulting from surge current corresponds to an abrupt change of the spindle speed from low (as the spindle starts) to the rotational speed required to obtain 300 m/min of cutting speed. When the tool inserts start cutting, the level of power signal slightly shifts up as the spindle motor is loaded by resistance in cutting point. The power signal gradually increases until reaching the half of cutting tool path or about half of workpiece radius, causing the second spike.

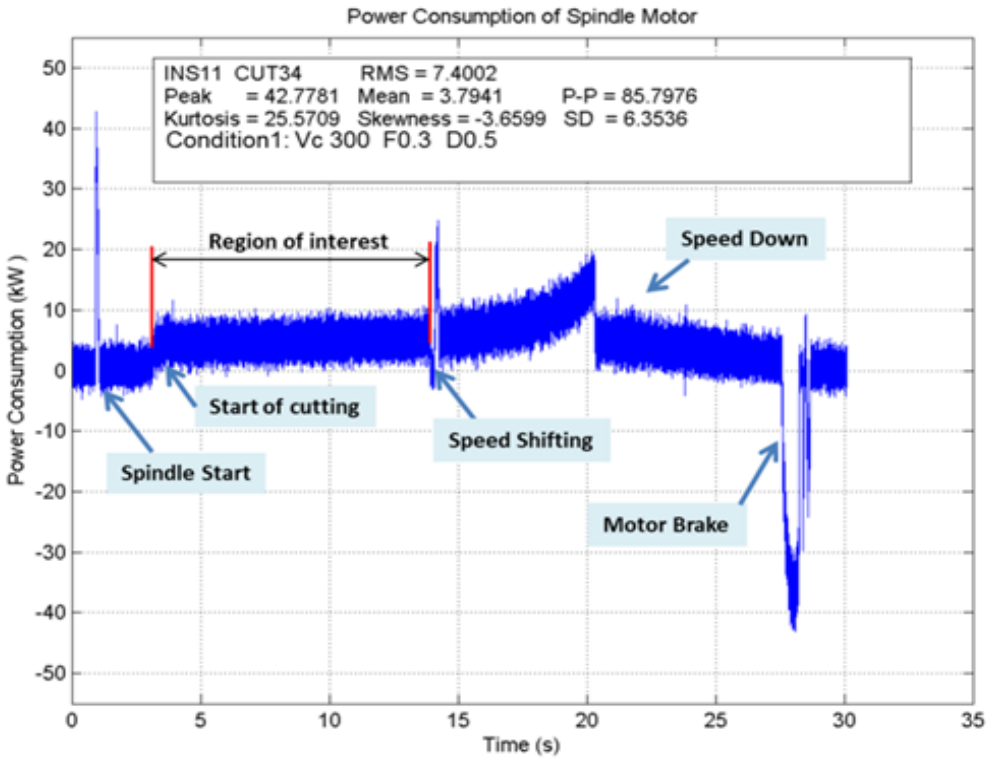

Figure 6.34 An example of typical power consumption signal in one cutting cycle

The spindle motor controller of machine tool used in this study is designed to adapt the speed automatically in order to maintain its constant cutting speed which normally decreases due to reducing workpiece radius. This spike stems from an increase of spindle speed from the first value to second value. After speed shifting, the spindle motor continuously consumes more power corresponding to the increase of power signal until 20 seconds have elapsed. The power signal then drops because the resistant force in the cutting zone reduces when cutting inserts nearly reach workpiece centre. As resistance cutting force decreases, the spindle speed is decreased, resulting in a decrease of power used. Finally, large amount of power is used to stop rotation of the spindle motor.

In practice, it is inappropriate to use the power consumption signal in all signal range to extract sensory features because some signal region such as spikes at spindle start, speed shifting and motor brake does not correlate to tool wear. To make an accurate monitoring of tool wear, the power signal during steady cutting is segmented from whole signals and then denoted as a region of interest in Figure 6.34. This part of signal was used to extract the features for feature selection and neural network training in this study. The RMS of power consumption was then used to correlate to the tool wear observed.

6.5.4.1 The Effect of Cutting Speed and Feed on Power Consumption of Spindle Motor

RMS power consumption of spindle was calculated and is shown in Figure 6.35.

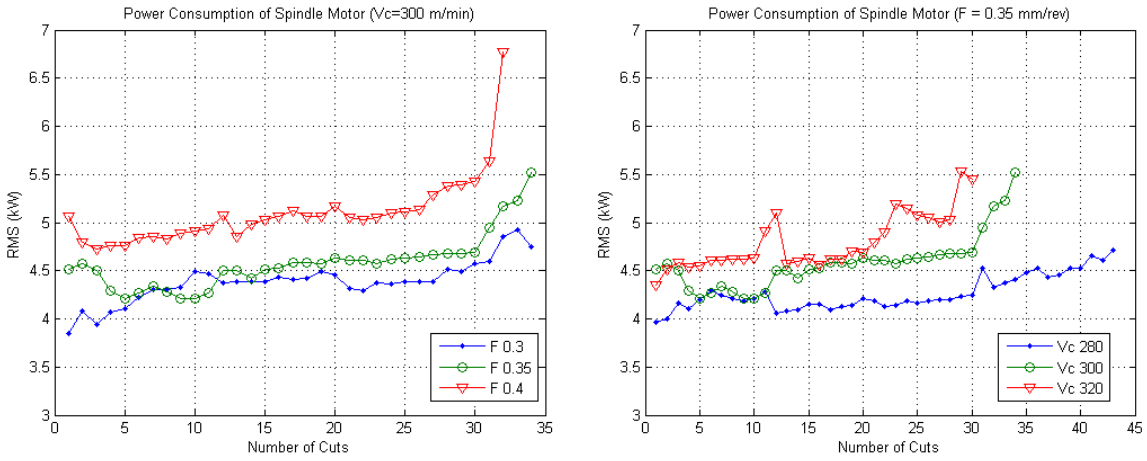

(a) *(b)*

Figure 6.35 Power consumption of spindle motor at different cutting conditions: *(a)* at constant cutting speed *(Vc=300* m/min), and *(b)* at constant feed rate (F=0.35 mm/rev)

From Figure 6.35*(a)*, it can be clearly seen that cutting by higher feed consumes higher power than used for the rotation of the spindle. The power consumption of each cutting condition gradually grows until reaching the final tool wear state. Then, the power use rapidly increases and an abrupt change can be found after 30th cut. Figure 6.35*(b)* similarly shows that the higher cutting speed consumes higher power.

These results are as expected, and are the reasons why power consumption is commonly used in this way. However, Figure 6.35 also shows the potential limitations of relying on power consumption solely as a tool wear monitoring system. The power consumption obviously declines at cut number 5-10 of feed 0.35 (Green line). This particular experiment was conducted across two working days so it is thought that is drop in power consumption is due to the temperature of the spindle motor. Similarly, in the 13th cut of the experiment with a constant feed 0.4, the machine was also stopped for an extended period of time so that the temperature of spindle motor cool down resulting in less power consuming when the machine continued using.

6.5.4.2 Relationship of Power Consumption of Spindle Motor and Flank Wear

Figure 6.36 shows example results of the relationship between power consumption and flank wear progression and all results can be found in Appendix B.

The results show that the RMS value of power consumption gradually increases, which correlates with the flank wear progression seen in Figure 6.36. The abrupt change can be found in failure wear region as expected. As flank wear width increases, the contact area between the flank face and workpiece increases, requiring more cutting force and consequently the spindle motor requires more power to rotate the workpiece at the desired speed to overcome the increasing friction force on cutting contact area. These

results agree with the reviews of Siddhpura *et al* [9], in which power can represent the tool wear effectively.

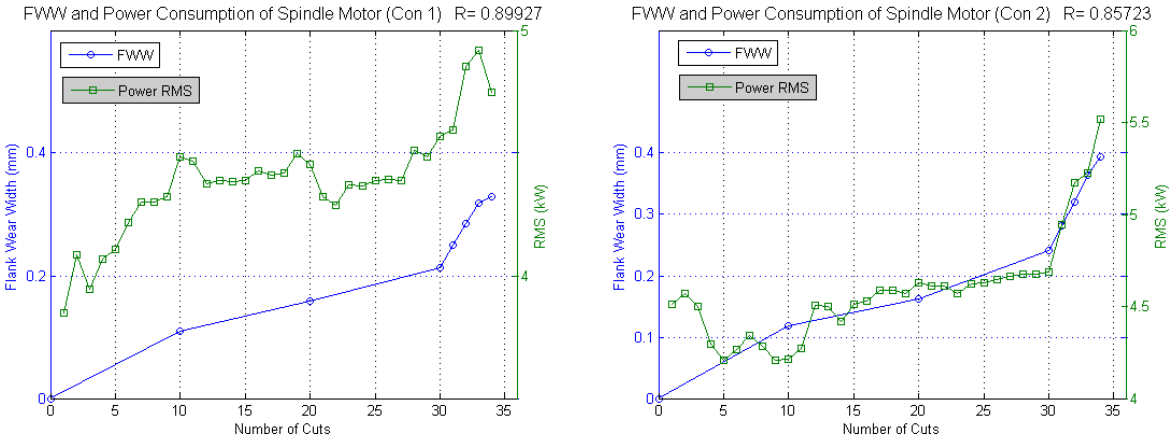

(a) *(b)*

Figure 6.36 Power consumption of the spindle motor and flank wear width

However, monitoring the tool wear using spindle power consumption is not adequate for low cutting force turning operations, and also has fluctuated pattern resulted from the temperature effect of the spindle motor. Power monitoring of the main spindle is widely used in the industry to define specific thresholds to prevent overload of the machine tool due to undesirable cause such as tool wear. These limitations further support the hypothesis that developing a system that utilises multiple sensors can have advantages.

6.6 Concluding Remarks

Most research in tool condition monitoring has been studied under laboratory controlled cutting conditions (e.g. a dry machining condition), few studies are conducted under real industrial conditions, which is in this case of the work presented here. However, conducting the machining in a real industrial environment produces several problems to be overcome, such as machine availability, high interference noise from a nearby machine, and maintenance interruption. This study performs machining in a wet condition which has several effects on the experimental results. For example, the useful lifetime of a particular tool is much longer compared to dry machining and therefore more time and workpiece material needs to be consumed to produce measurable wear. High pressure cutting fluid is the predominant attenuating noise on sound signal recorded by a microphone and the sensors used in the cutting point need to be well-protected from any damage that might happen.

From the results presented in this chapter, each sensing signal can be used to show significant change during turning process. Although AE signals are sensitive to tool wear, the burst type signal has an effect on the RMS value and it should be separated

before feature extraction in order to obtain an accurate tool wear result. The microphone is the easiest installation and most flexible method under real machining, but the interfering noise from the local environment causes problems. Using power consumption of spindle motor shows a significant warning of tool wear, but is susceptible to temperature effects and cannot detect the power consumed in low cutting force turning.

In conclusion, the three sensor signals used in this study are useful to monitor tool wear in the range of experimental trials. However, the experimental results confirm that using only single sensor signal cannot be used effectively due to its characteristics under various machining conditions. Therefore, multiple sensors and sensor fusion have been used for developing the tool wear monitoring system in order to increase reliability of the monitoring system.

Chapter 7

Development of Sensor Fusion Methodology

Feature Selection

Tool Wear Prediction

Tool Wear State Classification

Remaining Useful Life Time

This chapter presents the modelling results based on the sensor fusion concept using an artificial neural network. This chapter begins with the results of feature selection. Two algorithms: correlation coefficient (R) and correlation based feature selection (CFS) using WEKA were used to select the features for neural network training. Then, a flank wear width prediction method using artificial neural networks with several network configurations were developed. Finally, the tool wear states of cutting tool were classified by the neural networks and the potential utilisation of predicted flank wear and predicted state of tool wear are described in order to estimate the remaining tool life time.

7.1 Feature Extraction and Feature Selection

7.1.1 Feature Extraction

To improve the prediction accuracy and reduce training time, it is important to select the most building on the work presented in Chapter 6, each sensor signal (AE, microphone, and power consumption of spindle motor) was post-processed to extract seven features in time domain and seven in frequency domain, 42 features in total, denoted by letter and number as shown in Table 7.1.

Table 7.1 Feature lists and short name

Domain	Feuture Name	Feature Variables		
		Acoustic Emission (A)	Microphone (M)	Power Sensor (P)
Time	(1) Root Mean Square	(A1) AE_tRMS	(M1) MC_tRMS	(P1) PW_tRMS
	(2) Mean	(A2) AE_tMean	(M2) MC_tMean	(P2) PW_tMean
	(3) Maximum Amplitude	(A3) AE_tMax	(M3) MC_tMax	(P3) PW_tMax
	(4) Peak to Peak	(A4) AE_tPP	(M4) MC_tPP	(P4) PW_tPP
	(5) Kurtosis	(A5) AE_tKur	(M5) MC_tKur	(P5) PW_tKur
	(6) Skewness	(A6) AE_tSkew	(M6) MC_tSkew	(P6) PW_tSkew
	(7) Standard Deviation	(A7) AE_tSD	(M7) MC_tSD	(P7) PW_tSD
Frequency	(8) Mean Frequency	(A8) AE_fMean	(M8) MC_fMean	(P8) PW_fMean
	(9) Maximum Frequency	(A9) AE_fMax	(M9) MC_fMax	(P9) PW_fMax
	(10) Peak Frequency	(A10) AE_fPeakFreq	(M10) MC_fPeakFreq	(P10) PW_fPeakFreq
	(11) Max per Mean ratio	(A11) AE_fMaxpMean	(M11) MC_fMaxpMean	(P11) PW_fMaxpMean
	(12) Kurtosis	(A12) AE_fKur	(M12) MC_fKur	(P12) PW_fKur
	(13) Skewness	(A13) AE_fSkew	(M13) MC_fSkew	(P13) PW_fSkew
	(14) Standard Deviation	(A14) AE_fSD	(M14) MC_fSD	(P14) PW_fSD

The number of extracted features is very large, some of them are very distorted and irrelevant to tool wear. The features that are relevant and sensitive to tool conditions need to be selected. Thus, the subsequent step is to select the most appropriate features correlating with tool wear, a process called as feature selection. Figure 7.1 illustrates three types of feature sets being used for the neural network training in order to develop a tool wear monitoring system.

Firstly, the RMS of three sensors (A1, M1, and P1) were defined as FS1 since several studies suggested that the RMS value in time domain represents tool wear effectively as reviewed in Chapter 4 and Chapter 6 [9, 82]. The feature sets (FS2-FS5) were then selected by data mining software named WEKA [118] (described in Section 7.1.3). Lastly, feature set (FS6), selected from the ranking of highest correlation coefficient, is the proposed feature set.

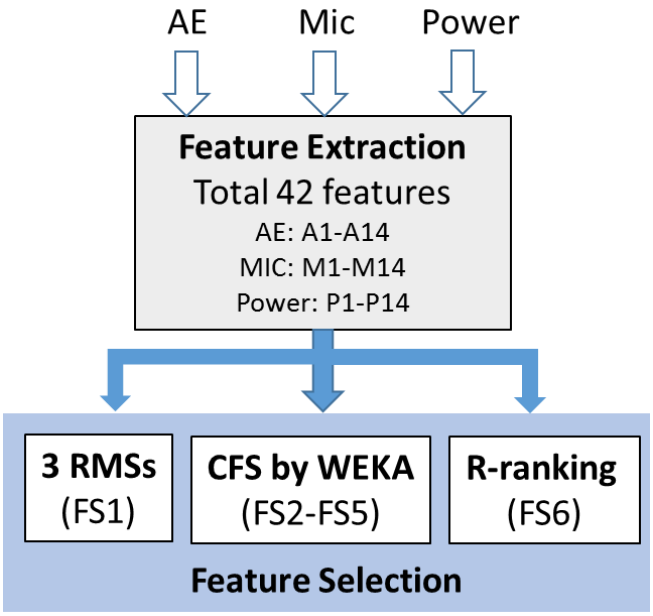

Figure 7.1 Schematic of feature selection in this study

7.1.2 Feature Selection Based on Correlation Coefficient

The combination of data sets obtained from machining experiment was compared by considering the average correlation coefficient (R) value (Chapter 4). This selection method is supported by Quan *et al*, Jemielniak *et al*, and Olufayo *et al* [97, 117, 148] who used the correlation coefficient to find the most meaningful features that can characterise tool wear conditions and then determine the best data set for use in neural network training. The performance of three sensors used in the machining experiment was also evaluated. Correlation coefficients between all features and flank wear width were ranked in order to select the first top three both in time and frequency domains of each sensor for FS6 (18 features in total).

Using data from the experimental trials presented in Section 6.4.3, seven cutting conditions were performed with two replications. The total cutting cycles in one replication are 253 cuts (or instances) and dataset 'totR1' and 'totR2' stand for the instances of replication 1 and 2, respectively. Dataset 'totR1R2' combines the instances of two replications (506 instances in total), while 'totAVG' is computed by average of those two replications (253 instances). The mean absolute value of the correlation coefficient (as a percentage) was used to evaluate the best data set and the best tool wear classifier.

Table 7.2 shows the average correlation coefficient between all features of each dataset and three tool wear locations or classifiers (FWWN, FWWR, and FWWL, as defined in Chapter 6). The average correlation coefficient of three classifiers is illustrated in Figure 7.2.

Table 7.2 Average correlation coefficient between 42 features and 3 classifiers

Data sets	no. of instances	Mean Absolute Value			AVG.
		FWWN	FWWR	FWWL	
totR1	253	20.14	19.17	17.60	**18.97**
totR2	253	17.57	15.70	16.59	**16.62**
totR1R2	506	18.00	16.87	16.43	**17.10**
totAVG	253	19.97	18.60	18.48	**19.02**
	AVG.	**18.92**	**17.58**	**17.28**	

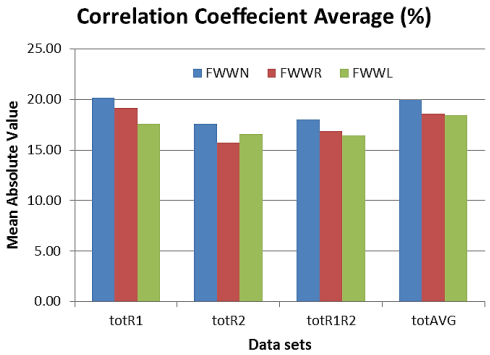

Figure 7.2 Average correlation coefficient of three classifiers

From Table 7.2, 'totR1' provides the best correlation value between sensory features and FWWN at 20.14%. The result shows that the flank wear width of nose radius (FWWN) has the best average correlation (18.92%) and the second place is the flank wear width of right side (FWWR) (17.58%). It is reasonable that these FWWN and FWWR are ranked highest as they are the major cutting edges as mentioned in the previous chapter (Section 6.5.1). Consequently, these two classifiers will be used as targets in neural network training. The 'totAVG' averaged of two replications is the best dataset (19.02%), while 'totR2' has the lowest correlation on average as can be clearly seen in Figure 7.2.

Table 7.3 and Figure 7.3 show the average correlation coefficient grouped by sensors. The result shows the features of power consumption have the best correlation with flank wear, approximately 25-30%, while the AE sensor is on the second place with 13-14% and microphone is the bottom of the group. It can be concluded that the features extracted from the power consumption signal have better correlation with the tool wear than other sensors in this machining experiment. This agrees with the results presented in Chapter 6 (Section 6.5.4).

Table 7.3 Average correlation coefficient grouped by sensors

Classifier	totR1				totR2				totR1R2				totAVG			
	AE	Mic	Power	Average	AE	Mic	Power	Average	AE	Mic	Power	Average	AE	Mic	Power	Average
FWWN	14.95	13.94	31.55	**20.14**	11.59	10.73	30.39	**17.57**	12.6	10.5	30.9	**18.00**	13.35	13.16	33.40	**19.97**
FWWR	15.42	13.11	28.99	**19.17**	13.58	11.34	22.17	**15.70**	14.5	10.7	25.5	**16.87**	14.72	12.85	28.24	**18.60**
FWWL	12.71	12.96	27.14	**17.60**	15.49	10.17	24.10	**16.59**	13.8	9.9	25.6	**16.43**	13.92	12.68	28.84	**18.48**
Average	14.36	13.34	29.23	**18.97**	13.56	10.74	25.55	**16.62**	13.6	10.4	27.3	**17.10**	14.00	12.90	30.16	**19.02**

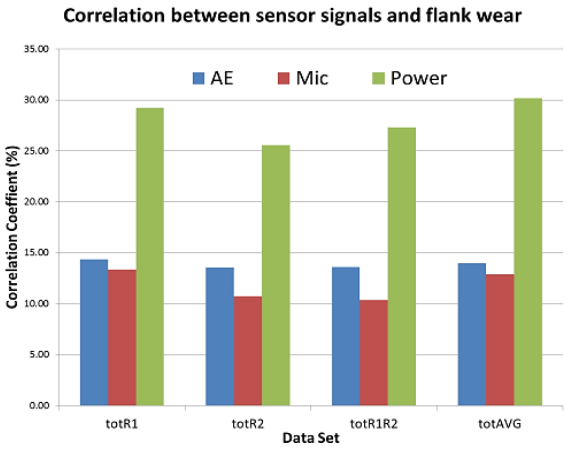

Figure 7.3 Average correlation coefficient of three sensors separated by data set

Table 7.4 and Table 7.5 show the ranking of the average value of absolute correlation value (in percent) of each classifier in all data sets. It is clear that power consumption ranks highest for the top twenty of the each sensor, and this is in agreement with the results shown in Figure 7.3. Next, the top-three features of each sensor both time and frequency domains were selected as a representative feature set (FS6, representing ranking method). These highly-correlated features will be then used for training the neural networks. The selected features of FS6 will be summarised in Table 7.6 (Section 7.1.3).

Note: Score represents the average value of the absolute correlation coefficient (expressed as a percentage)

Table 7.4 Top 20 features of each data set calculated by a correlation coefficient

Rank	totR1						totR2					
	FWWN		FWWR		FWWL		FWWN		FWWR		FWWL	
	score	Feature Name	score	Feature Name	score	Feature Name	score	Feature Name	score	Feature Name	score	Feature Name
1	63.28	'PW_tRMS'	60.29	'PW_tRMS'	56.24	'PW_tRMS'	58.44	'PW_tRMS'	48.40	'PW_tMax'	47.27	'PW_tMax'
2	61.71	'PW_tMean'	58.55	'PW_tMean'	55.22	'PW_tMean'	56.05	'PW_tMean'	45.47	'PW_tRMS'	46.00	'PW_tPP'
3	53.51	'PW_tMax'	52.04	'PW_tMax'	48.88	'PW_tMax'	50.78	'PW_tMax'	44.97	'PW_tPP'	45.64	'PW_tRMS'
4	46.69	'PW_fMean'	43.11	'PW_fMean'	37.97	'PW_fMean'	45.73	'PW_tPP'	43.30	'PW_tMean'	43.10	'PW_tMean'
5	41.91	'PW_tSkew'	40.71	'PW_tSkew'	36.81	'PW_tSkew'	44.58	'PW_fMean'	36.40	'MC_tMean'	36.46	'MC_tMean'
6	37.87	'PW_tPP'	38.78	'PW_tPP'	34.39	'PW_tPP'	37.71	'PW_fMaxpMean'	35.15	'AE_tMax'	35.43	'AE_tMax'
7	34.76	PW_fMaxpMean'	32.36	'AE_tPP'	29.67	'MC_tMean'	37.03	'AE_tMax'	31.66	'AE_tPP'	32.03	'AE_tPP'
8	32.98	'AE_tPP'	31.79	'MC_tMean'	29.45	'PW_fMaxpMean'	36.44	'PW_tSkew'	29.94	'PW_tSkew'	31.80	'PW_tSD'
9	32.63	'MC_tMean'	31.61	'PW_tSD'	28.62	'AE_tPP'	36.12	'AE_tPP'	29.26	'PW_tSD'	28.84	'PW_tSkew'
10	31.12	'PW_tSD'	31.08	'AE_tMax'	27.24	'AE_tMax'	34.07	'MC_tMean'	25.15	'PW_fMean'	26.23	'PW_fMaxpMean'
11	30.50	'AE_tMax'	30.77	'PW_fMaxpMean'	26.91	'PW_tSD'	33.10	'PW_tSD'	22.15	'PW_fMaxpMean'	24.09	'PW_fMean'
12	22.46	'MC_tSD'	22.59	'MC_tSD'	21.73	'MC_tSD'	18.76	'MC_tPP'	19.19	'MC_tPP'	20.70	'AE_tSD'
13	21.49	'MC_fKur'	22.54	'AE_tRMS'	20.52	'MC_tRMS'	17.75	'AE_tKur'	17.46	'MC_tMax'	20.70	'AE_tRMS'
14	21.21	'PW_tKur'	22.54	'AE_tSD'	20.15	'MC_fKur'	17.00	'MC_tMax'	16.94	'AE_tKur'	19.51	'AE_fMean'
15	21.02	'MC_tRMS'	20.76	'MC_tRMS'	19.12	'PW_tKur'	15.89	'PW_fSkew'	16.30	'MC_fKur'	19.34	'AE_tKur'
16	19.99	'AE_tRMS'	19.82	'AE_tKur'	18.58	'MC_tPP'	15.73	'PW_fPeakFreq'	15.17	'AE_tSD'	16.01	'PW_fSD'
17	19.99	'AE_tSD'	19.74	'MC_fKur'	17.53	'MC_fSkew'	14.06	'MC_fKur'	15.17	'AE_tRMS'	15.54	'MC_fKur'
18	18.89	'MC_fSkew'	19.20	'MC_tPP'	16.57	'AE_tRMS'	13.97	'MC_tRMS'	14.56	'AE_fKur'	14.41	'AE_fKur'
19	18.71	'MC_tPP'	17.34	'PW_tKur'	16.57	'AE_tSD'	13.71	'MC_tSD'	13.55	'AE_fMean'	13.01	'AE_fSkew'
20	18.69	'AE_fSD'	16.84	'AE_fMean'	15.35	'MC_tMax'	12.79	'PW_fKur'	13.28	'AE_fSkew'	12.82	'MC_tPP'

Table 7.5 (cont.) Top 20 features of each data set calculated by a correlation coefficient

Rank	totR1R2						totAVG					
	FWWN		FWWR		FWWL		FWWN		FWWR		FWWL	
	score	Feature Name	score	Feature Name	score	Feature Name	score	Feature Name	score	Feature Name	score	Feature Name
1	60.31	'PW_tRMS'	53.41	'PW_tRMS'	51.11	'PW_tRMS'	60.19	'PW_tMax'	57.12	'PW_tMax'	54.92	'PW_tMax'
2	58.39	'PW_tMean'	51.48	'PW_tMean'	49.43	'PW_tMean'	60.13	'PW_tRMS'	54.67	'PW_tRMS'	52.53	'PW_tRMS'
3	51.79	'PW_tMax'	50.36	'PW_tMax'	48.02	'PW_tMax'	59.14	'PW_tMean'	53.56	'PW_tMean'	51.68	'PW_tMean'
4	45.28	'PW_fMean'	40.97	'PW_tPP'	39.00	'PW_tPP'	49.72	'PW_tSkew'	48.33	'PW_tPP'	46.27	'PW_tPP'
5	41.13	'PW_tPP'	35.70	'PW_tSkew'	33.46	'PW_tSkew'	49.36	'PW_tPP'	44.67	'PW_tSkew'	43.28	'PW_tSkew'
6	38.76	'PW_tSkew'	34.91	'PW_fMean'	31.83	'MC_tMean'	42.82	'PW_fMean'	37.42	'MC_tMean'	37.70	'MC_tMean'
7	36.38	'PW_fMaxpMean'	32.82	'AE_tMax'	31.49	'PW_fMean'	39.55	'MC_tMean'	37.01	'PW_tSD'	34.69	'PW_tSD'
8	34.47	'AE_tPP'	32.67	'MC_tMean'	30.99	'AE_tMax'	38.33	'PW_tSD'	36.38	'PW_fMean'	32.93	'PW_fMean'
9	33.85	'AE_tMax'	31.94	'AE_tPP'	30.11	'AE_tPP'	37.32	'PW_fMaxpMean'	35.10	'AE_tMax'	32.78	'AE_tMax'
10	32.84	'MC_tMean'	30.51	'PW_tSD'	28.71	'PW_tSD'	34.95	'AE_tPP'	33.77	'AE_tPP'	31.64	'AE_tPP'
11	31.54	'PW_tSD'	26.80	'PW_fMaxpMean'	28.11	'PW_fMaxpMean'	34.93	'AE_tMax'	29.27	'PW_fMaxpMean'	31.36	'PW_fMaxpMean'
12	18.16	'MC_fKur'	19.16	'AE_tSD'	18.21	'MC_fKur'	23.17	'MC_tPP'	22.81	'MC_tPP'	21.74	'MC_fKur'
13	18.10	'MC_tPP'	19.15	'AE_tRMS'	18.08	'AE_tSD'	21.49	'MC_fKur'	21.03	'MC_fKur'	20.43	'MC_tPP'
14	16.51	'PW_tKur'	18.46	'AE_tKur'	18.08	'AE_tRMS'	20.99	'MC_tSD'	20.38	'MC_tMax'	18.37	'AE_tSD'
15	16.11	'PW_fPeakFreq'	18.33	'MC_tPP'	15.04	'AE_fMean'	20.89	'MC_tMax'	20.18	'AE_tKur'	18.37	'AE_tRMS'
16	15.95	'MC_tSD'	18.07	'MC_fKur'	14.86	'AE_tKur'	20.62	'MC_tRMS'	20.06	'MC_tSD'	17.78	'MC_tMax'
17	15.90	'MC_tRMS'	15.91	'MC_tMax'	14.46	'MC_tPP'	19.21	'PW_tKur'	19.59	'MC_tRMS'	17.20	'MC_tSD'
18	15.53	'MC_tMax'	15.66	'MC_tSD'	14.34	'MC_fSkew'	16.51	'AE_tRMS'	19.58	'AE_tSD'	16.96	'MC_tRMS'
19	15.39	'AE_tKur'	15.35	'AE_fMean'	13.67	'AE_fKur'	16.50	'AE_tSD'	19.58	'AE_tRMS'	16.06	'PW_tKur'
20	14.73	'AE_tRMS'	15.30	'MC_tRMS'	13.25	'PW_tKur'	15.12	'AE_tKur'	14.58	'PW_tKur'	15.94	'AE_tKur'

In conclusion, as they are major cutting edges on a tool, FWWN and FWWR provide a good correlation to the extracted features. In neural network training, these two classifiers will be used as targets (output layer) of the neural networks. The proposed features set (FS6), consisting of the first-three ranked features in both time and frequency domains and will be used as an initial feature set for the data training process.

The features extracted from power consumption signals show better correlation than any other sets as this signal are correlated with the tool wear. 'totAVG' calculated by the average value of two replications is the most suitable data set since it provides the best correlation score from averaged data. However, in neural network training, enough data instances are required to train the neural networks for tool wear estimation and classification. Consequently, 'totR1R2' contained with 506 instances from replication 1 and 2, will be used as the training data set.

7.1.3 Correlation Based Feature Selection (CFS) by WEKA

The '*cfsSubsetEval*' module of WEKA software was used to analyse the effect of input feature sets on the output target and determine the representative feature sets for neural network training. The output targets or classifiers used are the flank wear width of the three locations on tool cutting edge. As discussed in Chapter 4, several searching algorithms of '*cfsSubsetEval*' module in WEKA can be used to provide possible feature sets and to test their performance before reporting the end result.

The best feature sets of each searching algorithm determined by WEKA are summarised in Table 7.6 for FS2-FS5. The root mean squared value of three sensor signals (A1, M1, and P1) was manually selected and named as FS1 and the last feature set (FS6) stemmed from the ranking of highest correlation coefficient as mentioned previously.

Table 7.6 The selected features used for training the classification and regression models

Feature Sets	Search Algorithms	Total	Feature lists
FS1	Manually selected 3 RMSs	3	A1, M1, P1,
FS2	Greedy Step Wise	24	A9, A10, A13, A5, A3, A2, A4, A1, A6, M12, M9, M11, M10, M2, M4, M1, M7, P11, P3, P2, P4, P1, P7, P6
FS3	Genertic Search	24	A12, A9, A10, A5, A3, A2, A4, A6, M12, M9, M11, M8, M10, M3, M2, M1, M7, P11, P3, P2, P4, P1, P7, P6
FS4	Evaluation Search	24	A9, A11, A10, A14, A13, A5, A3, A2, A4, A1, A6, M12, M9, M11, M10, M2, M4, M1, P3, P2, P4, P1, P7, P6
FS5	LinearForward Selection	25	A9, A10, A14, A13, A5, A3, A2, A4, A1, A6, M12, M9, M11, M10, M2, M4, M1, M7, P11, P3, P2, P4, P1, P7, P6
FS6	Ranking	18	A1, A2, A7, A8, A11, A10, M1, M2, M7, M8, M11, M10, P1, P2, P7, P8, P11, P10

The application of neural networks in this study can be grouped into two categories: tool wear prediction and tool wear state classification. To obtain the artificial models for monitoring the tool wear, the feature sets listed in Table 7.6 and cutting parameters (cutting speed, feed, and cutting depth) will be used as input variables and fed into the input layer of the neural network. Two classifiers (FWWN and FWWR) are also used as targets in output layer of the neural network as shown in Figure 7.4.

The network was trained off-line using 503 training patterns (instances) from the seven cutting conditions. Multifold cross validation (Section 4.4.3) was performed in order to obtain the highest performance network structures in tool wear prediction. Also, 70/30 training and testing ratio was used for training the data in tool wear state classification.

To determine the best configuration, several neural network architectures were created by changing the network parameters. Feed forward neural networks, with different activation functions and training algorithms, were used to produce the artificial models for flank wear prediction and tool wear classification. The network performance between single and double hidden layer networks was compared and the error of each configuration can be calculated by subtracting the predicted value from ANN output

and the measured values (actual value). After evaluating combinations of several networks, the neural network with the lowest error was chosen.

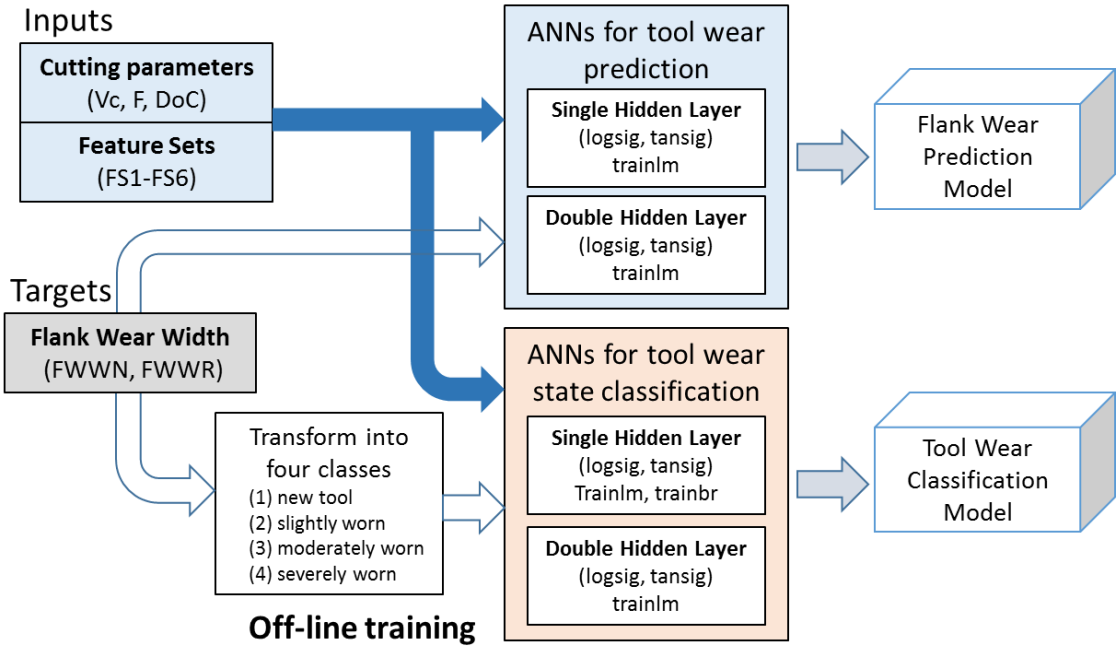

Figure 7.4 Diagram of neural network training procedure for tool wear prediction and classification

7.2 Flank Wear Prediction by Neural Network

7.2.1 General Information of Neural Network Training

The feed forward neural networks with single hidden layer (SHL) and double hidden layer (DHL) were used to estimate the tool wear value as shown in Figure 7.5 and Figure 7.6. These networks were trained by the *Levenberg-Marquardt* algorithm (*trainlm)* because this training algorithm (TA) offers good accurate results with short training time [26]. Two activation functions (AF) or transfer functions (*logsig* and *tansig*) were selected to activate the nodes in the hidden layer (NHL). Cutting parameters (cutting speed, feed, and cutting depth) and feature sets (FS1-FS6) from Table 7.6 were fed into the input layer of the networks, while the flank wear values (FWWN and FWWR) were set as the targets of the networks. The number of nodes in the hidden layer (NNHL) was varied.

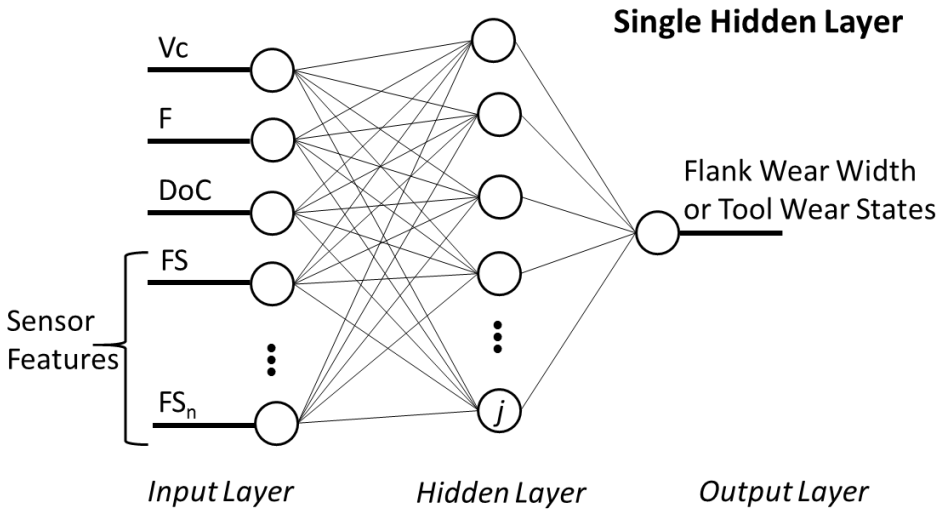

Figure 7.5 Architecture of nerual networks used in this study: single hidden layer

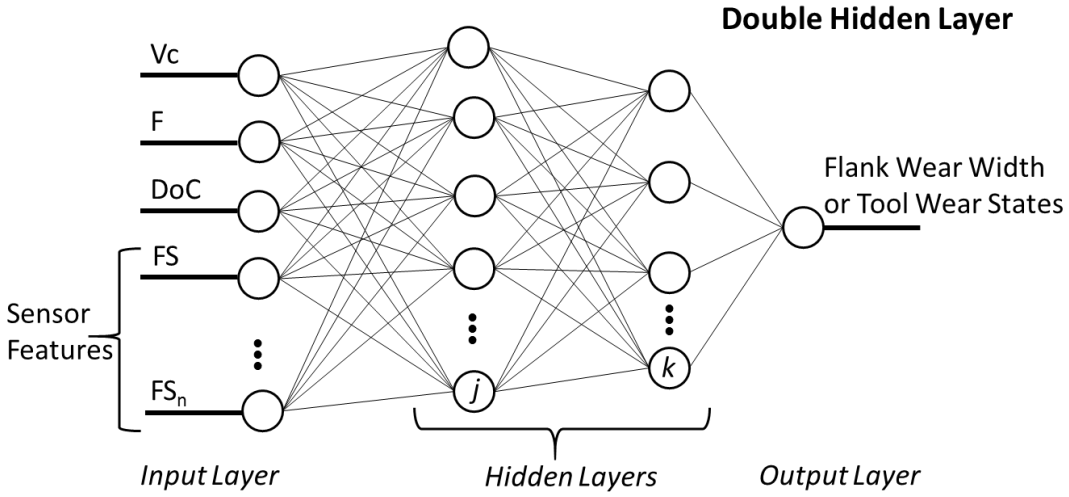

Figure 7.6 (cont.) Architecture of nerual networks used in this study: double hidden layer

The generic name of network configuration is defined as X-H_1-Y (SHL), and X-H_1-H_2-Y (DHL), where X stands for feature set fed into input layer of the network, H_1 and H_2 represent the NNHL of each hidden layer, and Y is the number of node in output layer.

The data set 'totR1R2', consisting of 503 data records from two replications, was used for network training. All data records were rearranged randomly before training the network. The 10-fold cross validation method (described in Chapter 4) was used to divide the data into training and validating groups. This validation method was used to determine the average network performance. The network in the fold that provides the best accuracy of prediction will be selected as the representative network.

Mean Absolute Error (MAE), Root Mean Squared Error (RMSE), and Sum of Squared Error (SSE) were used as criteria for evaluating the model accuracy. These evaluators are described in Chapter 4. The least MAE, RMSE, and SSE within a reasonable training time was used as criteria to select the representative network. The function

used to measure the network's performance is '*mse*' (mean squared error), and the learning rate was set to 0.3. The stopping criteria used for neural network training are shown in Table 7.7. Weights of network connections were randomly selected by MATLAB software.

Table 7.7 Stopping criteria for neural network training

Training Parameters	Value	Stop criteria for training
Epochs	500	Maximum number of epochs
min_grad	0.0000000001	Minimum gradient magnitude
goal	0.000000001	Minimum performance value

The modelling results will be separated into two main parts according to network structures used (i.e. single and double hidden layers).

7.2.2 Flank Wear Prediction by ANNs: Single Hidden Layer

From SHL architecture in Figure 7.6*(a)*, the NNHL was varied from 10 to 100 nodes in this study. The Figure 7.7 shows that mean absolute error (MAE) of FS1 increases when the NNHL increases. Interestingly, FS1 comprising of 3 RMS values extracted from three sensor signals has the least error when the NNHL is equal to 10 and 20 both *logsig* and *tansig*. Due to increasing error, only RMS values of three sensory signals are not capable of predicting the tool wear when the NNHL increases. However, as the machining process data is very noisy and complex, the number of input features for the networks should be used as much as the network performance does not decrease to increase robustness and generalisation of the prediction model [149]. FS1 was not therefore in consideration and was omitted due to divergent error.

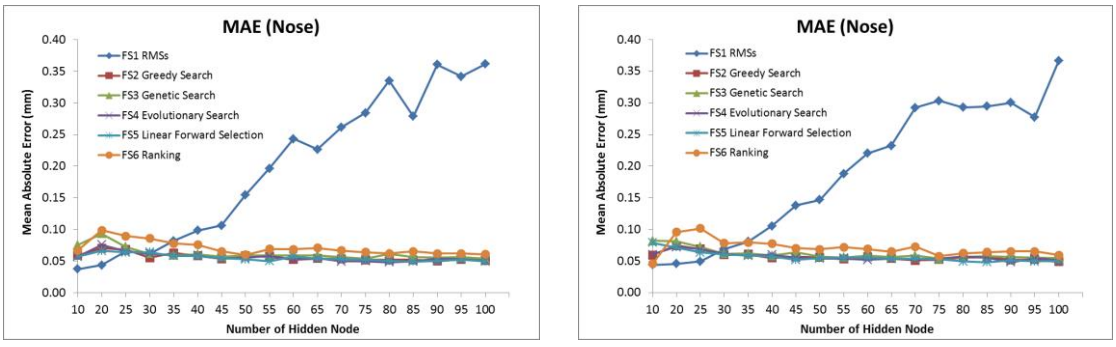

(a) logsig *(b) tansig*

Figure 7.7 Mean absolute error of flank wear prediction from single hidden layer neural networks

In following sections, the tool wear prediction results are divided into two sections according to the activate functions used: *logsig* and *tansig*. Only feature sets (FS2-FS6) will be considered and the discussed.

7.2.2.1 Flank Wear Prediction by ANNs (Single Hidden Layer, AF: logsig, TA: trainlm)

The feature sets (FS2-FS6) and two flank wear targets (FWWN and FWWR) were used as inputs and outputs of the networks respectively. The function *logsig* was used to activate the hidden nodes in hidden layer of the networks. The NNHL was varied from 10 to 100. Figure 7.8 illustrates the prediction error of each feature set, grouped by two wear targets.

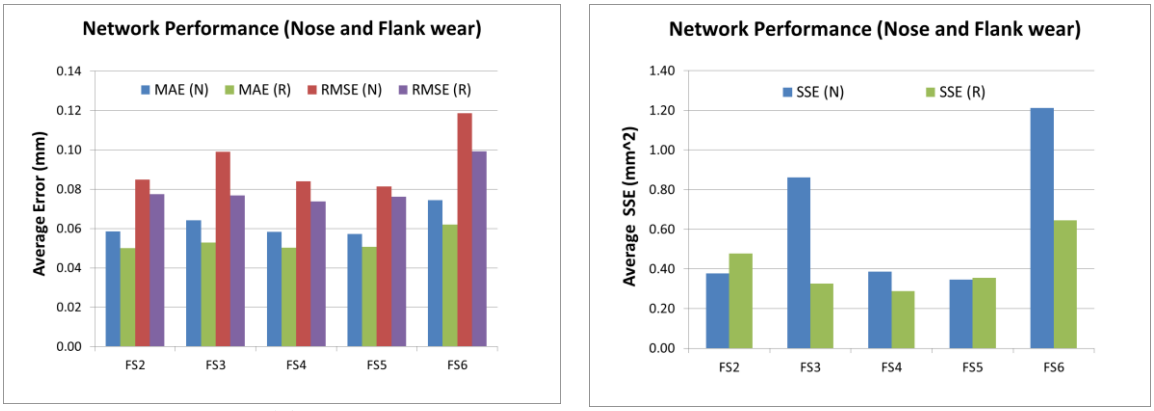

(a) *(b)*

Figure 7.8 Average error of each feature set categorised by two locations of tool wear

The graphs in Figure 7.8 show that networks training by FWWR provides more accurate prediction results than the ones trained by FWWN due to lower MAE, RMSE and SSE. Conversely, SSE of FWWN is less than that of FWWR in some feature set (i.e. FS2 and FS5) due to the inconsistency of the noisy data.

As regards training time in Figure 7.9, the time used for training the networks significantly increases where the NNHL increases. FS2, as selected by WEKA with the greedy search algorithm, requires less time to train the networks, but an outlier was found in 90 of hidden nodes (Figure 7.9*a*). Interestingly, both targets of FS6 spent longer training time in 20 and 25 nodes than any other feature sets. On average, it can conclude that the training time to predict FWWR is shorter than FWWN.

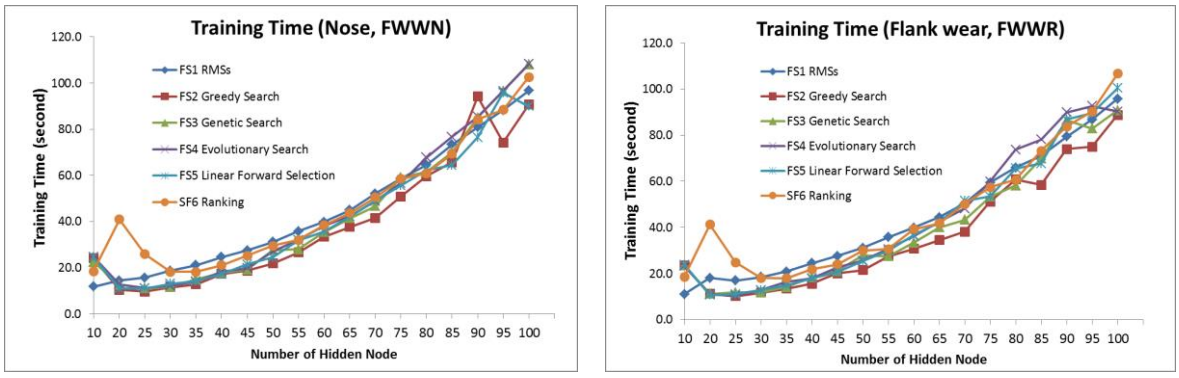

(a) *(b)*

Figure 7.9 Training time used for training the networks: *(a)* FWWN and *(b)* FWWR

As the FWWR provides higher accuracy, MAE, RMSE, and SSE of the networks trained with FWWR as targets are then illustrated in Figure 7.10, Figure 7.11, and Figure 7.12, respectively. Overall, the neural networks trained by feature sets (FS2-FS5) obtained by WEKA produces good prediction accuracy compared to that one obtained by a ranking method (FS6). It is apparent that the prediction errors of SF6 are significantly high, while the error of FS2 is low on average. This, therefore, could be the best feature set used to feed into the neural networks, but the lowest error was actually found in FS5.

In summary, the well-trained network is FS5-70-1. The network is activated by *logsig* function with 70 nodes in the hidden layer, and FS5 is used as inputs. This network can be able to predict flank wear width at right side or FWWR with the minimum errors (MAE=0. 042124, RMSE=0. 059558, and SSE=0. 17946).

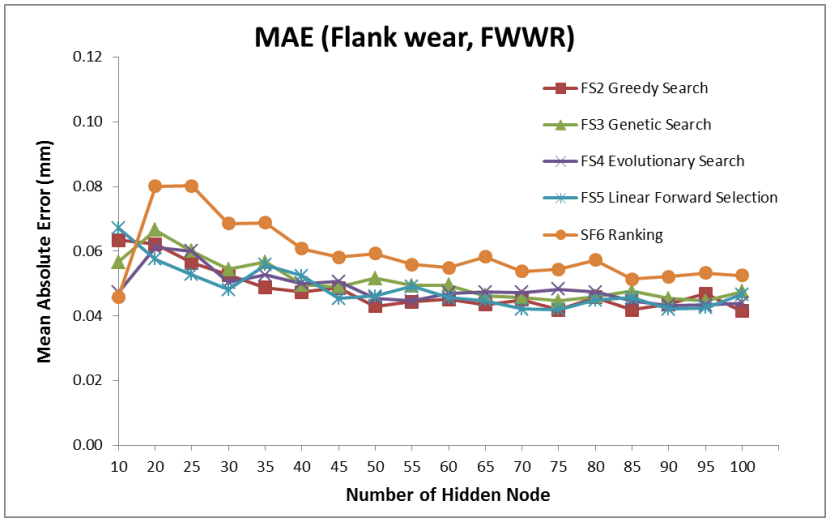

Figure 7.10 Mean absolute error of flank wear prediction by SHL, *logsig*

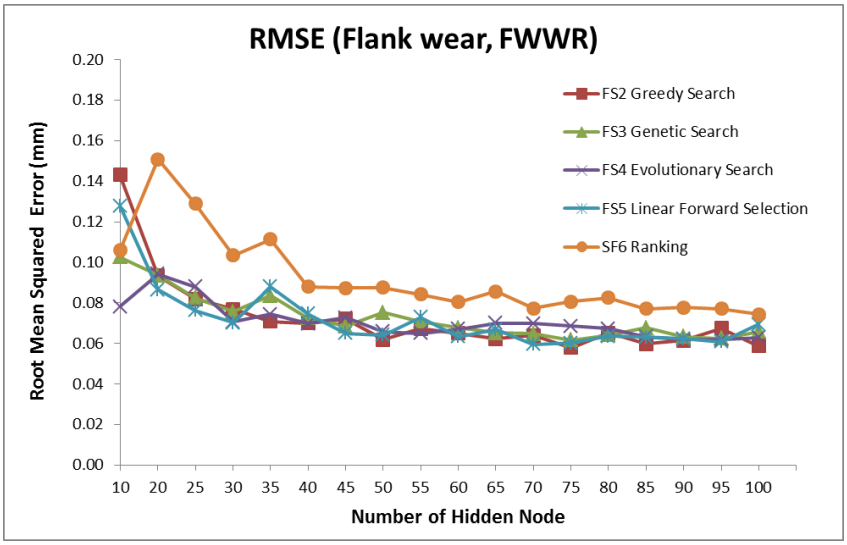

Figure 7.11 Root Mean Squared error of flank wear prediction by SHL, *logsig*

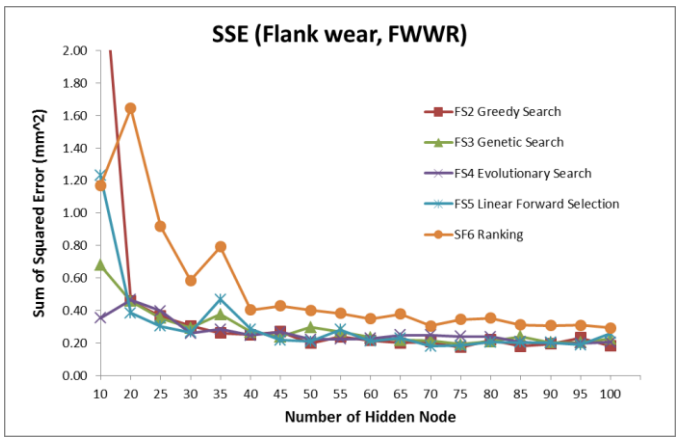

Figure 7.12 Sum squared error of flank wear prediction by SHL, *logsig*

7.2.2.2 Flank Wear Prediction by ANNs (Single Hidden Layer, AF: tansig, TA: trainlm)

This section explains the results when *tansig* was used as an activate function for the NHL of the neural networks. Clearly seen in Figure 7.14 that training by flank wear progressed on the right side of cutting inserts or FWWR, still has a good prediction accuracy as its average error is lower than FWWN for all feature sets. As well as, FWWR used shorter training time on average (Figure 7.13). The MAE, RMSE, and SSE of the trained networks are shown in Figure 7.16, Figure 7.17, and Figure 7.18, respectively.

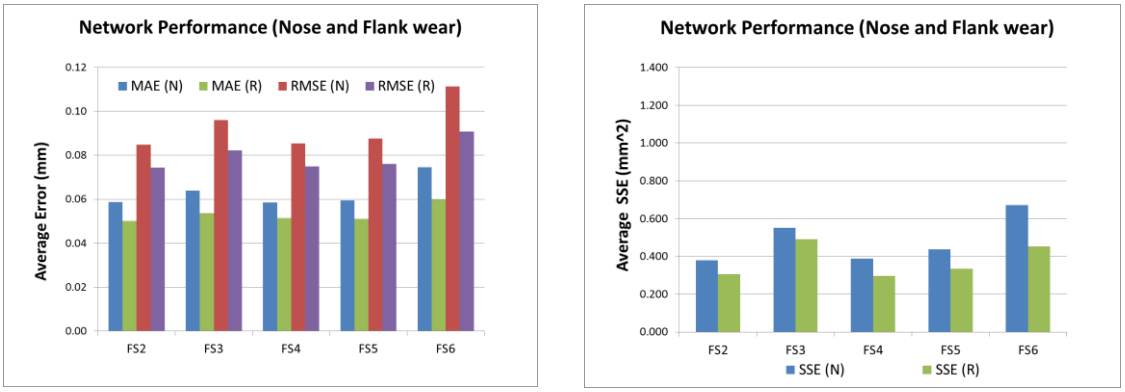

(a) *(b)*

Figure 7.14 Average error of each feature set categorised by two locations of tool wear

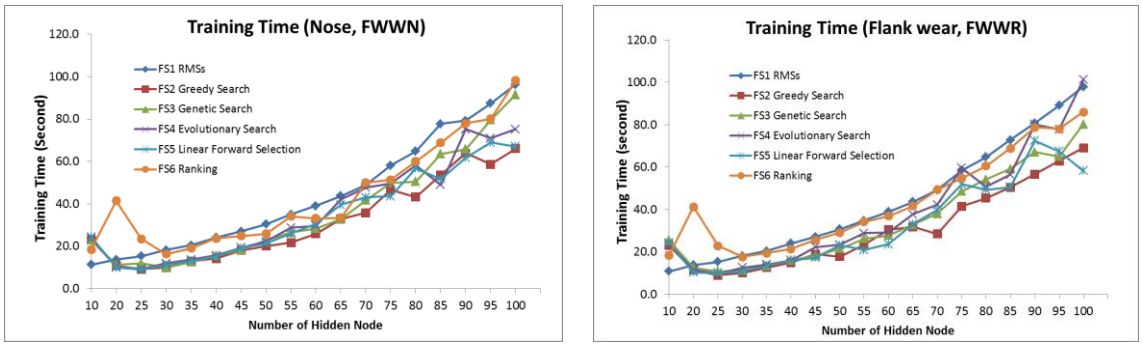

(a) *(b)*

Figure 7.15 Training time used for training the networks: *(a)* FWWN and *(b)* FWWR

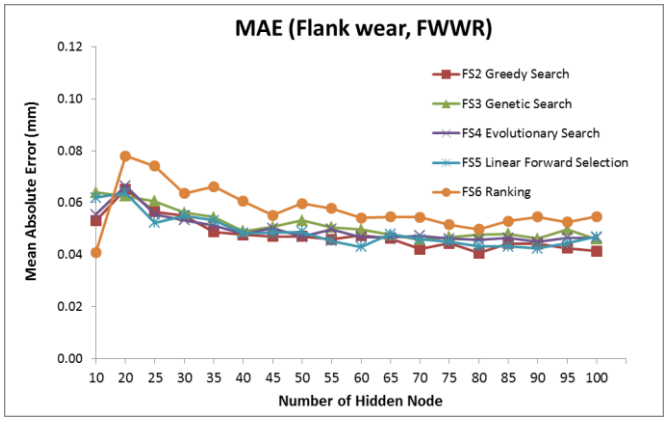

Figure 7.16 Mean absolute error of flank wear prediction by SHL, *tansig*

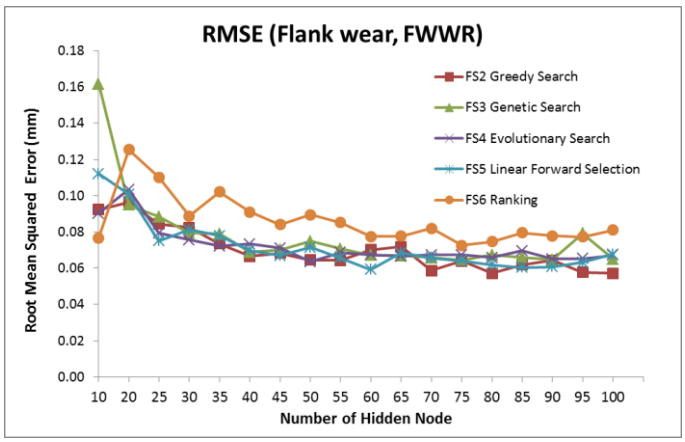

Figure 7.17 Root Mean Squared error of flank wear prediction by SHL, *tansig*

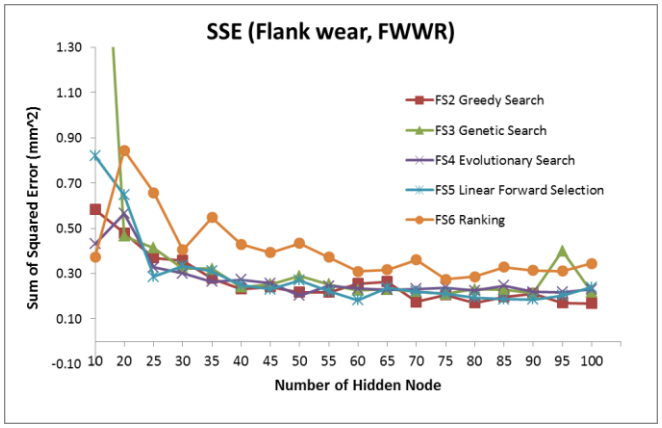

Figure 7.18 Sum squared error of flank wear prediction by SHL, *tansig*

The prediction error of feature set (FS6) is significantly higher compared to other feature sets. Interestingly, Figure 7.16 show that SF6 with 10 hidden nodes is the lowest MAE and could be the representative feature set but RMSE and SSE are also high. Alternatively, the best networks should select from the network where the lowest prediction errors can be obtained in this case FS2-70-1 with MAE=0.042075, RMSE=0.058600, and SSE=0.174680.

7.2.2.3 Comparison of Two Activation Functions (Single Hidden Layer)

The average prediction errors of two activation functions was compared and illustrated in Figure 7.19. Also, average training time of these functions was compared as shown in Figure 7.20.

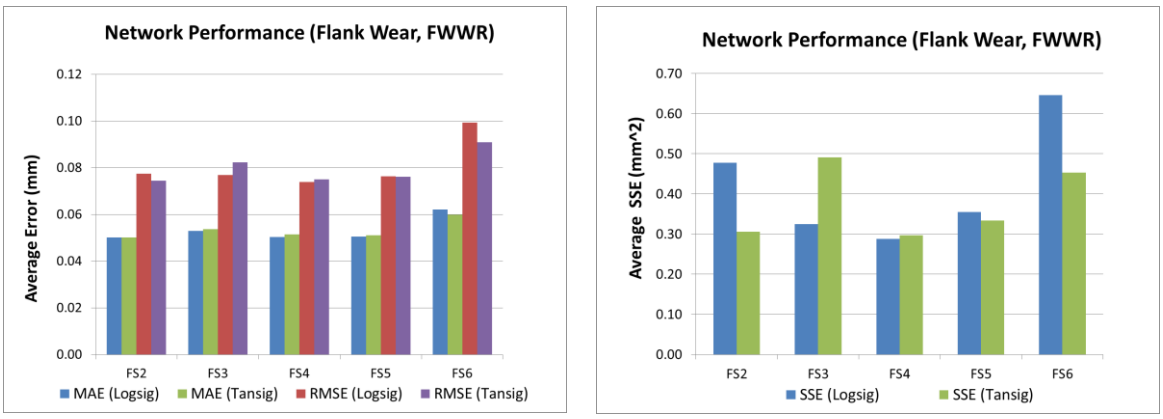

(a) *(b)*

Figure 7.19 Average prediction error compared between *logsig* and *tansig*

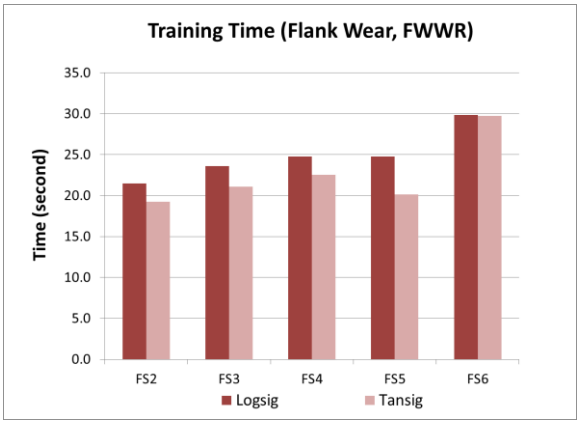

Figure 7.20 Training time used to train the networks classified by two activated functions

In Figure 7.19*(a)*, average MAE values between *logsig* and *tansig* are slightly different, while average RMSE and SSE have significant difference value. These results agree with the finding of other studies, in which *logsig* and *tansig* provide almost the same performance [124]. Overall, it seems that the error of using *logsig* is lower than *tansig* on average. Furthermore, *logsig* activation function tends to take longer time to train the networks as can be seen in Figure 7.20.

In conclusion, although *logsig* provides lower on average prediction errors than *tansig*, the best network structure, which has the lowest errors, is the network activated by *tansig* function. The neural network having single hidden layer with 70 nodes activated by *tansig* and the input feature set FS2 will be used to predict the flank wear (FS2-70-1). The error of this network provides 0.042075 of MAE, 0.058600 of RMSE, and 0.174680 of SEE. However, this network will be compared with the representative networks having double hidden layers in following sections.

7.2.3 Flank Wear Prediction by ANNs: Double Hidden Layers

In this section, DHL of feed forward neural network were trained with backpropagation training algorithms (*trainlm*) for flank wear prediction. From Figure 7.6*(b)*, the NNHL in each hidden layer was varied as follows:

1st hidden layer (H_1): 30, 35, 40, 45, 50, 55, 60

2nd hidden layer (H_2): 10, 20, 30, 40, 50, 60

The previous result in SHL (Section 7.2.2) found that FS2 selected by the greedy search algorithm is the best feature set which provides the least RMSE when used as inputs to train the neural networks for flank wear prediction. Additionally, the proposed feature (FS6) manually calculated by ranking of average correlation coefficient was selected to compare the results with the FS2. The flank wear values at two locations (FWWN and FWWR) were also used as target values for network training. The results of two activation functions (*logsig* and *tansig*) were compared. The prediction accuracy can be represented by the minimum errors between the predicted values and actual values. MAE, RMSE, and SSE were used to evaluate the best network structure. The 10-fold cross validation approach was performed to calculate the average network performance and errors. The training parameters and stopping criteria are the same as described in Section 7.2.1.

7.2.3.1 Flank Wear Prediction by ANNs (Double Hidden Layer, AF: logsig, TA: trainlm)

The combination of the 42 networks activated by *logsig* was trained by FS2 and FS6 as inputs, and the two targets as outputs. The Figure 7.21 presents the MAE of tool wear prediction, while Figure 7.22 shows RMSE, and Figure 7.23 illustrates SSE.

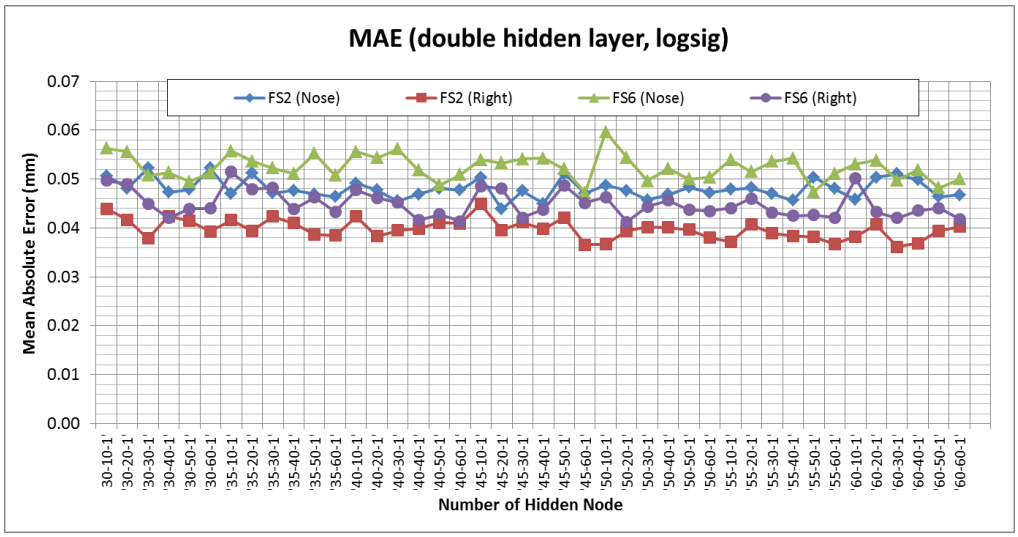

Figure 7.21 Mean absolute error of flank wear prediction by DHL, *logsig*

From Figure 7.21, on average, the networks trained by FWWR give better results than the ones trained by FWWN for both FS2 and FS6. Additionally, FS2 has a higher

prediction accuracy than FS6 as it produces less MAE. Similarly to RMSE (Figure 7.22) and SSE (Figure 7.23), FS2 and FWWR are still the best pair of data fed into network inputs and targets for training the neural networks.

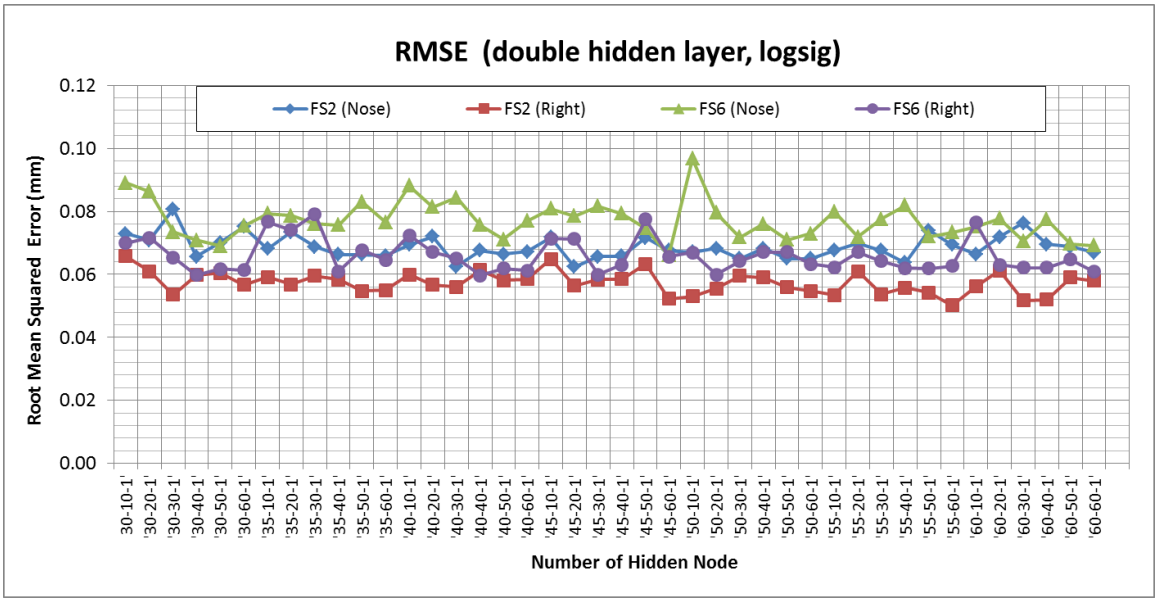

Figure 7.22 Root mean squared error of flank wear prediction by DHL, *logsig*

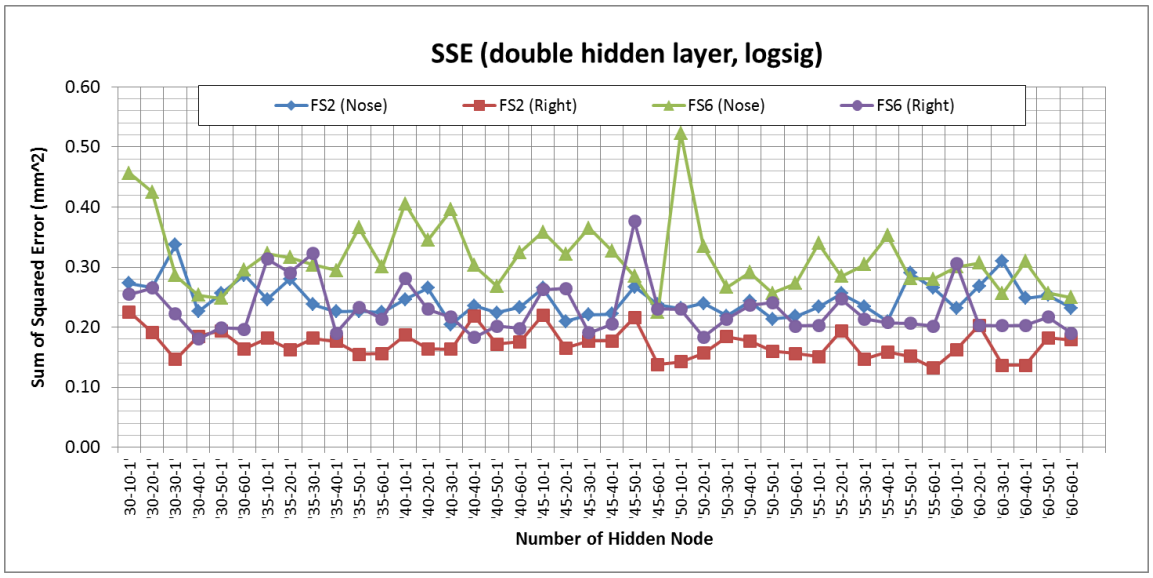

Figure 7.23 Sum of squared error of flank wear prediction by DHL, *logsig*

The training time of the networks is shown in Figure 7.24. Obviously seen that the time used for training the network increases, according to the number of hidden nodes. Interestingly, there is slightly increase of training time when the number of hidden nodes in 1st hidden layer increases, but on the other hand, the training time increases significantly if the number of nodes in 2nd hidden layer increases. The networks trained by FS2 spent less time on training than those trained by FS6, although FS2 comprises of 24 features which is higher than FS6 (18 features).

There is no evidence to describe effects of the number of input features on the training time. Most of studies mentioned only the effect of the hidden layer size [26]. It is difficult to explain this result, but it might be related to the correlation between input features and output targets. FS2, which has higher correlation, performs very well in neural network training. The network training will meet the stopping criteria faster than FS6 which has lower correlation between input and output features.

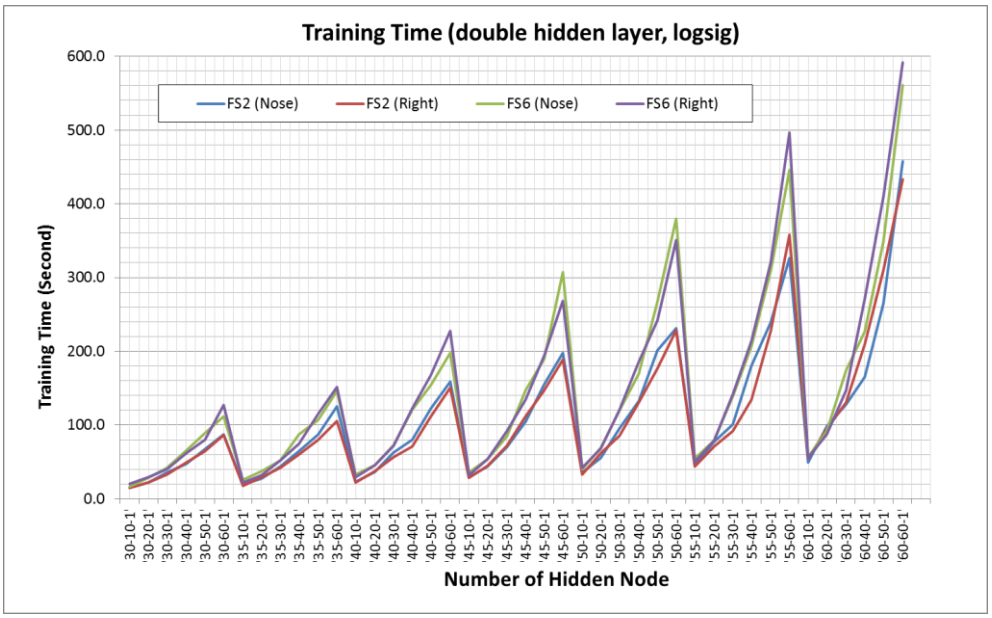

Figure 7.24 Training time used for training the DHL networks, *logsig*

From three evaluators, it can be found that FS2-55-60-1 using *logsig* in hidden layers is the best network for tool wear prediction as it produces the lowest prediction errors (MAE=0.0368, RMSE=0.0502, SSE=0.1320). The FS2 is used as network inputs and the output of this network can predict the flank wear width (FWWR). The performance of this network was later compared with the other network configurations to find the best representative network for tool flank wear prediction. This will be compared and summarised in Section 7.2.4.

7.2.3.2 Flank Wear Prediction by ANNs (Double Hidden Layer, AF: tansig, TA: trainlm)

In this section, the networks using *tansig* to activate the nodes in hidden layers were compared with ones activated by *logsig* so that the most accurate network for determining tool wear value can be obtained.

Figure 7.25 to Figure 7.27 illustrate the comparison of MAE, RMSE, and SSE, respectively. The prediction errors of the two feature set were both considered.

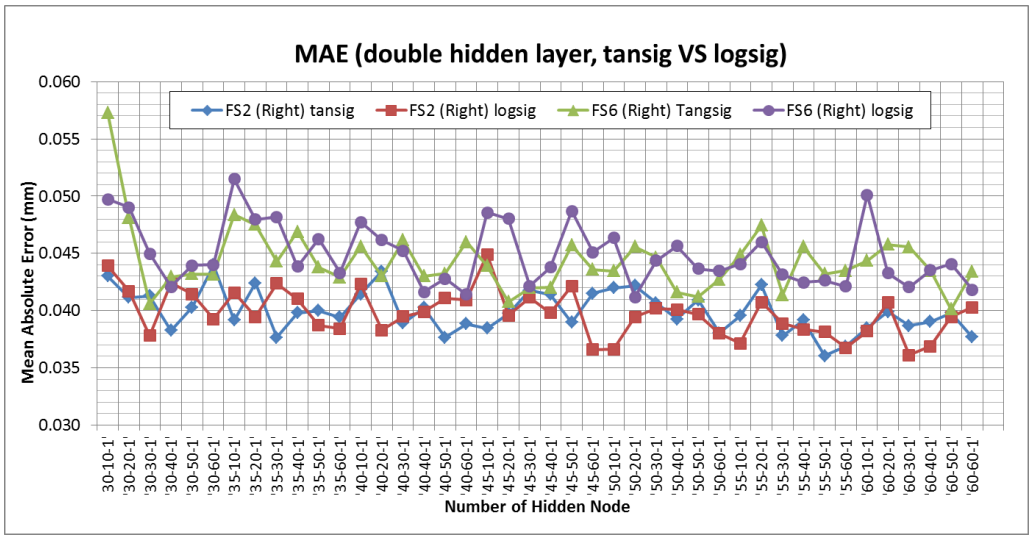

Figure 7.25 Mean absolute error of flank wear prediction by double hidden node

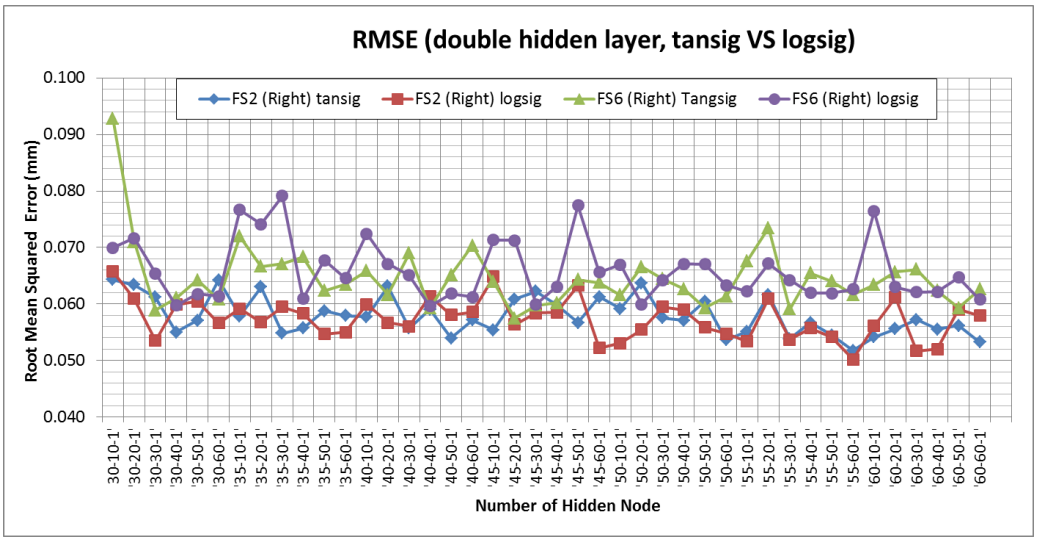

Figure 7.26 Root mean squared error of flank wear prediction by DHL

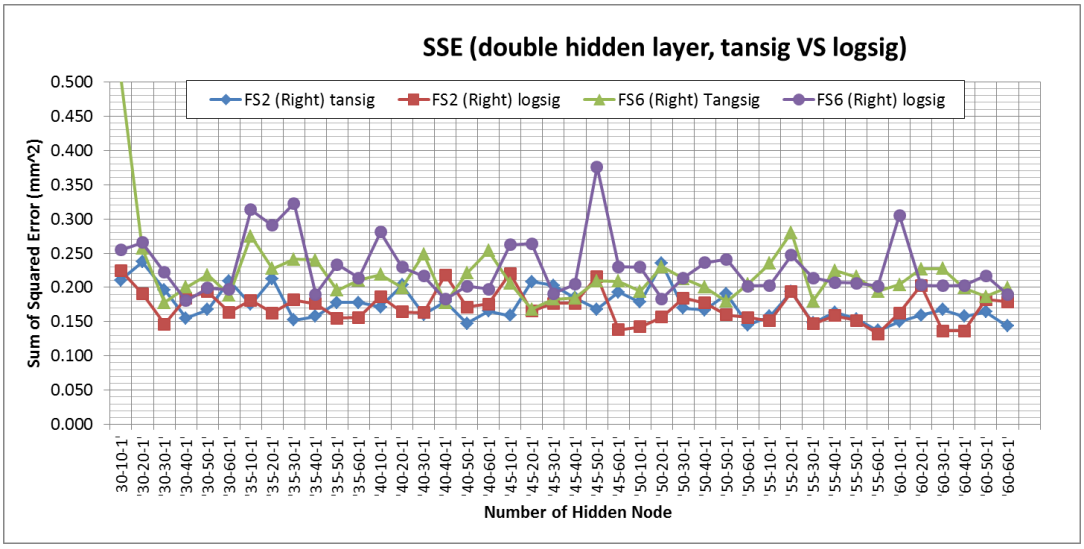

Figure 7.27 Sum of squared error of flank wear prediction by DHL

On average, the networks that nodes in hidden layers were activated by *logsig* provide slightly higher accuracy than ones activated by *tansig* in the cases of the FS2 and FWWR, but the networks using *logsig* function require more training time. Conversely, with respect to SF6, the prediction errors of the networks having *tansig* function in hidden layers is lower than the *logsig* networks.

Figure 7.25 shows that the network using *tansig* for activating the hidden nodes, structured FS2-55-50-1 is the lowest MAE but other evaluators are obviously higher than the *logsig* networks such as FS2-45-60-1 and FS2-50-10-1. Alternatively, SSE and RMSE of the *logsig* network (FS2-55-60-1) are lower than the FS2-45-60-1 and FS-50-10-1 networks, but MAE of FS2-55-60-1 is higher than those two sturctures. Therefore, using only one evaluator is not enough to justify the selection of the best network for use.

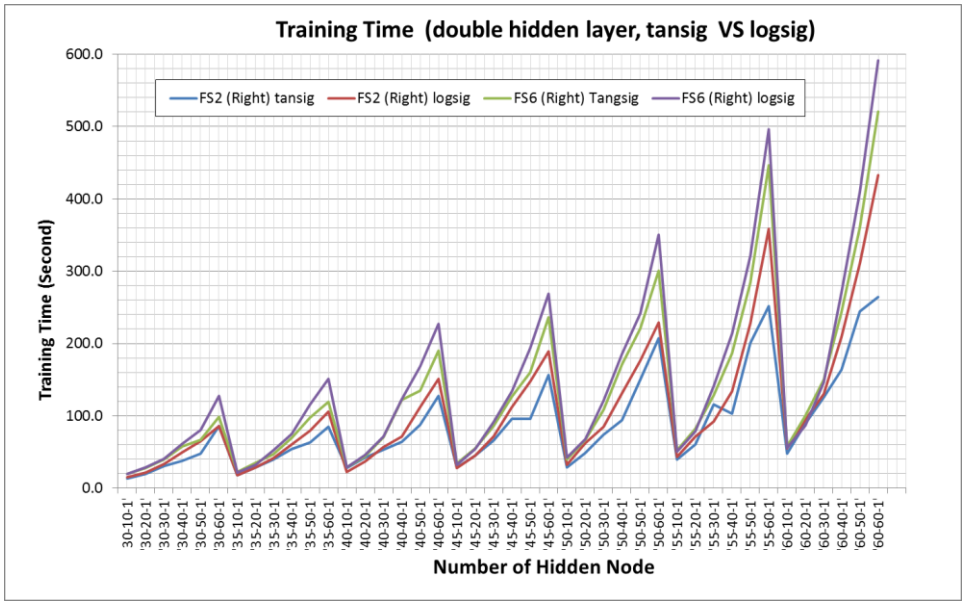

Figure 7.28 Training time used for training the DHL networks

It is seen in Figure 7.28 that the *logsig* networks spend longer training time than *tansig* networks for FS2 and FS6. Furthermore, the training time depends upon the number of elements in the networks. The NNHL have a direct influence on the time used for training. It is seen that the larger network structure requires longer time for training. Interestingly, there is slightly increase of training time when the NNHL of the first layer (H_1) increases, on the other hand, the training time increases rapidly if the NNHL of the second hidden layer (H_2) increases.

These results match those observed in the review of Basheer and Hajmeer [26], in which the training becomes immensely time-consuming with an increasing number of hidden nodes. Several previous studies in this review attempted to find generic formula to choose the optimum NNHL in terms of input/output vector sizes such as [150, 151]. However, these methods face the problems of nonlinearity and hysteresis. The most popular approach finding the optimal NNHL is by trial and error.

An alternative method is to start with a small NHN and increase as needed to meet the desired model accuracy. Similarly to the previous section, the networks trained by FS2 as inputs spend shorter time for training than trained by FS6, although the number of features of FS2 is more than FS6 (18 features).

7.2.3.3 Comparison of Two Activation Functions (Double Hidden Layer)

The average prediction errors of two activation functions was compared and illustrated in Figure 7.29. Also, average training time of these functions was compared as shown in Figure 7.30. In Figure 7.29, the average errors of 42 networks compared between *logsig* and *tansig* are very close. Similar to AsiltÜerk *et al* [124], they commented that using *logsig* and *tansig* for activating the hidden nodes produces almost the same performance. Overall, it seems that the error of using *logsig* is on average lower than *tansig* in case of FS2. Furthermore, *logsig* function takes longer time for training the networks as can be seen in Figure 7.30. As for FS6, *tansig* function has better prediction performance than *logsig*.

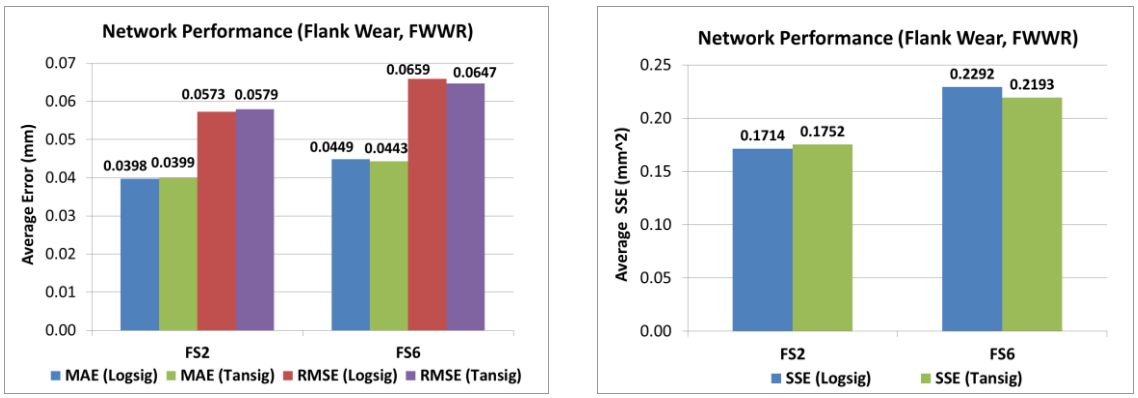

(a) *(b)*

Figure 7.29 Average prediction error compared between *logsig* and *tansig*

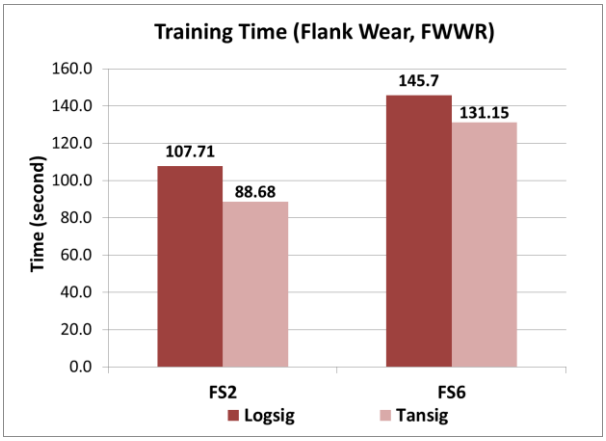

Figure 7.30 Training time used to train the networks classified by two activated functions

In double hidden layer, considering to errors of the networks activated by two activation functions, the best network structure is FS2-55-60-1 providing the lowest prediction errors (MAE=0.0368, RMSE=0.0502, and SSE=0.1320). This network was activated by *logsig* function, and it uses FS2 as network inputs in order to predict the tool wear value. This network performance will be later compared with the best one of the single hidden layer.

7.2.4 Summary of Tool Wear Prediction by Neural Network

Six feature sets obtained from machining data were used to train the several network configurations for tool wear prediction. The networks with different functions activating the hidden nodes were also used to compare to find the best representative network. From the first observation, FS1 was ruled out the possibility to use with the neural network due to increasing of prediction errors. It is clearly seen that feature sets selected by WEKA (FS2-FS5) produce a good performance in tool wear prediction rather than the proposed feature sets (FS1 and FS6).

In sum, the results of both single and double hidden layer networks found that a flank wear width of right side of cutting inserts (FWWR) is more suitable to be used as network targets during data training because training by FWWR provides a more accurate prediction result than by FWWN. Network training by FWWR spends less time compared to by FWWN. Interestingly, the MAE of a single hidden layer is significantly higher than the MAE of double hidden layers. This result is in agreement with the study of Venkata *et al* [32], but is contradictory to Srikant *et al* [152] where they concluded that the error is consistently less for a single hidden layer when compared to a network with two hidden layers, for the same number of hidden layer nodes.

Regarding training time, the longer training time of *logsig* networks offers better results that the prediction errors are mostly lower *tansig* networks. It is generally viewed that the training time of the networks depends on the number of hidden nodes in both single and double hidden layers. The larger structure of the neural network

needs more time to train. The time used for training the networks significantly increases where the NNHL increases. Remarkably, in double hidden layer networks, an increase of hidden nodes in the first hidden layer has a slight effect on training time only, contrasting with the large increase when the hidden nodes in the second hidden layer increase.

As previously mentioned, the representative networks trained by several network configurations are summarised in Table **7.8**. In conclusion, the best network having the minimum errors is a double hidden layer feed forward network, which consists of 50-60 nodes in two hidden layers activated by *logsig*, and FS2 is used as the network inputs. The training and validating results of FS2-50-60-1 (*logsig*) are shown in Figure 7.31.

Table 7.8 Summary of network configurations for tool wear prediction

Network Types	Hidden Nodes	Activated Function	Input Features	Targets	MAE	RMSE	SSE
Single hidden layer	70	logsig	FS5	FWWR	0.042124	0.059558	0.179460
Single hidden layer	70	tansig	FS2	FWWR	0.042075	0.058600	0.174680
Double hidden layer	**55-60**	**logsig**	**FS2**	**FWWR**	**0.036752**	**0.050166**	**0.132047**
Double hidden layer	55-60	tansig	FS2	FWWR	0.036887	0.051755	0.137014

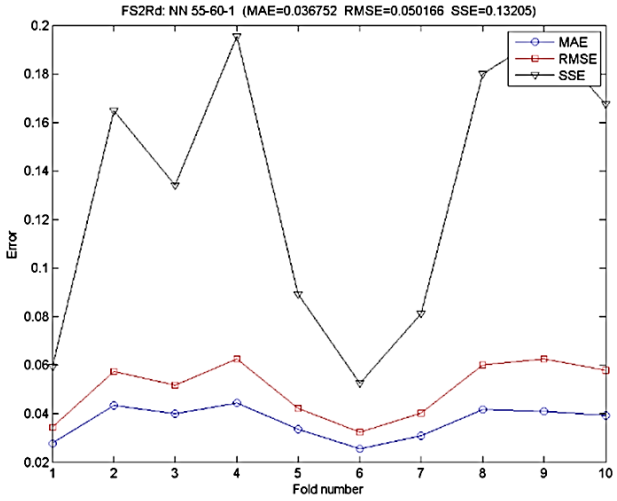


```
FFNN: FS2Rd  Model: 55-60-1
Date: 16/08/14  8:23 AM

Fold,  MAE,      RMSE,     SSE,      Time
01,    0.027783, 0.034443, 0.059316, 307.503000
02,    0.043325, 0.057433, 0.164930, 224.590000
03,    0.040097, 0.051812, 0.134224, 345.919000
04,    0.044301, 0.062539, 0.195554, 616.496000
05,    0.033732, 0.042238, 0.089201, 372.587000
06,    0.025482, 0.032396, 0.052476, 225.579000
07,    0.030808, 0.040309, 0.081239, 400.750000
08,    0.041608, 0.059993, 0.179958, 333.120000
09,    0.041056, 0.062605, 0.195971, 409.500000
10,    0.039329, 0.057897, 0.167604, 347.022000

AVG,   0.036752, 0.050166, 0.132047, 358.306600

Fold 06 has minimum MAE = 0.025482
Fold 06 has minimum RMSE = 0.032396
Fold 06 has minimum SSE = 0.052476

Start Time:  8:23:06 AM      End Time:  9:22:56 AM
Total Training Time : 59 mins, 49.8 secs
```

Figure 7.31 Training and validating results of the flank wear prediction model

7.3 Tool Wear State Classification

Tool wear state is an important piece of information used for monitoring the tool conditions. Wear state transformation (between states) can warn the machine control system to change the cutting parameter autonomously or can warn machine operators to prepare for changing tool or regrind the cutting edge. In this section, tool wear state in a turning process was classified by the feed forward neural networks, to classify tool wear state, flank wear values were transformed into four classes before using as targets in network training as shown in Figure 7.4. Six feature sets (FS1-FS6) were also used as network inputs. Several network architectures and different configurations were used to train the classification model to obtain the best results for tool wear state classification as described in following sections.

7.3.1 General Information of Neural Network Training

First of all, the flank wear values obtained from the experiment were classified into four classes (i.e. 1-new, 2-slightly worn, 3-moderately worn, and 4-severely worn) as detailed in Table 7.9. When the flank wear width on cutting tools (V_b) is lower than to or equal to 0.1 mm, this tool is considered as new tool (N, class 1). If the flank wear value is larger than 0.1 mm and lower than or equal to 0.2 mm, it is classified as slightly worn tool (U1, class 2). Moderately worn tool (U2, class 3) is defined where the flank wear value is larger than 0.2 mm and lower than or equal to 0.3 mm. Last class, above of this range is classified as severely worn tool (W, class 4). Training parameters, stopping criteria, training algorithms, activation functions used for the networks are previously mentioned in 7.2.1 and summarised in Table 7.10.

Table 7.9 Definition of the tool condition classes

Class	Code	V_b (mm)
1-New	N	$V_b \leq 0.1$
2-slightly worn	U1	$0.1 < V_b \leq 0.2$
3-moderately worn	U2	$0.2 < V_b \leq 0.3$
4-severely worn	W	$V_b > 0.3$

Table 7.10 Training parameters used for classification

Activation function / transfer function	Log-Sigmoid (*logsig*), Tan-Sigmoid (*tansig*)
Training algorithms	trainlm, trainbr
Network performance evaluators	MAE, RMSE, SSE, % Classification Accuracy
Network Performance function	'mse' - mean square error
Learning rate	0.3
min_grad	0.0000000001
Goal	1e-9
Epochs	500
Input layer	Feature sets (FS1- FS6)
Target layer	FWWN, FWWR (transformed to 4 classes)

7.3.2 Tool Wear State Classification Results: Single Hidden Layer

This section describes how the single hidden layer neural networks with varying the number of nodes were trained. The number of nodes in single hidden layer (NNHL) includes 10, 20, 25, 30, 35, 40, 45, 50, 55, and 60. Two activation function (AF) used for activating the nodes in hidden layer are *logsig* and *tansig* functions. These networks were trained and tested by 70/30 schemes where the total of 503 instances were randomly separated into 70 % for training, and 30 % for testing and validating. Two training algorithms (TA) are *trainlm* and *trainbr*. The network performance was determined to obtain the best network model for predicting the tool wear state. The "Percentage of correctly-classified instance" is a major evaluator for selecting the representative model. Furthermore, MAE, RMSE, and SSE are also minor criteria. These are described in Chapter 4 (Section 4.4.4).

7.3.2.1 Tool Wear State Classification by ANNs (SHL, AF: logsig, TA: trainlm)

This section describes the classification results of the networks which hidden nodes were activated by *logsig* function and the networks were trained by *trainlm*. Figure 7.32 shows the average classification accuracy (ACC) and average errors (MAE, RMSE) of six feature sets, where two classifiers (FWWN and FWWR) were denoted by N and R, respectively.

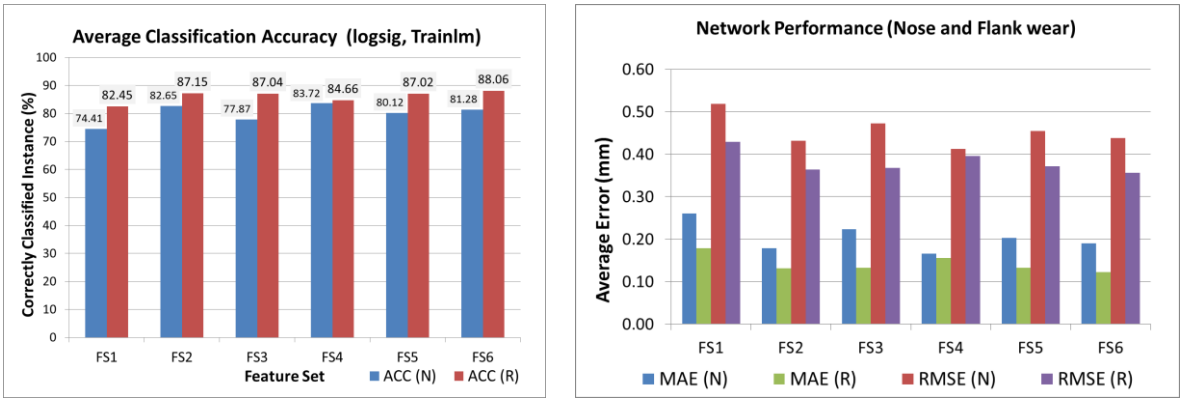

(a) *(b)*

Figure 7.32 Classification accuracy and average errors (AF: *logsig*,TA: *trainlm*)

As shown in Figure 7.32*(a),* it is obviously seen that classifier FWWR produces the better classification than FWWN for all feature sets. This is also confirmed by Figure 7.32*(b)* that average errors of FWWR are almost lower than FWWN. The highest ACC (88.06 %) can be obtained when FS6 was fed into the input layer of the networks. Most interestingly, this feature set was selected by the ranking method proposed in Section 7.1.2.

Figure 7.33 presents the classification accuracy of all feature sets where the different network structures varied by the NNHL were trained. Although FS6 produces the highest accuracy on average (Figure 7.32*(a)*), the best network can be found when FS2 is used as inputs. It is clearly seen in Figure 7.34 that MAE value of FS2 at hidden

node 35 is at the bottom. Therefore, the representative network from this section is FS2-35-1, consisting of FS2 on the input layer, 35 of NNHL activated by *logsig*, and tool wear states in the output layer. This network produces 92.89 % of correctly-classified instance.

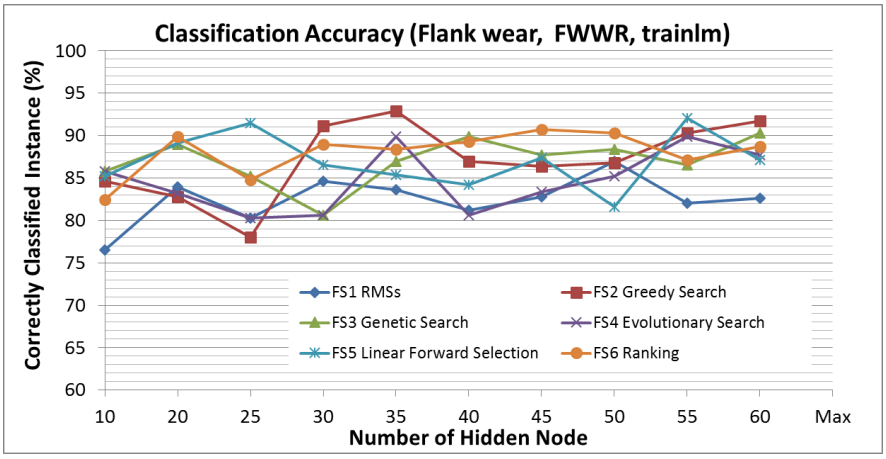

Figure 7.33 Classification accuracy of tool wear state prediction (AF: *logsig*,TA: *trainlm*)

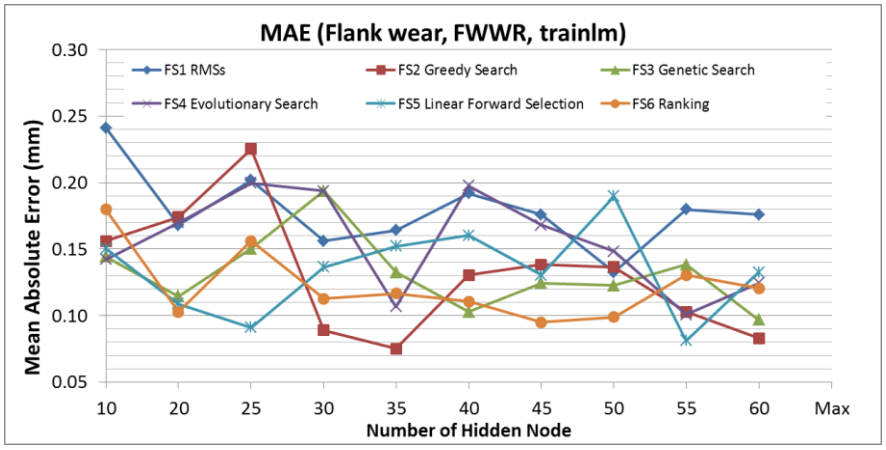

Figure 7.34 Mean absolute error (AF: *logsig*,TA: *trainlm*)

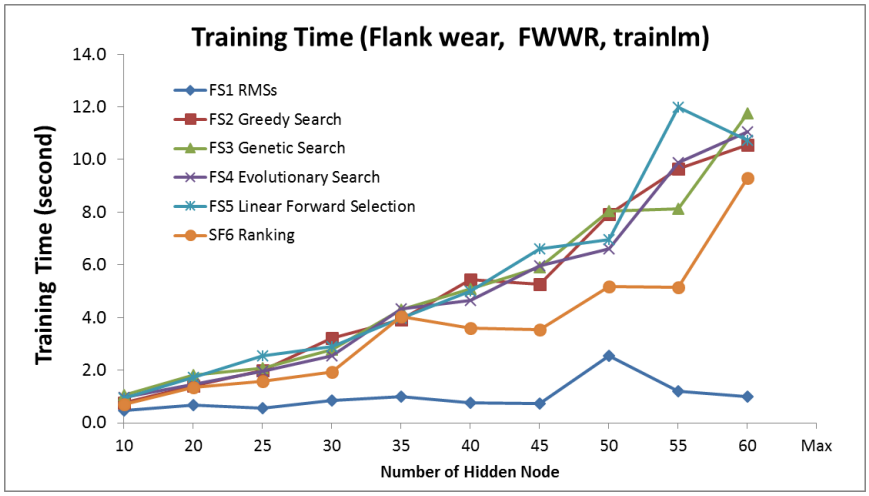

Figure 7.35 Training time (AF: *logsig*,TA: *trainlm*)

Figure 7.35 shows that the training time significantly increases when the NNHL increases. Clearly, FS1 having 3 RMS features spent the shortest time for training, while FS6 consisted of 18 features spent more time than FS1, and other sets contained 24-25 features inside are the highest value on average. From this results, it can be summarised that training time depends on the number of network elements, including the number of hidden nodes and the input features.

7.3.2.2 Tool Wear State Classification by ANNs (SHL, AF: tansig, TA: trainlm)

This section describes the classification results where the hidden nodes in the neural networks were activated by *tansig* function. The result in Figure 7.36 shows that on average, FS2 is the best feature set for use that provides the highest accuracy (ACC = 88.42 %) with the classifier (FWWR). Similar to *logsig* mentioned previously (Section 7.3.2.1), MAE and RMSE of FWWR are lower than the errors of FWWN unanimously.

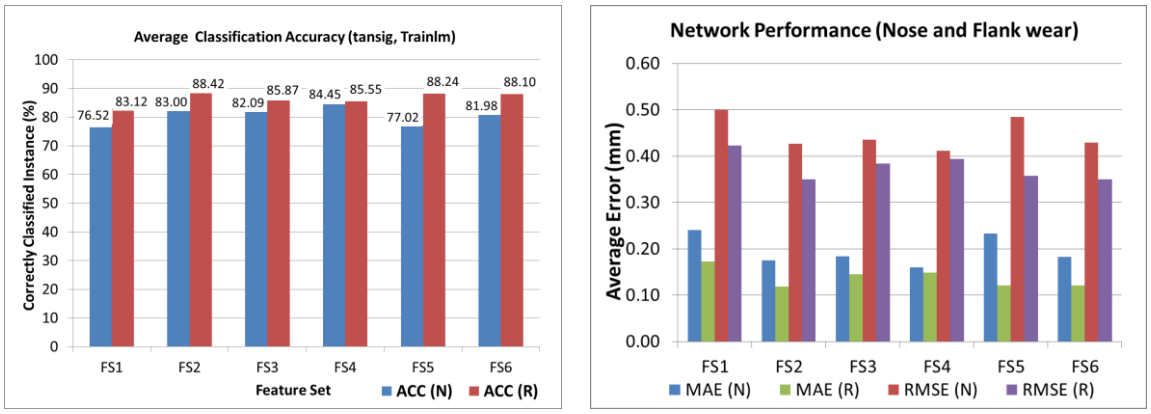

(a) *(b)*

Figure 7.36 Average error and classification accuracy (AF: *tansig*, TA: *trainlm*)

As regards the classification accuracy of each network structures in Figure 7.37, it is found that on average the top three of average accuracy consist of FS2, FS5, and FS6. However, it is easier to find the best result by considering the lowest MAE in Figure 7.38. Therefore, FS3, selected by a genetic search algorithm, produces the highest accuracy (92.09 %) with the network having 35 nodes in the hidden layer. Similarly, training time in Figure 7.39 is in agreement of the previous conclusion that the time usage increases due to the complexity of neural networks.

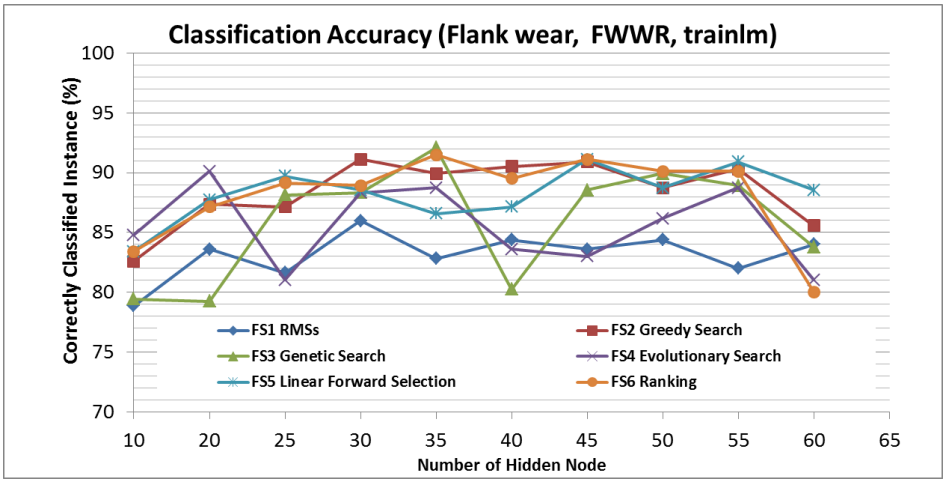

Figure 7.37 Classification accuracy of tool wear state prediction (AF: *tansig*, TA: *trainlm*)

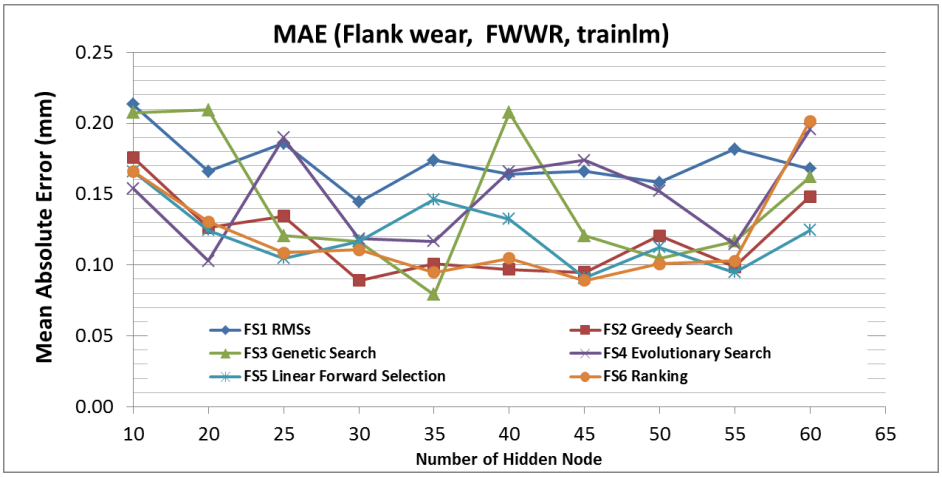

Figure 7.38 Mean absolute error (AF: *tansig*, TA: *trainlm*)

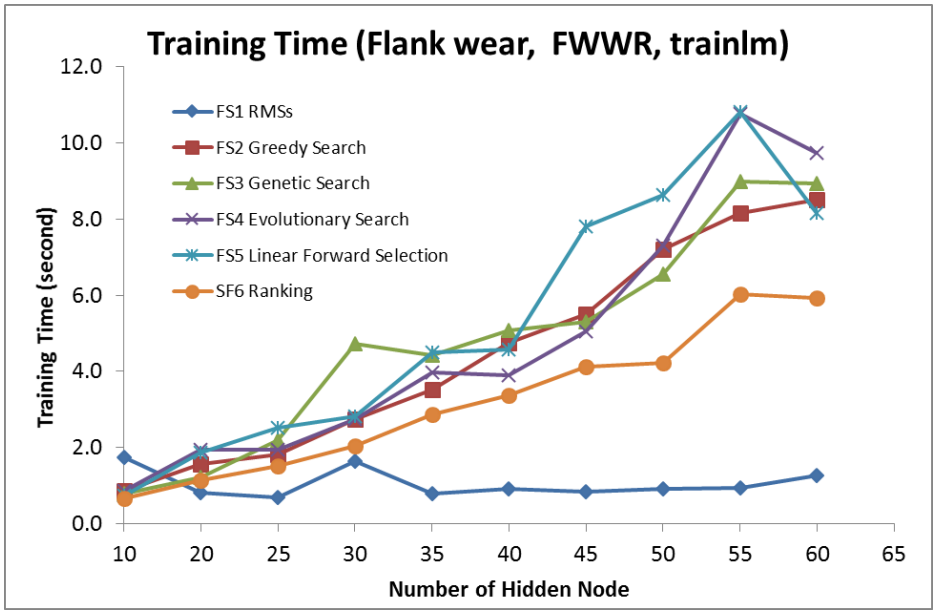

Figure 7.39 Training time (AF: *tansig*, TA: *trainlm*)

In a comparison of the two activation functions, the neural networks that the hidden nodes were activated by *logsig* can produce more accurate classification results than ones activated by *tansig* although previous study of Asiltuerk *et al* found that using *logsig* and *tansig* for activating the hidden nodes provide almost the same result [124]. Furthermore, compared between and Figure 7.39, it is found that the training time of *logsig* (Figure 7.35) is clearly longer than of *tansig*. It is reasonable to take more time to train the networks producing an accurate result.

The *trainlm* is one of the fast training algorithms, however, the classification results remain unsatisfied. Therefore, on the next section, these neural networks activated by two activation functions will be retrained by *Bayesian Regularisation* algorithm or *trainbr*. It is expected that *trainbr* can be able to produce more accurate results and the higher classification accuracy can be obtained.

7.3.2.3 Tool Wear State Classification by ANNs (SHL, AF: logsig, TA: trainbr)

Bayesian Regularisation algorithm (*trainbr*) was used to retrain the neural networks in previous sections. Surprisingly, the ACC of each feature set is greatly improved by this training algorithm (Figure 7.40). On average, training by *trainbr* produces the ACC about 80 - 95 %, while *trainlm* offers only 75 - 88 %. It can be seen that the accuracy results of two classifiers are very close as seen in Figure 7.40*(a)* and the errors between FWWN and FWWR in Figure 7.40*(b)* looks indifferent. The highest ACC is in the networks trained with FS6 as inputs and FWWR as targets. This configuration can offer 95.36 % of average accuracy.

Regarding to Figure 7.41, the classification accuracy of FS1 is outstandingly under the others. This means FS1 should not be used for tool wear state classification. Most interestingly, the proposed feature set (FS6), with 25 of *logsig* nodes in hidden layer, is the best network which provide 97.04 % of correct classification.

As for training time, Figure 7.43 shows similar increasing trend of the time usage of each feature set due to an increase of the NNHL. Most interestingly, training the networks by *trainbr* spent much greater time, approximately 120 % compared to the *trainlm* used as shown in Figure 7.39. Also, the number of features inputs to the networks have a significant influence on the time used for training.

As can be seen that FS1 having only 3 features, it spends shorter time than any other feature in the group.

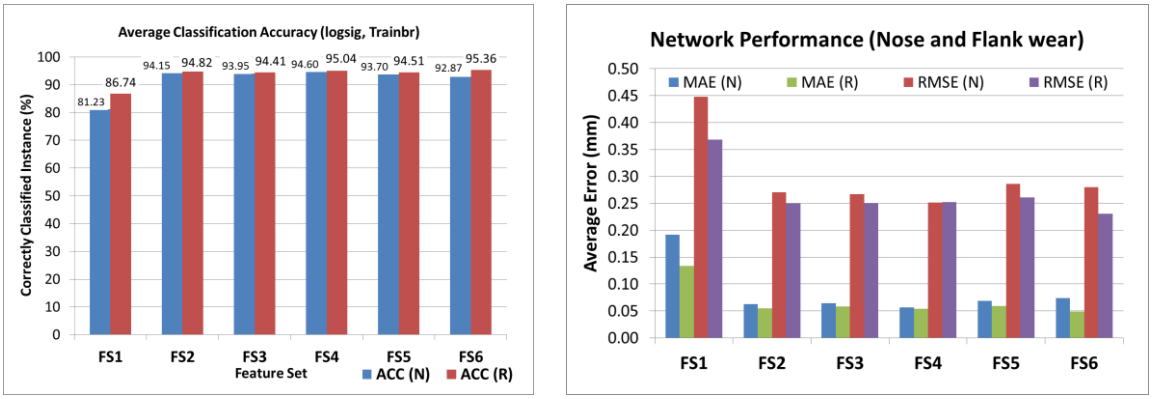

(a) *(b)*

Figure 7.40 Average error and classification accuracy (AF: *logsig*, TA: *trainbr*)

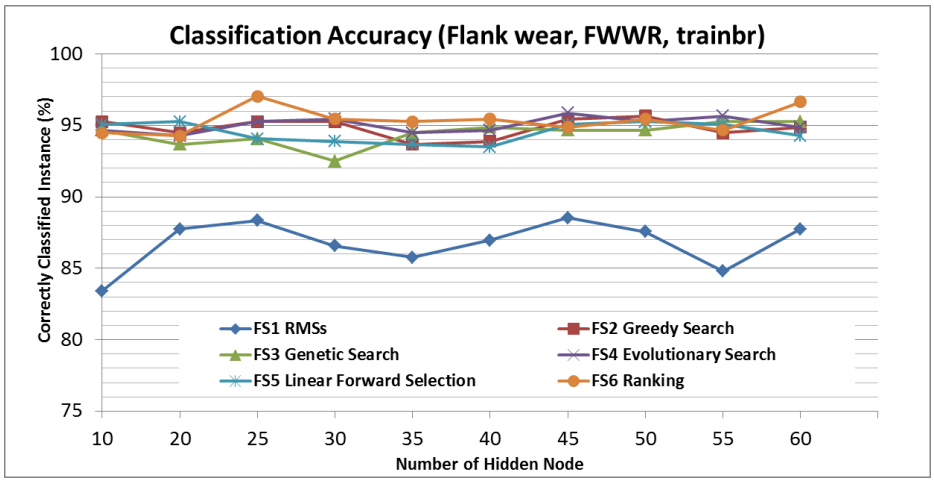

Figure 7.41 Classification accuracy of tool wear state prediction (AF: *logsig*, TA: *trainbr*)

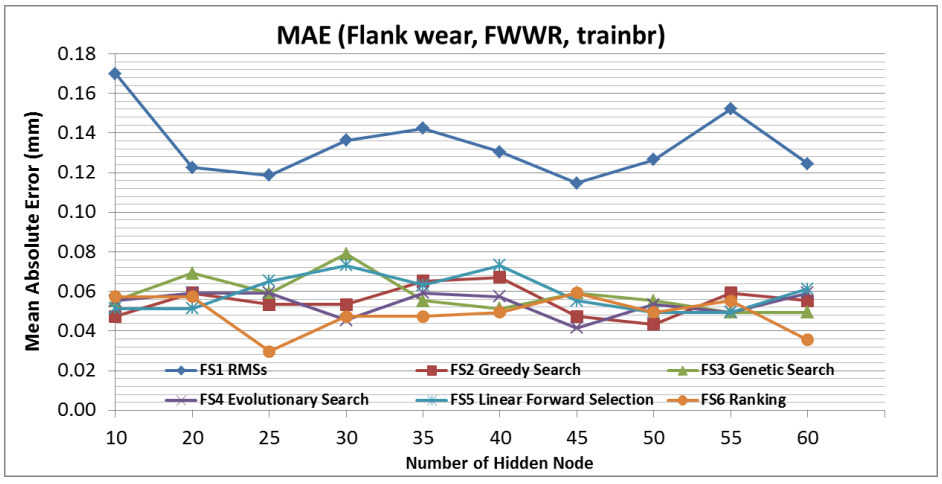

Figure 7.42 Mean absolute error (AF: *logsig*, TA: *trainbr*)

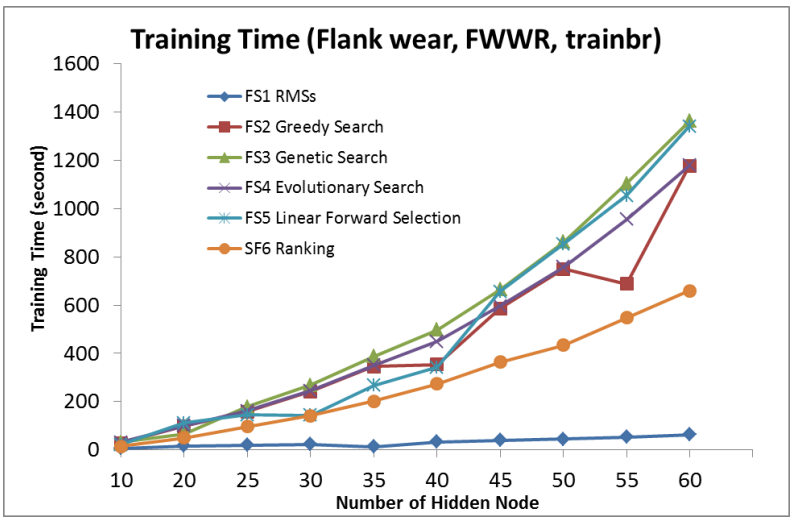

Figure 7.43 Training time (AF: *logsig*, TA: *trainbr*)

7.3.2.4 Tool Wear State Classification by ANNs (SHL, AF: tansig, TA: trainbr)

In this section, the *tansig* function was used to activate the nodes in hidden layer of the neural networks and the *trainbr* was used to train those networks. The Figure 7.44 presents the similar results as mentioned in previous section. It is found that the highest ACC is 95.24 % in both FS4 and FS6 where the FWWR was used as target values in output layer of the networks.

It can be found in Figure 7.45 that the network with 20 nodes in hidden layers activated by *tansig*, provides the maximum correct classification (96.44 %). The lowest accuracy was found in FS1 with 40 nodes in hidden layer (78.65 %). The training time of using *tansig* is shorter than using *logsig* by about 18 % as shown in Figure 7.47.

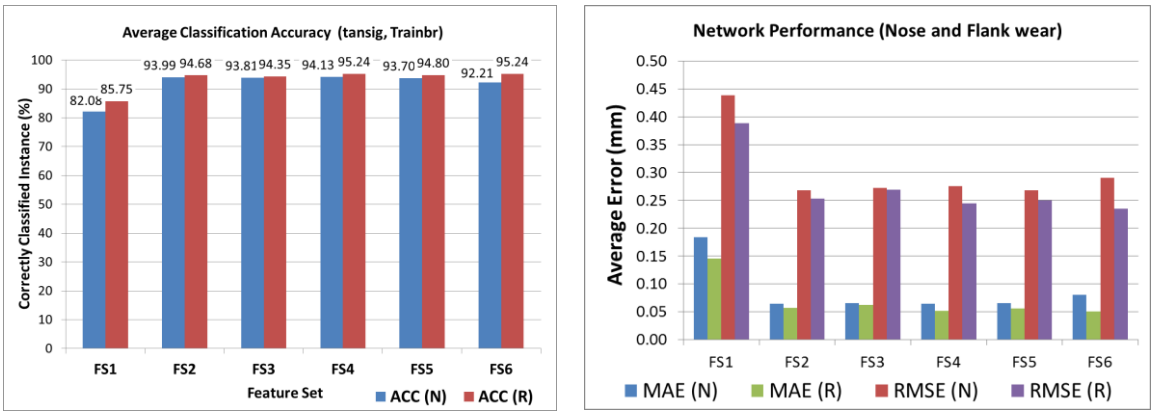

(a) *(b)*

Figure 7.44 Average error and classification accuracy (AF: *tansig*,TA: *trainbr*)

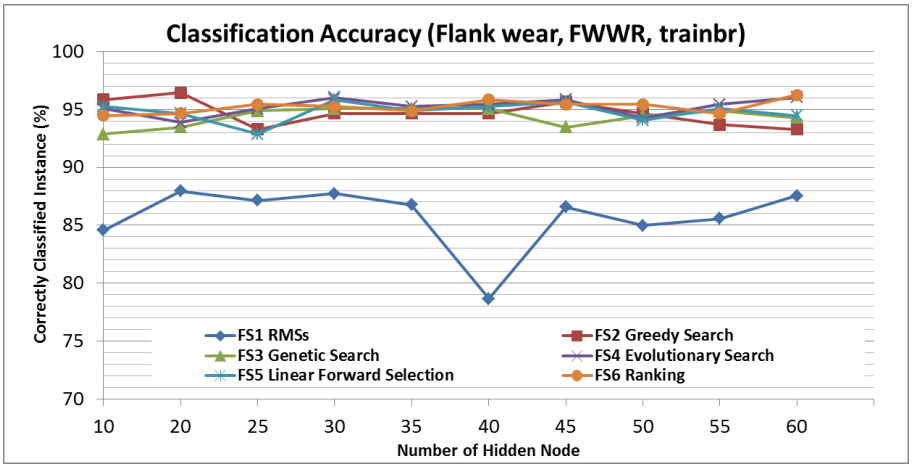

Figure 7.45 Classification accuracy f tool wear state prediction (AF: *tansig*,TA: *trainbr*)

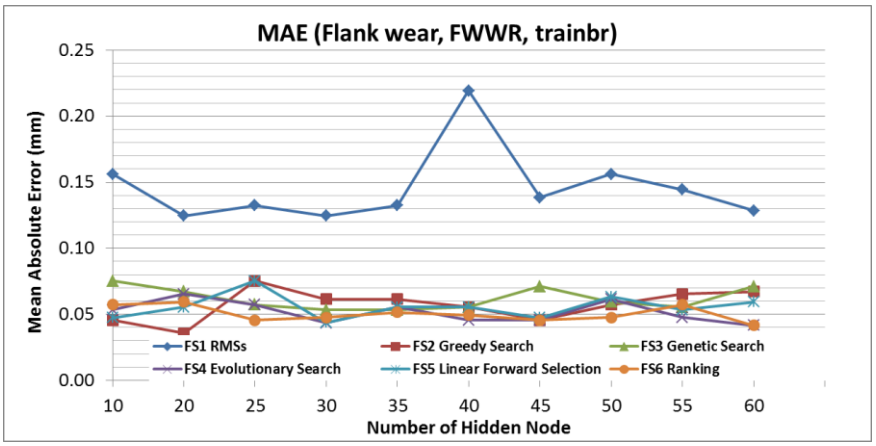

Figure 7.46 Mean absolute error (AF: *tansig*,TA: *trainbr*)

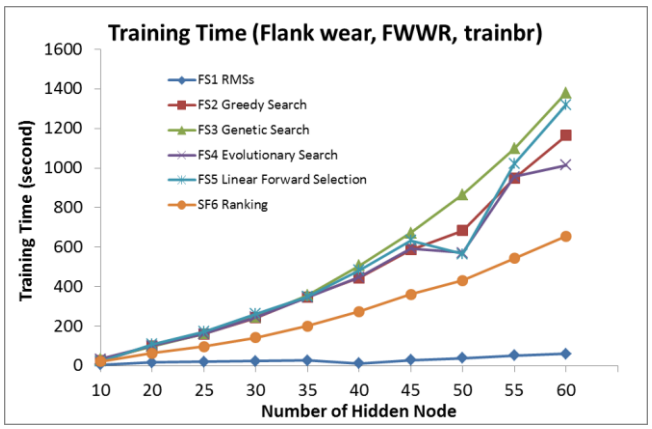

Figure 7.47 Training time (AF: *tansig*,TA: *trainbr*)

7.3.2.5 Summary of Tool Wear State Classification by SHL Neural Networks

The average and maximum accuracy of a tool wear state classification by several training configurations and feature sets are summarised in Table 7.11, while Figure 7.48 shows the comparison of classification accuracy between *trainlm* and *trainbr* with different feature sets and activation functions.

Table 7.11 Summary result of classification accuracy of single hidden layer ANNs

Feature set	Activate Function	Nose Waer (FWWN)				Flank Wear (FWWR)			
		Trainlm		Trainbr		Trainlm		Trainbr	
		mean	max	mean	max	mean	max	mean	max
FS1	logsig	74.4071	80.4348	81.2253	82.8063	82.4506	86.9565	86.7391	88.5375
	tansig	75.2767	82.4111	82.0751	83.7945	79.8617	84.3874	85.751	87.9447
FS2	logsig	82.6482	89.3281	94.1502	95.2569	87.1541	92.8854	94.8221	95.6522
	tansig	83.004	86.9565	93.9921	95.4545	88.419	91.1067	94.6838	96.4427
FS3	logsig	77.8656	85.7708	93.9526	95.2569	87.0356	90.3162	94.4071	95.2569
	tansig	82.0949	90.3162	93.8142	95.4545	85.8696	92.0949	94.3479	95.0593
FS4	logsig	83.7154	87.3518	94.6047	95.6522	84.664	89.9209	95.0395	95.8498
	tansig	81.9565	87.1542	94.1304	95.4545	84.3281	90.1186	95.2371	96.0474
FS5	logsig	80.1186	87.747	93.6956	94.2688	81.7787	92.0949	94.5059	95.2569
	tansig	77.0158	89.1304	93.6956	94.664	85.7115	91.1067	94.8024	95.8498
FS6	**logsig**	81.2846	85.7708	92.8656	94.8617	88.0633	90.7115	**95.3557**	**97.0356**
	tansig	79.4862	87.9447	92.2134	93.8735	88.1028	91.502	95.2371	96.2451
Max Accuracy.		-	**90.3162**	-	**95.6522**	-	**92.8854**	-	**97.0356**

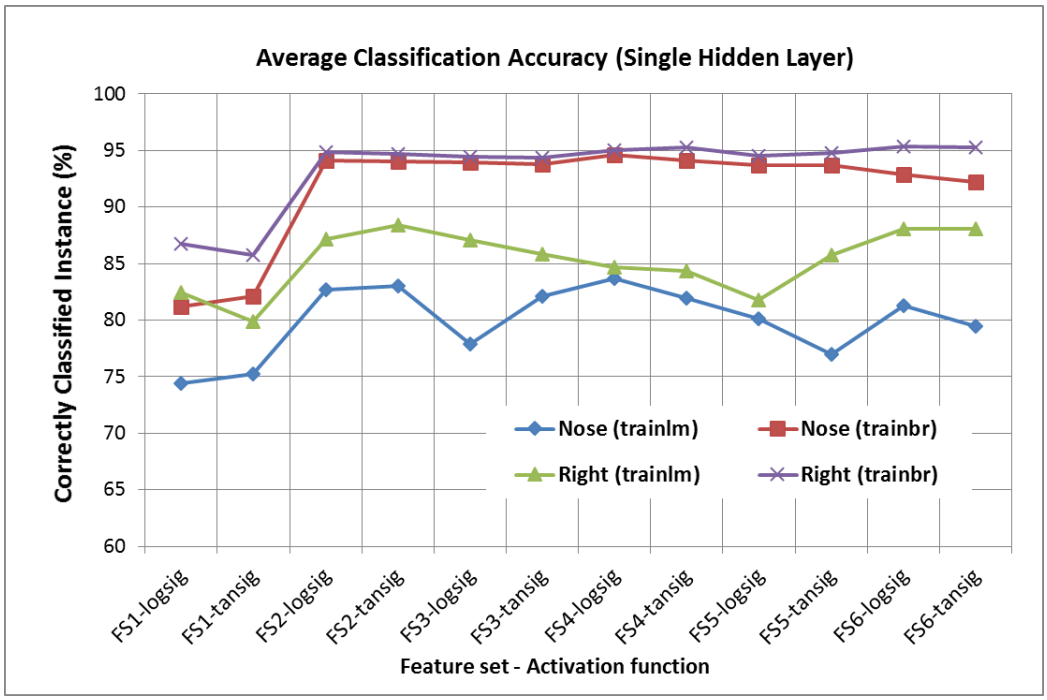

Figure 7.48 Comparison of two training algorithms

From the Table 7.11, the networks trained by *trainbr* produces the better classification models compared to the networks trained by *trainlm*. The average classification accuracy of the networks trained by *trainbr* is approximately 93-95 %, except the FS1 which is lower than others. Also, using *trainbr* algorithm can produce the highest accuracy of classification model when FS6 was used in input layer, FWWR was used in output layer, and the hidden nodes were activated by *logsig* function. The ACC is 95.35 % and the maximum accuracy (97.04 %) was found in the network, having 25 of hidden nodes as shown in Table 7.12 and Figure 7.49.

Table 7.12 Training results of FS6

FFNN-Class: CFS6Rlsbr (Single Hidden Layer-logsig) Date: 28/08/14 8:13 PM

Model	MAE	RMSE	SSE	Accuracy	Recall (TP)	Precision	Time
10	0.05731	0.24752	31	94.4664	0.931511	0.92505	14.922
20	0.05731	0.2394	29	94.2688	0.942713	0.92052	48.918
25	**0.02964**	**0.17218**	**15**	**97.0356**	**0.975452**	**0.9531**	**97.009**
30	0.04743	0.22668	26	95.4545	0.944885	0.94499	141.661
35	0.04743	0.21779	24	95.2569	0.942064	0.95117	201.306
40	0.04941	0.2394	29	95.4545	0.940778	0.94581	273.615
45	0.05929	0.28116	40	94.8617	0.936057	0.94618	363.897
50	0.04941	0.2394	29	95.4545	0.956292	0.93966	433.787
55	0.05534	0.24349	30	94.664	0.921586	0.94038	547.313
60	0.03557	0.19881	20	96.6403	0.956639	0.95914	659.589
			mean	**95.3557**			
			max	**97.0356**			

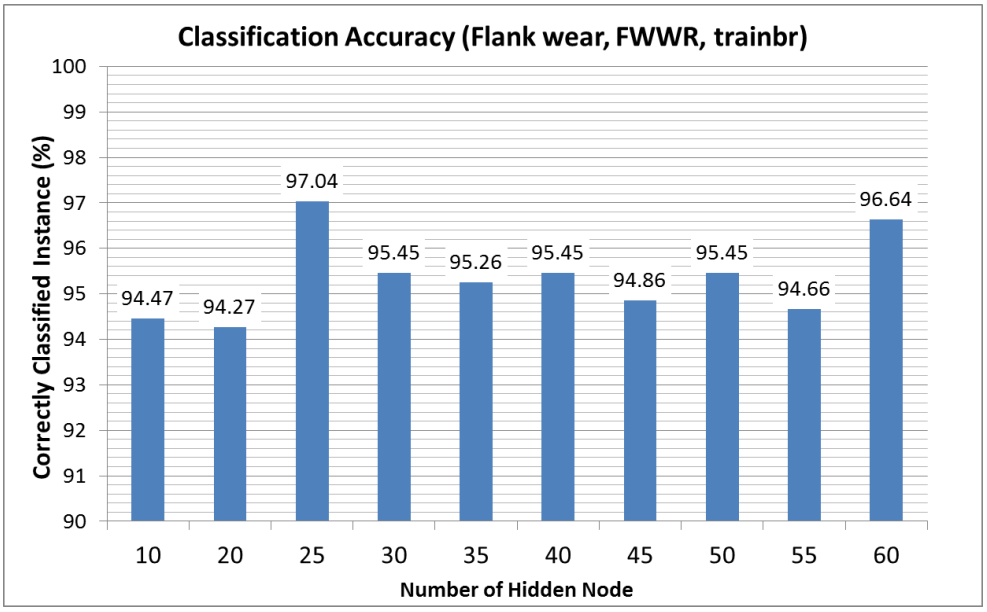

Figure 7.49 Percent of correct classification of FS6

The training results of the representative network (FS6-25-1) used for tool wear state classification is shown in Figure 7.50. It is observed that actual class of total instances were almost replaced by predicted class values. There are few red stars representing the incorrectly classified instances or miss-class. Considering the confusion matrix, the precision and recall determined from this matrix are 97.55 %, and 95.31 %, respectively. Obviously, large numbers down the main diagonal and small off-diagonal cells confirms that this classification network has a good performance.

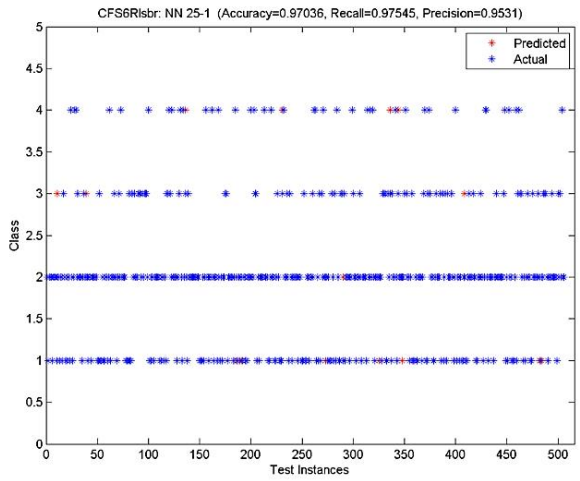


```
FFNN-Class: CFS6Rlsbr  Model: 25-1 (logsig) - Trainbr
Date: 28/08/14  8:14 PM

Fold MAE     RMSE    SSE Accuracy Recall(TP) Precision  Time
01   0.0296  0.1722  15  97.0356  0.9755     0.9531     97.0090

AVG  0.0296  0.1722  15  97.0356  0.9755     0.9531     97.0090

Confusion Matrix
130     1       0       0
7       249     3       0
0       0       73      4
0       0       0       39

Fold 1 has minimum MAE = 0.029644
Fold 1 has minimum RMSE = 0.172175
Fold 1 has minimum SSE = 15.000000
Fold 1 has maximum accuracy = 97.0356

Start Time:  8:14:34 PM      End Time:  8:16:14 PM
Total Training Time : 1 min, 40.2 secs
```

Figure 7.50 Flank wear classification results of the best network
(25 nodes in hidden layer, trained by trainbr, FS6 was used as inputs)

However, it is expected that the networks which have more complex structure can predict tool wear state more effectively. The following sections summarise the classification results which obtain from double hidden layer neural networks. The best network of both single and double structures of the networks will be compared to select the best representative network for tool wear classification.

7.3.3 Tool Wear State Classification Results: Double Hidden Layer

Several network structures with varying the NNHL were trained by *trainlm* in order to classify the tool wear state. The number of hidden nodes in two hidden layers was varied as follows:

1st hidden layer (H1): 30, 35, 40, 45, 50, 55, 60
2nd hidden layer (H2): 10, 20, 30, 40, 50, 60

As the classification results of SHL in section 7.3.2 found that FS2 and FS6 are the first two feature sets having the highest ACC as well as FS6 is also the proposed features by R-ranking method. Therefore, to save training time, only FS2 and FS6 were used as inputs to train the DHL networks. The flank wear values at two locations (FWWN and FWWR) were also used as target values for network training.

The training algorithm used in this section was *trainlm*, and activation functions (*logsig* and *tansig*) were used to activate the hidden nodes in the networks. The training results of these functions were compared and discussed. 70/30 validation scheme was used to evaluate network performance as it is faster training time for large network structure than multifold cross validation method.

The classification accuracy is represented by the percent of correctly-classification instance where the predicted classes are equal to actual classes. MAE, RMSE, and SSE were also help to find the best network structure.

7.3.3.1 Tool Wear State Classification by ANNs (DHL, AF: logsig, TA: trainlm)

The Figure 7.51 shows the fluctuated results of classification accuracy. It can be seen that the best classification result (94.46 % of accuracy) is the DHL network structured FS6-40-50-1, which is trained with FS6 and FWWR. This is in agreement with the lowest mean absolute error shown in Figure 7.52. Similar to other results in the previous sections, the flank wear (FWWR) keeps good results compared to the wear at nose radius (FWWN) on average. Training by the proposed feature (FS6) can give better accuracy than training by the FS2 obtained by WEKA software. It is apparent from the Figure 7.53 that there is no correlation between feature sets and classifiers in terms of training time. On average, the training time increase as the NNHL increases.

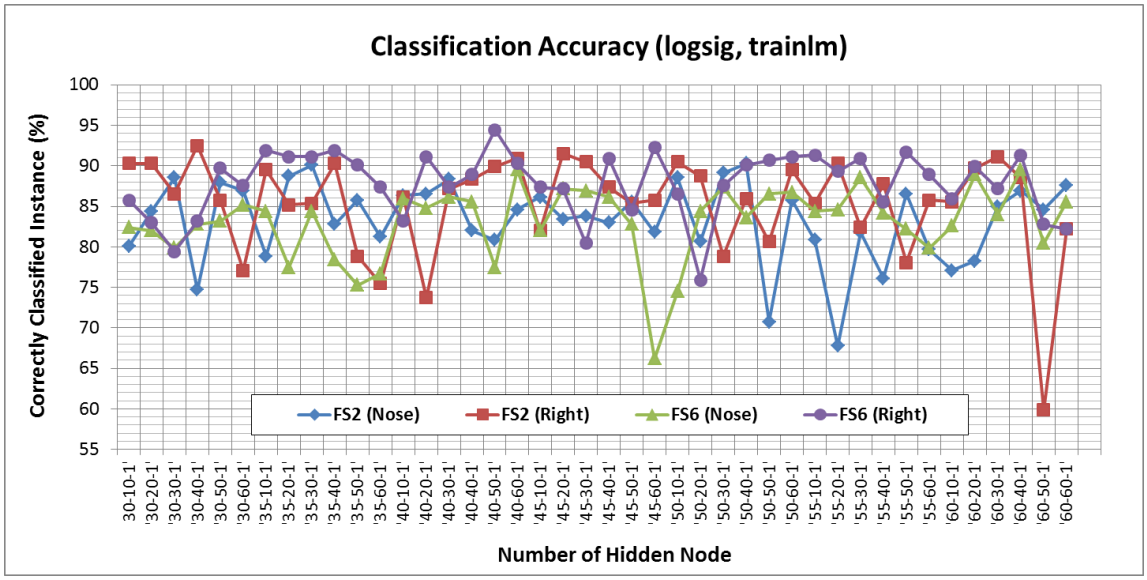

Figure 7.51 Classification accuracy of tool wear state prediction (AF: *logsig*, TA: *trainlm*)

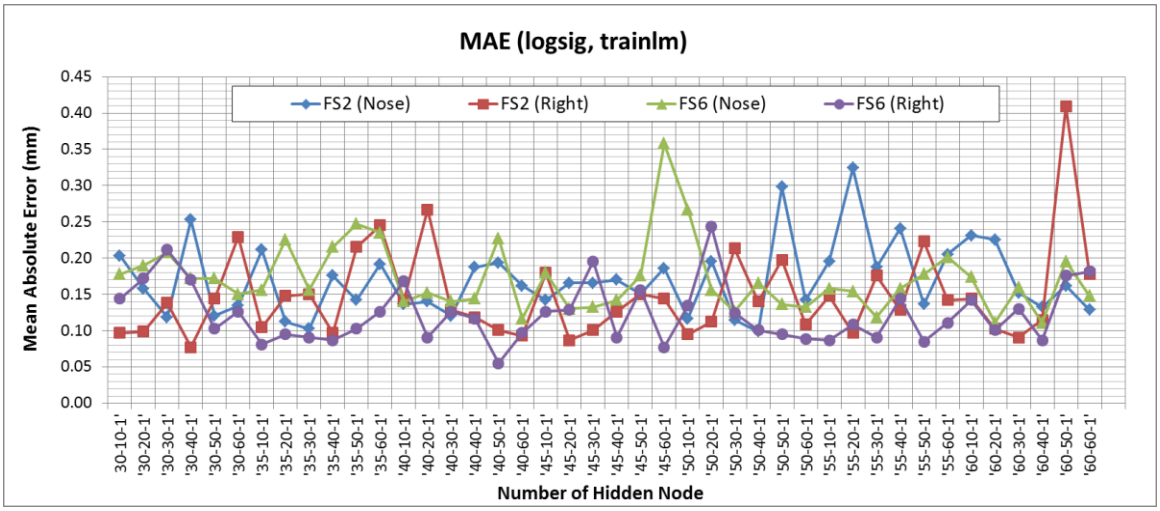

Figure 7.52 Mean absolute error (AF: *logsig*, TA: *trainlm*)

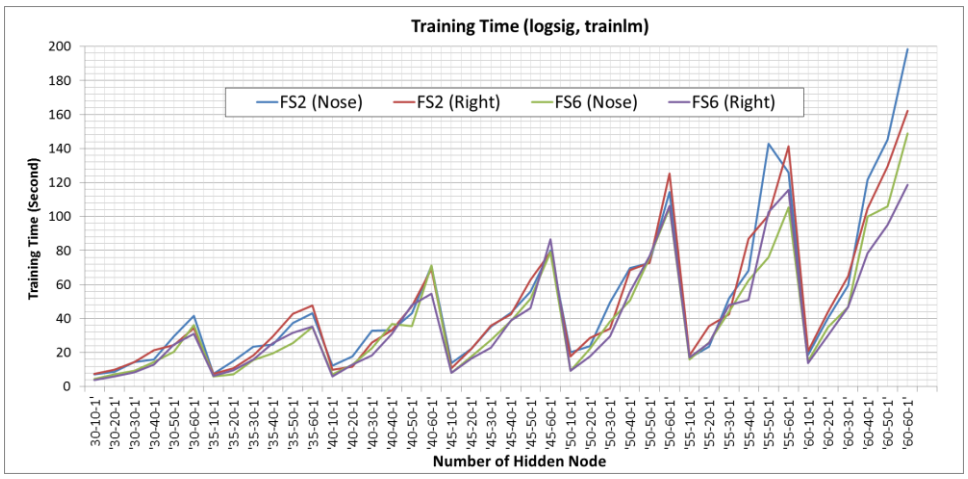

Figure 7.53 Training time (AF: *logsig*, TA: *trainlm*)

7.3.3.2 Tool Wear State Classification by ANNs (DHL, AF: tansig, TA: trainlm)

Figure 7.54 summarises the classification accuracy of the networks that the hidden nodes in hidden layers were activated by *tansig* function, while the mean absolute error of those networks is illustrated in Figure 7.55. Similar to previous section, the accuracy of networks is unpredictable trend. Considering to the peak point, outstandingly seen that the highest classification accuracy can be obtained by the network (FS6-30-50-1) where FS6 is used as inputs and FWWR is used as outputs. This network can be able to correctly classify the tool wear state about 94.86 %. The training time of this configuration is shown in Figure 7.56 and can be seen that the training time depends on the number of nodes in hidden layer. The more the hidden nodes have, the longer training time the network needs.

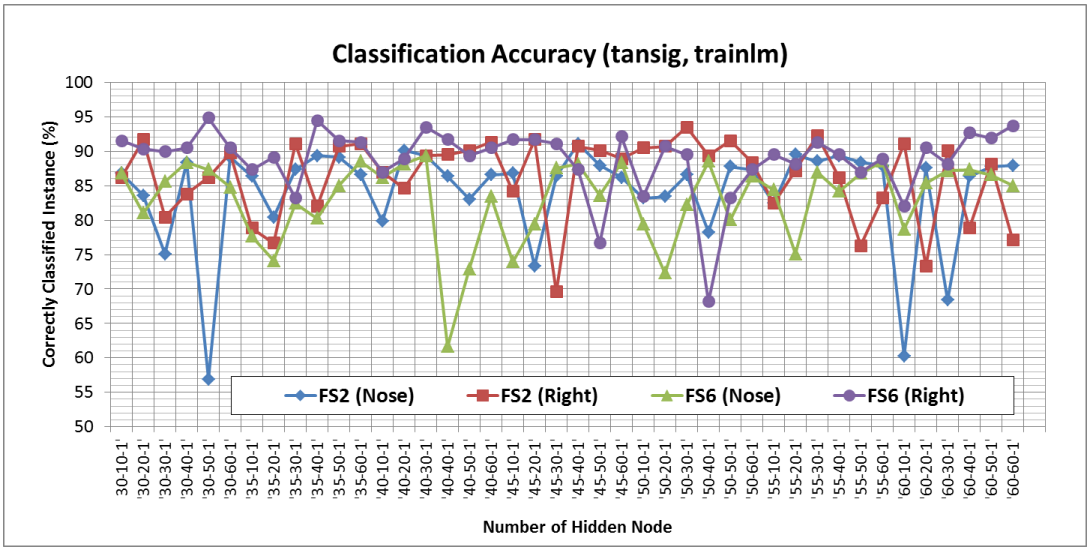

Figure 7.54 Classification accuracy of tool wear state prediction (AF: *tansig*, TA: *trainlm*)

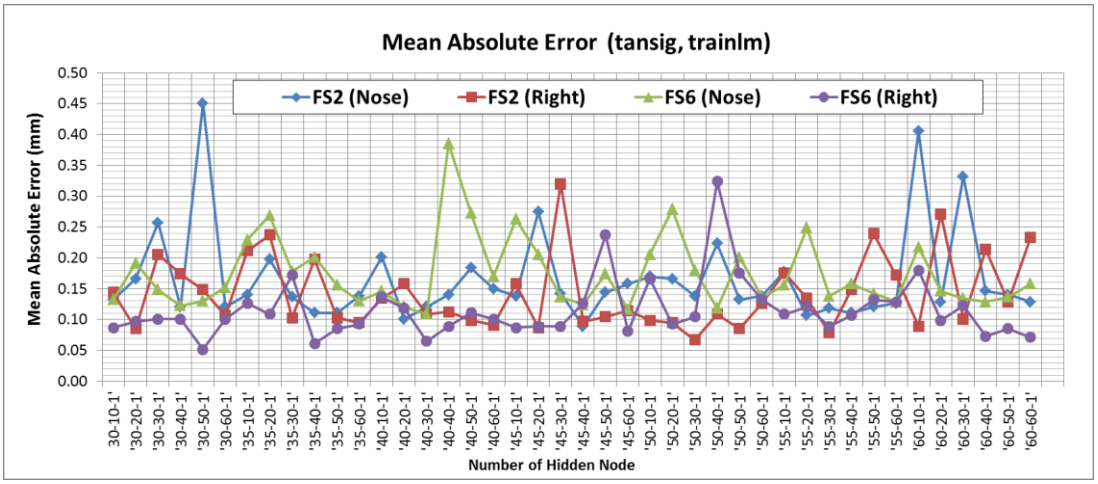

Figure 7.55 Mean absolute error (AF: *tansig*, TA: *trainlm*)

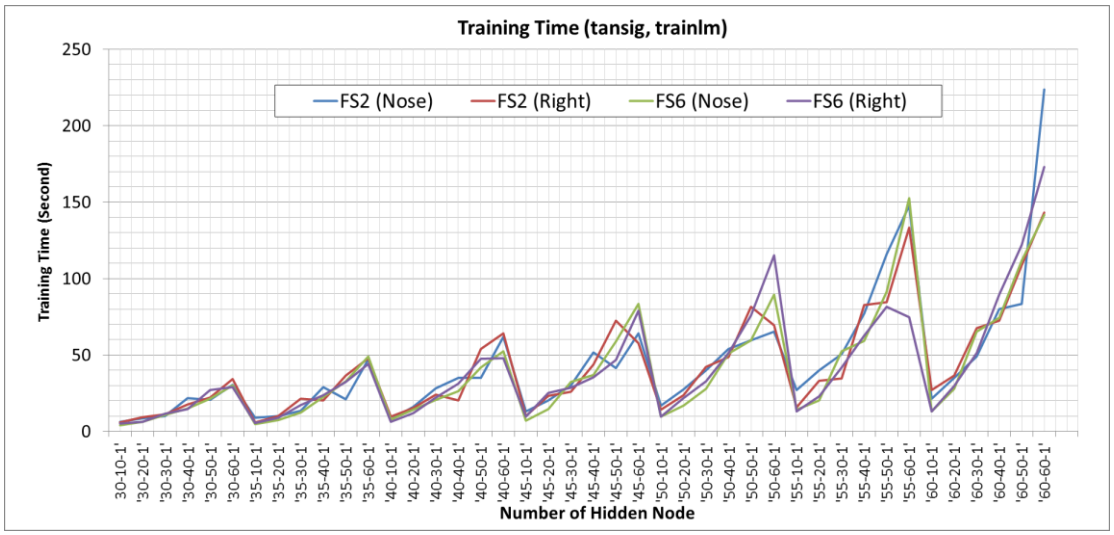

Figure 7.56 Training time (AF: *tansig*, TA: *trainlm*)

7.3.3.3 Summary of Tool Wear State Classification by DHL Neural Networks

Comparing the two activation functions, the ACC and maximum accuracy of the DHL neural networks are compared as shown in Figure 7.57 to find the best DHL network for tool wear state classification. It is seen that the networks were trained by FWWR as targets produce higher classification accuracy than by FWWN for all feature sets. Variation of the nodes in each hidden layer did not improve classification efficiency. The FS6 stemmed from the ranking technique (described in Section 7.1.2) is the best input features used for feeding into the input layer of the DHL neural networks. Clearly seen the use of FS1 as inputs of the DHL network provides the unsatisfied accuracy due to lower ACC.

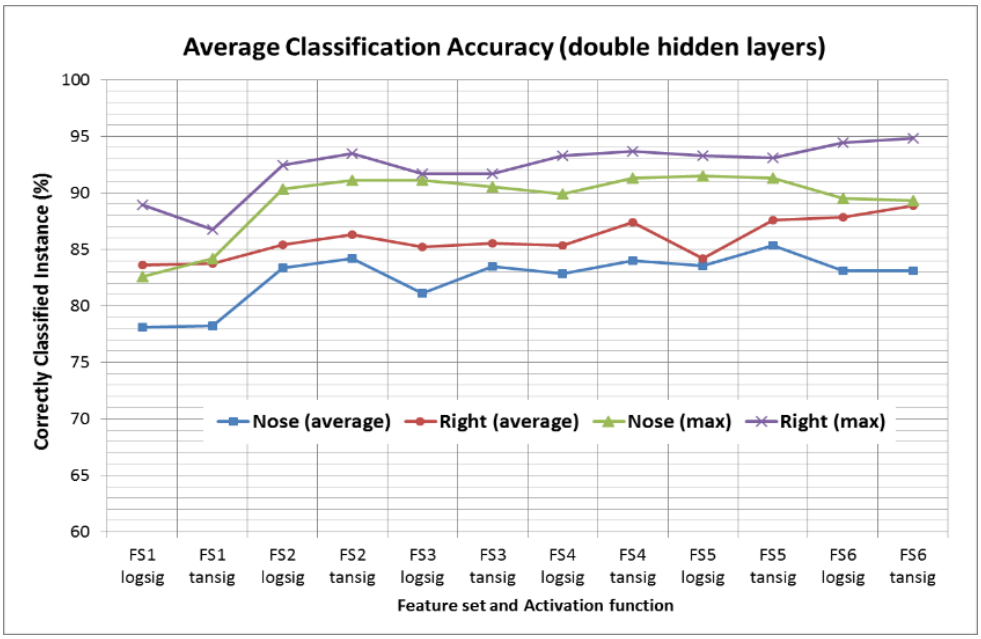

Figure 7.57 Comparison of two training algorithms

Compared between the results in section 7.3.3.1 and 7.3.3.2, the best network of DHL is the network that the hidden nodes were activated by *tansig* function. The structure of nodes in hidden layers is FS6-30-50-1 and FS6 is used as inputs. This classification model can be used to predict the tool wear states with 94.86 % of correct classification. The classification plots and confusion matrix of this network is shown in Figure 7.58.

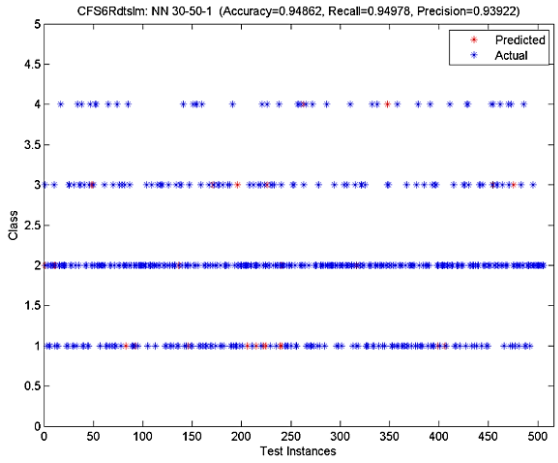


```
FFNN-Class: CFS6Rdtslm  Model: 30-50-1 (tansig)
Date: 30/08/14  3:06 AM

Fold MAE     RMSE    SSE    Accuracy  Recall(TP) Precision  Time
01   0.0514  0.2267  26.00  94.8617   0.9498     0.9392     27.0440

AVG  0.0514  0.2267  26.00  94.8617   0.9498     0.9392     27.0440

Confusion Matrix
128     3       0       0
11      243     5       0
0       3       72      2
0       0       2       37

Fold 1 has minimum MAE = 0.051383
Fold 1 has minimum RMSE = 0.226679
Fold 1 has minimum SSE = 26.000000
Fold 1 has maximum accuracy = 94.8617

Start Time:  3:06:57 AM      End Time:  3:07:28 AM
Total Training Time : 30.8 secs
```

Figure 7.58 Flank wear classification results of the best network
(25 nodes in hidden layer, trained by trainbr, FS6 was used as inputs)

As shown in Figure 7.58, the predicted tool wear state from the this neural network model has come very close to the tool state values measured experimentally, it can be finally concluded that this model can be used for classifying the tool wear state during turning operation. However, the DHL networks (FS6-30-50-1, *tansig*) will be finally compared with the SHL network which has the highest classification accuracy in order to obtain the representative model for tool wear state classification.

7.3.4 Summary of Tool Wear State Classification by Neural Network

The accuracy of networks with different configurations were compared to find the best representative network for tool wear state class. The results of both SHL and DHL networks found that flank wear at the right side of cutting inserts (FWWR) is more effective to be used as network targets during training process. This result agrees with the tool wear prediction in Section 7.2.4 that training by FWWR as target can obtain more accurate results.

With regard to training time, it is generally viewed that the training time of the networks depends on the number of hidden nodes in both single and double hidden layers. The larger structure of the neural network the more time it needs to train, especially in the DHL neural networks. Very reasonably, the longer training time of *logsig* function offers the better results as can be seen that the prediction errors are mostly lower than *tansig* function. The representative neural networks from several network configurations are summarised in Table 7.13.

Table 7.13 Summary of networks for tool wear prediction

Network Types	Hidden Nodes	Activated Function	Input Features	Targets	Training Algorithm	Accuracy%	MAE	RMSE	SSE
Single hidden layer	35	logsig	FS2	FWWR	trainlm	92.89	0.075099	0.288104	42.0
Single hidden layer	35	tansig	FS3	FWWR	trainlm	92.09	0.079051	0.281161	40.0
Single hidden layer	**25**	**logsig**	**FS6**	**FWWR**	**trainbr**	**97.04**	**0.029644**	**0.172175**	**15.0**
Single hidden layer	20	tansig	FS2	FWWR	trainbr	96.44	0.035573	0.188608	18.0
Double hidden layer	40-50	logsig	FS6	FWWR	trainlm	94.47	0.055300	0.235200	28.0
Double hidden layer	30-50	tansig	FS6	FWWR	trainlm	94.86	0.051400	0.226700	26.0

In conclusion, the best network for tool wear state classification is a SHL neural network, which consists of 25 nodes in hidden layer activated by *logsig* function. Training by *trainbr* algorithm produces the highest accuracy when FS6 was used as inputs, and FWWR was used in output layer. This network model can predict the state of tool wear and the average percent of correct classification is 97.04 %.

In this study, four tool wear states including: new tool, slightly worn, moderately worn, and severely worn are used. The simplest way to make use of tool wear state is using as a warning signal. For instance, once the tool state has been changed from moderately to severely worn, several actions such as tool changing or tool sharpening will take actions to extend the tool life or to prevent the rejection of finished workpiece due to tool wear progressed.

7.4 Tool Remaining Useful Life Estimation

Three common methods wildly used for expressing tool life are time units, number of workpieces machined, and volumetric loss of cutting tool. It is expected that the cutting tool should be used for long life time in order to save time for regrinding or tool replacement because these lower productivity of the machine. The assessment of remaining useful life (RUL) of the cutting tool was studied by [38]. In this work, they develop a model used for RUL estimation of cutting tool. Interestingly, Mei Wang and Jie Wang used Continuous Hidden Markov Model (CHMM) to classify tool wear states, and Gaussian regression model to estimate RUL of cutting tool [19]. However, this section describes a much simpler method to estimate the RUL.

The tool wear prediction model can be used to estimate the flank wear width (V_b) by using input features including sensor features and three cutting parameters to feed into the flank wear prediction model, while the states of tool wear can be obtained when input features were passed through the classification model as shown in Figure 7.59. This online tool wear monitoring system can be performed during the operation. Current flank wear width and tool wear state are the essential information for decision making (tool or cutting parameter change) and estimating the remaining useful life time.

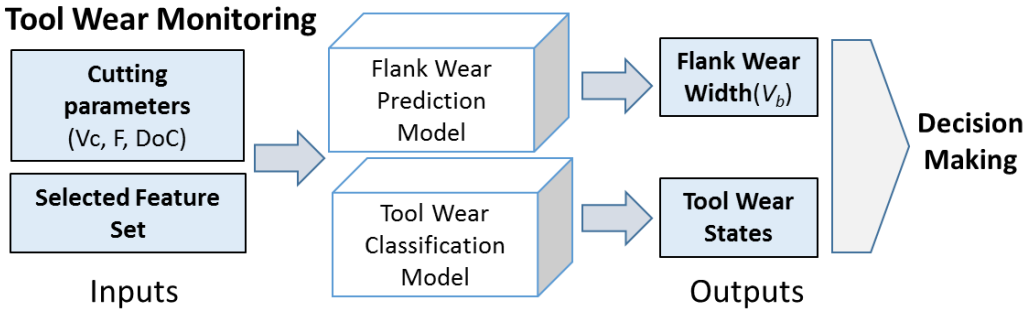

Figure 7.59 Tool wear monitoring system

As described in Chapter 2, tool life or useful life of cutting tool can be generally defined as the length of cutting time that a tool can be used until catastrophic failure or reaching of the wear limit (e.g. V_b=0.3 mm due to ISO 3685-1997).

In Figure 7.60, the RUL is simply calculated by the subtraction of overall tool life time at wear limit (T_a , measured value) and consumed time (T_c) at the current wear value (predicted value) under the cutting conditions of use. For example, if the measured cutting time up to flank wear of 0.3 mm is 65 minute and the currently useful life time at predicted flank wear is 45 minute, the remaining time to use the cutting tool is equal to 65-45 = 20 minute. It should be noted that the tool wear curve in Figure 7.60 can be used for one particular cutting condition only as different cutting parameters have different tool wear curve characteristics as discussed in Chapter 2.

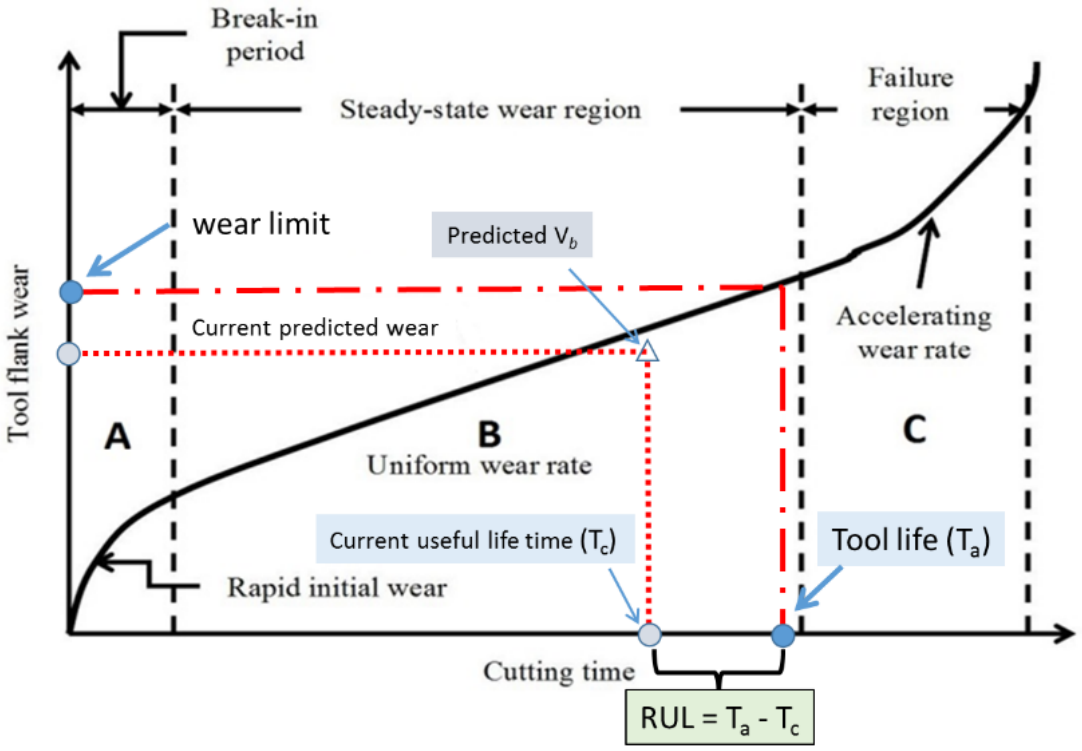

Figure 7.60 Remaining useful life time estimation from predicted flank wear

Then, making use of tool wear states, Figure 7.61 illustrates the tool wear curve and four tool wear states. For example, when the tool wear state is changing into the fourth state (severely worn), its remaining useful life ($RUL_{3\text{-}4}$) could be utilised to make a right decision before the tool wear reach the limit, to avoid the damage to the workpieces.

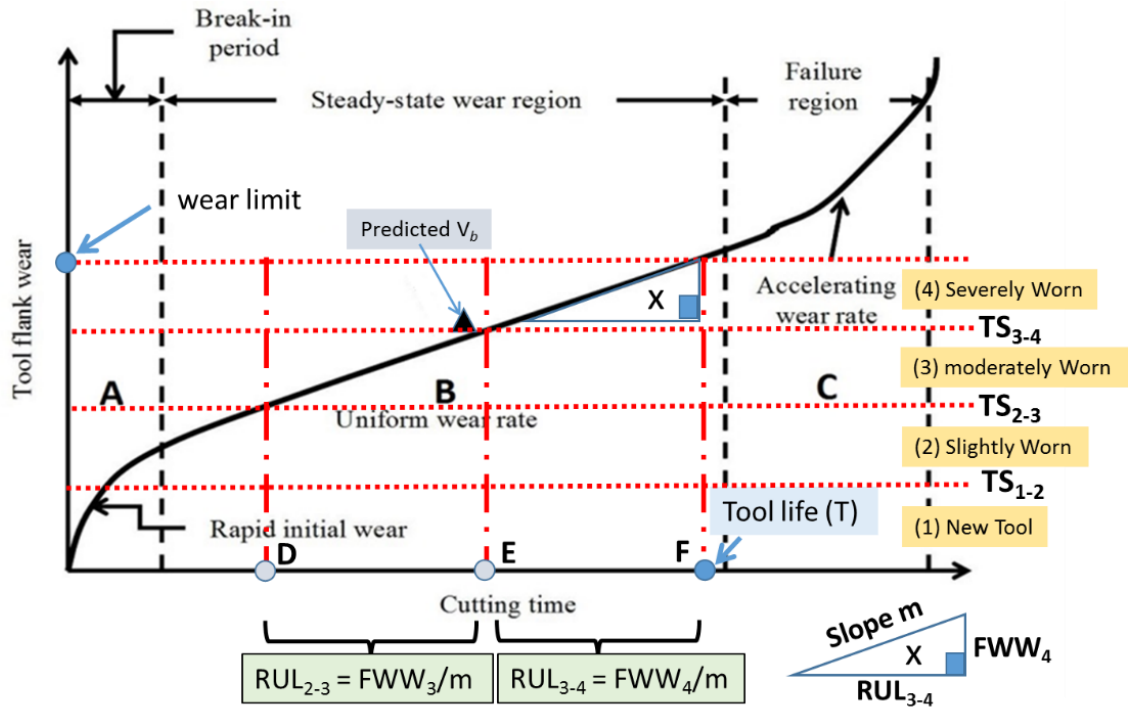

Figure 7.61 Remaining useful life time estimation from the change of tool wear state

As can be seen in Figure 7.61, the wear limit is selected in order to limit the tool life time (T). The horizontal red dot lines represent the transition of tool wear state (TS_{x-x}). The change of state transitions (e.g. TS_{3-4}, moderately worn-to-severely worn) can be used as warning signal to inform the operator for taking an actions before reaching the tool life (point F). Once the tool wear state crosses the TS_{3-4}, the remaining life time (RUL_{3-4}) can be then estimated using geometry/trigonometry. This method can be applied only in the steady-state wear region as the tool wear curve is constant. The wear rate (mm/min) or slope (m), can be obtained experimentally for individual cutting condition. Consequently, RUL_{3-4}, time form point E to F, can be calculated as the formula in Figure 7.61.

Also, this state transition can give the feedback signal to the machine control system to adapt the cutting parameter promptly in order to extend the RUL_{3-4} and obtain longer tool life. On the contrary, the decrease of cutting parameters also increase the machining cycle time that lower productivity. Therefore, the extended tool life and reduced production rate, should be balanced to meet the maximised machining operation.

7.5 Summary

Several sensory features of three sensor signals used in machining experiment have been extracted both in time and frequency domains. Some of the all 42 features are irrelevant to tool wear and those features have to be eliminated to increase speed in data training process and enhance the model performance. In consequence, feature selection process is normally performed to select the most meaningful features for training. Six Feature sets coming from manual selection of 3 signal RMS values, from WEKA software, and proposed Ranking of correlation coefficient method were used to train the prediction and classification models.

The feature sets and cutting parameters were used as inputs of the neural network being trained with flank wear targets. Several network configurations, with varying network architectures have been attempted to find the best representing model for tool wear prediction and tool wear state classification. The best tool wear prediction network is FS2-50-60-1, where FS2 was used as model inputs, the $NNHL_1 = 50$ and $NNHL_2 = 60$ activated by *logsig* function. This model can predict the accurate FWWR with lowest MAE.

In case of tool wear state classification, it is necessary to define the tool wear state into classes (new, slightly, moderately, and severely worn tool) before training the neural networks. The networks were retrained by classified flank wear as targets. The successful classification of tool state with respect to 4 wear classes was 97.04 % of correctly-classified instance. The SHL neural network FS6-25-1 is the best network where the hidden nodes were activated by *logsig* function and the network was trained by *trainbr*. It can be conclude that the proposed method (ranking of correlation coefficient) can be suitable for tool wear state classification.

Predicted flank wear and classified tool wear states can be used to estimate the remaining useful life time of the cutting tool. These parameters are commonly used for tool condition monitoring systems. the point at which the tool state begins to change can be then used as a warning signal to the machine or operator. The benefit of knowing the tool wear state can warn the machine operator to prepare the new cutting tool for substitution or to sharpen the cutting tool. In conclusion, tool condition monitoring based on sensor fusion can be effectively applied to monitor the wear of cutting tool in turning process.

Chapter 8

A Novel Feature for Tool Wear Monitoring in Machining Processes

In this chapter, consideration has been made of the spindle noise from the turning experiments (Chapter 6) and of previous attempts using sound signal for tool wear monitoring. A spectrogram has been used to indicate the source of spindle noise and the relationship between the magnitude of spindle noise frequency and tool wear in turning experiment is discussed. Finally, a feasibility study of using spindle noise to monitor drill bit wear on special milling machine is reported.

8.1 Introduction & Background

During the work presented in Chapter 6 the mean sound pressure level, with background noise removed, of the noise from turning experiment was used as a feature for tool condition monitoring. During this work, the sound emitted from the main spindle motor was noted as an interesting feature and named 'spindle noise'. It was hypothesised that this feature had the potential to be used in isolation to monitor tool wear and as there would be no requirement for further sensors (AE, cameras etc.) could form the basis of a low cost monitoring system. To investigate this, further analysis of the data obtained for the work presented in Chapter 6 was performed and then expanded by means of another machining experiment to investigate if the method is viable in other machining processes.

In the literature review presented in Chapter 4, audio signature in machining processes were reviewed as extracted features would be sensitive to tool wear. Much of the vibrations being excited in the cutting zone during machining are in the range at which they can be heard by the operator, and therefore be recorded by a standard audio microphone. Machine operators have been effective in the detection of unacceptable cutting conditions, inferred through the audible emissions from the cutting process. Microphones, being a non-contact sensor, are very easy and flexible to install in the machine and there are a wide variety of inexpensive models with different performance characteristics. Microphones have been used extensively for chatter detection, and have also been used on occasion to monitor tool wear in turning processes [99, 103, 104].

In previous studies, Teti *et al* [8] reviewed several sound measurement techniques used to monitor flank wear during turning process. Several studies confirm that tool wear state is correlated to the sound emitted during the machining found in the following reviews.

Sound signature in turning processes was studied in order to find the relationship between sound signal and cutting speeds and feed rates. Sound pressure in time domain has been used by several studies to observe the change in amplitude during tool wear [100, 103-105].

Tekiner used a microphone connected to a computer to record the cutting sounds in order to determine the best cutting parameters for cutting AISI 304 stainless steel according to process sound [105]. It was observed by Raja that the change of cutting parameters, cutting sound pressure levels also change and an increase in tool wear resulted in an increase of sound signal amplitude [104]. Similarly, Kopac *et al* concluded that progressive tool wear correlates with an increase in amplitude of the record sound between 6 and 20 kHz which is above the frequency range within which machine background noise is normally found [103]. Audio techniques were also used by Quintana to determine the stability lobe diagram (SLD) in a milling process by applying 3D sound mapping methodology. A microphone was mounted inside the milling machine and audio signals from 600 cutting conditions were recorded and processed. The sound pressure level of each condition was plotted on a grid to identify the stable and unstable cutting conditions that are a key to avoiding chatter in the milling process [100].

The analysis of Fast Fourier Transforms (FFT) of audible sound generated from the turning process was used by Lu *et al* to introduce the model for tool wear monitoring [84]. This model includes the main effects of tool wear on system dynamics during stable cutting of lathe machine. Alonso *et al* proposed a sound processing technique using singular spectrum analysis (SSA). This processing technique was used to extract the sound features from the cutting zone during turning process. The results showed that the extracted features from sound and feed motor current signals correlate with tool wear state [147]. Raja used sound signal analysis, using the Hilbert-Huang Transform (HHT), to monitor flank wear [104, 153]. Cutting sounds from three state of tool wear (fresh, slightly worn, and severely worn) were recorded under several cutting conditions and it is claimed that this signal processing method can be considered as a simple and reliable for flank wear monitoring.

Nevertheless, the major limitation of using a microphone to record the cutting sound is the background noise from the environment. This can be from vibrations in the cutting zone, vibrations caused by the machine tool drive system, external sources and in particular noise from the flowing coolant.

8.2 Observation of the Sound from a Cutting Cycle in Turning Process

The audio recorded from each test (as described in Section 6.4) was further analysed in the time-frequency domain by short-time Fourier transform (STFT) in order to establish the frequency content in the audio signature that could be then used for tool condition monitoring. The analysis produced a spectrogram that represents the sound signal resulting from the machining process. The example spectrogram shown in Figure 8.1 displays magnitude of frequency spectrum of the cutting sound recorded by

the microphone during a 25 second cutting cycle at cutting condition 1. The horizontal axis represents time, while the vertical axis displays frequency. The amplitude of a particular frequency is represented by the colour intensity of each point.

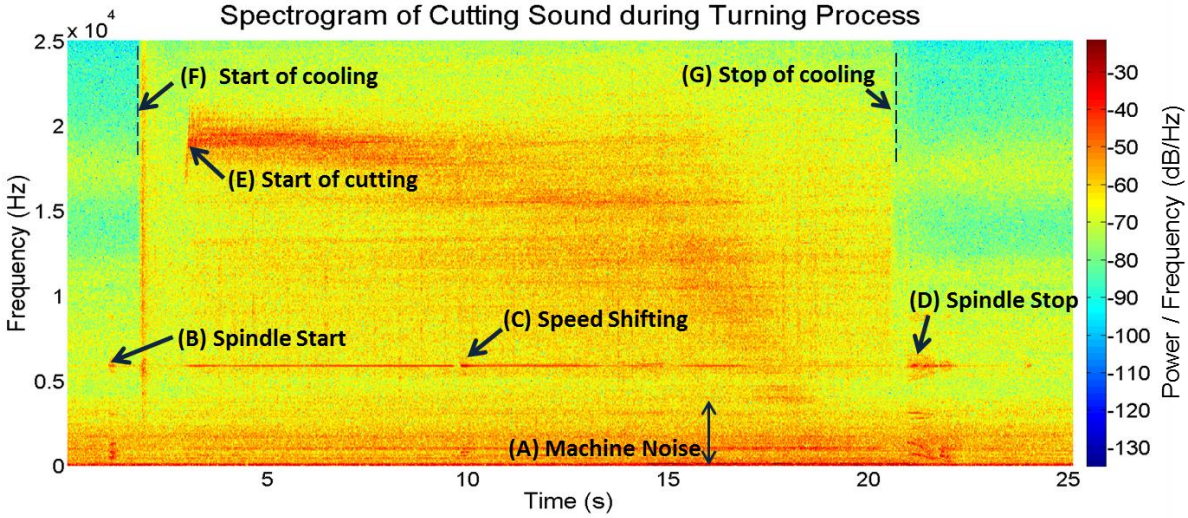

Figure 8.1 Spectrogram of audio recorded from cutting cycle

The various events that occurred during the turning process are labelled. Each of these is clearly heard by the human ear when observing the machining process. It is seen that throughout the cycle, the sound signal was contaminated by machine background noise (A). As mentioned in Chapter 6, the machine background noise frequency is in the range of 0 - 3 kHz, and the several studies agree that background machine noise can be identified in the range of 0 - 2 kHz [103]. It should be noted that although the machine used in these experiments has not been studied to fully characterise the stability of its noise output, the data presented in Figure 8.2 can be considered typical across all the experiments conducted for this work. This means that this part of the signal can be easily filtered without any effect to the signal of interest. It should be noted, that whilst chatter detection systems should include this frequency content, the tool condition monitoring objective in this case study, under non-chatter conditions, may benefit from removing this data.

As all trials were conducted in a wet condition a broadband frequency of coolant being applied to the cutting zone is also depicted (F to G). The noise from the main spindle motor can be seen as a long horizontal high intensity line from point (B) to (D). It is this sound at this frequency defined here as 'Spindle Noise'. It is the sound generated by the spindle motor during cutting in CNC turning machine. However, the origin of this noise frequency is not clear but it may have some mechanisms or mechanical parts emitting this noise. Presumably, it might be related to the percussion or rubbing of mechanical parts such as driving gear, and roller/ball bearings. The spindle noise was found at 5.86 kHz as shown by power spectrum in Figure 8.2.

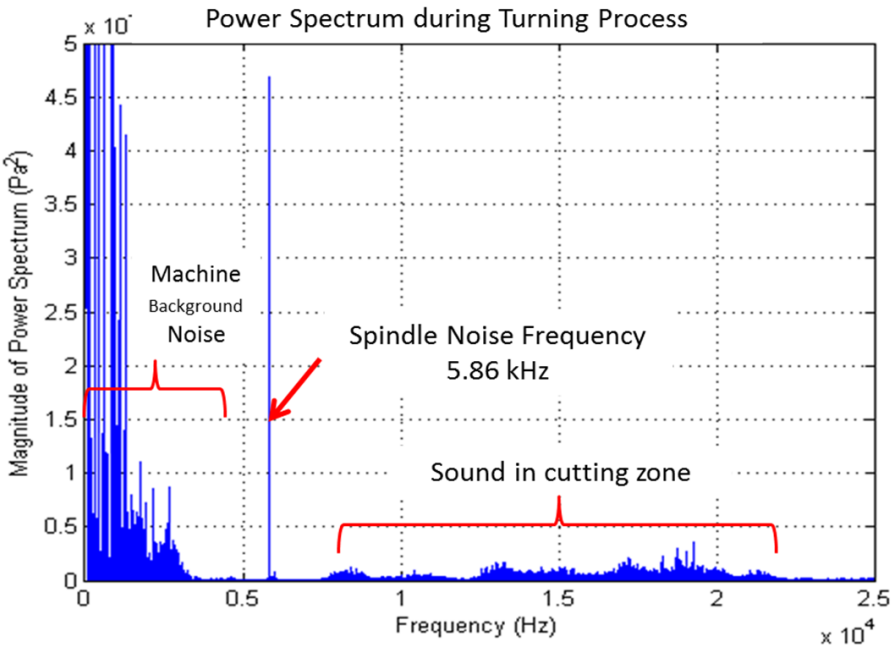

Figure 8.2 Power spectrum of cutting sound

Point (B) depicts the spindle start time as the motor is speeding up to the desired rotational speed. Note the spindle is accelerating due to the facing operation requiring constant surface speed. The maximum RPM of the spindle is reached in the middle of cutting time (point C), where the spindle increased its rotational speed automatically to keep the surface speed constant. Finally, the spindle was stopped (point D). The frequency band representing the coolant entering the cutting zone can be seen from point F to G.

Over the range of spindle noise frequency, it can be observed that during cutting both intensity and frequency of cutting sound change from high to low represented by the broad sweep of higher intensity from top left to bottom right of Figure 8.1.

The changes in frequency and magnitude of spindle noise were observed by FFT as shown in Figure 8.2. This observation was repeated for all of the machining trials performed and it was observed that the spindle noise was detected at 5.86 kHz regardless of cutting conditions used on this particular machine and there is no significant correlation between the frequency of spindle noise and the development of tool wear.

From the results, a possible source of this spindle noise is paid to the rubbing/hitting of the gear's teeth since the sound frequency of hitting/rubbing between gear teeth is constant (5.86 kHz) throughout the experiment regardless of speed changes, while the sound intensity (magnitude of this frequency) will be increased according to an increase of rotating speed (i.e. more frequent hitting/rubbing).

In order to study the influence of cutting parameters on the magnitude of spindle noise frequency, the power spectrum of spindle noise frequency was plotted in combination of cutting speeds and feed rates which are now discussed.

8.3 The Effect of Feed Rate on the Spindle Noise and Detecting Tool Wear

For the trials where cutting speed was held constant and feed rate was varied (Figure 8.3), it is clearly seen that the magnitude of spindle noise is low in the first half period, increases sharply and then decreases significantly in the final wear state. When compared to the three wear classification states, the magnitude of spindle noise starts increasing about the middle of steady-state wear (II) region, and the magnitude increases rapidly and then decreases before the tool wear state reaches the failure wear state (III). Therefore, these significant changes can be used as a warning signal in order to detect the tool wear.

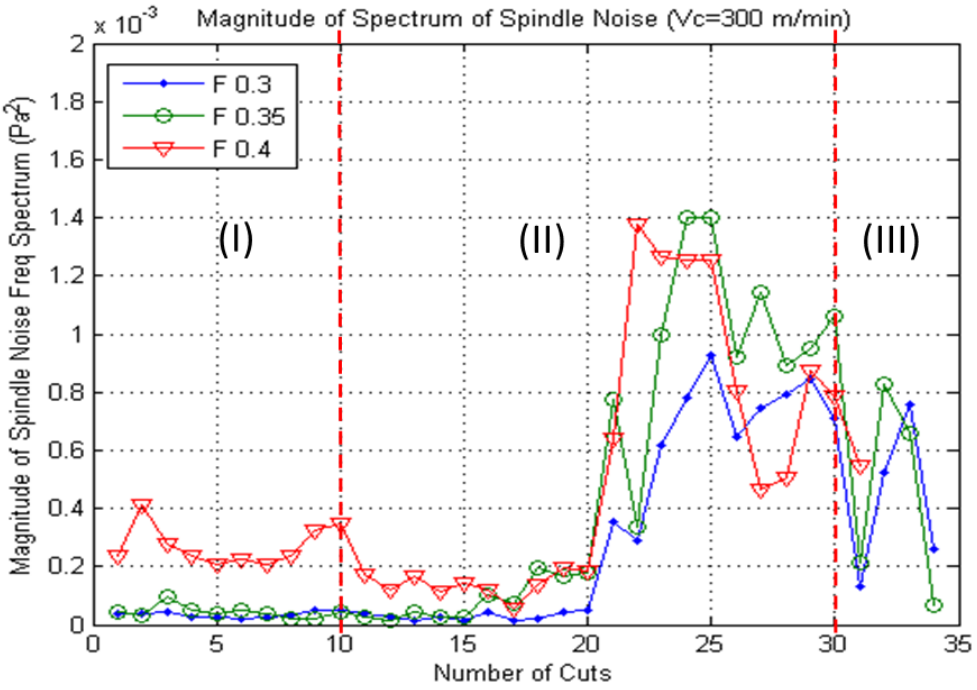

Figure 8.3 Peak spindle-sound frequency magnitude vs number of cuts for a varying feed rate and constant cutting speed.

It is seen that the onset of the rise in magnitudes of the power spectrum of spindle noise occurs earlier as the feed rate is increased. This means that the amount of warning (time) the system can give the operator is dependent on the feed rate being used (i.e. the greater the feed, the earlier the warning). Furthermore, the cumulative magnitude of spindle noise frequency was plotted in Figure 8.4 that each of the curve was clearly separated and has a warning signal at the turning point itself.

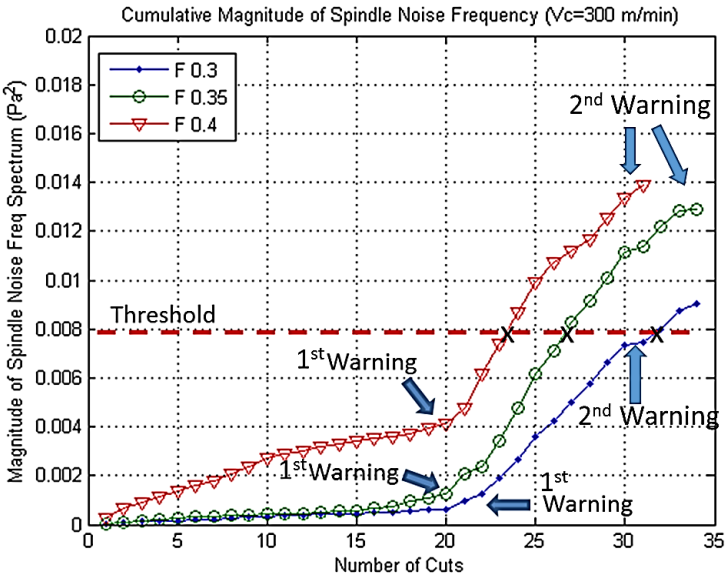

Figure 8.4 Cumulative magnitude for a varying feed rate and constant cutting speed

It is apparent that when the data appears to significantly increase its rate of growth, this is the point at which the tool should be replaced or warning occurs. In this case, for simplicity, a threshold value has been set as a tool change criteria. For example, using a threshold do 0.008, the ending points of tool usage are about cut number 25, 30, 35 in feed 0.3, 0.35 and 0.4, respectively.

Alternatively, the slope of these curves can be used to detect the tool warning signal. For example, If the cumulative curve has an abrupt change in slope from low to high, this can indicate the 1st warning (the middle of steady wear region) and the second change in slope from high to low could be used as the tool replacement point.

Also, it is seen that the magnitudes of spindle noise increase, according to increasing of feed, which suggests that the amount of warning (time) the system can give the operator is dependent on the feed rate being used i.e. the greater the feed, the earlier the warning.

8.4 The Effect of Cutting Speed on the Spindle Noise and Detecting Tool Wear

In order to observe the effect of cutting speed on spindle noise, the magnitude of the spindle noise frequency performed at constant feed rate (0.35 mm/rev) as shown in Figure 8.5. It can be seen that the spindle noise frequency of a new tool has a low magnitude in the power spectrum (cut 1st -20th) and high magnitude for the worn tool. The magnitude of spindle noise frequency gradually decreases until the cutting insert becomes dull and broken.

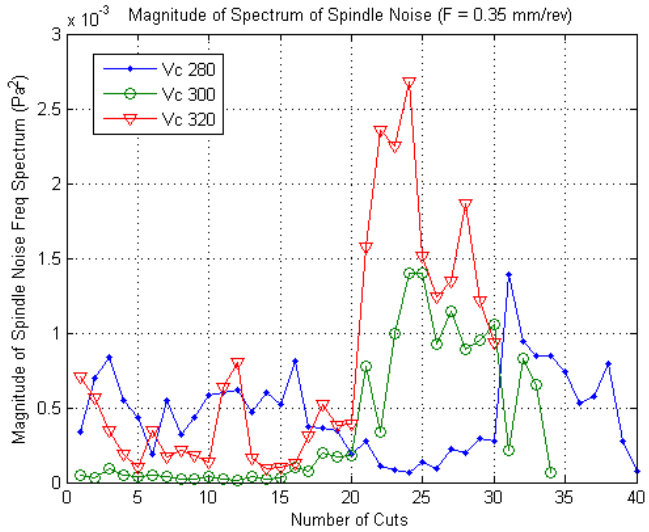

Figure 8.5 Spindle noise for each individual cut at different cutting conditions

The average magnitude of spindle noise increases with cutting speed (V_c). As is expected, the cuts performed at a higher cutting speed (V_c=320) have shorter tool life (cut 30) compared to the lower cutting speed (V_c=280) (cut 40). Due to Section 8.3, the warning signals can be indicated by the rate of increase of magnitude, observed in the cumulative plot as cut number 20 at cutting speed 300, 320 and 30 at 280 m/min, as shown in Figure 8.6.

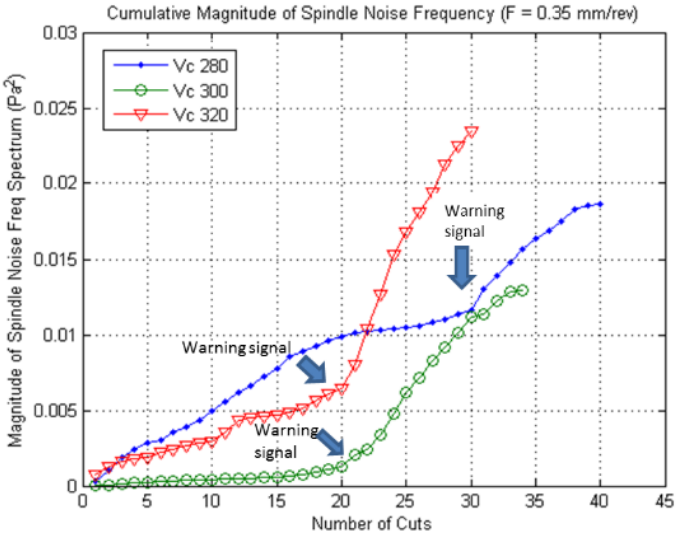

Figure 8.6 Cumulative magnitude of spindle noise for each cut at different cutting conditions

It can be concluded that the magnitude of spindle noise frequency has a good agreement with altered cutting conditions. When the cutting process performs at a high metal removal rate (MRR), the spindle motor emits the noise with a higher magnitude of power spectrum of spindle noise frequency. The abrupt change in power spectrum magnitude of spindle noise can be used as a warning signal for tool replacement.

It is worth noting that prior to the characteristic increase in magnitude indicating the onset on tool failure the relative magnitudes of the signals from each of the different cutting speeds vary with the number of cuts (Figure 8.5). Similarly, when considering the cumulative magnitude, although the warning signals are in the positions expected the relative magnitude of the signals prior to those points are not as expected (Figure 8.6). It is suggested that the cutting conditions used in these experiments are not different enough from each other to ensure any variation in the results due to non-uniformity of workpiece material and error in the experimental setup (e.g. changing workpiece position in the machine as it is consumed) do not overlap.

8.5 Tool Wear Detection in Turning

Although the frequency of the spindle noise remains constant, this study found that the magnitude of spindle noise frequency alters in conjunction with the tool wear progression. Power spectra of all cuts were individually calculated and illustrated that the magnitude of power spectra of the spindle noise frequency (multiple green lines) varies with tool wear (single blue line) as cutting takes place for the cutting conditions used in the machining trials (Figure 8.7).

a) V_c = 280, F = 0.35 *b)* V_c = 300, F = 0.35 *c)* V_c = 320, F = 0.35

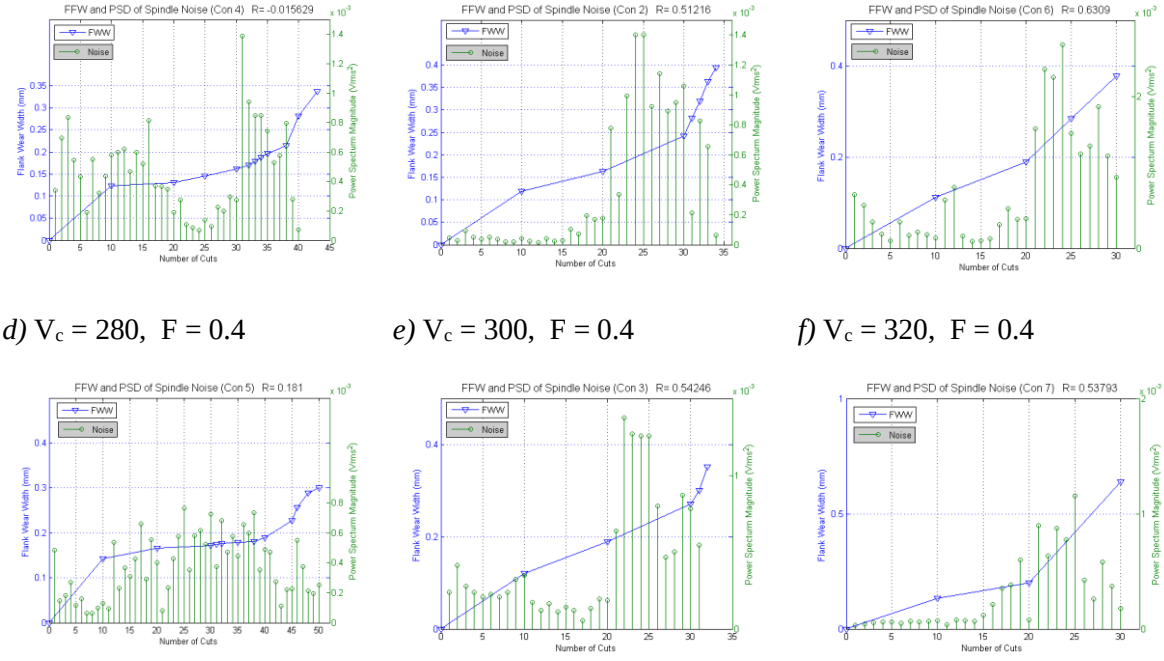

d) V_c = 280, F = 0.4 *e)* V_c = 300, F = 0.4 *f)* V_c = 320, F = 0.4

Figure 8.7 Magnitude of power spectrum of spindle noise and flank wear width (FWW) vs. varying cutting speed and feed

In general, and regardless of either considering the effect of varying cutting speed or feed, the magnitudes of power spectrum of spindle noise are low when the tools are in their break-in period and until halfway through their steady-state wear region. As

cutting progresses, the power spectrum magnitudes of spindle noise increase rapidly until reaching their maximum value just prior to a sudden decrease just before tool failure.

The cumulative spectra magnitudes compared to flank wear during cutting are shown in Figure 8.8. It is observed that the trends of the cumulative data slightly increase from the start to half of steady-wear period. Later, an abrupt change is observed in the second half of steady-state wear period. This can be used as a warning signal to indicate imminent tool failure.

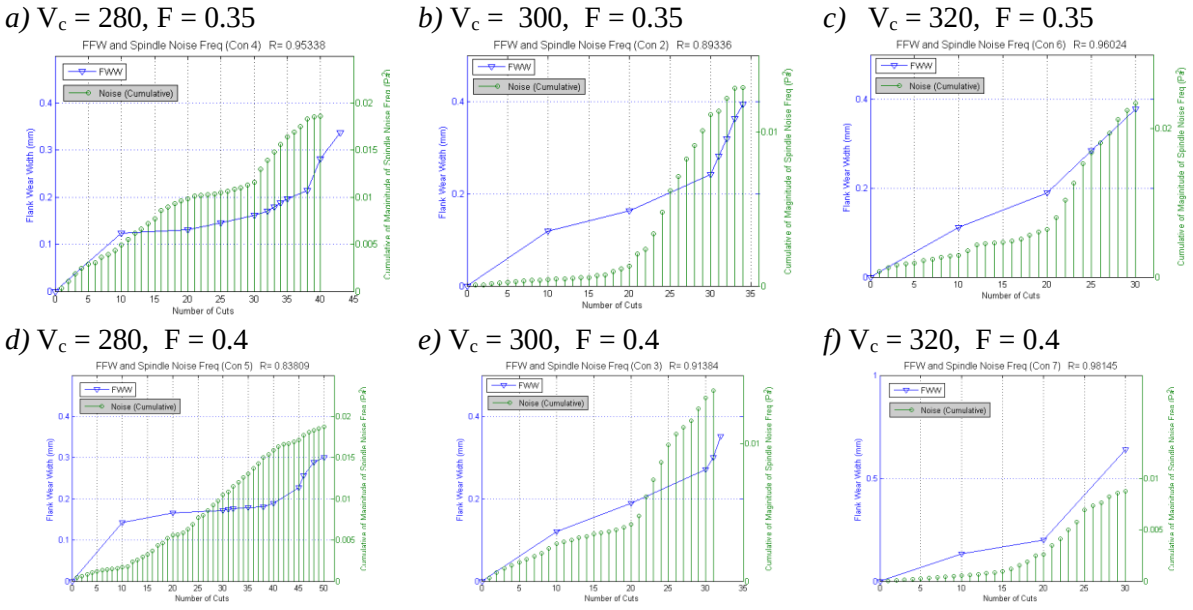

Figure 8.8 Cumulative of power spectrum magnitude of spindle noise and flank wear width (FWW)

By considering the derivative of the cumulative value the condition of the tool can be monitored. It is normally low in the first and middle of the second periods of tool wear curve or tool flank wear less than 0.2 mm. The significant change of derivative value is at the middle of steady wear. In failure region of tool wear curve, the derivative value intends to decrease to zero, which is the point of tool failure.

It has been seen that an increase in spectrum magnitude of spindle noise results from tool wear. As flank wear width increases, the contact area between the flank face and workpiece increases, which requires more cutting force and consequently the spindle motor requires more power to rotate the workpiece at the desired speed to overcome the increasing friction force on cutting contact area.

The power consumption of spindle motor was monitored (Section 6.5.4) and Figure 6.34 shows the power used of spindle motor during cutting, which increases significantly with the increase in tool wear. This increasing power for workpiece rotation produces more spindle noise. The increase in noise that this process produces is clearly recorded by the microphone and can be used as an indicator of the onset of unwanted levels of

tool wear, therefore using spindle noise can be a candidate feature for tool wear monitoring in a turning process.

It should also be noted that although a constant depth of cut was used in this work (as discussed in Section 6.4.3), it is expected that a similar relative change in the signal would be observed if it was also varied because the power consumption of a cutting process is related to the material removal rate (i.e. the product of depth of cut, cutting speed and feed). Similarly, it would be expected that repeating this work using different workpiece materials would produce measurable differences, for example using a workpiece of higher hardness (e.g. Inconel) would lead to higher tool wear (and therefore more noise) for a given cutting condition.

8.6 Feasibility Study of Using Spindle Noise to Monitor Drill Bit Wear

After observing the spindle noise in a turning experiment, this spindle noise was introduced to use for tool wear monitoring in a drilling process in order to investigate whether the proposed features extracted from the sound of the spindle motor can be monitored for a drilling process.

8.6.1 Scope of the Study

The drilling experiment was performed by very large heavy-duty vertical turning/milling/drilling lathe (VTL) as shown in Figure 8.9. Wear on drill bits was monitored. The Dorries Scharmann VTL, capable of working on pieces of up to five metres diameter and three metres height, was used to drill 10-millimetre holes on S275JR with high speed steel drill bit (Sandvik product number A777). This machine was selected because it is difficult to use traditional tool condition monitoring techniques due to its size. The sound of the drilling process was analysed to observe the spindle noise in this machining process.

Figure 8.9 VTL milling machine used for drilling experiment

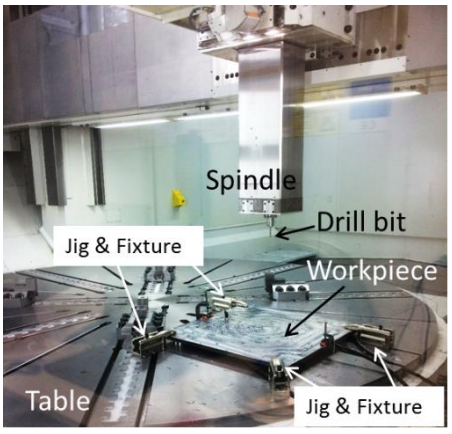

Figure 8.10 Material workpiece on the machine table

8.6.2 Tools, Equipment and Methodology

The workpiece material was an unalloyed low carbon mild steel (S275JR) which provides low strength with good machinability. A plate of S275JR (1m x 1m x 30mm) was clamped by jigs and fixtures on the machine table as shown in Figure 8.10. An A777 high speed steel drill bit (10 mm diameter) was used to perform benchmark drilling in wet machining condition at feed (f) = 0.228 mm/rev and surface cutting speed (V_c) = 30 m/min. 190 holes were drilled in total as it was assumed the drill would reach a failure wear state or the progression of drill bit wear could be found. The same data acquisition equipment as was used for the previous experiments (Chapter 6) was used here. The microphone (in an enclosure box) was fixed on machine wall by a flexible magnetic stand located 2 metres from the drilling point and connected to the data acquisition equipment (NI-9234 / cDAQ-9217). The rate of sampling used to collect the sound signal was 50 kS/s and during the experiment, the drill bit wear on cutting edges was observed with a digital microscope as shown in Figure 8.11. Wear images of the drill bit were taken every ten holes to see the progression of wear.

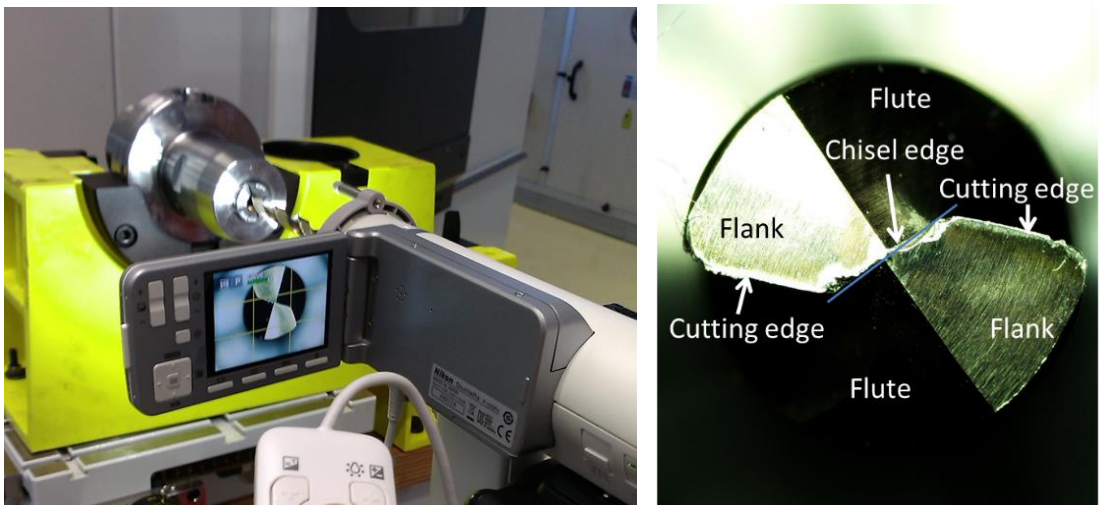

Figure 8.11 Tool wear image on a drill bit taken by the ShuttlePix P-400R

Note: Due to rules and regulations, the author could not be authorised to access to the NAMRC building. Therefore, the drilling experiment was carried out by NAMRC's researchers with the tools and equipment prepared by the author.

8.6.3 Spectrogram of Drilling Sound

An example of the drilling sound recorded from two consecutive holes was transformed into the spectrogram as shown in Figure 8.12.

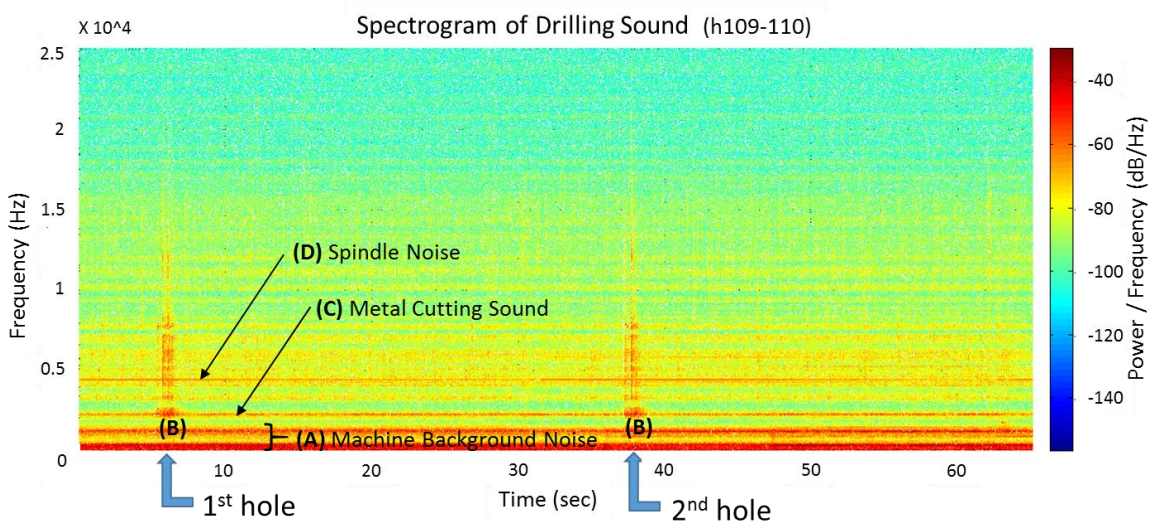

Figure 8.12 Spectrogram of machining sound in the drilling process

From the spectrogram, it is clearly seen that the low frequency 0-3 kHz is the machine background noise (A) as previously mentioned (Section 8.2). Two groups of wide frequency band (B) can be seen and represent the starting point of drilled holes. The long stretch line represents the metal cutting sound (C) as can be seen the impact sound when the drill bit engage the workpiece. The spindle noise frequency (D) was found constantly at 4.39 kHz for all 190 holes as shown in Figure 8.13. The change of the magnitude of this frequency was considered likely to be useful for monitoring tool wear.

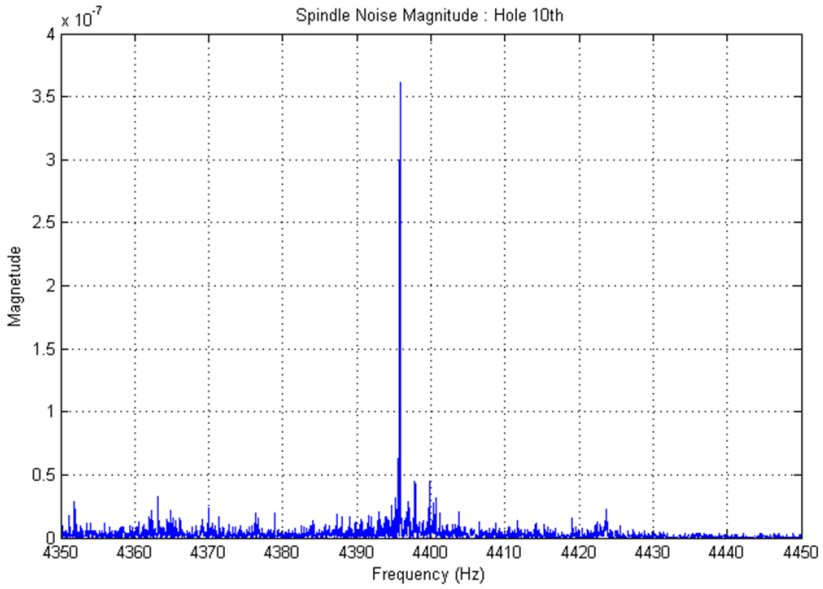

Figure 8.13 Spindle Noise of VTL machine found about 4.3 kHz.

8.6.4 Magnitude of Spindle Noise during Drilling Test

Figure 8.14 shows the drill bit wear during the drilling experiment. Roughly, the slightly worn tool was observed at the hole 40th, a moderately worn tool was imaged at hole 100, and severe wear image was observed at hole 160.

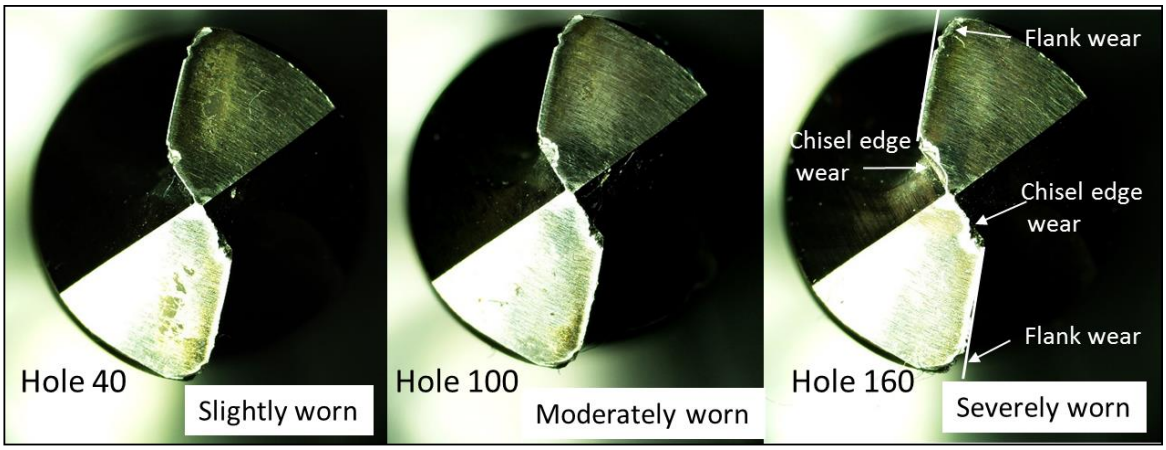

Figure 8.14 Typical drill bit wears during the drilling experiment

Figure 8.15 shows the progression of magnitude of spindle noise frequency during the endurance drilling. The number of drilled holes representing the drilling time was used to represent the progressive wear of the drill bit.

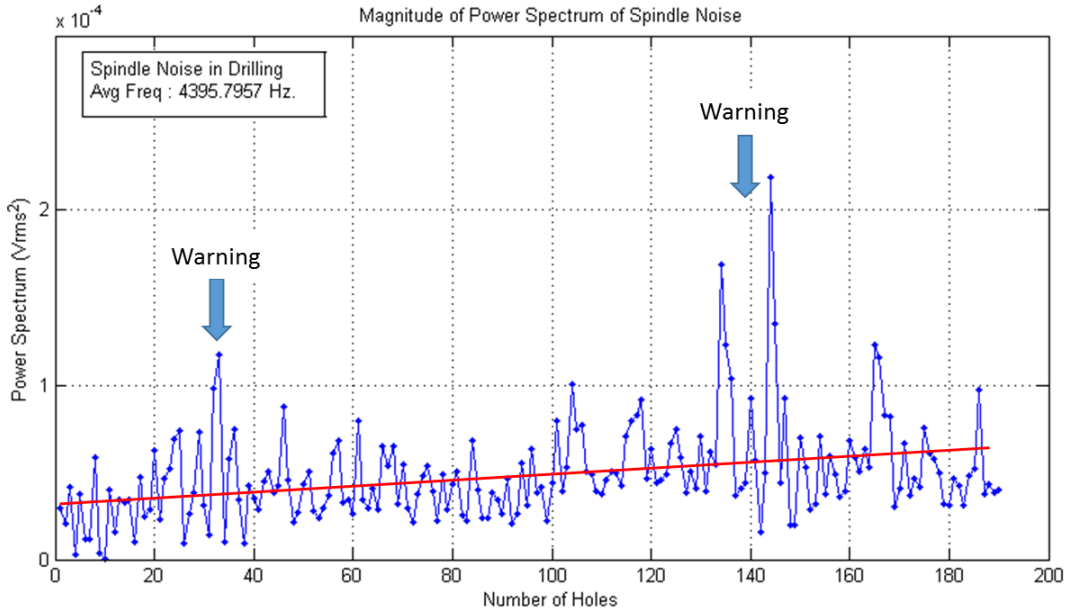

Figure 8.15 Magnitude of power spectrum of spindle noise during drilling experiment

It is found that the magnitude of power spectrum gradually increased, which correlated with an increase of drill bit wear. Interestingly, significant peak magnitude was found during holes 30-40. This could be the transition point of the tool wear state from break-in to steady-state. After that, the magnitude gradually increases until holes 130-150 where the second warning was found. Also, this could be the middle of the second tool wear state or the transition state from steady-state wear region to failure

wear region. To confirm this assumption, the drill bit wear should be measured to obtain enough data points so that the region of tool wear state can be indicated like Figure 8.3. However, this increasing trend could be possibly used to monitor the drill bit wear.

When compared to the results from turning (Section 8.3), in which the magnitude of spindle noise significantly increases in the middle of the steady-state wear region, the magnitude values in drilling fluctuate. This may be due to an amount of undefined ambient noise in the very large machine room and very low signal-to-noise ratio of the spindle noise frequency. Also, the absolute position of the drilling varied during the experiments, as each hole was drilled in the plate, and therefore damping, distance from the microphone and superposition of waves will vary; and any variation in the period over which the magnitude of the signal is analysed versus the period of drilling could have a strong effect.

The cumulative plot of magnitude of spindle noise frequency in drilling is shown in Figure 8.16. The figure shows the linear relationship between cumulative magnitude of spindle noise frequency and the number of drilled holes or drilling time. This is different to the cumulative values from the turning experiments (Figure 8.8) where the turning point of the curve can be clearly found on the cumulative plot in turning experiment.

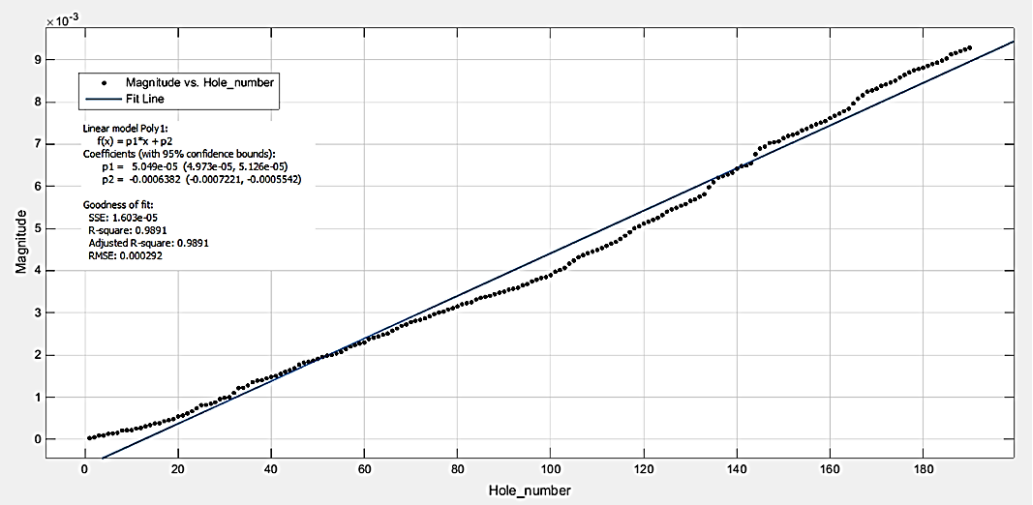

Figure 8.16 Cumulative magnitude of power spectrum of spindle noise during drilling experiment

Although it appears that less information can be derived from a drilling process compared to a turning process, it is proposed that a thresholding method can be applied to indicate when to replace or sharpen the drill bit when the cumulative magnitude of the spindle noise frequency reaches a limiting value. In conclusion, this benchmarking result of using spindle noise in the drilling process suggests that the magnitude of spindle noise frequency could be used as a monitoring feature for tool condition monitoring system, but further work is required.

8.7 Concluding Remarks

In conclusion, it has been shown that the use of relatively simple and inexpensive instrumentation can produce data that is of high enough quality to contribute to the condition monitoring of a running cutting process. The initial sound analysis process described can be used to easily characterise a particular machining process by recording its audio signature. For the particular machine and cutting process used here, noise from spindle motor was detected at the frequency of 5.86 kHz in turning (4.39 kHz in drilling experiment) and from the machine itself between 0-3 kHz. There is no significant correlation between the frequency of spindle noise and tool wear, but it is possible to infer basic knowledge about tool condition from the response of the magnitude of power spectrum of noise from the spindle to changing cutting speed and feed rate. The magnitude of spindle noise frequency spectrum or its cumulative value could be used as monitoring features in tool condition monitoring to assist with the selection of more expensive instrumentation hardware.

It might be worth only using 'the magnitude of spindle noise frequency' extracted from cutting sound to be a monitoring features in turning and drilling processes. To gain more reliability, this proposed feature can be also used in sensor fusion concept. It is expected that the spindle noise frequency magnitude will be selected and used as training data in order to obtain the accurate prediction model for use in tool wear monitoring system.

Chapter 9

Conclusions

In this final chapter, the outcomes and findings are related back to project aims and objectives. Later, the following sections summarise significant research findings made from the present study, recommendation for future work, and the publications and major scientific contributions.

9.1 Achievements against Project Aim and Objectives

The main studies of this thesis can be split into two separate, but closely linked studies: the Barkhausen noise (BHN) technique for coating depth measurement (off-line method) in coated high speed steel and condition monitoring of tool wear (on-line method) in turning. The objectives of these studies were achieved as the following description.

9.1.1 Objective 1

The fundamentals of machining processes were reviewed to understand the influences of tool wear in machining operations. The potential sensors and common signal processing widely used in the tool condition monitoring system and several methods commonly used to extract the monitoring features are described and feature selection methods were also established. This work enabled the identification of likely condition monitoring techniques to be used to create the low cost systems that would be able to monitor the machining processes of interest. From the literature, there were a number of gaps identified from previous research efforts and understanding which are summarised here.

Barkhausen Noise Technique for Coating Depth Measurement (off-line method)

Although extensive research has been carried out on BHN, no single study exists using BHN technique to measure the coating layer of coated HSS cutting tool. From the literature, the BHN technique is likely to measure the coating layers due to the different characteristics of coating materials and the substrate materials. The work presented here shows that this is possible.

Although some commercial systems can offer a BHN measuring system which can be used in several applications, they are relatively expensive and are for general quality control purposes. Therefore, a cost-effective system based on the BHN technique was developed in this study and successfully used to measure the coating layer on coated HSS specimens.

Condition Monitoring of Tool Wear (on-line method)

It was noted that the most-recent research on tool condition monitoring in turning processes was performed in a dry machining conditions as they attempted to accelerate tool wear in order to lower the cost and time used. In addition, some sensing

techniques, such as cutting sound measurement, are very sensitive to interference from noise caused by using coolant. However, several studies proposed the tool condition monitoring systems obtained from the dry machining experiment to use in the real machining conditions that the coolant is normally used. This leads to the systematic error of tool wear prediction and tool wear state classification.

Furthermore, most of the monitoring systems proposed in the literatures use high performance sensors such as dynamometers, acoustic emission sensors for monitoring the tool conditions, but they are considered relatively-expensive and seem to be used in the laboratory only. To achieve the practical use, a cost-effective tool wear monitoring system was developed and performed in the wet machining condition to obtain prediction and classification models for use in the real machining.

9.1.2 Objective 2

In the study of coating layer depth evaluation, in-house equipment, including a bipolar power amplifier, signal amplifier, and passive filter were built to use in the BHN measuring system. Assembled from laboratory devices, it costs less, but can perform as well as commercial equipment. Furthermore, an exciting coil was successfully designed and built for inducing the electromagnetic field (H) into the coated HSS specimens. Basic experiments were performed in order to identify capabilities of BHN, an uncoated specimen was first tested with the measuring system and the thickest coating layer was then checked. The different results of these specimens confirmed that the BHN can be used to indicate the difference of coating thickness.

A low-cost USB microscope camera and lighting system were added to the tool condition monitoring system (AE sensor, microphone, power monitoring) and combined to sense the tool wear in turning process indirectly. The introduction of this allowed the monitoring of the tool wear progression with the expectation that this vision system can be used instead of the high cost system.

The sensor signals in the two studies were collected by the combination of data acquisition systems described in Chapter 4. The data collection programs were developed using LabVIEW. All acquired signals were conditioned electronically and the signal processing was performed by MATLAB and LabVIEW.

9.1.3 Objective 3

The cost-effective BHN system was developed to do the feasibility study of coating depth measurement of the HSS specimen. The proposed BHN system could prevent the excessive current that might cause damage to the system by measuring the current and resistor temperature in the circuit of the exciting coil. The proposed BHN system could then be used in other BHN based condition monitoring systems, if the higher field generation of the exciting coil was used.

Several sensory features were extracted from the BHN signal received by the pick-up coil and some features successfully correlated with the thickness of the coating layer on HSS specimens. The results presented in Chapter 5 suggest that the BHN system developed in this study can successfully indicate the different thickness of the coating layer on CrN/TiN coated HSS specimens. The cost of the proposed system is relatively low compared to the commercial systems.

9.1.4 Objective 4 and 5

A measuring system for tool condition monitoring system based on sensor fusion was developed. First, multiple sensors (AE, microphone, Power) were selected to monitor the wear on cutting inserts during the machining process as described in Chapter 6. Those signals were acquired and processed appropriately. Several sensing features were then extracted and only sensitive features were used to correlate with the tool wear value (also coating layer depth in BHN study). To reduce the influence of dimensionality, the most significant features were used in monitoring systems. The feature selection was subsequently performed to find the best feature sets to use in the modelling step. Those features were fused by selected AI algorithms to obtain a tool wear prediction model and a tool wear state classification model for on-line use.

In developing the monitoring model, several AI algorithms have been used in the data fusion step as found in the literature. However, artificial neural networks were used as a modelling tool in this thesis as they offer fast modelling time and high performance in predicting the tool wear and classifying the tool wear states. As found in Chapter 7, several network configurations and selected features were trained and validated to achieve the highest performance for use.

9.2 Critical Reflection on the Work and Recommendations

9.2.1 Reflection on the Whole Project vs. the Aim

The work presented here has developed two inexpensive tool condition monitoring methods. It is confirmed that the Barkhausen noise methods can characterise the difference of coating thickness in TiN/CrN HSS tool. This can be applied to measure the coating thickness for any other application if there are the different characteristics of coating and core materials.

Tool wear monitoring in turning machines with the combination of multiple, inexpensive sensors can be an alternative system for practical use as they can be justified for use (and potentially destruction) in wet machining. This study also proposed '*spindle noise*', as a novel feature for tool wear monitoring, which may be the basis of a useful method to monitor tool wear using only machining sound instead of very expensive monitoring systems.

Finally, the cost-effective systems proposed in this study can be particularly utilised in small and medium sized engineering companies and will improve productivity by reduction of machine downtime due to tool wear.

9.2.2 Further Work on Barkhausen Noise Technique

The Minimum Coating Depth Difference

In this thesis, coating depth measurement was studied for only two coating materials (CrN and TiN) which have three different thicknesses. From the experimental results, the BHN profile curve could be clearly separated, however, future work should evaluate the minimum depth difference that the BHN technique can be used to indicate the difference of the coating depth layer. Practically, the thickness of coating layer could be reduced by etching or mechanical technique, but the actual thickness value should be measured by the precisely-measuring method in order to validate with the BHN sensing technique. Further study is also required for ensuring that this magnetic method would be used in other metal coating materials.

The Design of BHN System

Due to the limitations of the existing coil used in this study, the BHN signal could be obtained only in the range that the exciting current is up to 1 A. To obtain more measuring range, the new exciting coil should be redesigned and constructed as suggested in Sections 5.6 - 5.7.

Some components of the BHN measuring system developed in this study used some laboratory equipment which is large size and heavy. It would be convenient to develop a small portable system that can be easily used on-site. Most importantly, the compact design of the BHN probe increases the accessibility of the probe to access the surface of testpiece for particular applications.

Fusion the Sensing Features

As discussed in Chapter 5, RMS, peak count, and signal energy extracted from the BHN signal in Stage III, are the significant features used to correlate with the coating layer depth. Although they can be used individually to indicate the thickness of the coating layer, the measured values would be more accurate if these three features are fused together by methods such as neural networks and fussy logic. Similarly, the proper calibration and sufficient data for training are also required.

9.2.2 Further Works on Tool Condition Monitoring Based on Sensor Fusion

Attempt to Use Other AIs to Recognise the Machining Data

Neural networks (backpropagation) are commonly used to train the machining data as they offer acceptable accuracy in estimation and classification with a fast modelling time. However, there are many other neural networks and AIs which could be used to

train the machining data (e.g. fussy logic, ANFIS, PCA). A comparative study is required to obtain the best AI method to be used as a monitoring model for monitoring of tool wear.

Tool Wear Monitoring by Image Technique during Wet Machining Condition

Although several studies have succeeded in developing image processing technique for measuring tool wear, their techniques can only be utilised in dry machining. In real machining operations, coolant is normally used to prolong tool life and help chip removal. Nevertheless, the various difficulties of using a vision system in wet machining condition (as raised in Section 6.5.1) make it challenging to use in the real machining process. These difficulties might have a much greater influence on the results presented by previous researchers if these issues are unaccounted for.

Using Spindle Noise Feature in Other Machining Processes

A novel feature (spindle noise) has been introduced to be used for monitoring the tool wear in the turning process and drilling processes as presented in Chapter 8. However, in drilling, the extremely large vertical turning lathe machine used as a drilling platform in this study has a huge working area and very large of the working room that might have an effect on the recorded sound. It is suggested that the use of the spindle noise in the drilling process could be confirmed by using a general drilling machine, or any other machining process which has a rotary spindle, such as milling and grinding, could be used for further studies. It would be worth investigating if using only spindle noise extracted from the cutting sound to indicate the tool wear states in several machining processes can be used instead of expensive tool wear monitoring system like AE and dynamometers.

9.3 Publication and Contributions

9.3.1 Publications

N.Seemuang, T.McLeay, T.Slatter, "Using Spindle Noise to Monitor Tool Wear in a Turning Process", The International Journal of Advanced Manufacturing Technology, 2016, DOI 10.1007/s00170-015-8303-8

9.3.2 Conference Paper and Poster

Poster Presentation

- "Evaluation of Case-depth Layer in Coated Cutting Tool by Using Barkhausen Noise and Electromagnetic Acoustic Emission Techniques", 2nd Annual EPSRC Manufacturing the Future Conference, 17th- 18th September 2013, Vincent Building, Cranfield University, UK.
- "The Relationship between Spindle Sound and Tool Performance in Turning" MachMan2015, 21st October 2015, the KTC at the Advanced Manufacturing Research Centre (AMRC) with Boeing, Sheffield, UK.

Oral presentation

- "The Relationship between Spindle Sound and Tool Performance in Turning" ICMMM 2015: 17th International Conference on Machining and Machinability of Materials, 13th -14th August 2015, NH Laguna Palace, Venice, Italy

9.3.3 Knowledge Contributions and Industrial Impact

In this study, the author gains support from the University of Sheffield Advanced Manufacturing Research Centre (AMRC) with Boeing, which is a world-class centre for advanced machining and materials research for aerospace and other high-value manufacturing sectors. The author has a valuable opportunity to perform the machining experiment with the real industry environment, but it did not disturb the production. The machining experiment was performed with the recently-technological turning machine. Furthermore, this research centre provides the sensors, data acquisition, cutting tool insert, workpiece material, and other facilities to carry out the machining experiment throughout the study. General discussion due to the experimental work and the result was regularly made by the people who specialise in machining science.

At the end of the study, the experimental findings were discussed and reported to AMRC. Significantly, 'Spindle noise', a new feature found in this study, has been introduced to use as a monitoring feature for tool wear monitoring.

Furthermore, this sensing feature was introduced to engineers at NAMRC (Nuclear AMRC) which acts as a research factory for innovative and optimised processes in

machining, welding and other key areas of large-scale manufacturing technology. The drilling experiment was performed with a very large heavy-duty vertical turning/milling lathe to ensure that the spindle noise feature can be found in the drilling process. Moreover, other sensing techniques were used to monitor the drill bit wear such as acoustic emission, and vibration. In-house equipment (such as a signal amplifier, pre-amplifier, filter) was made to interface the AE sensors and an accelerometer and perform signal processing. From the preliminary results, it is confirmed that the spindle noise can be used to monitor the drill bit wear. However, the further experiment is required to complete the full experimental design.

The work focussing on the use of spindle noise to monitor tool wear in a turning process was published in the International Journal of Advanced Manufacturing Technology. It is expected that this proposed feature will be useful to use in the tool wear monitoring system in machining process.

Finally, the use of Barkhausen noise technique to measure the coating depth of coated HSS has been published in order to introduce the significant findings to public. Other researchers can make use of these results to develop a cost-effective tool or equipment to measure the remaining coating depth layer on coated high speed tool for tool breakage prevention, and production downtime is reduced accordingly.

References

[1] R. A. K. J T. Black, *Materials & Processes in Manufacturing*, 10 ed.: John Wiley & Sons, Inc., 2008.

[2] R. L. R L. Timings, *Manufacturing technology*, 3rd ed. vol. 1: Longman, 1998.

[3] F. Klocke, *Manufacturing Processes 1 - Cutting*: Springer Heidelberg Dordrecht London New York, 2011.

[4] S. R. S. Serope Kalpakjian, *Manufacturing Engineering and Technology* 5th ed.: Prentice Hall, 2005.

[5] M. P. Groover, *Fundamentals of modern manufacturing : materials, processes, and systems*, 3rd ed.: Hoboken, N.J. : Wiley, 2007.

[6] V. P. Astakhov, "The assessment of cutting tool wear," *International Journal of Machine Tools & Manufacture,* vol. 44, pp. 637-647, May 2004.

[7] T. Marwala, *Condition Monitoring Using Computational Intelligence Methodes*: Springer-Verlag, 2012.

[8] R. Teti, K. Jemielniak, G. O'Donnell, and D. Dornfeld, "Advanced monitoring of machining operations," *CIRP Annals - Manufacturing Technology,* vol. 59, pp. 717-739, 2010.

[9] A. Siddhpura and R. Paurobally, "A review of flank wear prediction methods for tool condition monitoring in a turning process," *International Journal of Advanced Manufacturing Technology,* vol. 65, pp. 371-393, Mar 2013.

[10] J. Abellan-Nebot and F. Romero Subirón, "A review of machining monitoring systems based on artificial intelligence process models," *The International Journal of Advanced Manufacturing Technology,* vol. 47, pp. 237-257, 2010/03/01 2010.

[11] J. C. Chen and W. L. Chen, "A tool breakage detection system using an accelerometer sensor," *Journal of Intelligent Manufacturing,* vol. 10, pp. 187-197, Apr 1999.

[12] X. Li, "A brief review: acoustic emission method for tool wear monitoring during turning," *International Journal of Machine Tools and Manufacture,* vol. 42, pp. 157-165, 1// 2002.

[13] M. C. Lu and B. S. Wan, "Study of high-frequency sound signals for tool wear monitoring in micromilling," *International Journal of Advanced Manufacturing Technology,* vol. 66, pp. 1785-1792, Jun 2013.

[14] Y. C. Zhou, P. Orban, S. W. Nikumb, and Ieee, "Sensors for intelligent machining - A research and application survey". New York: I E E E, 1995.

[15] S. Kurada and C. Bradley, "A review of machine vision sensors for tool condition monitoring," *Computers in Industry,* vol. 34, pp. 55-72, 10// 1997.

[16] B. Sick, "On-line and indirect tool wear monitoring in turning with artificial neural networks: A review of more than a decade of research," *Mechanical Systems and Signal Processing,* vol. 16, pp. 487-546, Jul 2002.

[17] K. Worden, W. J. Staszewski, and J. J. Hensman, "Natural computing for mechanical systems research: A tutorial overview," *Mechanical Systems and Signal Processing,* vol. 25, pp. 4-111, Jan 2011.

[18] O. Geramifard, J. X. Xu, J. H. Zhou, and X. Li, "Multimodal Hidden Markov Model-Based Approach for Tool Wear Monitoring," *Ieee Transactions on Industrial Electronics,* vol. 61, pp. 2900-2911, Jun 2014.

[19] M. Wang and J. Wang, "CHMM for tool condition monitoring and remaining useful life prediction," *International Journal of Advanced Manufacturing Technology,* vol. 59, pp. 463-471, Mar 2012.

[20] A. G. Vallejo, J. A. Nolazco-Flores, R. Morales-Menendez, L. E. Sucar, and C. A. Rodriguez, "Tool-wear monitoring based on continuous hidden Markov models," in *Progress in Pattern Recognition, Image Analysis and Applications, Proceedings*. vol. 3773, A. Sanfeliu and M. L. Cortes, Eds., ed Berlin: Springer-Verlag Berlin, 2005, pp. 880-890.

[21] J. F. Dong, K. V. R. Subrahmanyam, Y. S. Wong, G. S. Hong, and A. R. Mohanty, "Bayesian-inference-based neural networks for tool wear estimation," *International Journal of Advanced Manufacturing Technology,* vol. 30, pp. 797-807, 2006.

References

[22] J. Sun, G. S. Hong, M. Rahman, and Y. S. Wong, "Identification of feature set for effective tool condition monitoring by acoustic emission sensing," *International Journal of Production Research,* vol. 42, pp. 901-918, Mar 2004.

[23] S. Dey and J. A. Stori, "A Bayesian network approach to root cause diagnosis of process variations," *International Journal of Machine Tools and Manufacture,* vol. 45, pp. 75-91, 1// 2005.

[24] S. Cho, S. Asfour, A. Onar, and N. Kaundinya, "Tool breakage detection using support vector machine learning in a milling process," *International Journal of Machine Tools & Manufacture,* vol. 45, pp. 241-249, Mar 2005.

[25] A. Widodo and B.-S. Yang, "Support vector machine in machine condition monitoring and fault diagnosis," *Mechanical Systems and Signal Processing,* vol. 21, pp. 2560-2574, 8// 2007.

[26] I. A. Basheer and M. Hajmeer, "Artificial neural networks: fundamentals, computing, design, and application," *Journal of Microbiological Methods,* vol. 43, pp. 3-31, 12/1/ 2000.

[27] G. Byrne, D. Dornfeld, I. Inasaki, G. Ketteler, W. König, and R. Teti, "Tool Condition Monitoring (TCM) — The Status of Research and Industrial Application," *CIRP Annals - Manufacturing Technology,* vol. 44, pp. 541-567, // 1995.

[28] M. Rizal, J. A. Ghani, M. Z. Nuawi, and C. H. C. Haron, "Online tool wear prediction system in the turning process using an adaptive neuro-fuzzy inference system," *Applied Soft Computing,* vol. 13, pp. 1960-1968, 4// 2013.

[29] A. Gajate, R. Haber, R. del Toro, P. Vega, and A. Bustillo, "Tool wear monitoring using neuro-fuzzy techniques: a comparative study in a turning process," *Journal of Intelligent Manufacturing,* vol. 23, pp. 869-882, Jun 2012.

[30] V. S. Sharma, S. K. Sharma, and A. K. Sharma, "Cutting tool wear estimation for turning," *Journal of Intelligent Manufacturing,* vol. 19, pp. 99-108, Feb 2008.

[31] S. Kumanan, C. P. Jesuthanam, and R. A. Kumar, "Application of multiple regression and adaptive neuro fuzzy inference system for the prediction of surface roughness," *International Journal of Advanced Manufacturing Technology,* vol. 35, pp. 778-788, Jan 2008.

[32] K. Venkata Rao, B. S. N. Murthy, and N. Mohan Rao, "Prediction of cutting tool wear, surface roughness and vibration of work piece in boring of AISI 316 steel with artificial neural network," *Measurement,* vol. 51, pp. 63-70, 5// 2014.

[33] K. A. Risbood, U. S. Dixit, and A. D. Sahasrabudhe, "Prediction of surface roughness and dimensional deviation by measuring cutting forces and vibrations in turning process," *Journal of Materials Processing Technology,* vol. 132, pp. 203-214, 1/10/ 2003.

[34] W. H. Yang and Y. S. Tarng, "Design optimization of cutting parameters for turning operations based on the Taguchi method," *Journal of Materials Processing Technology,* vol. 84, pp. 122-129, 12/1/ 1998.

[35] N. Mandal, B. Doloi, B. Mondal, and R. Das, "Optimization of flank wear using Zirconia Toughened Alumina (ZTA) cutting tool: Taguchi method and Regression analysis," *Measurement,* vol. 44, pp. 2149-2155, 12// 2011.

[36] D. Montgomery, *Design and analysis of experiments*, 5th ed.: Wiley, New York, 2001.

[37] R. K. Roy, *Design of experiments using the Taguchi approach*: Wiley, New York, 2001.

[38] J. Gokulachandran and K. Mohandas, "Comparative study of two soft computing techniques for the prediction of remaining useful life of cutting tools," *Journal of Intelligent Manufacturing,* vol. 26, pp. 255-268, Apr 2015.

[39] B. Karpuschewski, O. Bleicher, and M. Beutner, "Surface integrity inspection on gears using barkhausen noise analysis," *Procedia Engineering,* vol. 19, pp. 162-171, // 2011.

[40] B. Raj, V. Moorthy, T. Jayakumar, and K. B. S. Rao, "Assessment of microstructures and mechanical behaviour of metallic materials through non-destructive characterisation," *International Materials Reviews,* vol. 48, pp. 273-325, 2003.

[41] M. Dubois and M. Fiset, "Evaluation of case depth on steels by barkhausen noise measurement," *Materials Science and Technology,* vol. 11, pp. 264-267, Mar 1995.

References

[42] J. W. Wilson, G. Y. Tian, V. Moorthy, and B. A. Shaw, "Magneto-acoustic emission and magnetic barkhausen emission for case depth measurement in EN36 gear steel," *Ieee Transactions on Magnetics,* vol. 45, pp. 177-183, Jan 2009.

[43] Z. D. Wang, Y. Gu, and Y. S. Wang, "A review of three magnetic NDT technologies," *Journal of Magnetism and Magnetic Materials,* vol. 324, pp. 382-388, Feb 2012.

[44] B. Zhu, M. J. Johnson, and D. C. Jiles, "Evaluation of wear-induced material loss in case-hardened steel using magnetic Barkhausen emission measurement," *Ieee Transactions on Magnetics,* vol. 36, pp. 3602-3604, Sep 2000.

[45] C. C. H. Lo, E. R. Kinser, Y. Melikhov, and D. C. Jiles, "Magnetic nondestructive characterization of case depth in surface-hardened steel components," in *Review of Progress in Quantitative Nondestructive Evaluation, Vols 25A and 25B*. vol. 820, D. O. Thompson and D. E. Chimenti, Eds., ed Melville: Amer Inst Physics, 2006, pp. 1253-1260.

[46] F. A. Franco, M. F. R. Gonzalez, M. F. de Campos, and L. R. Padovese, "Relation between magnetic barkhausen noise and hardness for jominy quench tests in SAE 4140 and 6150 steels," *Journal of Nondestructive Evaluation,* vol. 32, pp. 93-103, Mar 2013.

[47] S. Santa-aho, M. Vippola, A. Sorsa, K. Leiviskä, M. Lindgren, and T. Lepistö, "Utilization of Barkhausen noise magnetising sweeps for case-depth detection from hardened steel," *NDT & E International,* vol. 52, pp. 95-102, 2012.

[48] M. Lindgren and T. Lepistö, "Application of a novel type Barkhausen noise sensor to continuous fatigue monitoring," *NDT & E International,* vol. 33, pp. 423-428, 9// 2000.

[49] D. M. Stewart, K. J. Stevens, and A. B. Kaiser, "Magnetic Barkhausen noise analysis of stress in steel," *Current Applied Physics,* vol. 4, pp. 308-311, 4// 2004.

[50] V. Moorthy, B. A. Shaw, P. Mountford, and P. Hopkins, "Magnetic Barkhausen emission technique for evaluation of residual stress alteration by grinding in case-carburised En36 steel," *Acta Materialia,* vol. 53, pp. 4997-5006, 2005.

[51] V. Moorthy, B. A. Shaw, and P. Hopkins, "Surface and subsurface stress evaluation in case-carburised steel using high and low frequency magnetic Barkhausen emission measurements," *Journal of Magnetism and Magnetic Materials,* vol. 299, pp. 362-375, Apr 2006.

[52] A. Sorsa, K. Leiviska, S. Santa-aho, M. Vippola, and T. Lepisto, "A study on laser-processed grinding burn simulation and analysis based on Barkhausen noise measurement," *Insight,* vol. 52, pp. 293-297, Jun 2010.

[53] S. Santa-aho, M. Vippola, A. Sorsa, J. Latokartano, M. Lindgren, K. Leiviska*, et al.*, "Development of Barkhausen noise calibration blocks for reliable grinding burn detection," *Journal of Materials Processing Technology,* vol. 212, pp. 408-416, Feb 2012.

[54] S. Santa-aho, M. Vippola, A. Sorsa, M. Lindgren, J. Latokartano, K. Leiviskä*, et al.*, "Optimized laser processing of calibration blocks for grinding burn detection with Barkhausen noise," *Journal of Materials Processing Technology,* vol. 212, pp. 2282-2293, 11// 2012.

[55] L. Vrkoslavova, P. Louda, and J. Malec, "Analysis of surface integrity of grinded gears using barkhausen noise analysis and X-Ray diffraction," in *40th Annual Review of Progress in Quantitative Nondestructive Evaluation: Incorporating the 10th International Conference on Barkhausen Noise and Micromagnetic Testing, Vols 33a & 33b*. vol. 1581, D. E. Chimenti, L. J. Bond, and D. O. Thompson, Eds., ed Melville: Amer Inst Physics, 2014, pp. 1280-1286.

[56] S. Santa-aho, A. Sorsa, M. Hakanen, K. Leiviska, M. Vippola, and T. Lepisto, "Barkhausen noise-magnetising voltage sweep measurement in evaluation of residual stress in hardened components," *Measurement Science & Technology,* vol. 25, p. 6, Aug 2014.

[57] S. Santa-aho, M. Vippola, A. Sorsa, K. Leiviskä, M. Lindgren, and T. Lepistö, "Utilization of Barkhausen noise magnetising sweeps for case-depth detection from hardened steel," *NDT & E International,* vol. 52, pp. 95-102, 11// 2012.

References

[58] A. Sorsa, K. Leiviska, S. Santa-aho, and T. Lepisto, "Quantitative prediction of residual stress and hardness in case-hardened steel based on the Barkhausen noise measurement," *Ndt & E International,* vol. 46, pp. 100-106, Mar 2012.

[59] U. Alonso, N. Ortega, J. A. Sanchez, I. Pombo, S. Plaza, and B. Izquierdo, "In-process prediction of the hardened layer in cylindrical traverse grind-hardening," *International Journal of Advanced Manufacturing Technology,* vol. 71, pp. 101-108, Mar 2014.

[60] S. Santa-aho, M. Hakanen, A. Sorsa, M. Vippola, K. Leiviska, and T. Lepisto, "Case depth verification of hardened samples with Barkhausen noise sweeps," in *40th Annual Review of Progress in Quantitative Nondestructive Evaluation: Incorporating the 10th International Conference on Barkhausen Noise and Micromagnetic Testing, Vols 33a & 33b*. vol. 1581, D. E. Chimenti, L. J. Bond, and D. O. Thompson, Eds., ed Melville: Amer Inst Physics, 2014, pp. 1307-1314.

[61] M. Blaow, J. T. Evans, and B. A. Shaw, "Surface decarburisation of steel detected by magnetic Barkhausen emission," *Journal of Materials Science,* vol. 40, pp. 5517-5520, Oct 2005.

[62] S. Kahrobaee and M. Kashefi, "Hardness profile plotting using multi-frequency multi-output electromagnetic sensor," *NDT & E International,* vol. 44, pp. 335-338, 7// 2011.

[63] S. Ghanei, A. S. Alam, M. Kashefi, and M. Mazinani, "Nondestructive characterization of microstructure and mechanical properties of intercritically annealed dual-phase steel by magnetic Barkhausen noise technique," *Materials Science and Engineering a-Structural Materials Properties Microstructure and Processing,* vol. 607, pp. 253-260, Jun 2014.

[64] A. Drehmer, G. J. L. Gerhardt, and F. P. Missell, "Case depth in SAE 1020 steel using Barkhausen noise," *Materials Research-Ibero-American Journal of Materials,* vol. 16, pp. 1015-1019, Sep-Oct 2013.

[65] V. Moorthy, B. A. Shaw, and S. Day, "Evaluation of applied and residual stresses in case-carburised En36 steel subjected to bending using the magnetic Barkhausen emission technique," *Acta Materialia,* vol. 52, pp. 1927-1936, 4/19/ 2004.

[66] D. Kerr, J. Pengilley, and R. Garwood, "Assessment and visualisation of machine tool wear using computer vision," *International Journal of Advanced Manufacturing Technology,* vol. 28, pp. 781-791, Apr 2006.

[67] J. Jurkovic, M. Korosec, and J. Kopac, "New approach in tool wear measuring technique using CCD vision system," *International Journal of Machine Tools and Manufacture,* vol. 45, pp. 1023-1030, 7// 2005.

[68] W. K. Mook, H. H. Shahabi, and M. M. Ratnam, "Measurement of nose radius wear in turning tools from a single 2D image using machine vision," *International Journal of Advanced Manufacturing Technology,* vol. 43, pp. 217-225, Jul 2009.

[69] Y. Liao, D. A. Stephenson, J. Ni, and Asme, *Assessment Of Tool Wear Based On Surface Texture Parameters*. New York: Amer Soc Mechanical Engineers, 2009.

[70] S. Dutta, A. Datta, N. D. Chakladar, S. K. Pal, S. Mukhopadhyay, and R. Sen, "Detection of tool condition from the turned surface images using an accurate grey level co-occurrence technique," *Precision Engineering,* vol. 36, pp. 458-466, 7// 2012.

[71] S. Kurada and C. Bradley, "A machine vision system for tool wear assessment," *Tribology International,* vol. 30, pp. 295-304, 4// 1997.

[72] H. H. Shahabi and M. M. Ratnam, "In-cycle detection of built-up edge (BUE) from 2-D images of cutting tools using machine vision," *International Journal of Advanced Manufacturing Technology,* vol. 46, pp. 1179-1189, Feb 2010.

[73] T. Yesin and Z. Ozel, "A study of cutting-tool wear by neutron-activation technique," *Journal of Radioanalytical and Nuclear Chemistry-Articles,* vol. 99, pp. 441-445, Jun 1986.

[74] N. H. Cook, "TOOL WEAR SENSORS," *Wear,* vol. 62, pp. 49-57, 1980.

[75] Q. Ren, M. Balazinski, L. Baron, and K. Jemielniak, "TSK fuzzy modeling for tool wear condition in turning processes: An experimental study," *Engineering Applications of Artificial Intelligence,* vol. 24, pp. 260-265, Mar 2011.

References

[76] D. Gao, Z. Liao, Z. Lv, and Y. Lu, "Multi-scale statistical signal processing of cutting force in cutting tool condition monitoring," *The International Journal of Advanced Manufacturing Technology,* vol. 80, pp. 1843-1853, 2015/10/01 2015.

[77] D. Li and J. Mathew, "Tool wear and failure monitoring techniques for turning - a review," *International Journal of Machine Tools & Manufacture,* vol. 30, pp. 579-598, 1990.

[78] D. E. Dimla, "Sensor signals for tool-wear monitoring in metal cutting operations - a review of methods," *International Journal of Machine Tools & Manufacture,* vol. 40, pp. 1073-1098, Jun 2000.

[79] R. Teti, K. Jemielniak, G. O'Donnell, and D. Dornfeld, "Advanced monitoring of machining operations," *Cirp Annals-Manufacturing Technology,* vol. 59, pp. 717-739, 2010.

[80] S. K. Sikdar and M. Y. Chen, "Relationship between tool flank wear area and component forces in single point turning," *Journal of Materials Processing Technology,* vol. 128, pp. 210-215, Oct 2002.

[81] M. C. Cakir and Y. Isik, "Detecting tool breakage in turning aisi 1050 steel using coated and uncoated cutting tools," *Journal of Materials Processing Technology,* vol. 159, pp. 191-198, Jan 2005.

[82] A. G. Rehorn, J. Jiang, and P. E. Orban, "State-of-the-art methods and results in tool condition monitoring: a review," *The International Journal of Advanced Manufacturing Technology,* vol. 26, pp. 693-710, 2005/10/01 2005.

[83] C. Scheffer and P. S. Heyns, "An industrial tool wear monitoring system for interrupted turning," *Mechanical Systems and Signal Processing,* vol. 18, pp. 1219-1242, 9// 2004.

[84] M. C. Lu and E. Kannatey-Asibu, "Analysis of sound signal generation due to flank wear in turning," *Journal of Manufacturing Science and Engineering-Transactions of the Asme,* vol. 124, pp. 799-808, Nov 2002.

[85] F. J. Alonso and D. R. Salgado, "Analysis of the structure of vibration signals for tool wear detection," *Mechanical Systems and Signal Processing,* vol. 22, pp. 735-748, Apr 2008.

[86] D. E. Dimla, "The correlation of vibration signal features to cutting tool wear in a metal turning operation," *International Journal of Advanced Manufacturing Technology,* vol. 19, pp. 705-713, 2002.

[87] D. R. Salgado, F. J. Alonso, I. Cambero, and A. Marcelo, "In-process surface roughness prediction system using cutting vibrations in turning," *International Journal of Advanced Manufacturing Technology,* vol. 43, pp. 40-51, Jul 2009.

[88] F. Ding and Z. J. He, "Cutting tool wear monitoring for reliability analysis using proportional hazards model," *International Journal of Advanced Manufacturing Technology,* vol. 57, pp. 565-574, Nov 2011.

[89] D. Dornfeld, "Application of acoustic emission techniques in manufacturing," *NDT & E International,* vol. 25, pp. 259-269, 12// 1992.

[90] S. V. Kamarthi, S. R. T. Kumara, and P. H. Cohen, "Flank wear estimation in turning through wavelet representation of acoustic emission signals," *Journal of Manufacturing Science and Engineering-Transactions of the Asme,* vol. 122, pp. 12-19, Feb 2000.

[91] P. Kulandaivelu, P. S. Kumar, and S. Sundaram, "Wear monitoring of single point cutting tool using acoustic emission techniques," *Sadhana-Academy Proceedings in Engineering Sciences,* vol. 38, pp. 211-234, Apr 2013.

[92] B. M.S.H, C. I.A, and N. Y, "An innovative approach to monitor the chip formation effect on tool state using acoustic emission in turning," *International Journal of Machine Tools and Manufacture,* vol. 58, pp. 19-28, 7// 2012.

[93] S. Rangwala and D. Dornfeld, "Sensor integration using neural networks for intelligent tool condition monitoring," *Journal of Engineering for Industry-Transactions of the Asme,* vol. 112, pp. 219-228, Aug 1990.

[94] C. Chungchoo and D. Saini, "A computer algorithm for flank and crater wear estimation in CNC turning operations," *International Journal of Machine Tools and Manufacture,* vol. 42, pp. 1465-1477, 10// 2002.

References

[95] V. Sharma, S. K. Sharma, and A. Sharma, "Cutting tool wear estimation for turning," *Journal of Intelligent Manufacturing,* vol. 19, pp. 99-108, 2008/02/01 2008.

[96] A. Gajate, R. Haber, R. Toro, P. Vega, and A. Bustillo, "Tool wear monitoring using neuro-fuzzy techniques: a comparative study in a turning process," *Journal of Intelligent Manufacturing,* vol. 23, pp. 869-882, 2012/06/01 2012.

[97] K. Jemielniak, T. Urbanski, J. Kossakowska, and S. Bombinski, "Tool condition monitoring based on numerous signal features," *International Journal of Advanced Manufacturing Technology,* vol. 59, pp. 73-81, Mar 2012.

[98] S. Y. Liang, R. L. Hecker, and R. G. Landers, "Machining process monitoring and control: The state-of-the-art," *Journal of Manufacturing Science and Engineering-Transactions of the Asme,* vol. 126, pp. 297-310, May 2004.

[99] M. A. Mannan, A. A. Kassim, and M. Jing, "Application of image and sound analysis techniques to monitor the condition of cutting tools," *Pattern Recognition Letters,* vol. 21, pp. 969-979, 10// 2000.

[100] G. Quintana, J. Ciurana, I. Ferrer, and C. A. Rodriguez, "Sound mapping for identification of stability lobe diagrams in milling processes," *International Journal of Machine Tools & Manufacture,* vol. 49, pp. 203-211, Mar 2009.

[101] T. H. Chen, M. C. Lu, S. J. Chiou, C. Y. Lin, M. H. Lee, and Asme, *Study of Sound Signal for Tool Wear Monitoring System in Micro-milling Processes*, 2009.

[102] C. Aliustaoglu, H. M. Ertunc, and H. Ocak, "Tool wear condition monitoring using a sensor fusion model based on fuzzy inference system," *Mechanical Systems and Signal Processing,* vol. 23, pp. 539-546, 2// 2009.

[103] J. Kopac and S. Sali, "Tool wear monitoring during the turning process," *Journal of Materials Processing Technology,* vol. 113, pp. 312-316, Jun 2001.

[104] J. E. Raja, L. C. Kiong, and L. W. Soong, "Hilbert-Huang transform-based emitted sound signal analysis for tool flank wear monitoring," *Arabian Journal for Science and Engineering,* vol. 38, pp. 2219-2226, Aug 2013.

[105] Z. Tekıner and S. Yeşılyurt, "Investigation of the cutting parameters depending on process sound during turning of AISI 304 austenitic stainless steel," *Materials & Design,* vol. 25, pp. 507-513, 9// 2004.

[106] P. Bhattacharyya, D. Sengupta, S. Mukhopadhyay, and A. B. Chattopadhyay, "On-line tool condition monitoring in face milling using current and power signals," *International Journal of Production Research,* vol. 46, pp. 1187-1201, 2008.

[107] T. Szecsi, "A DC motor based cutting tool condition monitoring system," *Journal of Materials Processing Technology,* vol. 92–93, pp. 350-354, 8/30/ 1999.

[108] R. G. Silva, R. L. Reuben, K. J. Baker, and S. J. Wilcox, "Tool wear monitoring of turning operations by neural network and expert system classification of a feature set generated from multiple sensors," *Mechanical Systems and Signal Processing,* vol. 12, pp. 319-332, Mar 1998.

[109] A. Renones, J. Rodriguez, and L. de Miguel, "Industrial application of a multitooth tool breakage detection system using spindle motor electrical power consumption," *International Journal of Advanced Manufacturing Technology,* vol. 46, pp. 517-528, Jan 2010.

[110] S. P. Lo, "The application of an ANFIS and grey system method in turning tool-failure detection," *International Journal of Advanced Manufacturing Technology,* vol. 19, pp. 564-572, 2002.

[111] V. S. Sharma, S. K. Sharma, and A. K. Sharma, "An approach for condition monitoring of a turning tool," *Proceedings of the Institution of Mechanical Engineers, Part B: Journal of Engineering Manufacture,* vol. 221, pp. 635-648, April 1, 2007 2007.

[112] M. Malekian, S. S. Park, and M. B. G. Jun, "Tool wear monitoring of micro-milling operations," *Journal of Materials Processing Technology,* vol. 209, pp. 4903-4914, 6/1/ 2009.

References

[113] S. Tangjitsitcharoen, C. Rungruang, and N. Pongsathornwiwat, "Advanced monitoring of tool wear and cutting states in CNC turning process by utilizing sensor fusion," in *Manufacturing Process Technology, Pts 1-5*. vol. 189-193, Z. Y. Jiang, S. Q. Li, J. M. Zeng, X. P. Liao, and D. G. Yang, Eds., ed Stafa-Zurich: Trans Tech Publications Ltd, 2011, pp. 377-384.

[114] T. Segreto, A. Simeone, and R. Teti, "Sensor fusion for tool state classification in nickel superalloy high performance cutting," *Procedia CIRP,* vol. 1, pp. 593-598, // 2012.

[115] K. F. Zhang, H. Q. Yuan, and P. Nie, "A method for tool condition monitoring based on sensor fusion," *Journal of Intelligent Manufacturing,* vol. 26, pp. 1011-1026, Oct 2015.

[116] N. Fang, P. S. Pai, and S. Mosquea, "Effect of tool edge wear on the cutting forces and vibrations in high-speed finish machining of Inconel 718: an experimental study and wavelet transform analysis," *International Journal of Advanced Manufacturing Technology,* vol. 52, pp. 65-77, Jan 2011.

[117] Y. Quan, M. Zhou, and Z. Luo, "On-line robust identification of tool-wear via multi-sensor neural-network fusion," *Engineering Applications of Artificial Intelligence,* vol. 11, pp. 717-722, 12// 1998.

[118] M. Hall, E. Frank, G. Holmes, and I. H. Witten, "The WEKA data mining software: an update," *SIGKDD Explorations,* vol. 11, 2009.

[119] D. E. Dimla Sr and P. M. Lister, "On-line metal cutting tool condition monitoring.: II: tool-state classification using multi-layer perceptron neural networks," *International Journal of Machine Tools and Manufacture,* vol. 40, pp. 769-781, 4// 2000.

[120] J. M. Zhou, M. Andersson, and J. E. Stahl, "The monitoring of flank wear on the CBN tool in the hard turning process," *International Journal of Advanced Manufacturing Technology,* vol. 22, pp. 697-702, Nov 2003.

[121] U. Natarajan, V. M. Periasamy, and R. Saravanan, "Application of particle swarm optimisation in artificial neural network for the prediction of tool life," *International Journal of Advanced Manufacturing Technology,* vol. 31, pp. 871-876, Jan 2007.

[122] T. I. Liu and B. Jolley, "Tool condition monitoring (TCM) using neural networks," *International Journal of Advanced Manufacturing Technology,* vol. 78, pp. 1999-2007, Jun 2015.

[123] P. Wilkinson, R. L. Reuben, J. D. C. Jones, J. S. Barton, D. P. Hand, T. A. Carolan*, et al.*, "Tool wear prediction from acoustic emission and surface characteristics via an artificial neural network," *Mechanical Systems and Signal Processing,* vol. 13, pp. 955-966, 11// 1999.

[124] İ. Asiltürk and M. Çunkaş, "Modeling and prediction of surface roughness in turning operations using artificial neural network and multiple regression method," *Expert Systems with Applications,* vol. 38, pp. 5826-5832, 5// 2011.

[125] S. Zhang and W. Zhu, "TiN coating of tool steels: a review," *Journal of Materials Processing Technology,* vol. 39, pp. 165-177, 1993/10/01 1993.

[126] J. Rech, M. A. Djouadi, and J. Picot, "Wear resistance of coatings in high speed gear hobbing," *Wear,* vol. 250, pp. 45-53, 10// 2001.

[127] C. Y. H. Lim, S. C. Lim, and K. S. Lee, "The performance of TiN-coated high speed steel tool inserts in turning," *Tribology International,* vol. 32, pp. 393-398, Jul 1999.

[128] V. Moorthy, B. K. Choudhary, S. Vaidyanathan, T. Jayakumar, K. B. S. Rao, and B. Raj, "An assessment of low cycle fatigue damage using magnetic Barkhausen emission in 9Cr-1Mo ferritic steel," *International Journal of Fatigue,* vol. 21, pp. 263-269, Mar 1999.

[129] A. Vincent, L. Pasco, M. Morin, X. Kleber, and M. Delnondedieu, "Magnetic Barkhausen noise from strain-induced martensite during low cycle fatigue of 304L austenitic stainless steel," *Acta Materialia,* vol. 53, pp. 4579-4591, 10// 2005.

[130] X. J. Hao, W. Yin, M. Strangwood, A. J. Peyton, P. F. Morris, and C. L. Davis, "Off-line measurement of decarburization of steels using a multifrequency electromagnetic sensor," *Scripta Materialia,* vol. 58, pp. 1033-1036, Jun 2008.

[131] G. Bach, K. Goebbels, and W. A. Theiner, "Characterization of hardening depth by Barkhausen noise measurement," *Materials Evaluation,* vol. 46, pp. 1576-1580, Nov 1988.

References

[132] V. Moorthy, B. A. Shaw, and K. Brimble, "Testing of case depth in case carburized gear steels using magnetic barkhausen emission technique," *Materials Evaluation,* vol. 62, pp. 523-527, May 2004.

[133] S. Vaidyanathan, V. Moorthy, T. Jayakumar, and B. Raj, "Evaluation of induction hardened case depth through microstructural characterisation using magnetic Barkhausen emission technique," *Materials Science and Technology,* vol. 16, pp. 202-208, 2000.

[134] M. M. Blaow and B. A. Shaw, "Effect of excitation field strength on magnetic Barkhausen noise profile in case carburized EN 36 steel," in *4th International Congress in Advances in Applied Physics and Materials Science*. vol. 1653, A. Y. Oral, Z. B. Bahsi, M. Ozer, M. Sezer, and M. E. Akoz, Eds., ed Melville: Amer Inst Physics, 2015.

[135] O. Stupakov, O. Perevertov, I. Tomáš, and B. Skrbek, "Evaluation of surface decarburization depth by magnetic Barkhausen noise technique," *Journal of Magnetism and Magnetic Materials,* vol. 323, pp. 1692-1697, 6// 2011.

[136] M. Vashista and S. Paul, "Novel processing of Barkhausen noise signal for assessment of residual stress in surface ground components exhibiting poor magnetic response," *Journal of Magnetism and Magnetic Materials,* vol. 323, pp. 2579-2584, 11// 2011.

[137] D. O'Sullivan, M. Cotterell, S. Cassidy, D. A. Tanner, and I. Mészáros, "Magneto-acoustic emission for the characterisation of ferritic stainless steel microstructural state," *Journal of Magnetism and Magnetic Materials,* vol. 271, pp. 381-389, 2004.

[138] M. Vashista and V. Moorthy, "Influence of applied magnetic field strength and frequency response of pick-up coil on the magnetic barkhausen noise profile," *Journal of Magnetism and Magnetic Materials,* vol. 345, pp. 208-214, Nov 2013.

[139] Y. Isik, "Investigating the machinability of tool steels in turning operations," *Materials & Design,* vol. 28, pp. 1417-1424, // 2007.

[140] S. K. Sikdar and M. Chen, "Relationship between tool flank wear area and component forces in single point turning," *Journal of Materials Processing Technology,* vol. 128, pp. 210-215, 10/6/ 2002.

[141] S. H. Yeo, L. P. Khoo, and S. S. Neo, "Tool condition monitoring using reflectance of chip surface and neural network," *Journal of Intelligent Manufacturing,* vol. 11, pp. 507-514, Dec 2000.

[142] F. A. Farrelly, A. Petri, L. Pitolli, G. Pontuale, A. Tagliani, and P. L. N. Inverardi, "Statistical properties of acoustic emission signals from metal cutting processes," *Journal of the Acoustical Society of America,* vol. 116, pp. 981-986, Aug 2004.

[143] J. Bhaskaran, M. Murugan, N. Balashanmugam, and M. Chellamalai, "Monitoring of hard turning using acoustic emission signal," *Journal of Mechanical Science and Technology,* vol. 26, pp. 609-615, Feb 2012.

[144] V. S. S. Kumar, C. Ezilarasan, A. Velayudham, and Asme, *Acoustic Emission Based Tool Wear Condition Monitoring While Turning Nimonic C-263 Alloy Using Pvd Coated Carbide Insert*. New York: Amer Soc Mechanical Engineers, 2014.

[145] M. Balazinski, E. Czogala, K. Jemielniak, and J. Leski, "Tool condition monitoring using artificial intelligence methods," *Engineering Applications of Artificial Intelligence,* vol. 15, pp. 73-80, 2// 2002.

[146] C. Chungchoo and D. Saini, "On-line tool wear estimation in CNC turning operations using fuzzy neural network model," *International Journal of Machine Tools & Manufacture,* vol. 42, pp. 29-40, Jan 2002.

[147] F. J. Alonso and D. R. Salgado, "Application of singular spectrum analysis to tool wear detection using sound signals," *Proceedings of the Institution of Mechanical Engineers Part B-Journal of Engineering Manufacture,* vol. 219, pp. 703-710, Sep 2005.

[148] O. Olufayo and K. Abou-El-Hossein, "Tool life estimation based on acoustic emission monitoring in end-milling of H13 mould-steel," *International Journal of Advanced Manufacturing Technology,* vol. 81, pp. 39-51, Oct 2015.

[149] C. E. D. Cruz, P. R. de Aguiar, A. R. Machado, E. C. Bianchi, J. G. Contrucci, and F. C. Neto, "Monitoring in precision metal drilling process using multi-sensors and neural network," *International Journal of Advanced Manufacturing Technology,* vol. 66, pp. 151-158, Apr 2013.

References

[150] M. N. Jadid and D. R. Fairbairn, "Neural-network applications in predicting moment-curvature parameters from experimental data," *Engineering Applications of Artificial Intelligence,* vol. 9, pp. 309-319, 6// 1996.

[151] G. Lachtermacher and J. D. Fuller, "Backpropagation In Time-Series Forecasting," *Journal of Forecasting,* vol. 14, pp. 381-393, Jul 1995.

[152] R. R. Srikant, P. V. Krishna, and N. D. Rao, "Online tool wear prediction in wet machining using modified back propagation neural network," *Proceedings of the Institution of Mechanical Engineers Part B-Journal of Engineering Manufacture,* vol. 225, pp. 1009-1018, Jul 2011.

[153] J. E. Raja, W. Lim, and C. Venkataseshaiah, "Tool Condition Monitoring using Competitive Neural Network and Hilbert-Huang Transform," *Asian Journal of Scientific Research,* vol. 6, pp. 703-714, 2013.

Appendix Contents

A-1 CrN Coated HSS (depth of coated layer = 5 µm)

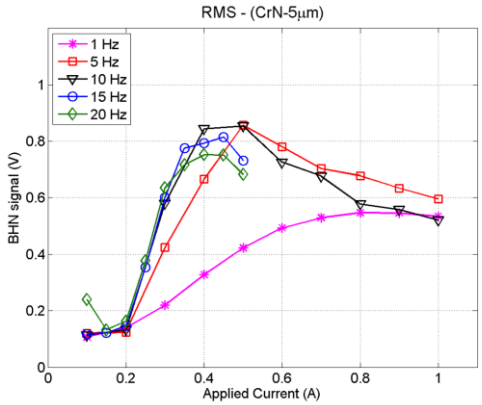

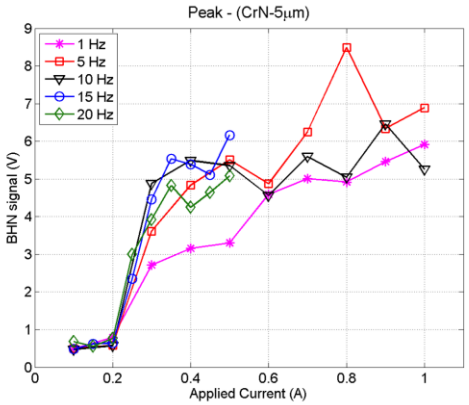

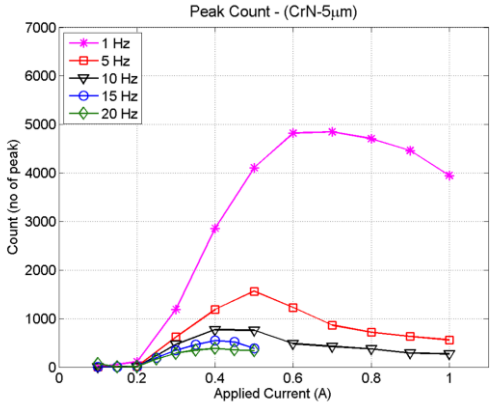

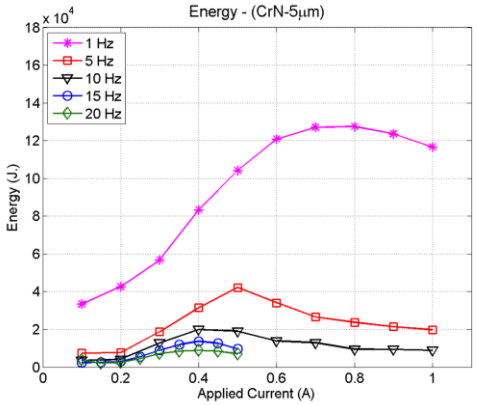

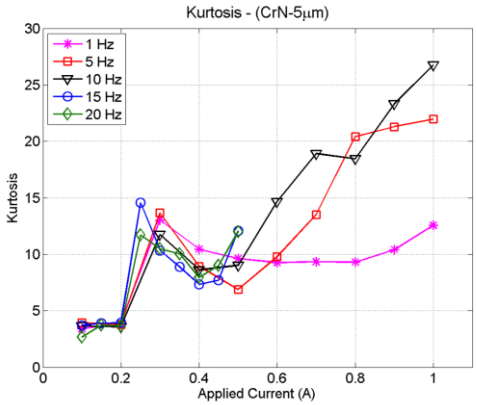

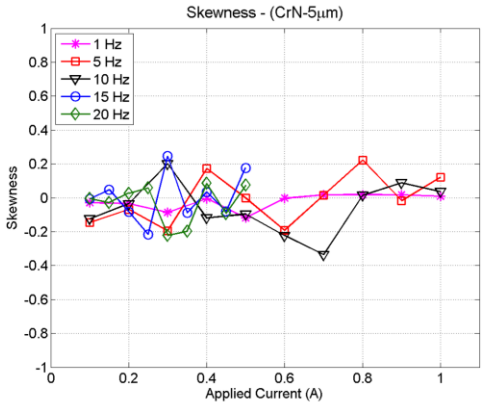

A-2 CrN Coated HSS (depth of coated layer = 10 µm)

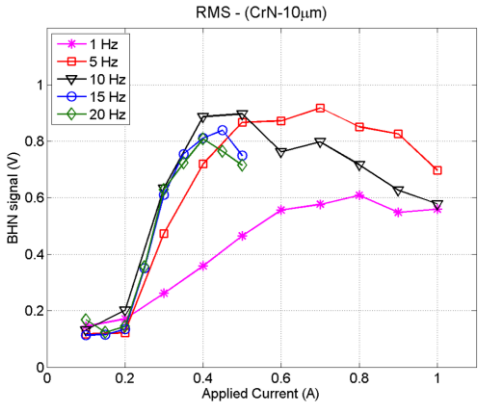

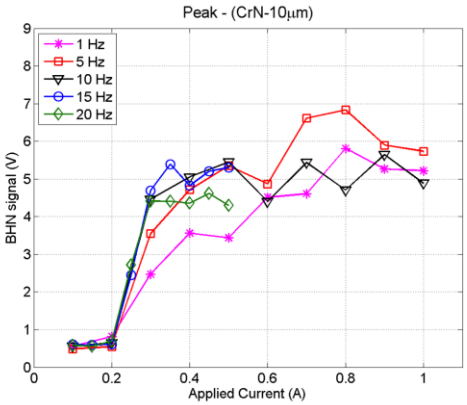

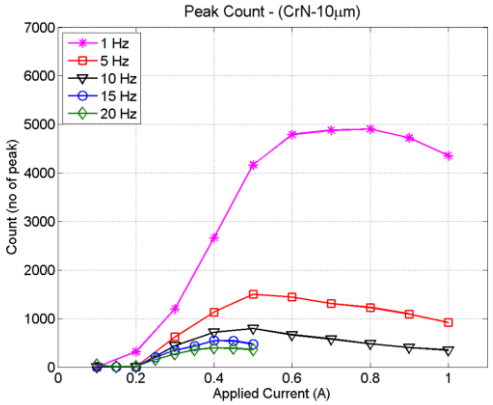

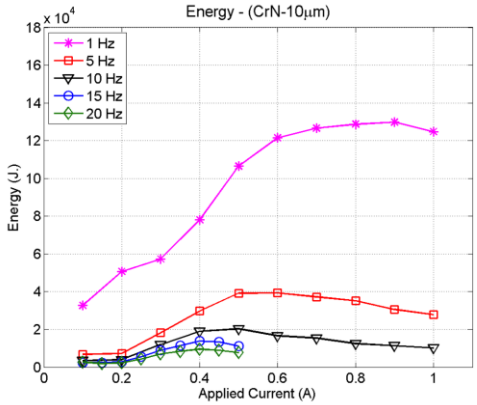

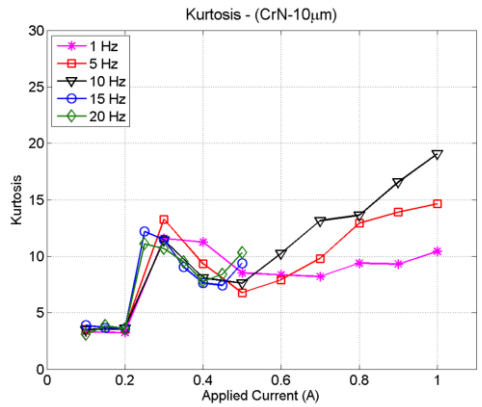

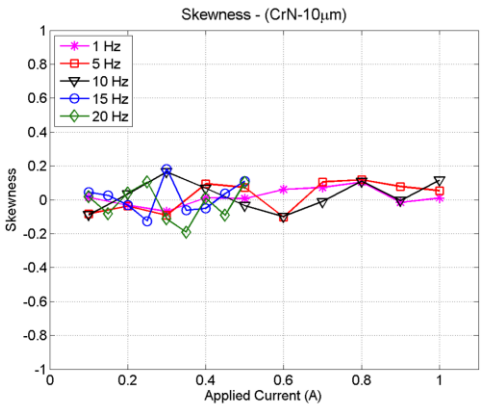

A-3 CrN Coated HSS (depth of coated layer = 15 µm)

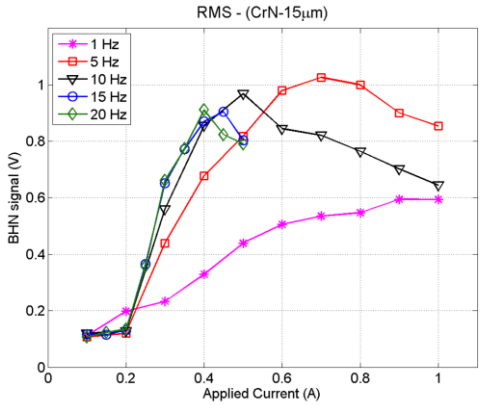

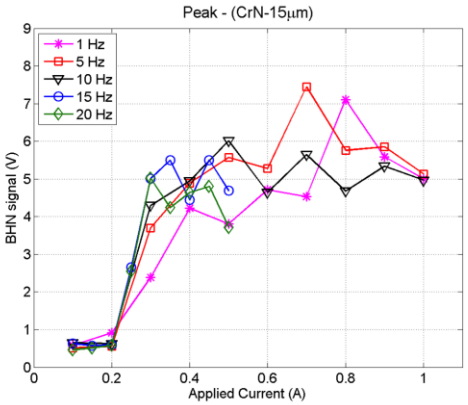

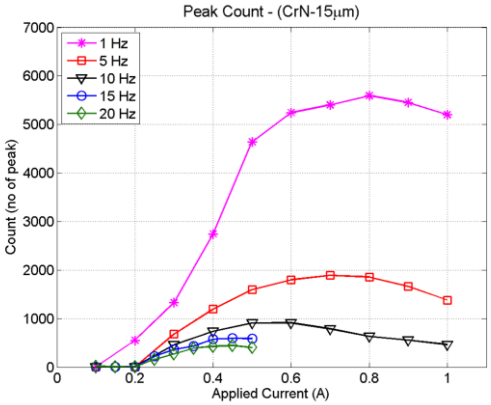

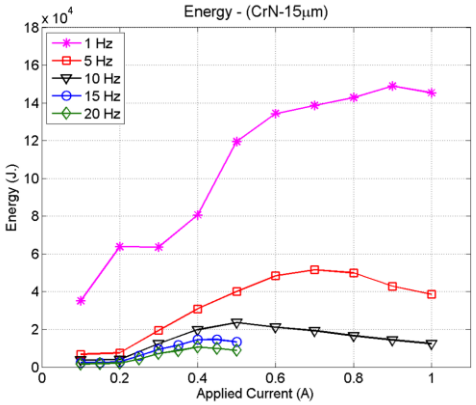

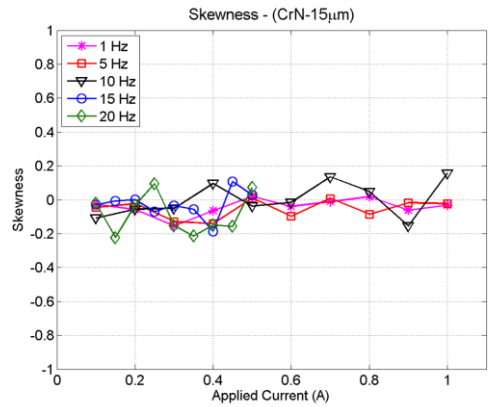

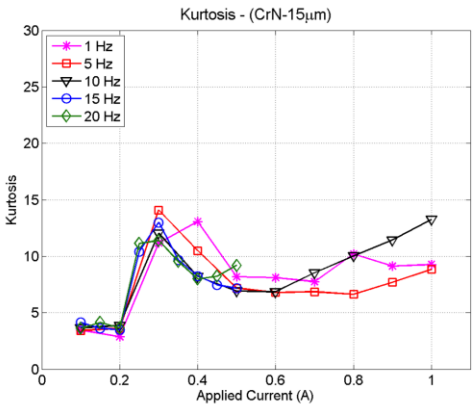

A-4 TiN Coated HSS (depth of coated layer = 5 µm)

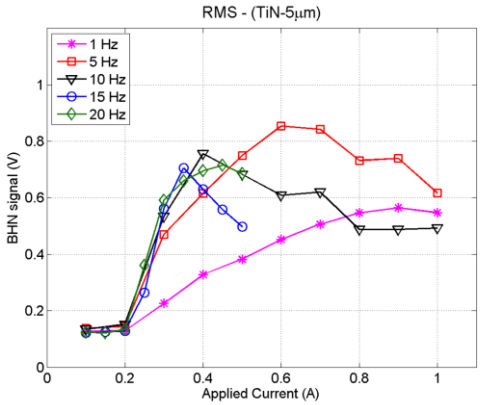

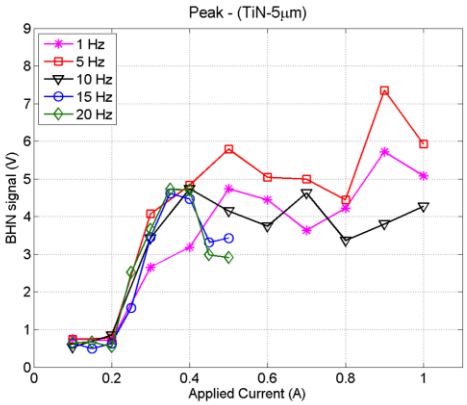

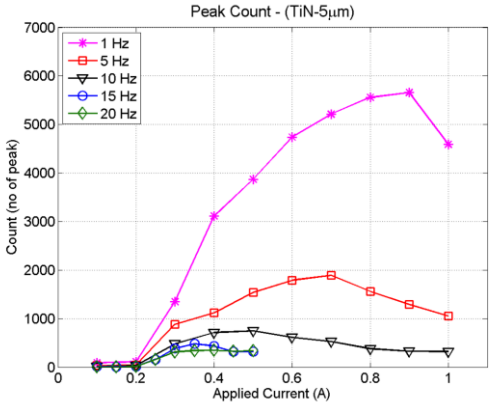

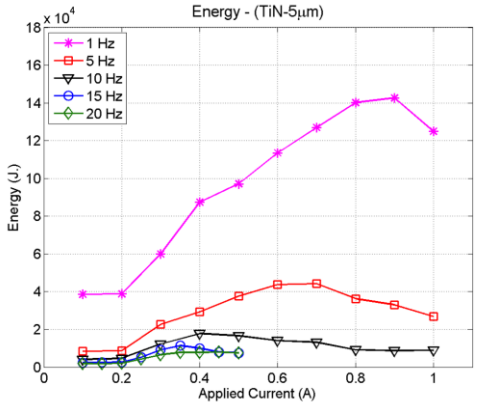

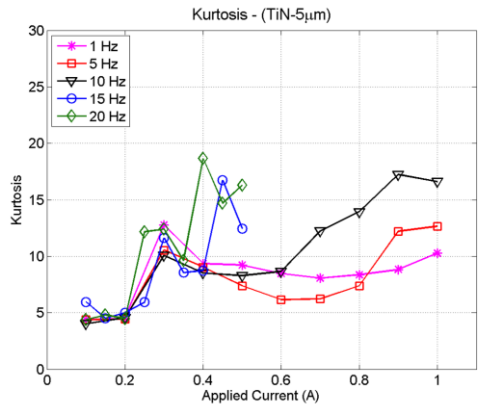

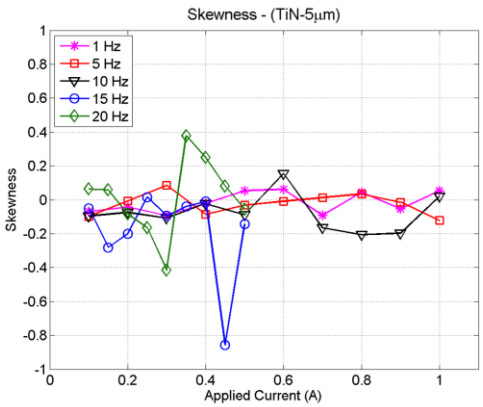

A-5 TiN Coated HSS (depth of coated layer = 10 µm)

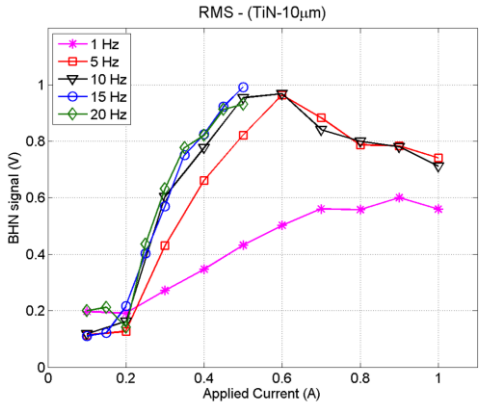

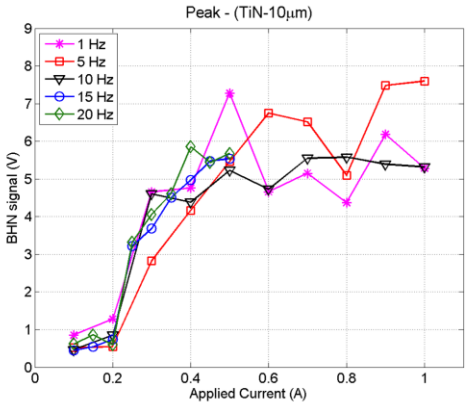

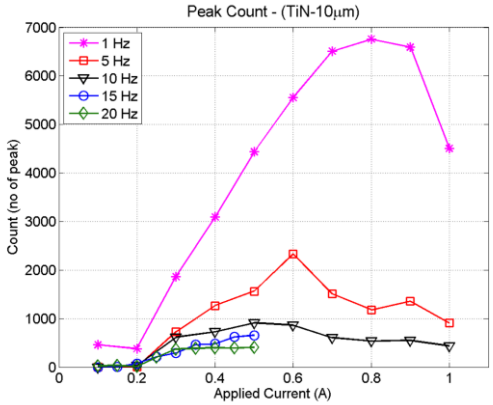

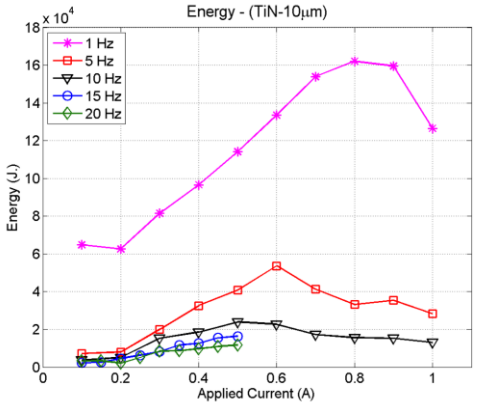

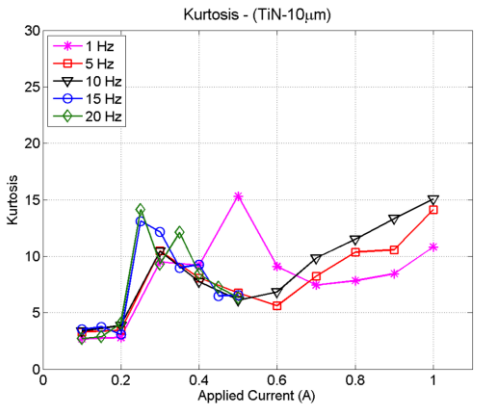

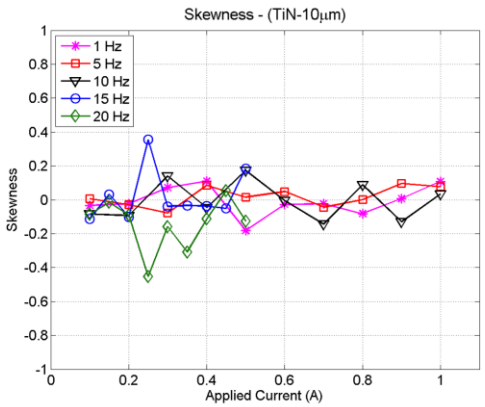

A-6 TiN Coated HSS (depth of coated layer = 15 µm)

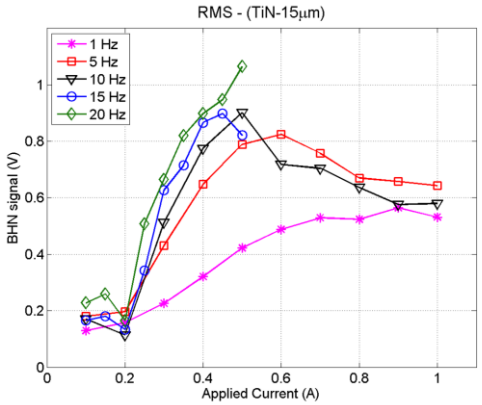

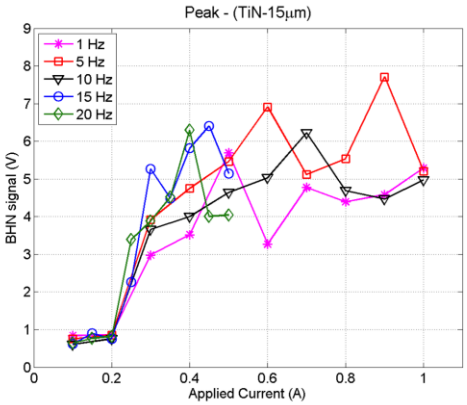

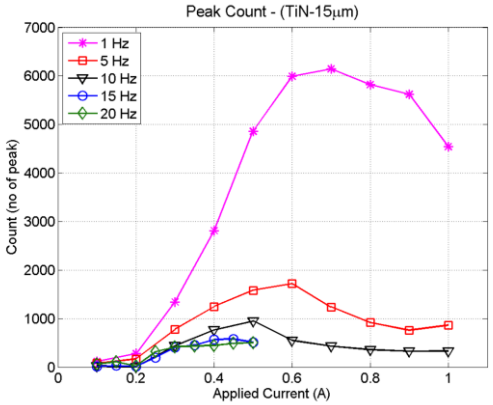

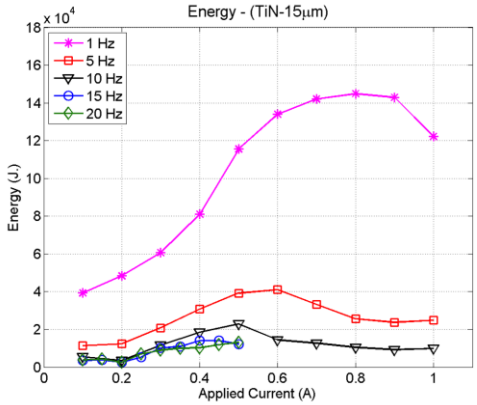

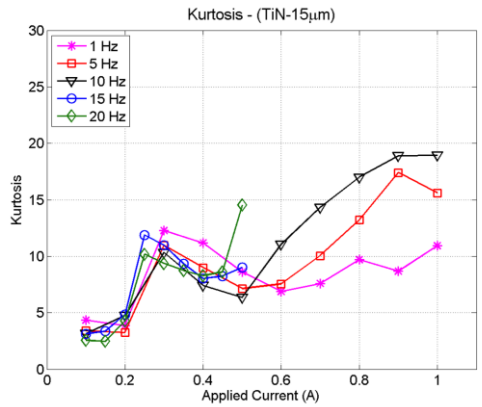

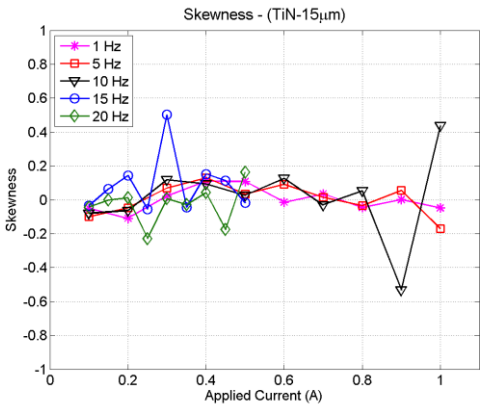

A-7 CrN Coated HSS (fe=1 Hz)

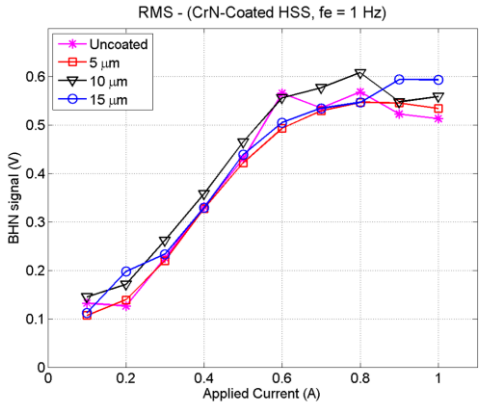

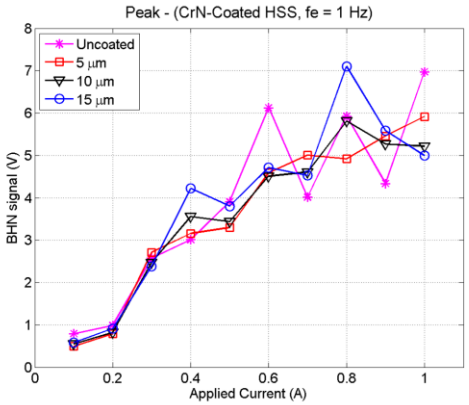

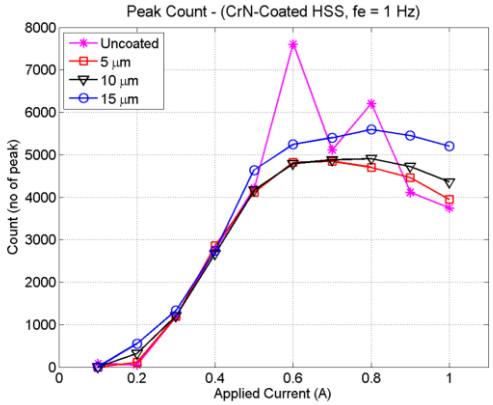

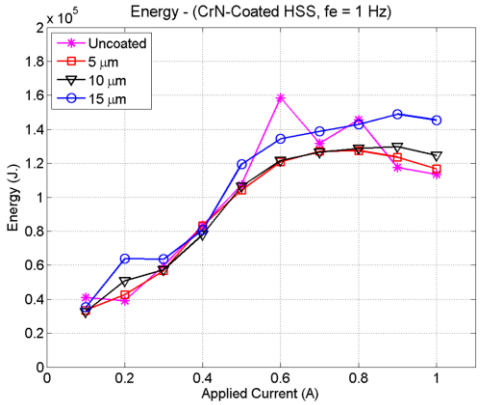

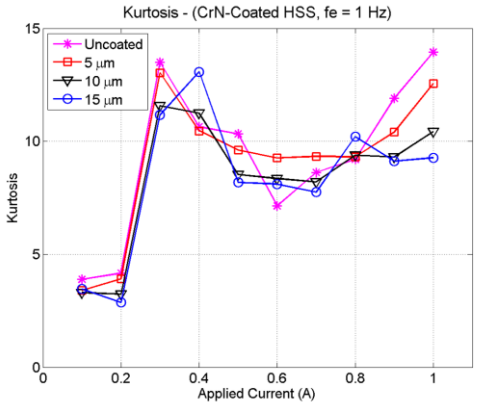

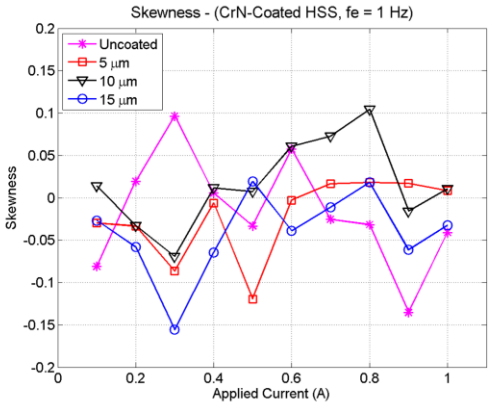

A-8 CrN Coated HSS (fe=5 Hz)

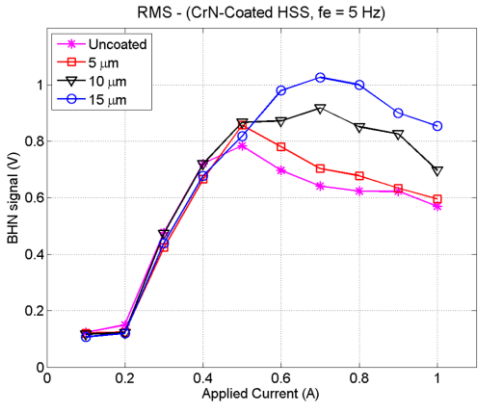

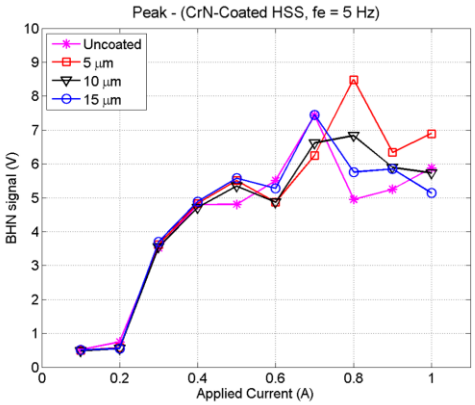

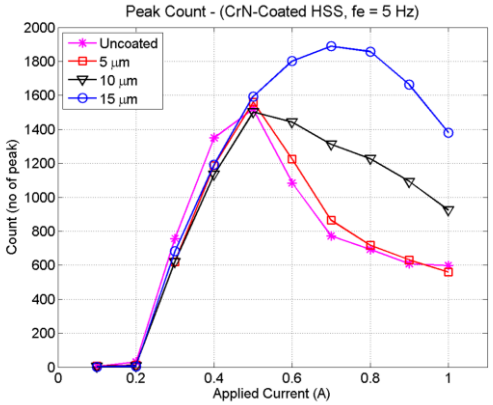

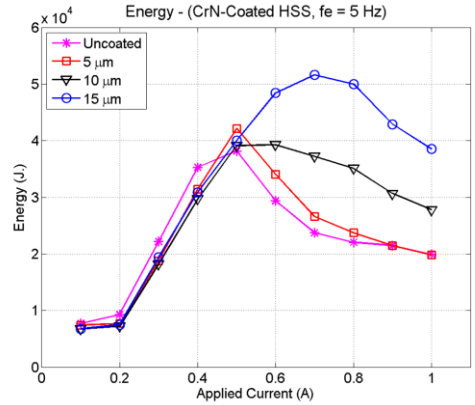

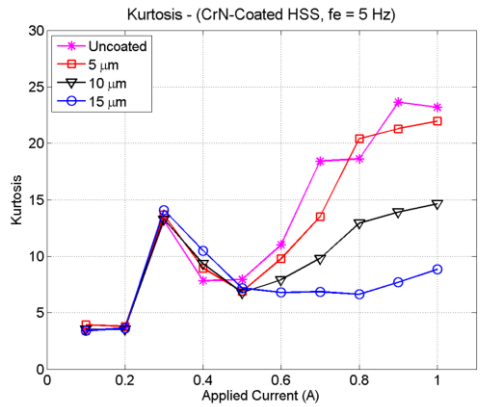

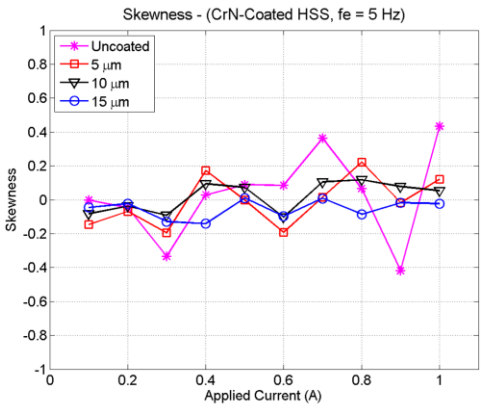

A-9 CrN Coated HSS (fe=10 Hz)

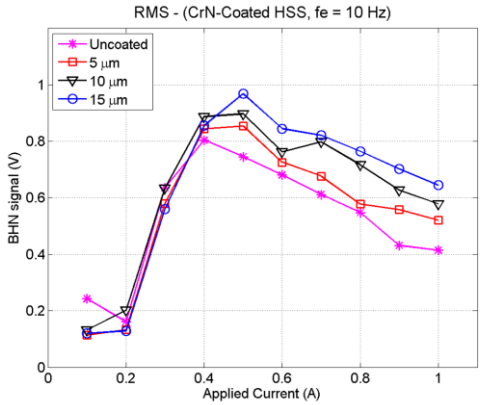

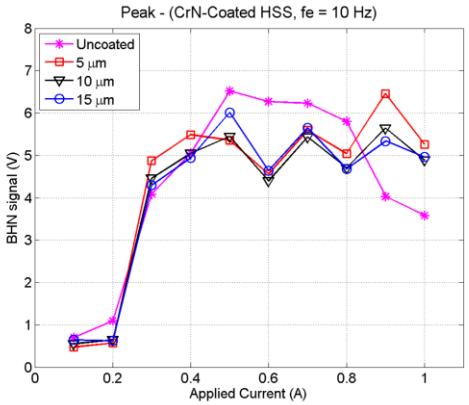

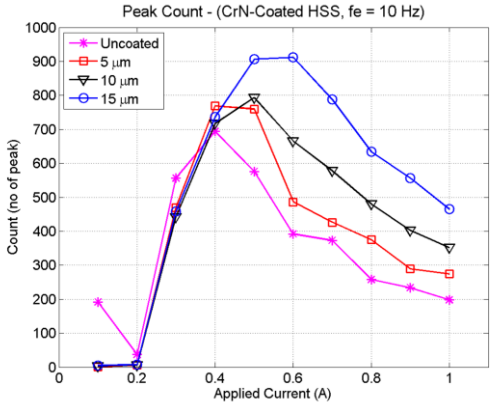

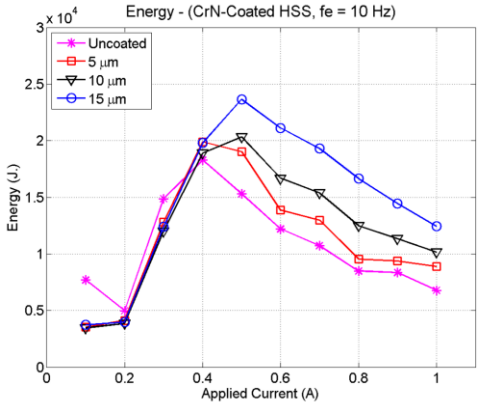

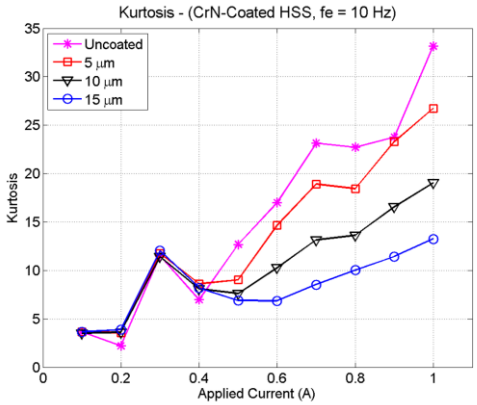

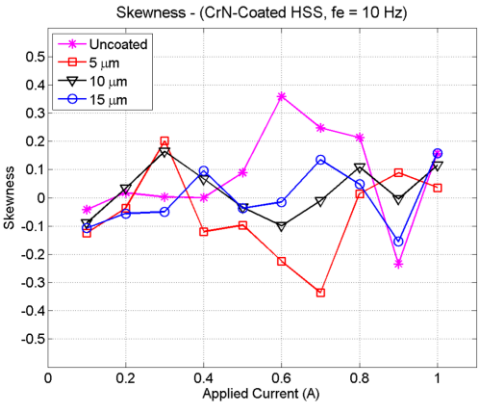

A-10 CrN Coated HSS (fe=15 Hz)

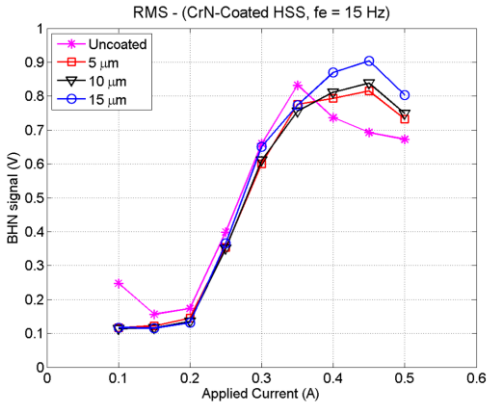

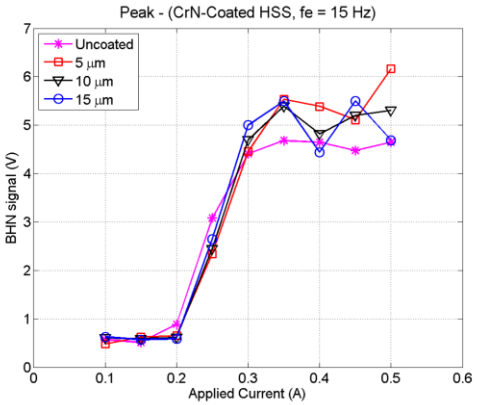

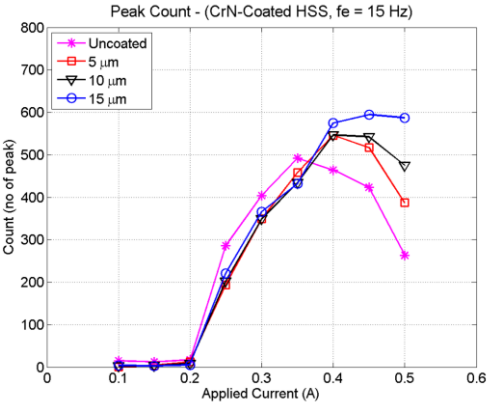

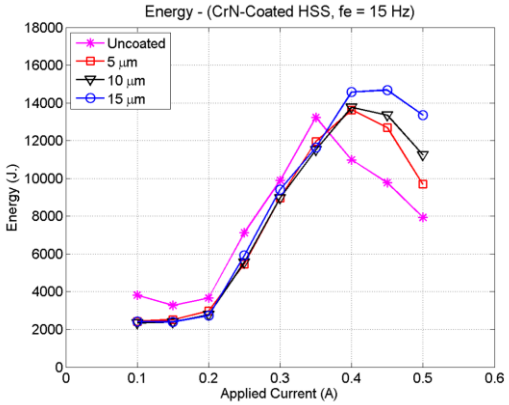

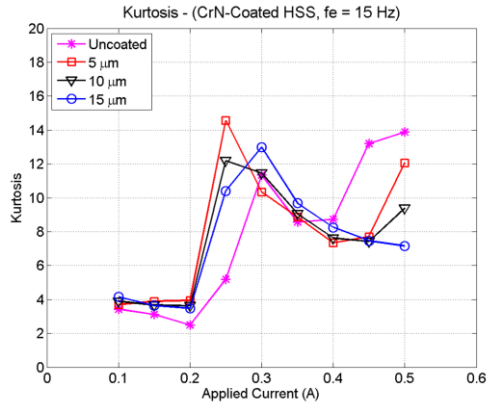

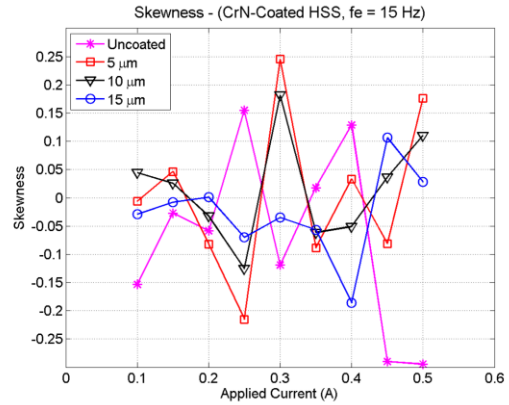

A-11 CrN Coated HSS (fe=20 Hz)

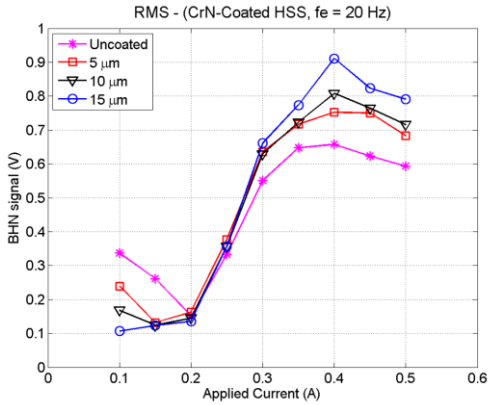

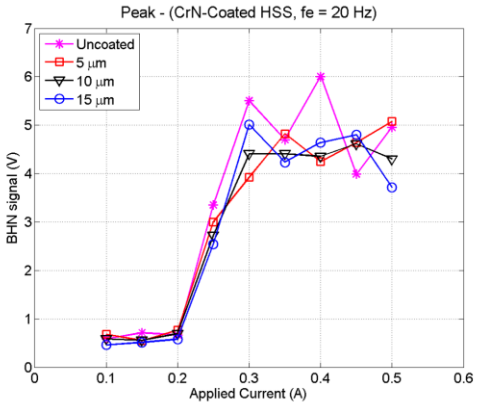

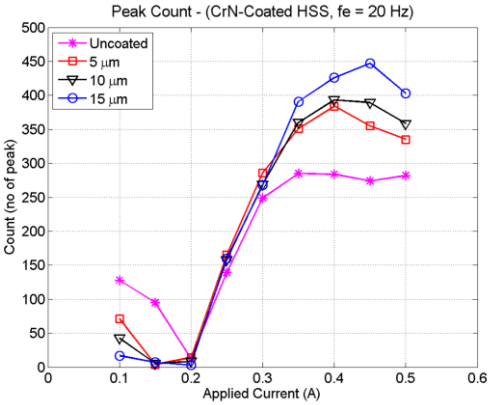

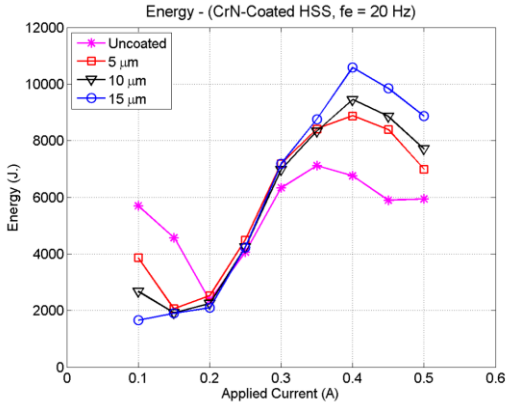

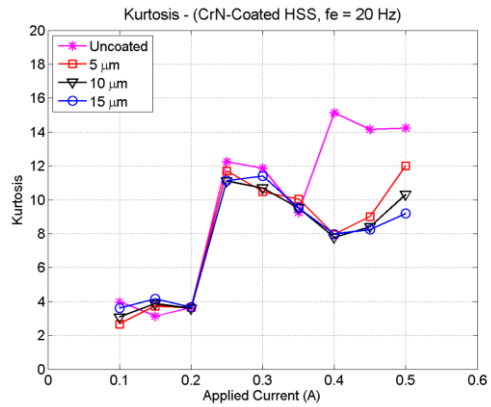

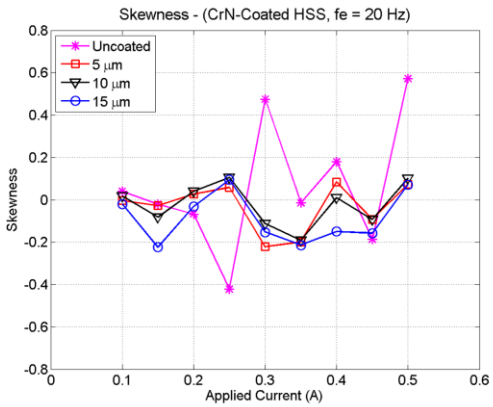

A-12 TiN Coated HSS (fe=1 Hz)

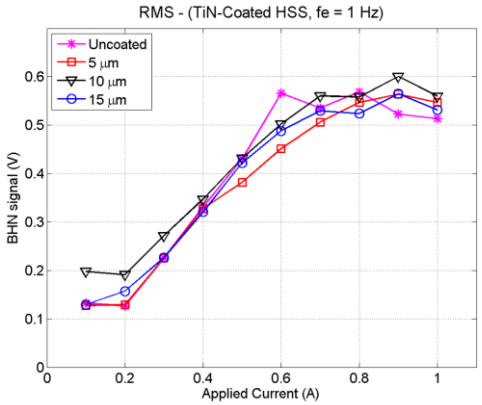

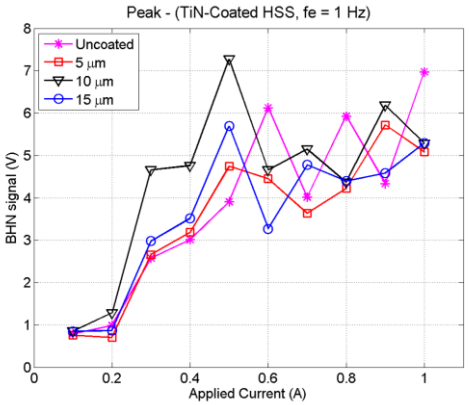

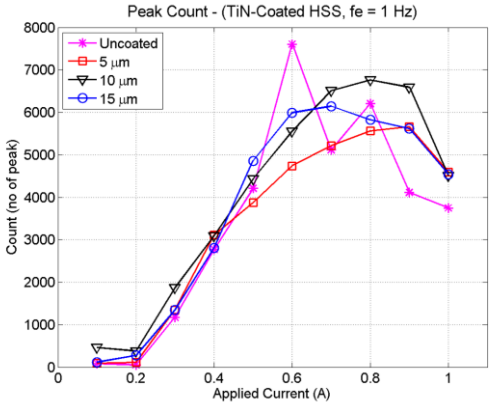

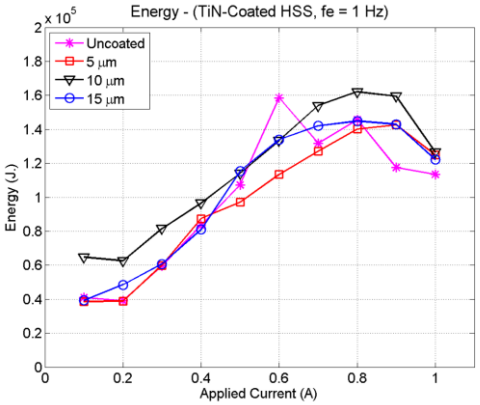

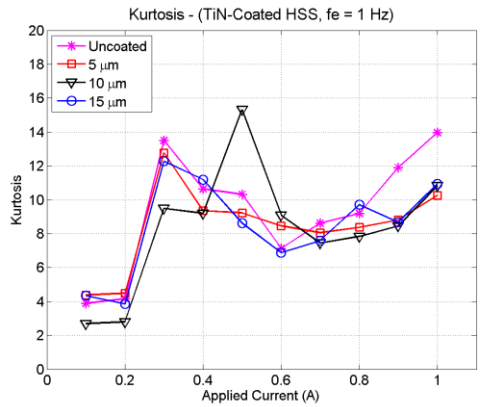

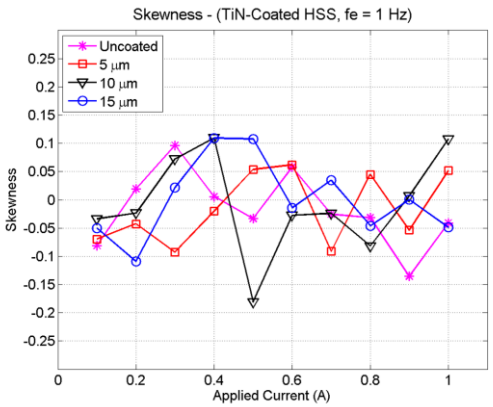

A-13 TiN Coated HSS (fe=5 Hz)

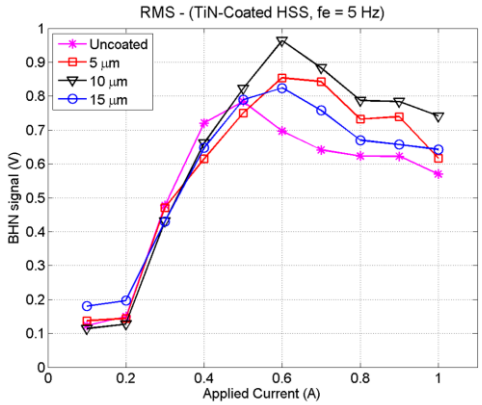

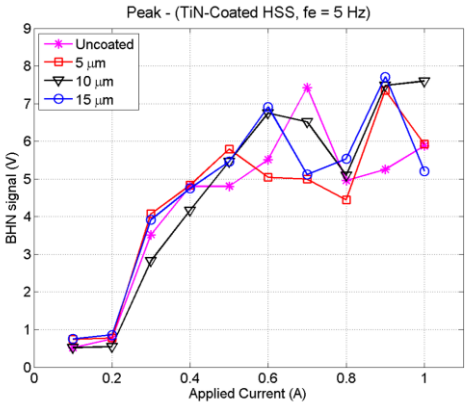

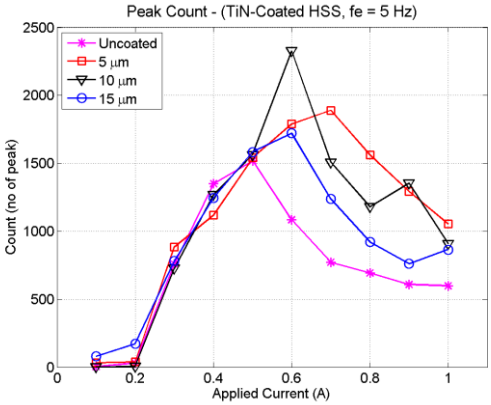

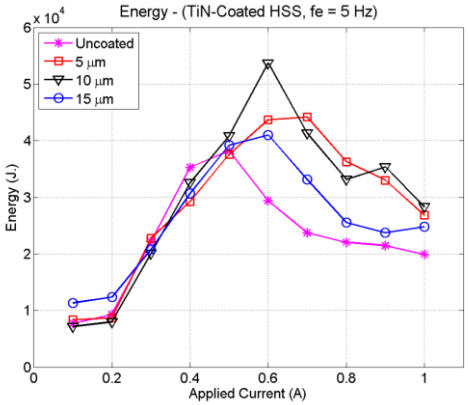

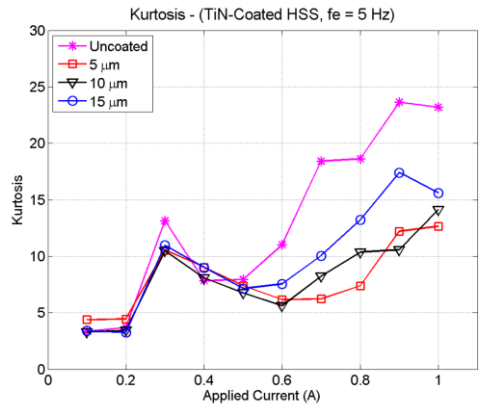

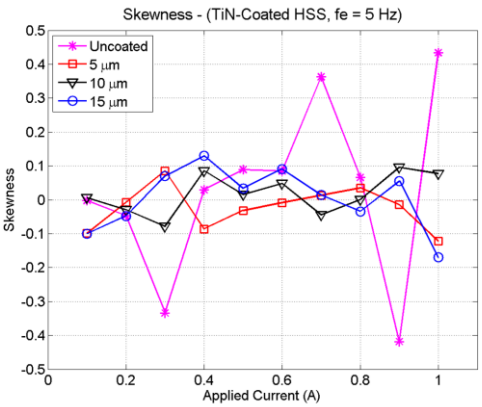

A-14 TiN Coated HSS (fe=10 Hz)

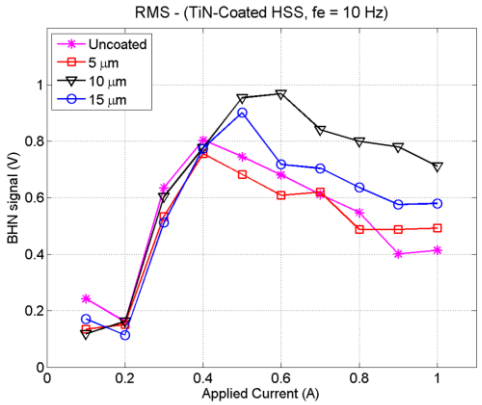

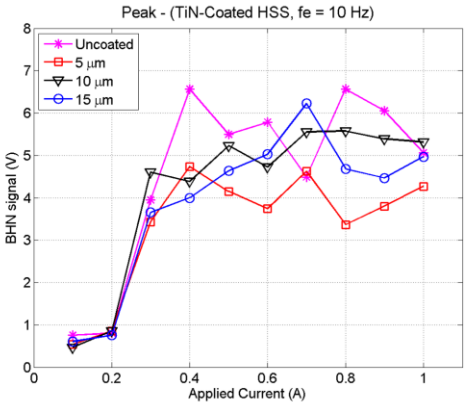

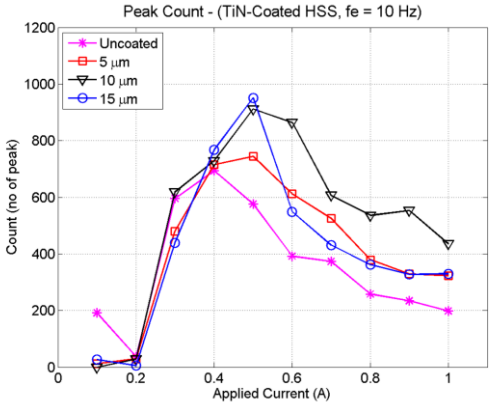

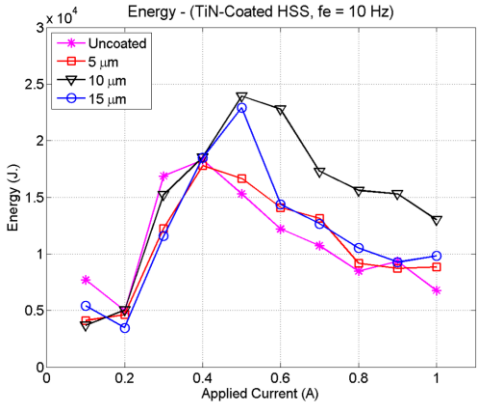

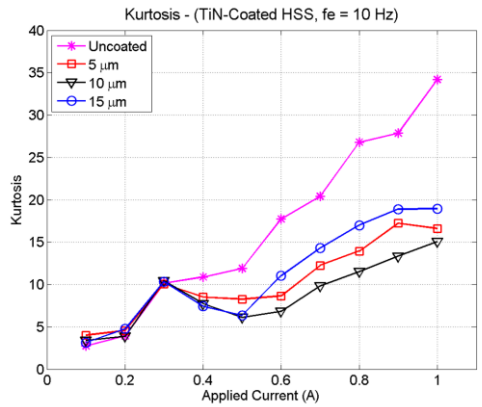

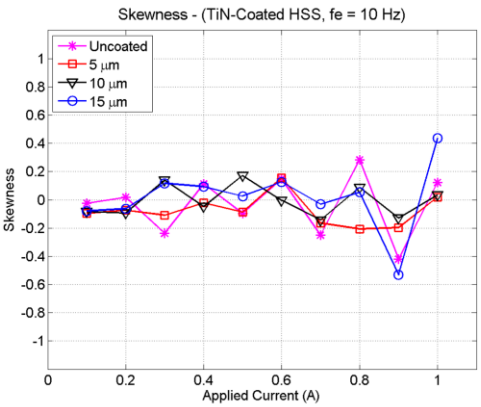

A-15 TiN Coated HSS (fe=15 Hz)

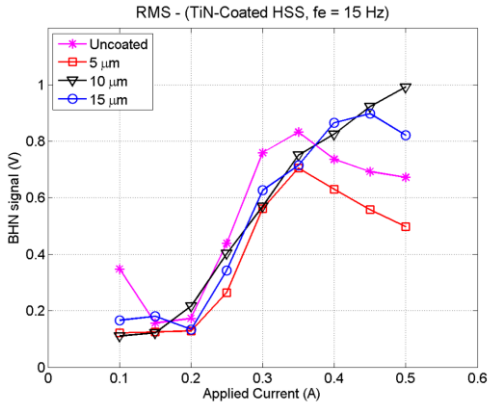

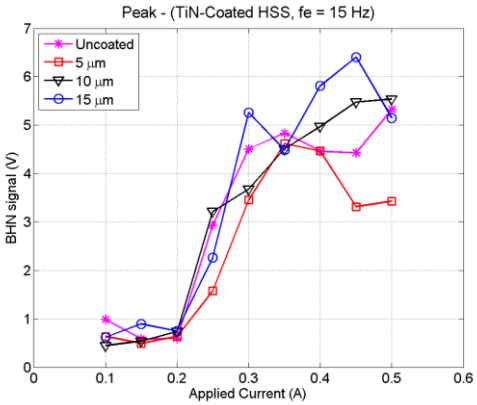

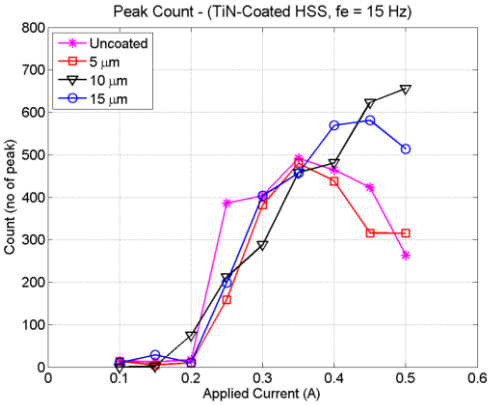

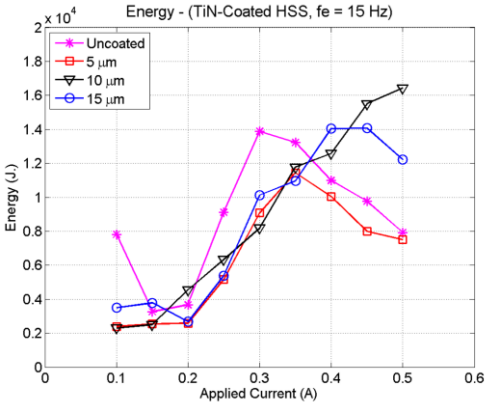

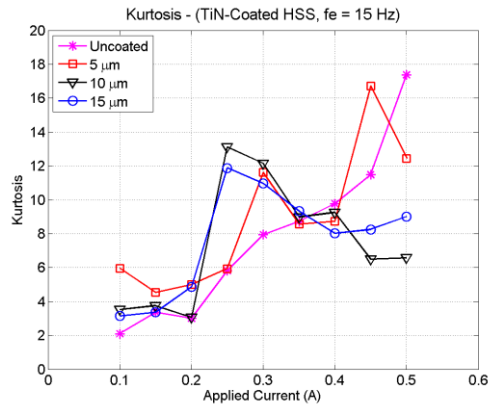

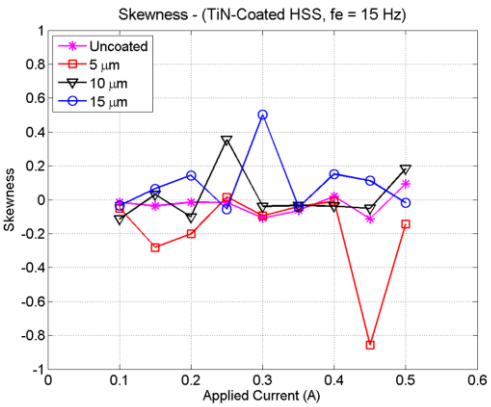

A-16 TiN Coated HSS (fe=20 Hz)

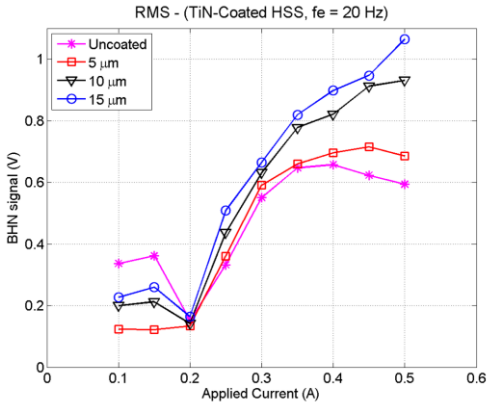

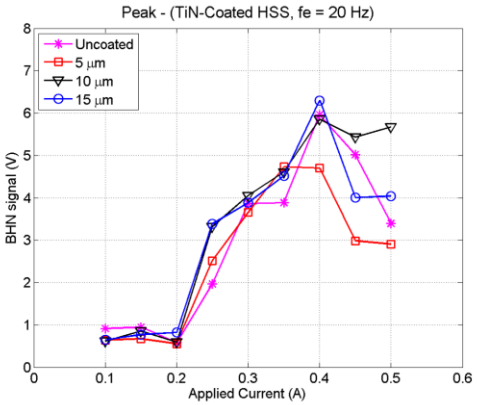

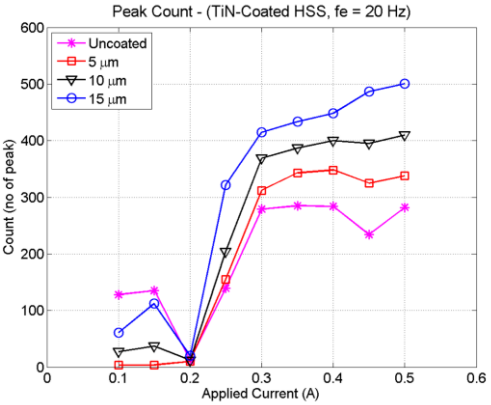

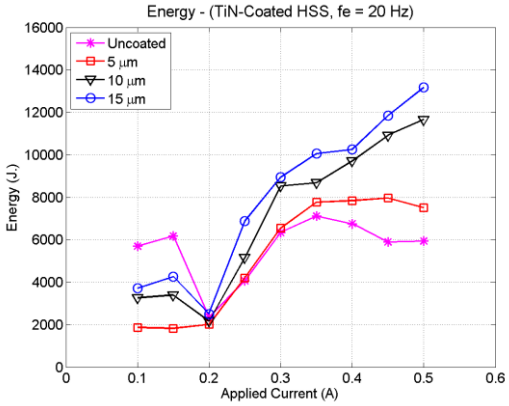

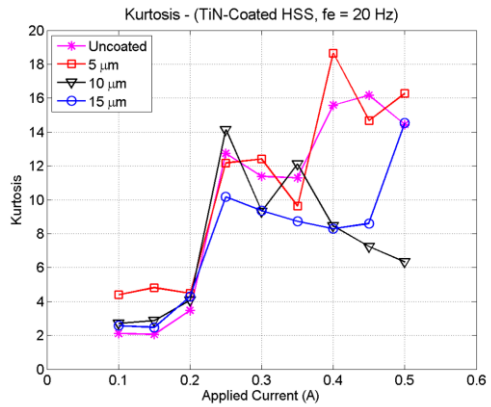

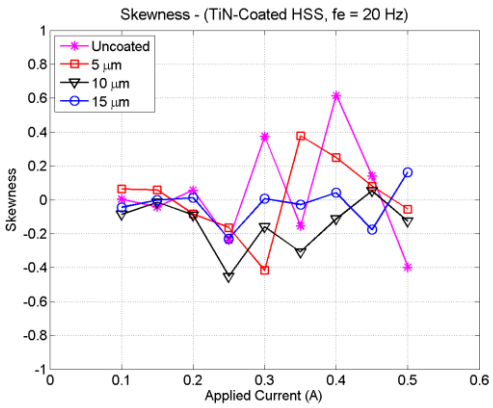

B-1 Flank Wear Values (replication 2)

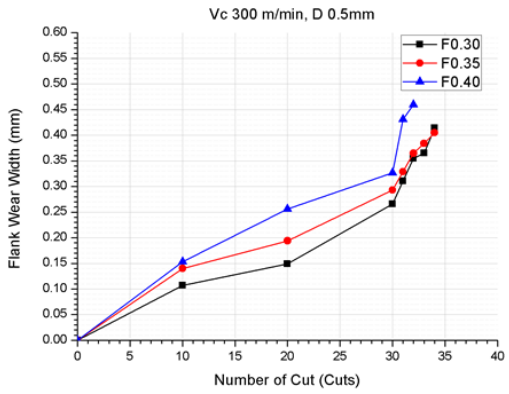

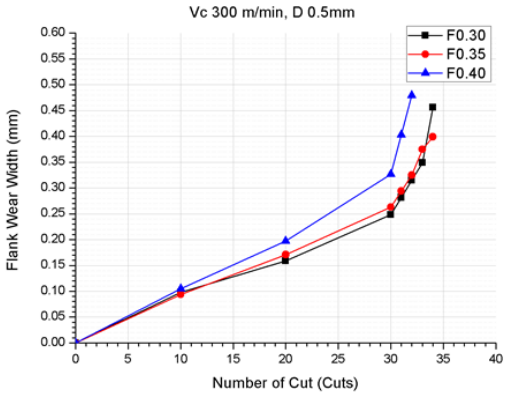

(a) *(b)*

Flank wear width at cutting speed 300 m/min on the main cutting edges:
(*a*) nose radius, (*b*) right side (replication 2)

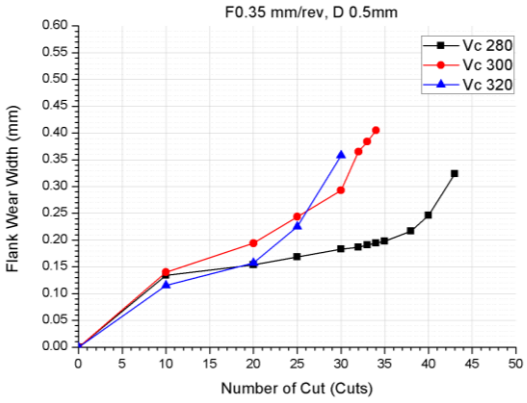

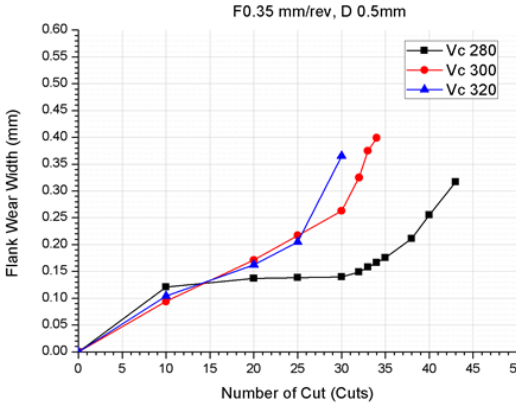

(a) *(b)*

Flank wear width at Feed rate 0.35 mm/rev on the main cutting edges:
(*a*) nose radius, (*b*) right side (replication 2)

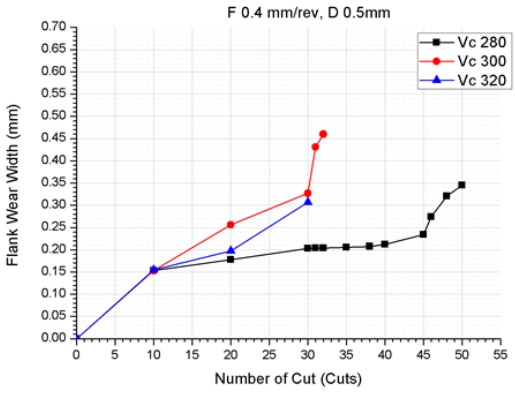

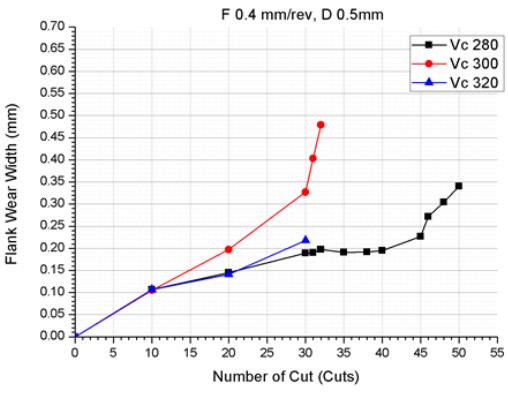

(a) *(b)*

Flank wear width at Feed rate 0.4 mm/rev on the main cutting edges:
(*a*) nose radius, (*b*) right side (replication 2)

B-2 AE Signal during the Experiment

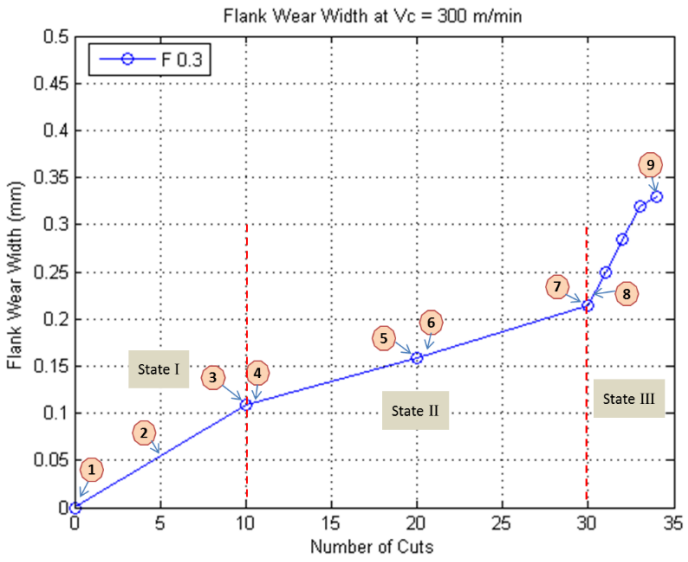

AE signals in Time domain and FFT graphs during tool wear progression from point 1 to 9.

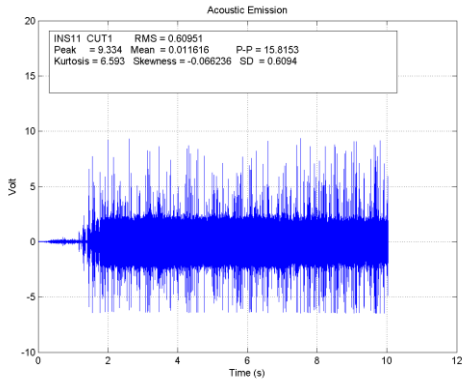

Time domain of point 1, 1st cut

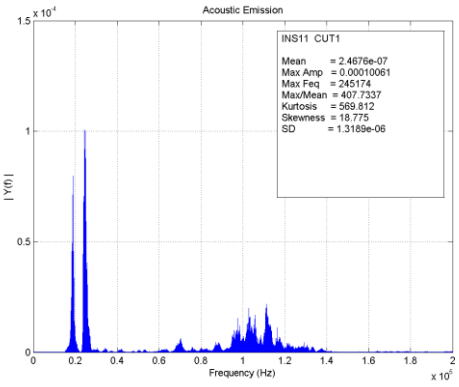

FFT of point 1, 1st cut

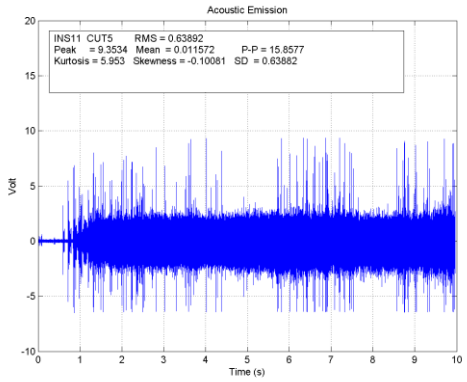

Time domain of point 2, 5th cut

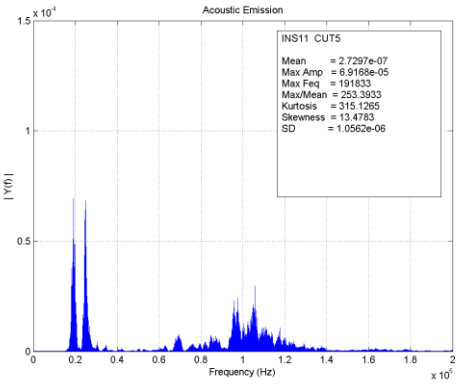

FFT of point 2, 5th cut

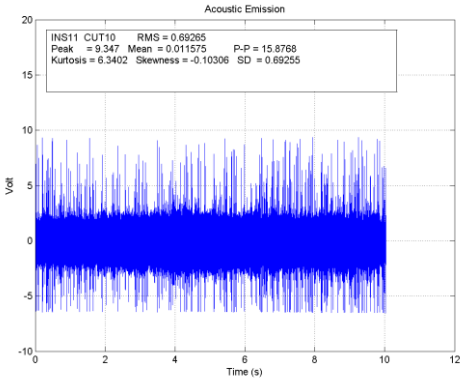

Time domain of point 3, 10th cut

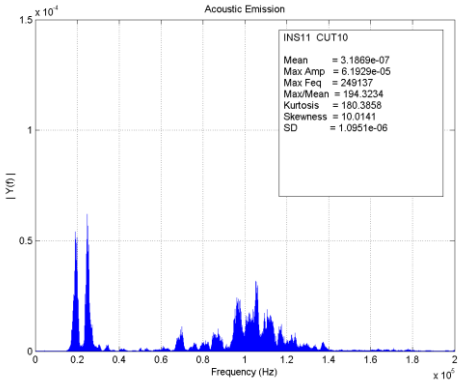

FFT of point 3, 10th cut

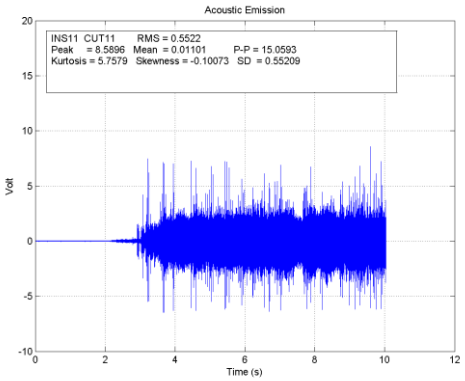

Time domain of point 4, 11th cut

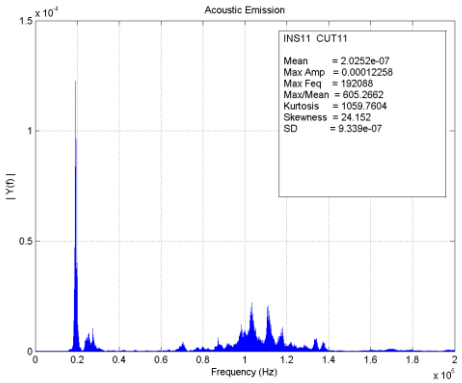

FFT of point 4, 11th cut

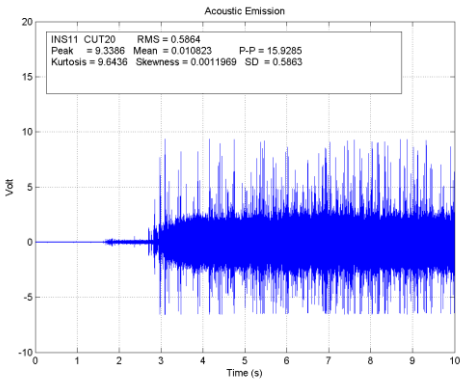

Time domain of point 5, 20th cut

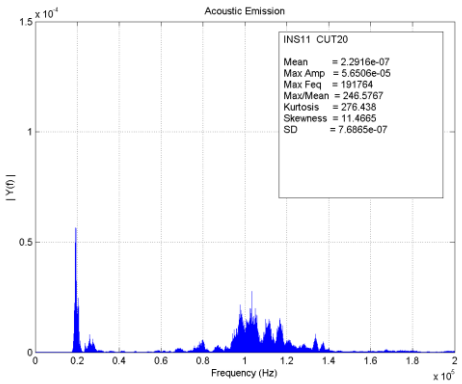

FFT of point 5, 20th cut

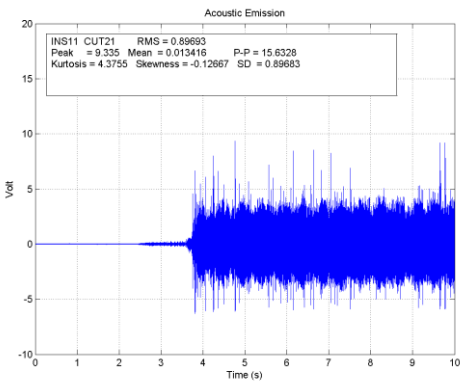

Time domain of point 6, 21st cut

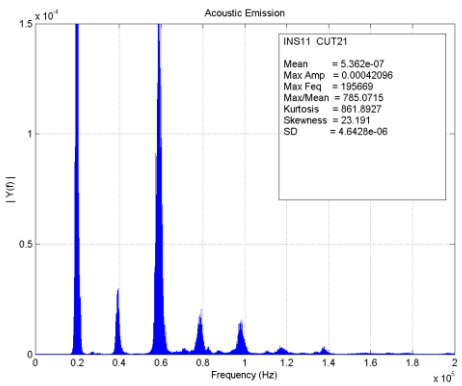

FFT of point 4, 21st cut

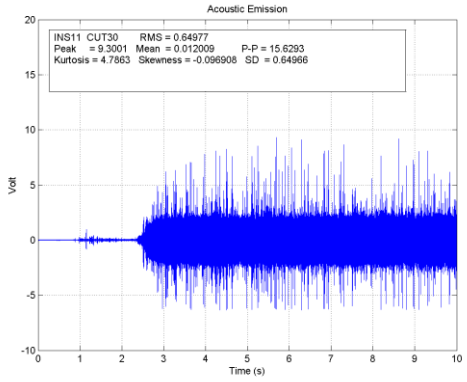

Time domain of point 7, 30th cut

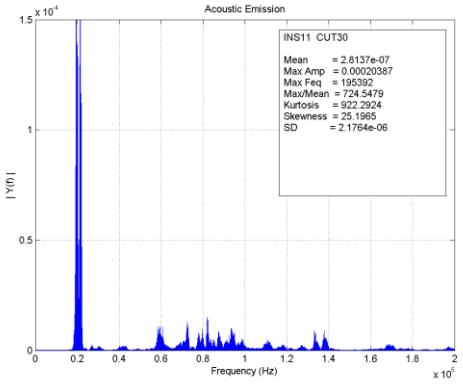

FFT of point 7, 30st cut

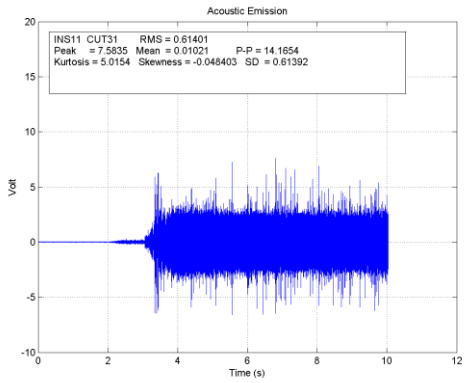

Time domain of point 8, 31st cut

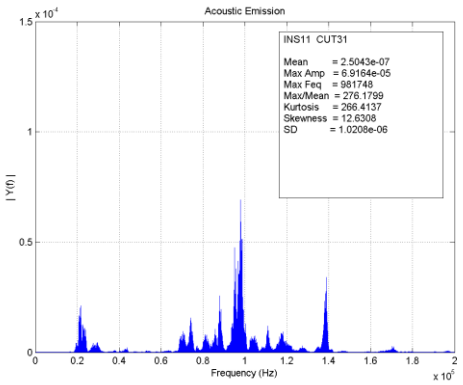

FFT of point 8, 31st cut

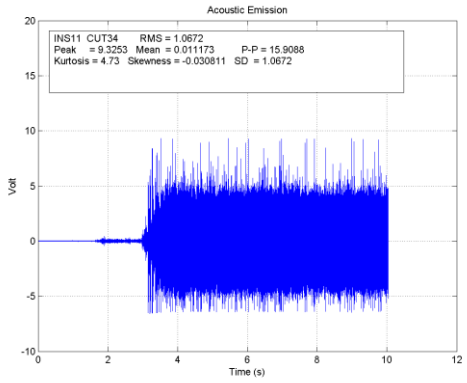

Time domain of point 9, 34th cut

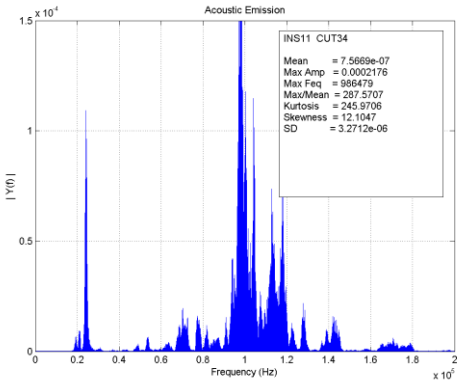

FFT of point 9, 34th cut

B-3 AE Features and Flank Wear

B-3.1 Relationship between AErms and Flank Wear

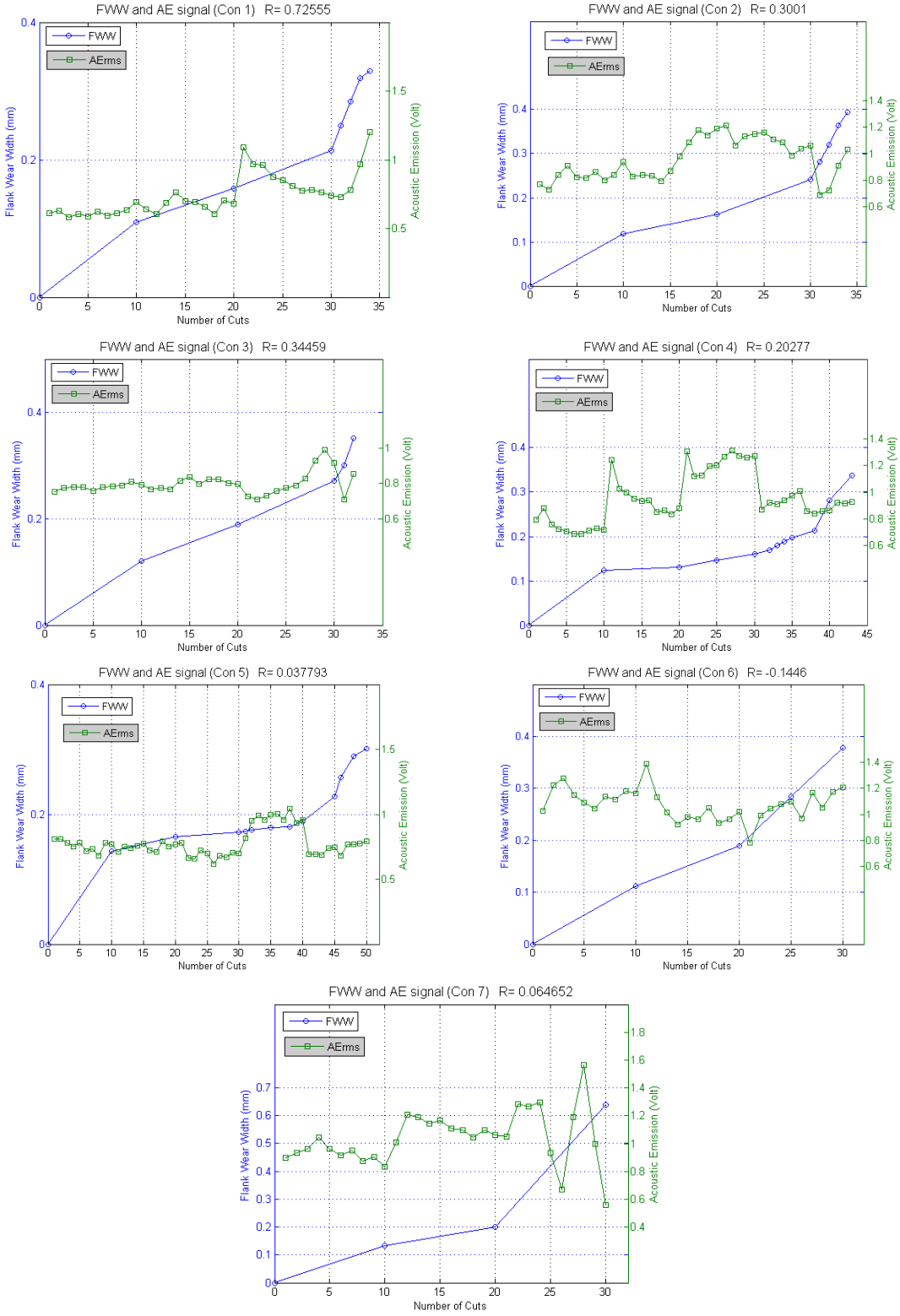

B-3.2 Relationship between AE_{p-p} and Flank Wear

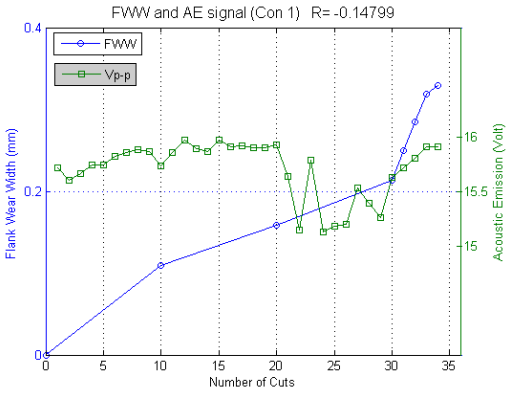

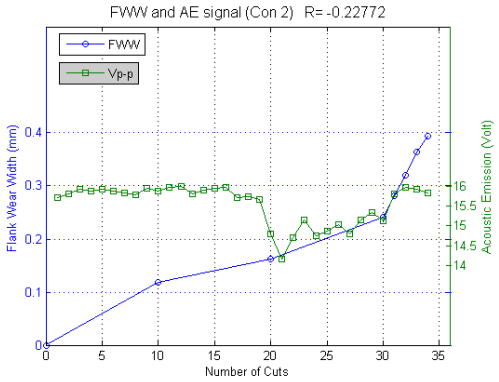

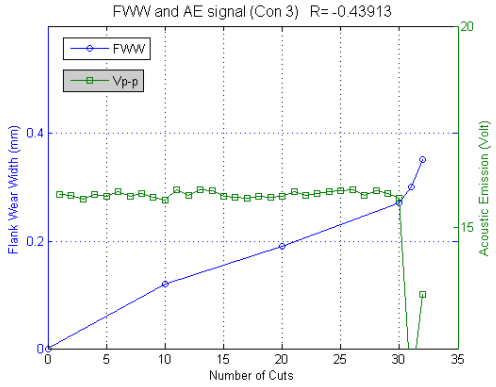

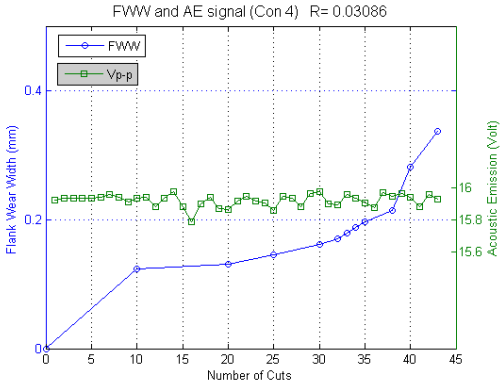

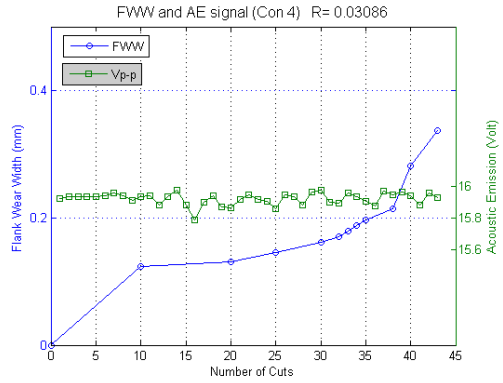

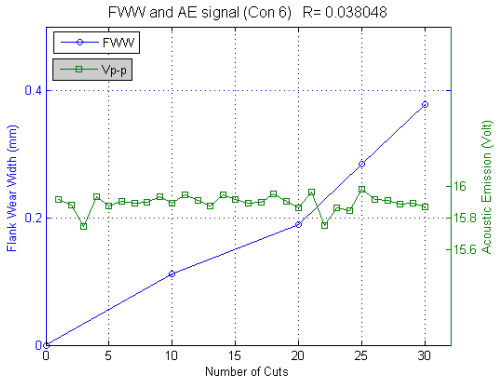

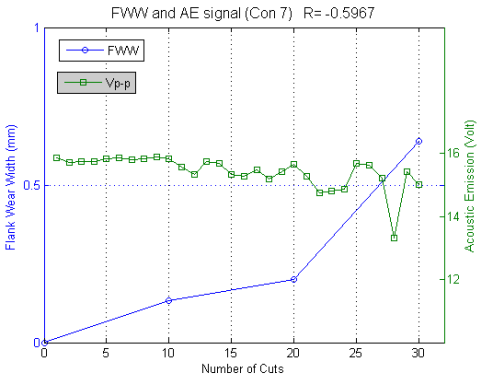

B-3.3 AE_{rms} and AE_{p-p} at Different Cutting Conditions

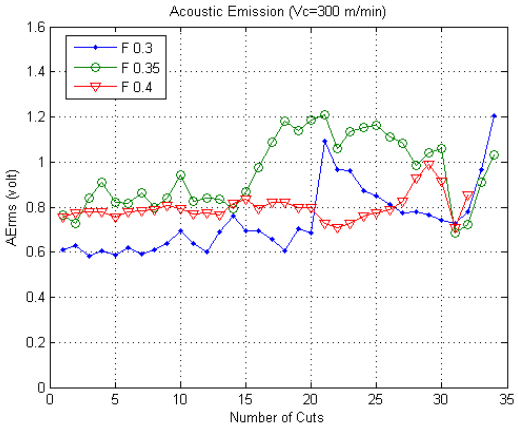

(*a*) AE_{rms} at constant cutting speed 300 m/min

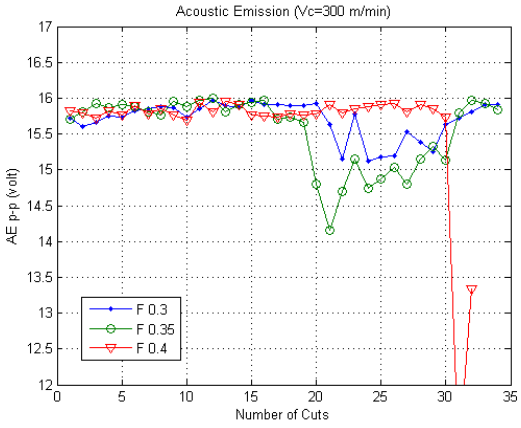

(*b*) AE_{p-p} at constant cutting speed 300 m/min

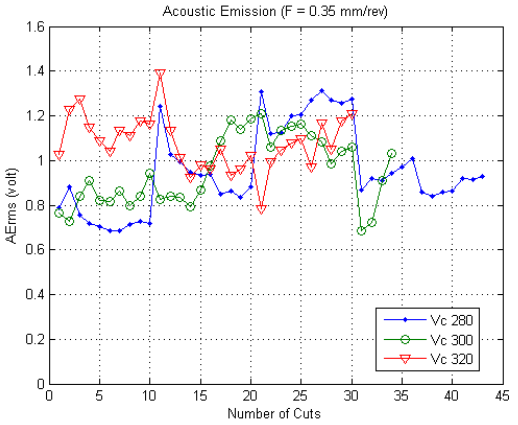

(*c*) AE_{rms} at constant feed rate 0.35 mm/rev

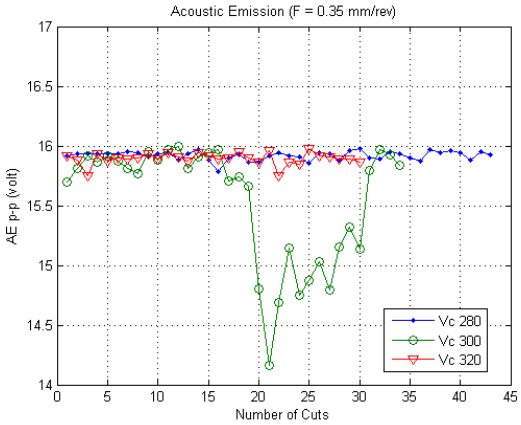

(*d*) AE_{p-p} at constant feed rate 0.35 mm/rev

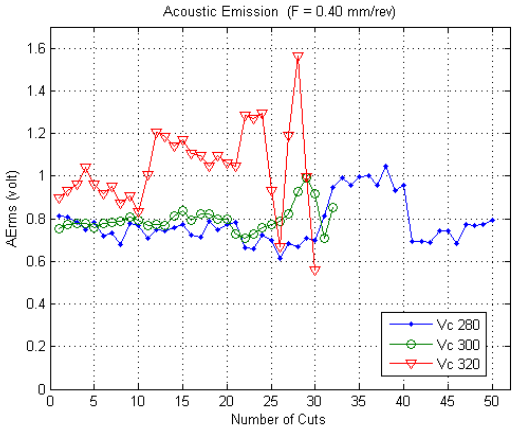

(*e*) AE_{rms} at constant feed rate 0.4 mm/rev

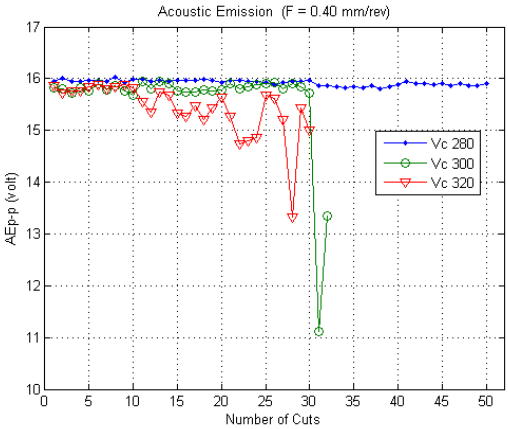

(*f*) AE_{p-p} at constant feed rate 0.4 mm/rev

B-4 Mean Sound Pressure and Flank wear

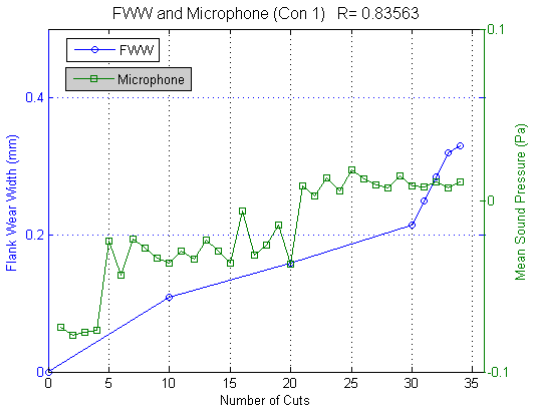

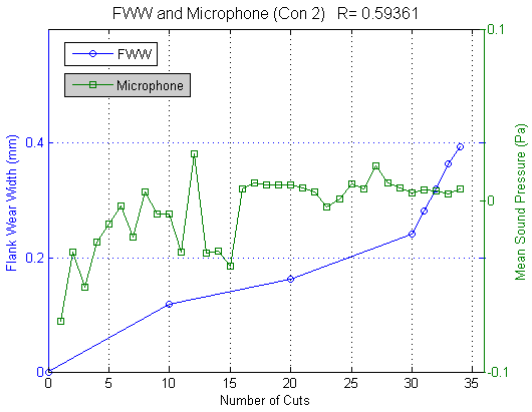

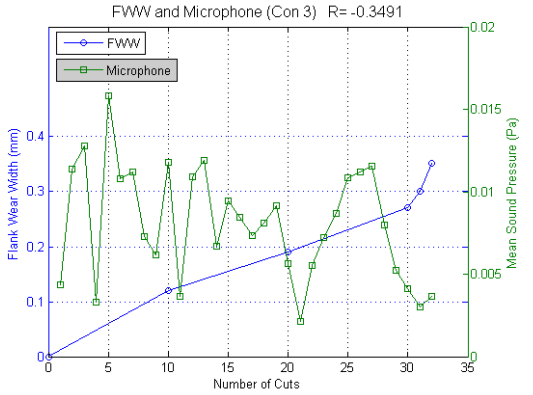

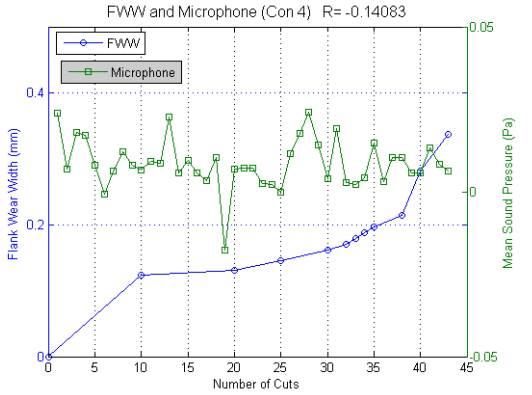

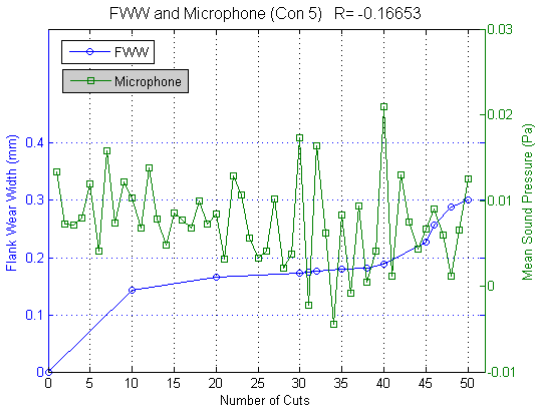

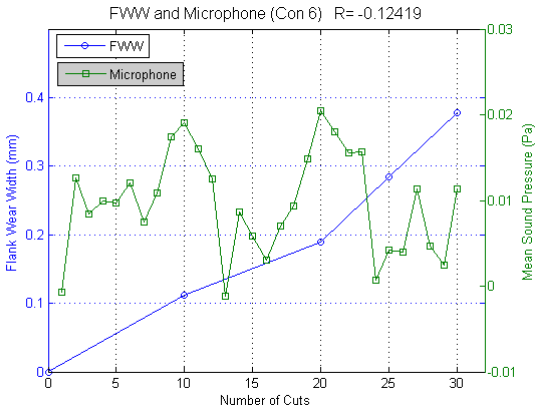

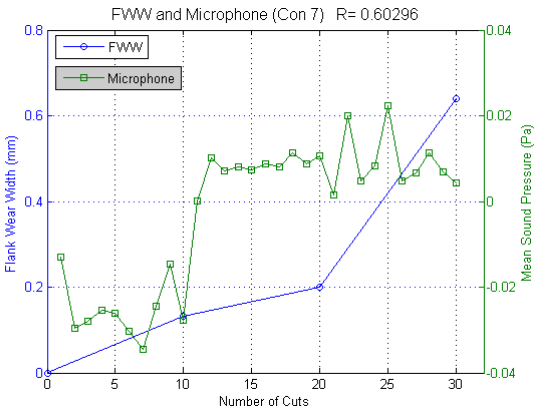

B-5 Mean Sound Pressure at Different Cutting Conditions

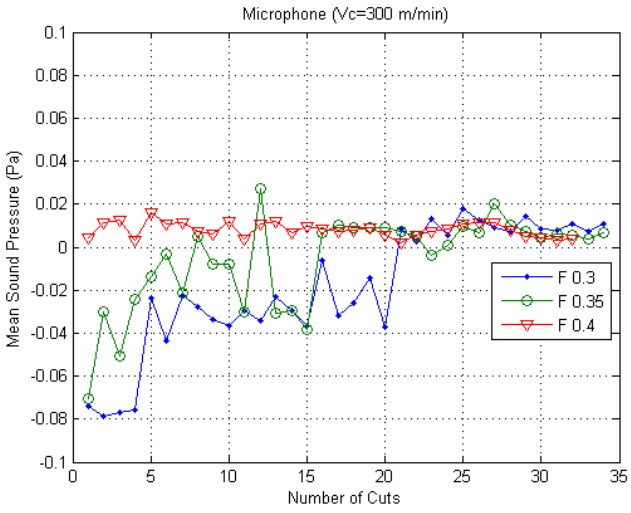

At constant cutting speed (Vc=300 m/min)

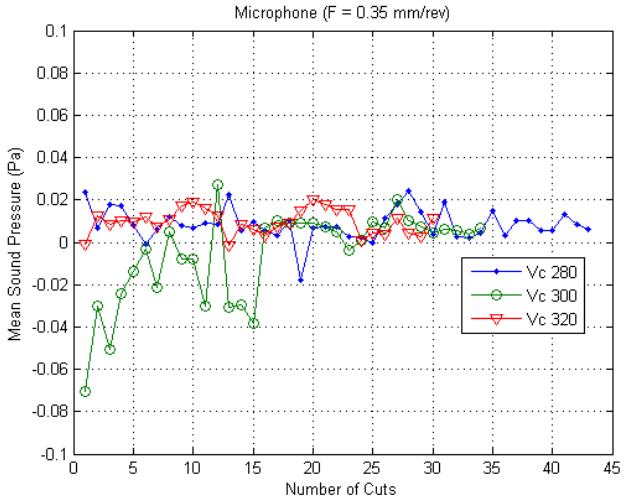

At constant feed (F=0.35 mm/rev)

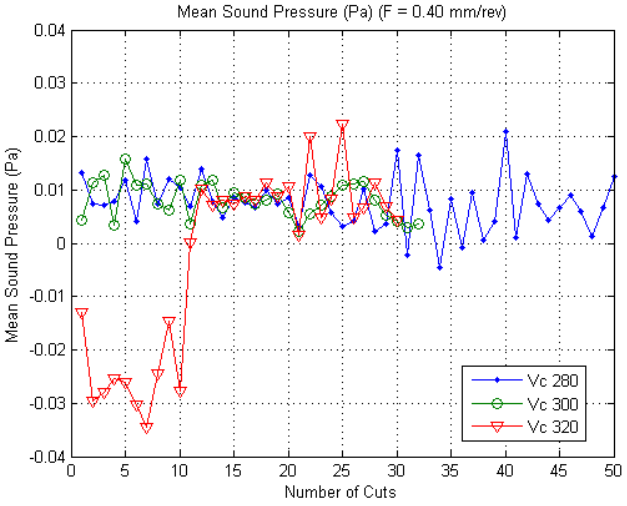

At constant feed (F=0.40 mm/rev)

B-6 Power Consumption of Spindle Motor (P_{rms}) and Flank Wear

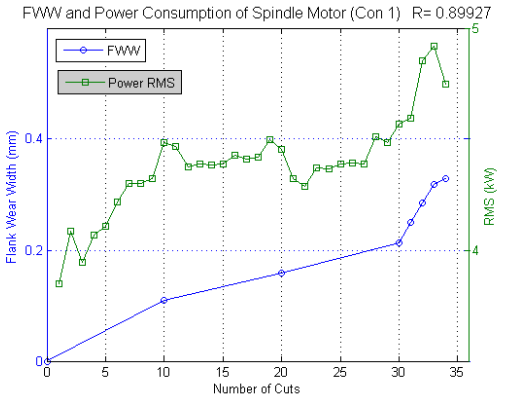

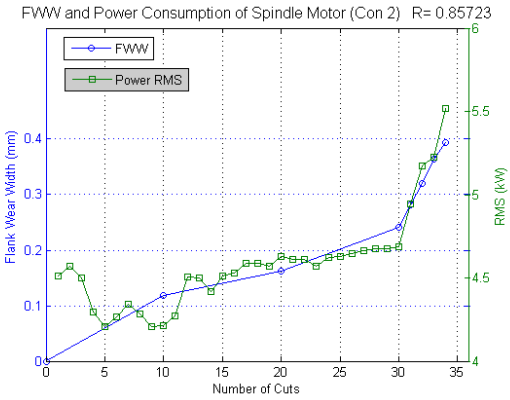

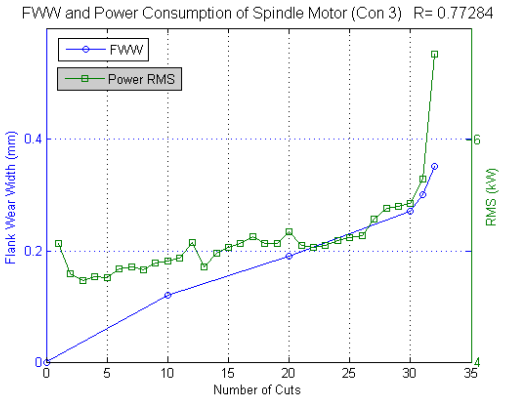

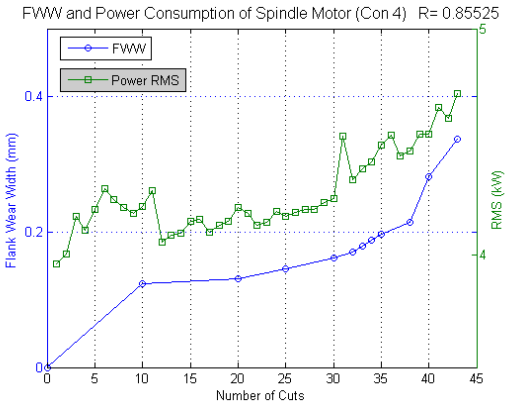

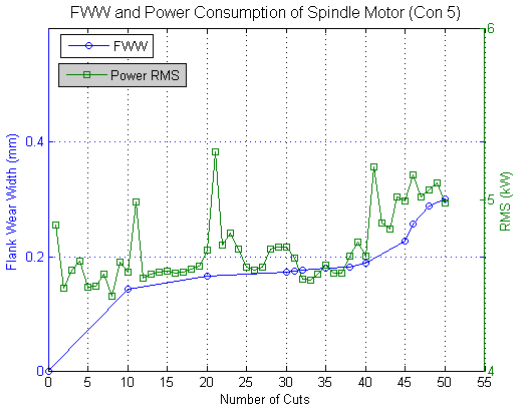

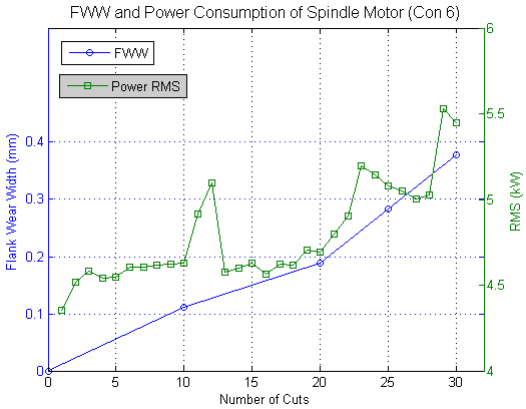

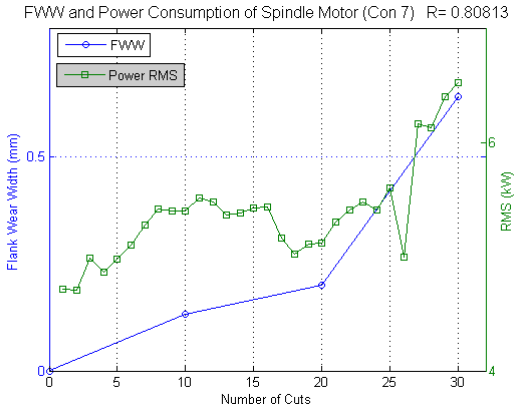

B-7 Power Consumption (P_{rms}) at Different Cutting Conditions

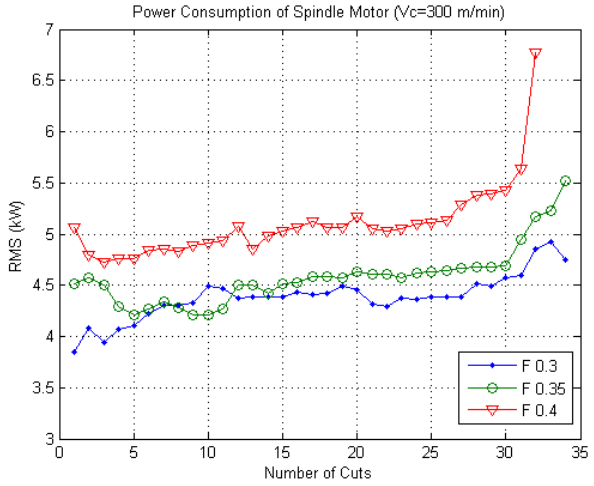

At constant cutting speed (Vc=300 m/min)

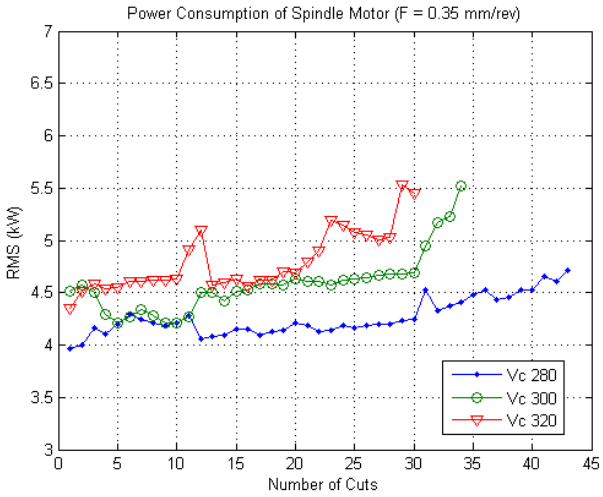

At constant feed (F=0.35 mm/rev)

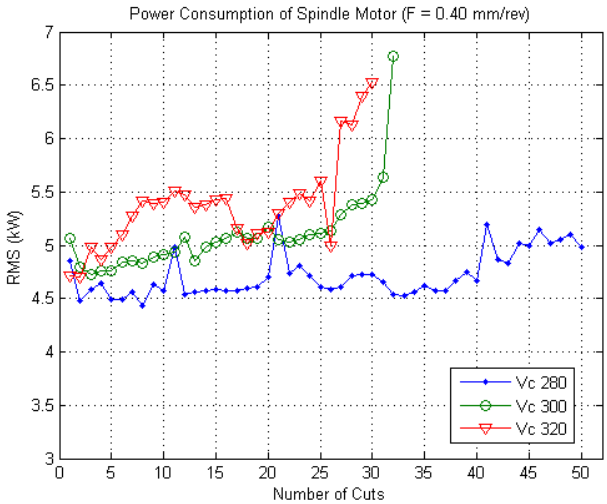

At constant feed (F=0.40 mm/rev)